Do Membranes Dream of Electric Tubes?

Advanced Membranes Using Carbon Nanotube - Polymer Nanocomposites

by

Charles-François Pedro Claude Karolek Ghislain de Lannoy

Department of Civil and Environmental Engineering
Duke University

Date: _____

Approved:

_____
Mark R. Wiesner, Supervisor

_____
Marc Deshusses

_____
Helen Hsu-Kim

_____
Jie Liu

_____
David Jassby

Dissertation submitted in partial fulfillment of the requirements for the degree of Doctor of Philosophy in the Department of Civil and Environmental Engineering in the Graduate School of Duke University

2014

Abstract

Do Membranes Dream of Electric Tubes? Advanced Membranes Using Carbon Nanotube - Polymer Nanocomposites

by

Charles-François Pedro Claude Karolek Ghislain de Lannoy

Department of Civil and Environmental Engineering
Duke University

Date: _____

Approved:

_____
Mark R. Wiesner, Supervisor

_____
Marc Deshusses

_____
Helen Hsu-Kim

_____
Jie Liu

_____
David Jassby

An abstract of a dissertation submitted in partial fulfillment of the requirements for the degree of Doctor of Philosophy in the Department of Civil and Environmental Engineering
in the Graduate School of Duke University
2014

Abstract

Membrane technologies represent an energy efficient, effective solution for treating municipal and commercial waters/wastewaters. Membranes are predominantly polymer-based and despite steady advances in polymeric materials, they continue to suffer from operational problems including biofouling and breakages. This work addresses these two disparate problems by developing novel CNT-polymer nanocomposite materials that contain variously functionalized carbon nanotubes (fCNTs) in low quantities ($< 0.5\,wt\%$). Several strategies have been employed to achieve highly functional CNT-polymer nanocomposite membranes including blend mixing, ionic charge association, and covalent cross-linking with monomer and oligomer constituents. These CNT-polymer nanocomposite membranes were compared to traditional polymer membranes across various properties including increased Young's Modulus, changes in surface hydrophilicity, fine control over molecular weight cut-off and flux, and surface electrical conductivity. Membranes with high surface electrical conductivity were further tested for their anti-biofouling properties. Finally, CNT stability and polymer compatibility were evaluated throughout membrane manufacture, use, and cleaning. The incorporation of CNTs mixed in bulk phase and linked through ionic associations in polymer matrices showed significant (50%) increases in Young's modulus for certain CNT functionalizations and derivatization percent. Membranes formed with high surface electrical conductivity demonstrated almost complete resistance to biofouling ($> 95\%$) in long-term bacterially challenged ex-

periments. CNTs and polymer mixtures that lacked covalent or ionic bonds were susceptible to significant (up to 10%) loss of CNTs during membrane non-solvent gelation and aggressive chemical cleaning treatment. Functionalized carbon nanotubes endow polymer membranes with their unique strength and electrically conductive properties. These added properties were demonstrated to greatly improve membrane operational efficiency and membrane longevity. CNT-polymer nanocomposite membranes offer low-energy, high-efficiency, and long-lifetime alternatives to traditional polymer membranes. With further advances in polymeric nanomaterials, membrane technology has the potential for wide applicability across many fields outside of water filtration and desalination.

My PhD Dissertation is dedicated to my mother, Prof. Krystyna Sieciechowicz. She was my intellectual inspiration, my rational stronghold, my co-investigator in life, my most avid cheerleader, my strength, and my calm. Above all she was my loving mother, and she lives through this dissertation.

Contents

List of Tables

List of Figures

List of Abbreviations and Symbols

Symbols

δ_x	Hildebrand solubility parameter of component x

Abbreviations

EPS	Extra polymeric substances produced by bacteria
MF	Microfiltration
UF	Ultrafiltration
NF	Nanofiltration
RO	Reverse Osmosis
PSf	Polysulfone
PES	Polyethersulfone
SPSf	Sulfonated Polysulfone
PVA	Poly(vinyl alcohol)
PA	Polyamide
MWCO	Molecular Weight Cutoff
MWCNT	Multiwalled Carbon Nanotubes
CNT	Carbon Nanotube
CNT-COOH	Carboxylated Carbon Nanotube
CNT-NH2	Amine Functionalized Carbon Nanotube
CNT-OH	Hydroxylated Carbon Nanotubes

ECPNC	Electrically Conductive Polymer Nanocomposite
kDa	kilo Daltons
MDa	Mega Daltons
TEM	Transmission Electron Microscopy
SEM	Scanning Electron Microscopy
FTIR	Fourier Transfrom Infrared Spectroscopy
XPS	X-ray Photoelectron Spectroscopy
XRD	X-ray Diffraction
CA	Contact Angle

Acknowledgements

The stars have not dealt me the worst they could do;
My pleasures are plenty, my troubles are two.
But oh, my two troubles they reave me of rest,
The brains in my head and the heart in my breast.

A. E. Housman

This is a five-year-long story of support and direction, of trust in my intellectual curiosity and independence, a test of my perseverance, of much needed distraction and welcome chaos, of scientific discovery and personal growth. It is a selfish story devoted to a single protagonist, but a story filled with many actors and supporting characters without whom this story might not have been nearly so successful and most certainly not so entertaining. This story is therefore entirely devoted to many segments of my life over the past five years: the science and engineering that filled my curious mind with insight, frustration, bewilderment, and purpose; the professors and mentors and post-docs and graduate students and undergraduates and high school students that fueled scientific discussions, triggered discoveries, and encouraged my determination to persevere despite innumerable failures and personal travails; the close family and friends that supported me in each their unique way along this tortuous path; and the music that never ceased to play in my head or in my voice — a continuous silk thread weaving its way through the fabric of my education. For helping me to write this great story, I tip my hat and don my ascot to each influence

that has supported me over the past five years.

I came to Duke University for the vague notion that I wanted to apply my physics and materials science knowledge to environmental issues, and the *specific* knowledge that I craved more education in materials engineering and environmental sciences. These pursuits were stymied initially by an unfortunate misalignment of goals in my first department. Uncertain of my fate at Duke, I started exploring my options. An impromptu discussion with Prof. Mark Wiesner that spanned such diverse topics as statistical mechanics, nanoparticles, environmental stewardship, quantum phenomena, french language and culture, the inspiration of music, and the importance of a varied educational and cultural background, opened a new and exciting path to me. After this discussion, on December 8th 2008, I knew that my advisor and mentor and intellectual guide would be Prof. Mark R. Wiesner.

In January 2009, I joined his group - sometimes endearingly referred to as the island of misfit toys - an haphazard group of acutely intelligent and multi-talented physicists, chemists, biologists, and economists, all striving to be successful environmental engineers in their own unique ways, and modeled on the brilliant yet unconventional career of Prof. Wiesner. His support of my scientific and engineering endeavors has been invaluable throughout my tenure as a PhD student and candidate. Mark's approach has always been to encourage my scientific exploration by giving me the freedom to pursue my own ideas, within the broad structure of his own creative vision. This type of open, collaborative, unbounded research environment is both inspiring and challenging to work in. That level of trust inspires commitment and spurs creativity, but it also requires an enormous amount self-discipline and personal focus that at times was challenging to achieve. As described in detail below, much-needed distractions from weeks spent in the lab often spilled over the brim, but I always returned to the scientific and engineering pursuit to which these past five years have been dedicated. Throughout this messy process, Mark has been

there to support me intellectually and financially. Like a choir conductor with musicians he has inspired with trust, he lets the music flow from his choir with only the most delicate guidance from his baton. The result is at times cacophonous, at times tremendous, but always artistic. I will be forever grateful for Mark's initial belief in me as a curious scientist, for his support in me to become an engineer and a researcher, his encouragement throughout my tumultuous doctoral journey, and his continued support in my future endeavors. Thank you Mark, for all that you have done.

The first person I met in Mark Wiesner's lab was David Jassby. The fast talking, energetic, hard-truth-spouting doctoral student that I met in that lab would eventually become one of my closest associates and collaborators, and a motivating force throughout my doctoral journey. He and I developed the idea to create electrically conducting membrane surfaces to combat biofouling. Together we fought through thick and thin to make that idea a reality. At times we butted heads, at times we disputed the division of labour, but throughout this chaotic discovery and invention process, we never lost respect for each other. In retrospect, it was in part his determination and drive that pushed me to succeed and publish my first first-authored-paper. I am forever thankful for his single-minded focus through the worst year of my life - the year that my mother died compounded by two other personal calamities. My response to grief and the passing of a parent, as in the past, has been to drown myself in work, but without David's manic energy, like a jet engine, firing me up to, for example, work the long hours in the lab running biofouling experiments, to focus on the materials development tasks ahead, to submit provisional patents to the office of licences and ventures, or to make a push in the Duke Start-Up Challenge, I would not have achieved the success that I can claim today. Thank you, David, for all of your support, for the discussions, for being a sounding board for crazy ideas, and for being a friend.

I thank the other members of my dissertation committee, Prof. Helen Hsu-Kim, Prof. Marc Deshusses, and Prof. Jie Liu, for their intellectual support, for educating me throughout my PhD, for all the continual constructive criticism, and for the perpetually helpful research suggestions. Prof. Claudia Gunsch has been invaluable in providing emotional support and encouragement in my pursuits of faculty positions. Her helpful and cheerful advice is always appreciated. Prof. Lee Ferguson's guidance, specifically in writing a grant with him, was instrumental in helping me develop my own ideas for my future research.

My experience in Istanbul at MEM-TEK at the Istanbul Technical University was made possible in part by the generous support of my host Prof. Ismail Koyuncu. His dedication to the engineering and scale-up of membrane technology, evidenced by the impressive facilities housed at MEM-TEK, has had a strong influence on my research motivations. Prof. Volodymyr Tarabara's innumerable reference letters and cheerful encounters at conferences kept me smiling. Prof. Hans Vrouwenvelder's praise for my work, his continued support throughout my research, and his insights on biofouling are greatly appreciated. Prof. Saifur Rahaman has also been a strong supporter and has been a valuable sounding board for my ideas as well as a constant source of encouragement for my future endeavors.

One of the highlights of working in the lab was my interactions with my colleague, collaborator, and friend Shi-Hong Lin. Never a dull day in the lab with him around, together we managed to juggle productive research with fascinating discussions that spanned religion, politics, theory of mind, quantum mechanics, the shortcomings of DLVO theory, the hydrophobic interaction, advanced membrane applications, and our respective futures. Days spent chatting with Shi-Hong were among my most cherished. Discussions were fruitful and entertaining with Jeff Farner Budarz, as well. I thank him for his patience with my cockamamie ideas and for leading us down research rabbit holes. Always there with a horrible pun, a 90s allusion, and

a soccer match in the background, Jeff was a great labmate. I thank Yingwen Chen for supplying me with the highest quality carbon nanomaterials. I was always impressed with his calm, collected attitude and how he made time available to help at the drop of a hat. Thomas Morse and Christina Arnout were both very helpful with all my amateur biological work. I thank both of them for their support in my bacterial genocide. Judy Wing-Lee and Alexis Wells Carpenter stimulated membrane discussions, forced me to question what I knew and what I took for granted, and helped develop brilliant research projects that I will continue to pursue with them.

Apart from the lab, Mathieu Therezien was a great help in my coding endeavors. Together with Jeff, the three of us pushed each other to excel in our qualifying and preliminary exams. Manuel Diaz was instrumental in getting me to write the entire dissertation in LaTeX. Elif Soyer sparked my initial interest in membrane science and taught me the most crucial fundamentals. Raju Badireddy, Benjamin Espinasse, Zachary Hendren, and Stella Marinakos all helped shape my understanding of membrane development, membrane testing, membrane treatment, nanoparticle formation, and the complex dynamics of polymer-nanoparticle interactions. Christine Hendren helped me see the bigger picture through her broad grasp of our work. Andreas Gondikas was instrumental in his expertise in instrumentation. I thank Turker Turken for spending an intense twelve days in a Turkish lab learning alongside me in the trenches of membrane scale-up. I must apologize to his wife, however, because I kept the newly weds apart for twelve days for the sake of our research, leaving her husbandless every day for twelve days from dawn until well passed midnight. I thank my wonderful Turkish hosts Esra Erdim, Rehyan Sengur, Serkan Guclu, and Recep Kaya, all of whom made my stay in Istanbul an amazing experience to remember. I thank Lauren Barton, Yao Xiao, Rob Ferris, and of course Marc Daniel Ryser. Marc's ability to form collaborations across a wide berth of research fields, and his ability to blatantly say no when needed, will serve me well in my future

research endeavors. Finally, I must thank my hard-working summer students in particular Katie Gloe, Sydney Stewart, Demi Davis, and Caroline Sorenson. I am much obliged to their hard work and patience with my sometimes chaotic research style. I am excited to see where your careers will lead you.

The SMIF at Duke University has been the single most important instrumentation facility for my doctoral research. My gratitude goes out to Mark Walters and I appreciate his patience, especially when I dropped my samples in the primary vacuum chamber of the XPS. My appreciation goes to Michelle Gignac and her expertise in microscopy. I thank Rebecca Dupre for making my transition from the department of Mechanical Engineering and Materials Science to the Department of Civil and Environmental Engineering as smooth and as problem-free as possible. Eileen Kramer has been a godsend in innumerable number of ways. She has also had unflinching faith in the success of my future exploits. Thanks to Dwina for chatting away the empty minutes spent on hold with customer service, to Glenda Kelly for exposing me to NanoDays and to all my fantastic summer students, to Patrick McGuire for letting me permanently borrow the wave generators and voltage sources, and to Eudys Estecumbre for all my computer troubles. While we never ended up going boxing together, the offer still stands, and maybe someday I'll meet him wrapped and gloved.

I thank all of my funding sources including the Duke Graduate School and the Duke Graduate School Conference Travel Awards, the Society of Duke Fellows (SDF), The Pratt School of Engineering, the Pratt-Gardner Fellowship, the EPA and the EPA funded Center for the Environmental Implications of NanoTechnology (CEINT), the internal CEINT Award, and the Certificate of Nanoscience Fellowship, all of which helped me to pursue my research and give talks at conferences around the world in Aachen, Buenos Aires, Istanbul, New Hampshire, New Orleans, Raleigh, San Antonio, Santa Barbara, and Toronto.

The single most important influence throughout my PhD was my loving mother, Prof. Krystyna Sieciechowicz, to whom this dissertation is dedicated. Although we didn't fully comprehend each other's work — she was a Cultural Anthropologist — we discussed our respective research and explained what intrigued us, where we saw hope for creativity and where it might fall short. Even during the year-and-a-half when she struggled to recover from intense bouts of chemotherapy, she was still curious about my progress and my ideas. Forever the proud mother, Mu'my was my most ardent supporter. After she died, in the middle of my fourth year, much of my determination to forge ahead in my PhD as adamantly as I did was for her; to live up to the faith she had in me and to let her memory live through my thoughts and ideas. In a similar way, the memory of my father, the modern-day Renaissance man, Prof. Jean-Louis de Lannoy, inspired my creativity and my desire for continued learning. My Babcia, Alicia Sieciechowicz, was equally inspirational. One of the earliest female computer programmers, an insatiable physics nerd, tech-geek, and life-long learner at 91 years old and still going strong, her curiosity about the world and beyond continues to inspire both my scientific career and my general quest for knowledge. I also thank the bed-rock of my support, my loving sisters, Maryna de Lannoy, Louise de Lannoy, Florence de Lannoy, Ines de Lannoy, and Val McDow ... burn, yo ... and my cousin Maya Sieciechowicz. Their level headedness, calm support, and loving distraction helped me recharge when I felt spent, and their consistent pride in me gave new purpose to my goals. Tommy and Ania Sieciechowicz, Konrad and Jill Sechley, and Pedro and Anne Leon were always there for me if and when I needed them. I especially thank Konrad for helping ease the tumultuous aftermath of my mother's passing, without whose understanding and stolid loyalty, this last year may have gone completely awry.

And who could possible do all this without friends — my local and international support group that did everything from discussing science and research ideas of my

own, to arguing and debating politics, social structure, history, literature, music, physics, monkeys, and more, to introducing me to all sorts of new music and old, to singing, to dining on fine foods, to drinking the endless nights away, to playing chess and complicated board games, to traveling and partying and booty shaking and party bus-ing and all sorts of hilarious debauchery, to inspiring my poetry, to pondering art, to planting my garden, to cooking up a storm, to boxing, to soccering, to running and pumping iron, to loving life, to distracting me from the lab and my computer, and to acting as the stimulating scaffold upon which my love of life is most firmly grounded. For these and all the other memories and shmemories, my dear neurotic, eccentric, and brilliant friends, I thank you all.

In particular I thank Marc D. Ryser, a cigarette pinched between two skinny jean fingers, redefining cool, but warm beyond reckoning, instilling in me that lust for success, lamenting academic fate, constantly introspecting, reminding me to strive for the important questions, and always seeking the ultimate truth. David Barrack, the brilliant monkey philosopher, an insatiable tornado devouring knowledge and propagating debauchery, inspiring a life of curiosity devoted to learning and rationality, a most loyal comrade, a common, happy sight on my morning couch, and a perpetual intellectual fount. Erica Dunkle, my cherished striped-sock friend, the huggiest fabric rainbow, the keeper of keepsakes with an enormous heart that emotionally helped me beyond measure. Sara Budarz, Shorty, the germanic intellectual, constantly seeking true happiness, engaging discussion on impossible subjects, and reminding me to pursue even the loftiest answers. Zach Russell, gamer-extraordinaire cum particle engineer, encouraging my entrepreneurial spirit, keeping me honest, and cracking the door to the industrial possibilities of my work. Steven Sherman, (the flux capacitor is now complete and the hover board is on the way), always supportive, who's New York apartment served as a skyward haven from the flat smallness of North Carolina, who welcomed me into his family when the chips were down. Miles Crosskey and

our epic chess battles, discussions of mathematical manifolds and protein folding, letting me peer into the realm of computational mathematics, all while debating Net Runner strategies. Steven Levin, the political weathervane, ardent supporter of my environmental conscience and fast-talking, jive-walking shenanigan creator. Liz Turner, a loving and thoughtful, motherly support that inspired me to pursue classroom flip methodologies. Allen Riddell, the brilliant computational literary analyst and fervent Canadiophile, who reminded me why my home country is so great. And happily, Abbie Langston, the ever-loyal, mischievous devil on my shoulder, opening my mind to literary philosophy and the appreciation of Tequila, and being the rock to which I know I can always turn.

Thanks to the Euro crew; together we discovered Durham and our place in it. Thank you especially Clement Ramos for kicking the walls, making them green, and keeping my eye on what really matters — the environment; Zvia Shwirtz for bioshockingly late nights and travelling with my face on a stick; Tamara Extian-Babiuk (honorary Euro) for cheek-pinchingly good harumphs and curmudgeonly jolly good times, old chap; Julian Henneberg for being the model suave intellectual; and Valeria De Luca for chocolate and wine and serving as a model for one of the sharpest and most practical engineers I know. The French Connection, who kept my french up to snuff and allowed me to be pedantically grammatical, especially the boxing crew, Fantine Mordelet and her promiscuously creative use of the English language, and Benjamin Espinasse for his invaluable support in darker times.

The residents of Manhattan and Brooklyn and of course Jimmy, Jimmy, Jimmy. Manhattan's king-pin, Manuel Diaz and his Dominican expressions, and the hipsters in the Brooklyn office, Jeff Farner Budarz and his bikes, Judy Wing-Lee and her question-time, and Amalia Marenberg and her colorful lead purses.

Jillian Powers, who saw me at the start of my research and helped me grow emotionally, intellectually, and creatively, who remained incredibly thoughtful at the

worst of times despite our falling out, and who will always have a special place in my heart. Paige Conn, who helped me through a transition, inspired me to share my poetry, and introduced me to one of the most beautifully written books I have ever read. Agnes Meleske, with whom I shared opera in the area and who's warm wine was always welcome.

Thank you to the home team that remembered where I came from. Bunny, aka Bobby-K, aka BBK, aka BB-King, aka Bobby-Backy, aka Bobak Shahriari, for being such a piss-taking, hilarious brat that called at all the wrong times, and who, despite his best efforts, filled me with pride for working on environmentally pertinent matters and Olga Trichtchenko for reminding me that we used to be physicists. And to all the other brilliant people I've met along the way that invited me to stimulating cocktail parties (Prof. Jonathan Mattingly), or titillating garden parties (Prof. Randall Love), or inspired poetry as the Duke poet in residence (Christophe Fricke), that DJ-ed the craziest raves (Daniel Real and Yoichi Horikoshi), and smiled the smiliest smiles (Mike Stanton) and all the rest that fueled my craving for life's passion, including such brilliant people as Cristian Ciraci, Meg Shea, Jean-Hubert and Anlo Olivier, Marc and Justine Sperber, Myriah Cornwell, Henri Roesch, Pierre Arroucau, Jesse Shaw, and Reginald Patterson.

For all the dance parties at the Pinhook, for all the drinks at the Fed, for all the 3 am Cosmic Cantina and taco truck runs, for all the Apex rave parties, the fantastic breakfasts, the feet that hurt in the morning, the dance shows, the expertly cooked meals and superb dinners, the thunderstorms on porches, the scientific discussions, the music in the gardens, and to all my friends for putting up with me when I was late, which was all the time, thank you.

Finally, music encouraged me when I was on fire with my ideas, music sustained me when I was pulling long hours in the lab, supported me when I was depressed, inspired me when I was intellectually distracted, comforted me when I needed to

cry and made my feet move when I needed to dance. I thank all the singers of Vespers and SONAM, specifically my friends Erica Dunkle and her melodious alto, Roman Testroet and sissy bounce, Stephen Pysnik my fellow bass, Mike Lyle and his boisterous laugh, and Chris Shreve for ticking me up a notch, and of course my wonderful conductor Allan Friedman. Singing had been my life in younger years, and in these past five, I rediscovered the joy and the beauty of making music with such highly talented musicians. Thank you for making such awe-inspiring music and for introducing and re-introducing me to the greats, specifically Palestrina, Tallis, Victoria, Purcell, Tchaikovsky, and Barnum.

Without so many wonderful people and such beautiful music to accompany them, these past five years are almost unimaginable. Thank you one and all.

1

Exordium

1.1 Introduction

1.1.1 Problem Statement

Water contamination causes severe environmental, global health, economic, geopolitical, and socio-environmental stresses. Decontaminating natural water sources and increasing access to clean, potable water can mitigate many of these ubiquitous global problems. This can be accomplished in two ways: either by treating current environmentally stressed and/or polluted waters (water and waste-water treatment) or by creating new fresh water (desalination). In either case, membrane technologies have proven to be an efficient and effective method to provide clean, usable water. Polymeric membranes are ubiquitously used for this purpose, however current membrane technologies are hamstrung by several limitations: susceptibility to biofouling, inconsistent selectivity, and low resistance to shear stresses. Membranes are plagued by biofilms that readily grow on their surfaces. Biofouled membranes suffer from reduced membrane flux, separation, and selectivity, which rapidly reduces the membrane's effectiveness and thus lifetime. The pores of polymer membranes form through thermodynamically driven processes, giving rise to pores of variable size.

Heterogeneity in pore size across a membrane surface hinders particle selectivity and reduces the effectiveness of membrane operation. During operation, membranes, in particular hollow fibers, are challenged by high pressures and vibrations, which cause shear stresses. Membranes composed of traditional polymers can break under these applied tensile forces.

Given these membrane limitations, we sought improvements to polymer materials through the addition of nanoparticles to form polymer nanocomposites. Specifically we studied the potential of multi-walled carbon nanotubes (CNTs) to improve the properties of polymers such that they could help prevent biofouling, improve particle selectivity, and resist breaking during membrane operation. Given a variety of chemical functionalizations and polymer-carbon nanotube interactions, we explored optimal polymer-CNT compatibilities to address these pressing issues for improved membrane materials. Throughout this research, we were cognizant of the environmental, public health, and economic concerns surrounding nanoparticles. The sustainable and responsible use of carbon nanotubes in material composites was a motivating factor in this research. To this end, we investigated the loss and leaching of CNTs from polymer nanocomposites in order to understand the compatibility and optimal chemical interactions of polymers with carbon nanotubes.

1.2 Hypothesis and Objectives

1.2.1 Hypotheses

Carbon nanotube (CNT)-polymer composites can serve as a platform for adding unique functionality to membranes. This includes creating membranes of varying permeability, rejection, tensile resistance, and electrical conductivity by altering CNT functionalization and content. Both the physical addition of CNTs and the chemical reaction of CNTs with the membrane polymers provide a means of controlling membrane properties. In this dissertation, six key hypotheses have been tested. These hypotheses concern the interaction of carbon nanotubes with polymers to form nanocomposite membranes, the properties and applications of these membranes, and the implications associated with the production and use of nanocomposite membranes. The hypotheses follow:

Preamble There is great potential in using electrically conductive permeable surfaces for environmental applications. Electrically conductive membranes, in particular, might be used as a platform to reactively degrade environmental contaminants, prevent bacterial attachment and long-term biofouling, and/or limit scaling. Highly electrically conductive thin films may be formed into membranes, and these nanocomposite electrically conductive thin film membranes can be formed with various membrane characteristics.

Hypothesis 1 Cross-linking linear polymers with functionalized CNTs produces physically stable, flux controllable, highly electrically conductive nanocomposites, that can be formed into ultrafiltration thin film nanocomposite membranes.

Cross-linking a hydrophilic linear polymer, such as poly(vinyl alcohol) (PVA), with functionalized CNTs may produce a highly electrically conductive network polymer whose interconnections are composed of CNTs. It is hypothesized that with

the addition of a catalyst, carboxylic functional groups on the CNT sidewalls react with the hydroxyl groups on the PVA backbone, in a hydrolysis reaction, to form a cross-linked interconnected CNT-PVA network. Much like a pure PVA cross-linked network, this electrically conductive nanocomposite network polymer may demonstrate separation properties as well as promising pure water flux characteristics, and may serve as an electrically conductive thin-film for a composite membrane. This system may provide a high degree of control over the density of cross-linking between the PVA chains, and thus a high level of control over the flux and separation characteristics of the resultant nanocomposite thin film membrane. It is hypothesized that the parameters affecting the cross-linking density of the PVA chains include CNT concentration, the degree of functionalization of the CNTs, and the addition of cross-linking entities such as dicarboxylic acids, specifically succinic acid. Further, it is hypothesized that the long, rigid, functionalized and cross-linked CNTs disrupt the PVA semi-crystalline structure. Reductions in PVA crystallinity may increase the permeability and reduce the rejection characteristics of the thin film.

Hypothesis 2 Interfacially polymerizing monomers about functionalized CNTs produces physically stable, highly electrically conductive nanocomposites, which can be formed into tight nanofiltration thin film nanocomposite membranes.

Using small quantities of CNTs reacted with a traditional reverse osmosis membrane polymer, such as polyamide (PA), may produce a membrane surface with high electrical conductivity, while minimally affecting the polymerized network, thus maintaining the flux and salt rejection properties required for reverse osmosis (RO) or tight nanofiltration (NF) membranes. Interfacial polymerization between an aqueous suspension, composed of hydroxylated CNTs and m-phenylenediamine (MPD), and a hexane solution of trimesoyl chloride (TMC) – the monomer constituents of PA – is hypothesized to form an interconnected nanocomposite network. It is hy-

pothesized that the hydroxyl groups of the CNTs and the amine groups of the MPD monomer will covalently bond to the chloride group of the TMC monomer across the water-hexane interface. The covalent bonds formed between the functionalized CNTs and the TMC may form a physically and chemically stable nanocomposite. This bonding may immobilize CNTs and prevent their leaching during normal RO or NF membrane operating conditions. Further, minimizing the polymer concentration and thereby maximizing the CNT surface exposure, may endow the salt-rejecting thin film composite membrane with high electrical conductivity.

Preamble Biofouling is one of the most common and detrimental problems faced by membranes. Membrane surface biofouling obstructs flux and disrupts particle and ion separation. The scientific literature is replete with various strategies, of varying degrees of success, for overcoming surface biofouling. Membranes are identified as high-risk surfaces subjected to ideal biofouling conditions. One strategy involving the application of an alternating electric potential to a conductive surface has shown strong promise in certain niche applications. Reduced bacterial deposition on an electrically conductive membrane may be expected based on a number of underlying physical-chemical phenomena including the generation of reactive oxygen species, direct oxidation/reduction of biological cellular material and exocellular products, and changes in the electrical double layer that may affect bacterial deposition and proliferation.

Hypothesis 3 Applying an alternating electric potential to the surface of an electrically conductive membrane prevents bacterial attachment and biofilm development on that surface.

Pressurized membrane separation of dense aqueous solutions of bacterial communities will lead to rapid flux decline and irreversible fouling caused by biofilm

development. It is hypothesized that the application of an external electric potential to the surface of an electrically conductive membrane will reduce the rate of flux decline and severely impeded or entirely prevent the development of biofilms. Applying a continuous alternating square wave to an electrically conductive membrane may enhance the anti-biofouling effect of the electrical potential. The application of a $\pm 1.5\,V$ square wave over-potential to the surface of an electrically conductive PA-CNT membrane is hypothesized to prevent surface biofouling during desalination of bacteria-rich saline waters. In particular, the application of this potential to those membranes is hypothesized to prevent the attachment, development, and proliferation of biofilms by the aggressively reproducing bacteria, *Pseudomonas Aeruginosa*. In this way, the rate of flux decline through the membrane due to bio attachment may decrease significantly, extending the amount of time before flushing or cleaning of the membrane is necessary. Moreover, the surface of the membranes may be cleaned, and the transmembrane flux entirely recovered during the desalination of these waters simply by increasing the speed of the feed solution and changing the direction of its flow (cross-flow flushing). This may demonstrate chemical-free membrane cleaning. It is hypothesized that the application of an external alternating square wave potential to the surface of the membrane will in no way affect the salt-rejecting properties of the membrane. Further, it is hypothesized that cross-flow flushing will not affect the efficacy of future filtration and desalination of the feed waters by the membrane, and that separation of these bacterially rich aqueous communities and transmembrane flux will be maintained regardless of applied potential and cross-flow flushing.

Preamble An important premise for the development of CNT-polymer nanocomposites, and the applications in membrane separations these nanocomposites inspire, is that they should be conceived to be sustainable and environmentally responsible as

viewed from the life-cycle perspective of technology production, use, and end of life. Unknown impacts of CNTs on human health and ecosystems suggest that it is desirable to minimize possible release of CNTs to the environment during the production, use, and end of life of CNT nanocomposite membranes. Ideally, CNTs found in composites would be stable and secure throughout the product lifetime and either have an absence of effects or demonstrate minimal or innocuous effects on both humans and the environment.

Hypothesis 4 CNTs unbound to the bulk polymer chains are unstable in polymer-CNT nanocomposites and leach from them.

Chemically unbound CNTs may leach from their polymer surroundings during all stages of a nanocomposite life cycle. Carbon nanotube-polymer nanocomposite membranes may be particularly susceptible to loss and leaching of CNTs during their product lifetime, because of the thermodynamic rearrangements the polymer chains undergo during membrane formation and the extreme conditions to which membranes are subjected during their use. Loss and leaching of CNTs may occur at three main stages throughout their lifetime: during membrane production by immersion precipitation of the polymer nanocomposite solutions, during membrane operation while these materials are subjected to high pressures, and during membrane cleaning with caustic chemicals. It is hypothesized that loss and leaching of both pristine and functionalized CNTs occurs from the polymer nanocomposite solutions during all three of these stages in a membrane's life cycle. Loss of CNTs may occur to varying degrees and may be greatest during immersion precipitation, but still significant and detectable during pressurized filtration and surface cleaning. It is hypothesized that functionalizing CNTs with hydrophilic moieties, such as carboxylic and hydroxyl groups, may increases their instability within the polymer matrices of membranes. Moreover, it is suggested that greater degrees of carboxylation cause

greater instabilities, which are realized as an increase in the loss and leaching of CNTs during the nanocomposite lifetime.

Preamble The concern over the loss and leaching of CNTs from polymer membrane matrices is primarily important because of the potential human health and environmental risks associated with nanomaterials. There are also concerns, however, regarding the practical material and commercial nature of these nanocomposites. CNTs are added to polymer materials for a variety of reasons, and in membranes discussed in this section, they are primarily added to increase the membrane's Young's Modulus and tensile strength. The efficient manufacture, effective use, and maximal property realization of nanocomposites are potentially jeopardized by nanoparticle instability. These considerations may further help motivate safe and responsible use of nano-additives in composites.

Hypothesis 5 Minimizing CNT instability within polymer-CNT nanocomposite membranes optimizes the mechanical, morphological, and chemical properties of these membranes.

Loss and leaching of CNTs from polymer systems reduces the total content of CNTs within polymer nanocomposites. It is hypothesized that this loss of CNTs may cause deviations from the expected nanocomposite material properties. Materials expected to perform in a given manner with a certain percentage of CNTs may not be observed to fulfill those expectations when unexpected loss and leaching of CNTs occurs. Specifically, expected increases in membrane tensile strength for a given amount of included CNTs may not be observed when loss or leaching of those CNTs from the polymer system occurs. Further, it is suspected that the dynamic losses of CNTs from the polymer matrices may disrupt internal morphologies, which in turn may affect membrane properties. CNT instability may cause inhomoge-

neous partitioning of CNTs within a nanocomposite, resulting in variable properties across the material. It is hypothesized that CNTs with greater functionalization, and therefore a greater propensity for leaching from membranes, will show greater deviations from expected material trends than CNTs functionalized to a lesser degree. In particular, membrane Young's Modulus and maximum tensile stress will increase more from the inclusion of CNTs functionalized to a lesser degree than from the inclusion of the same initial concentration of CNTs functionalized to a greater degree. It is hypothesized that uneven partitioning within polymer matrices and loss of CNTs during membrane formation increases membrane permeability and reduces the separation precision of solutes across the membrane. Further, inhomogeneous partitioning due to thermodynamic driving factors, may lead to the possibility of reduced reproducibility across membranes made in the same manner.

Hypothesis 6 Ionically or covalently binding CNTs to the polymer chains that comprise the composite eliminates or greatly limits the loss and leaching of CNTs from the polymer matrices.

Loss and leaching of CNTs from polymer systems hinders optimally realizing the advanced functionality or improved properties of those nanomaterials. This is of particular concern in polymer nanocomposite membranes. Further, loss and leaching of CNTs may contaminate the environments these membrane technologies are meant to remediate. It is hypothesized that ionic and covalent bonding of CNTs to polymer chains eliminates CNT loss and leaching, and prevents the release of CNTs into the environment during membrane production, use, and cleaning. The strong associations between the CNTs and the polymer chains may prevent losses of CNTs from the polymer matrix and in this way aid in achieving maximal property improvement. In particular, it is hypothesized that if CNTs are prevented from being lost from the nanocomposite membranes through ionic associations with the

polymer chains, then increased degree of functionalization of CNTs increases the membranes' Young's Modulus. However, CNTs bound to the polymer chains may inhibit polymer mobility, which may affect the kinetics of membrane gelation and in turn cause unexpected changes to membrane morphology and structure.

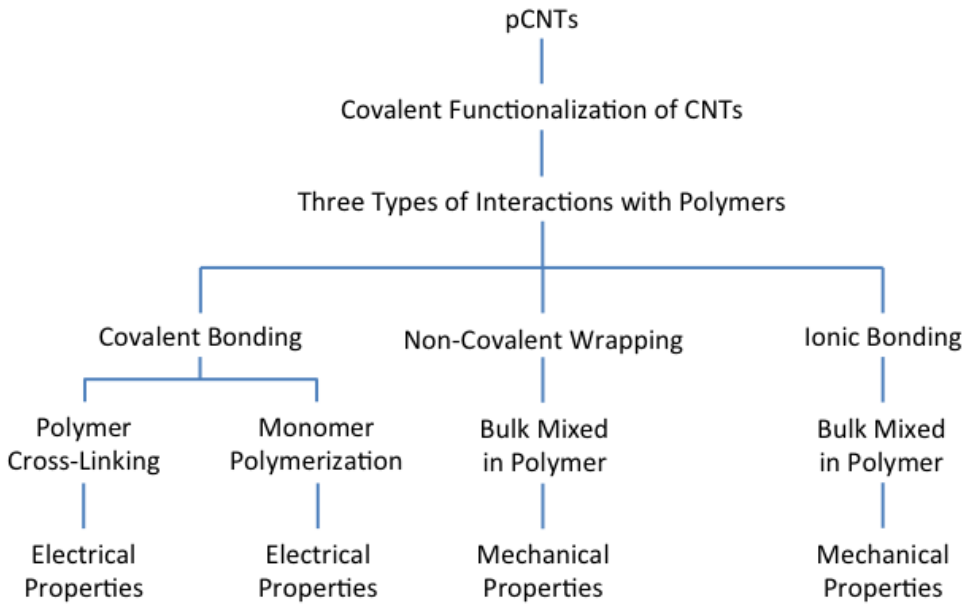

FIGURE 1.1: A flow-chart break-down of the research approach in this dissertation. Starting from pristine CNTs, these CNTs are then functionalized for interaction with polymers in various ways to achieve two distinct, specific properties.

1.2.2 Objectives

The objectives of this dissertation were to experimentally analyze, test, and prove or disprove the hypotheses outlined above. The three types of CNT-polymer interactions that were investigated - covalent bonding between polymers and CNTs, non-covalent wrapping of polymers about CNTs, and ionic bonding between poly-

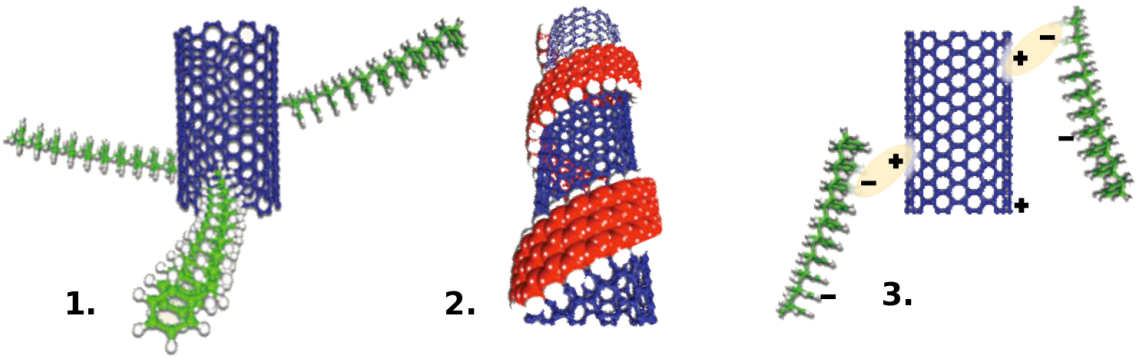

FIGURE 1.2: The three types of CNT-polymer interaction investigated in this dissertation are pictorially described above. 1. Covalent bonding between the functionalized sidewalls of the CNTs and the backbone of a polymer chian. This was established either through cross-linking or by interfacial polymerization. 2. Non-covalent associations between the polymer chain and the functionalized CNTs. Polymers were either adsorbed or wrapped around CNTs. 3. Ionic bonding between the charged functional groups on the CNT sidewalls and the the charged moities on the polymer chain.

mers and CNTs - are described pictorially in figure 1.2

An experimental materials science approach was used to test the hypothesis that linear polymers could be cross-linked with functionalized CNTs to form highly electrically conductive UF thin films with control over their permeability and rejection properties. Specifically, reactions were designed to cross-link long-chain PVA macromolecules with carboxylated CNTs (CNT-COOHs) and succinic acid catalyzed by dilute HCl to create nanocomposites of varying cross-linking density (Peng et al., 2010). Tasks were designed to form UF membranes of varying permeability, rejection, and electrical conductivity by altering CNT-COOH content with respect to the PVA concentration. The main objective of this work was to determine the optimal CNT content to achieve the maximal surface electrical conductivity (Koning et al., 2006), while still maintaining CNT stability within the composite. The goal in this case was to minimize the polymer content within the system while maintaining sufficient cross-linking to bind CNTs within a stable matrix in order to form a stable, highly

electrically conductive surface. Another main objective of this work was to develop polymer nanocomposite UF membranes with tunable surface parameters based on adjustments to carbon nanotube functionalization, content, and reactivity. The goal in this case was to test and investigate how CNT concentration, cross-linking degree, and CNT-to-polymer ratio affected thin film membrane permeability and rejection by comparing these variations across all membrane properties. A final objective was to determine the material and membrane properties of these electrically conductive UF membranes. Properties that were investigated include the membrane electrical conductivity, the surface hydrophilicity, the pure water transmembrane flux, and the membrane MWCO.

An experimental materials science approach was also taken to test the hypothesis that interfacial polymerization of monomer constituents about functionalized CNTs can form physically stable, highly electrically conducting, nanocomposite tight NF thin film membranes. Specifically, the objective of this research was to create highly electrically conductive, salt-rejecting thin films by polymerizing the monomer constituents of traditional RO polymer membranes (Lee et al., 2011) from the sidewalls of hydroxylated carbon nanotubes (CNT-OHs). CNT-OHs were employed to imbue the insulating polyamide (PA) thin films with high electrical conductivity. One of the main objectives of this work was to minimize the polymer content about CNTs and in this way maximize the CNT surface exposure in order to maximize the surface electrical conductivity. In contrast to the maximum electrical conductivity of these membranes, another objective of this work was to ensure that these thin film surfaces were mechanically and chemically stable, which required sufficient content and reaction of the monomer constituents with the functionalized CNTs. To this end, one of the goals of this work was to investigate the optimal CNT content, polymer concentration, and interfacial polymerization reaction time to achieve highly electrically conductive surfaces that were also mechanically and chemically stable

under NF operating conditions. A final objective was to determine the material and membrane properties of these electrically conductive NF membranes. Properties that were investigated include the membrane surface electrical conductivity, the surface hydrophilicity, the pure water transmembrane flux, and the membrane's salt rejection capability (Mulder, 1996).

Pursuant to the material development objectives, the next goal was to demonstrate the capabilities of electrically conductive thin film membrane surfaces to resist bacterial adhesion and biofilm growth. All biofouling experiments were performed in a configuration similar to a leaky capacitor. In this set-up, an alternating potential was applied to the electrically conductive membrane surface, a platinum, non-corrosive counter-electrode acted as the source or sink of the electric field lines, and salt water, nutrients, and bacteria acted as the dielectric material separating the charged plates. To demonstrate that an alternating electric potential prevents bacterial attachment and biofilm development when applied to the surface of an electrically conductive membrane (Hong et al., 2008), the main objective was to apply an alternating electric potential to the surface of these membranes, challenge the membranes with high concentrations of bacteria that were encouraged to grow in solution (Herzberg and Elimelech, 2007), and demonstrate against control experiments that biofouling was prevented on the surface of these electrically conductive membranes when an external electric potential was applied to them. To support the practical application of an externally applied electric potential to the surface of a conductive membrane, it was imperative to ensure that the salt rejecting properties of the electrically conductive membranes did not vary with the application of an external potential. Another objective of this work was to explore the rate of decline of trans-membrane flux as a function of time to demonstrate that flux decline was slower for membranes with an alternating electric potential applied than for control experiments. Following this, the next objective was to determine the extent

to which flux on the surface of a highly conducting membrane surface with an applied electric potential, could be recovered by cross-flow flushing. The final objective was to ensure that the cross-flow flushing maintained the membrane integrity and in so doing maintained the membrane rejection properties throughout the biofouling experiments.

To test the hypothesis that CNTs are unstable in polymer-CNT nanocomposites and leach from them, one main objective of this work was to determine the loss of CNTs from nanocomposite membranes during immersion precipitation of the nanocomposite solution, pressurized water filtration, and immersion in caustic chemical cleaning agents. This work therefore included tasks designed to evaluate CNT release during immersion precipitation, pressurized filtration, and caustic chemical cleaning (Zularisam et al., 2006). Experiments were conducted to test the hypothesis that chemically unbound CNTs are inherently unstable throughout the product lifetime, using both pristine CNTs and functionalized CNTs dispersed within the polymer matrices of membranes. After membrane gelation of polymer and polymer-nanocomposite membranes, non-solvent was collected to analyze CNT content. Solutions were also collected during pressurized membrane filtration and after membrane cleaning. An objective of this work was to determine the concentration of CNTs in the solutions associated with each phase of the membrane life-cycle. To achieve this goal, solutions were analyzed using UV-Vis and compared against various background and control spectra. A further objective was to understand what effect CNT-functionalization (Sun et al., 2002), or the lack thereof, had on their stability within polymer matrices. To pursue this goal, CNTs were functionalized to various degrees of carboxylation and tested for stability within the polymer membrane matrix under conditions of gelation, filtration, and chemical cleaning. The same UV-Vis analysis was used to determine the effect that the degree of functionalization had on the loss and leaching of CNTs from membrane matrices.

A traditional membrane analysis approach was used to test whether or not the instability of CNTs within polymer-CNT nanocomposites impacts the mechanical, morphological, and chemical properties of the nanocomposites. Experiments were conducted to investigate whether property changes and inhomogeneities of nanocomposite membranes occurred as a result of CNT loss during immersion precipitation of polymer nanocomposite solutions. Properties that were investigated included the membrane Young's Modulus and maximum tensile stress (Xie et al., 2005b), the surface hydrophilicity, and the pure water permeability. The goal of these experiments was to determine the optimal CNT carboxylation that achieves minimal loss and leaching with maximal benefit to the membrane material. To this end, a comparison of all the membrane properties was conducted across all the various CNT functionalization degrees. A further objective was to demonstrate that greater amounts of CNT loss from the membrane lead to reduced reproducibility of the membrane property results. This was achieved by demonstrating the increased variability in measured membrane properties correlated to membranes containing CNTs with greater functionalization degree.

To test the hypothesis that CNTs are stable in polymer matrices if they are bound through ionic or covalent bonds, functionalization and bonding conditions were sought that would reduce or eliminate loss and leaching of CNTs from polymer matrices. In particular, ionic associations between CNTs and polymer chains for enhanced stress-resistant membranes were pursued. One of the objectives of this work was to tailor CNT-functionalization for reaction with specific polymer functional groups and then to test for CNT stability within this polymer matrix. To this end, CNTs were functionalized with various positively and negatively charged functional groups, and polymers were sulfonated to add negatively charge moieties to their chains. The primary objective of this investigation was to determine whether loss and leaching of CNTs could be prevented through charge associations between

the polymer chains and the functionalized CNTs. Loss and leaching were analyzed as before using UV-Vis and releases of CNTs were analyzed from non-solvent solutions after immersion precipitation. A further objective of this work was to determine if increasing CNT functionalization degree improved membrane properties, such as increased membrane mechanical resistance, once CNT leaching from nanocomposite membranes was prevented. To this end, CNTs were functionalized to two different degrees of functionalization with positively charged functional groups, then included in the same concentrations in polymer membranes, and tested for variations in membrane properties.

2

Background

2.1 Preamble

Around the globe, shortages of safe and clean drinking water are commonplace and the effects are disastrous: 2.6 billion people live with little or no sanitation and of those, 1.2 billion people lack access to safe drinking water. This great dearth leads to millions of avoidable deaths annually, primarily from diseases transmitted through unsafe water or human excretion. Those fortunate enough to avoid this fate are nevertheless sickened from disease and contamination directly associated with contaminated water. While third world countries are the most heavily plighted, industrialized nations are confronting an ever-greater influx of contaminants entering the water supply from human activity including the traditionally worrisome heavy metal compounds and distillates to new micro- and nano-pollutants such as nitrosamines and a variety of nanoparticles. Water supplies once considered clean are now focal points of decontamination efforts (Shannon et al., 2008).

While the number of uncontaminated water sources is shrinking, the demand for clean, useable water is increasing. Growing global populations with first world

demands will strain water supplies for use in energy and food production, industrial output, and the environment: over 80% of all water for human consumption is used for agriculture, livestock and energy production. Of those sources currently tapped, many freshwater aquifers are being contaminated or overdrawn, oftentimes irreversibly, or are degraded by saltwater intrusions. To make matters worse, global climate change is foreseen to aggravate access to traditional water supplies as glaciers recede which may cause the flows of major arteries, such as the Ganges, Yellow, Brahmaputra, and Mekong rivers, to become irregular, to the detriment of 1.5 billion people during the dry months. Even developed countries in North America, Europe and South America could experience severe disruptions to agriculture, energy production, and drinking water supplies as a result of the fluctuations in snowmelts and loss of glaciers (Shannon et al., 2008). It is, therefore, imperative to find more effective, more efficient, and lower-cost methods to decontaminate waters from source to point-of-use without further aggravating the environment or imperiling human health. Fortunately, a recent surge in water treatment research provides hope that these disasters can be mitigated. Technology alone will not solve the world's water shortage, but it is a crucial step in understanding how to treat newly contaminated waters, and developing solutions to overcome those problems.

2.2 Conventional Water Processes

For millennia people have been finding ways to obtain clean, uncontaminated water either by collecting rain water or skimming surface waters from fast flowing rivers, digging wells to tap groundwater, or by treating waters in various ways such as boiling surface waters or fermenting additives in water to produce beer, mead, and other fermentation byproducts. Mass distribution of water to large population centers and farming communities was implemented as early as 3000 BCE by ancient civilizations such as the Harappan Indus Valley Civilizations, the Ancient Egyptians, and

the Mesopotamians. However, water and wastewater treatment and desalination for mass consumption by chemical or thermo-chemical means following a scientific understanding of some of the fundamental aquatic physico-chemical processes is a relatively recent development. Only in the past 120 years has mass treatment and distribution of waters for large population centers and agricultural operations been implemented (Juuti et al., 2007). Conventionally this was achieved through chemical and thermal methods, and more recently the current trend is away from these less sustainable (i.e. materially consumable and energetically unfavourable) methods towards more efficient processes involving membranes.

2.2.1 Conventional Water Treatment

Centralized water treatment revolutionized public health in developed nations. Centralized wastewater treatment also greatly improved public health and safety, while also drastically limiting environmental contamination and stress. Conventional water treatment is used to remove a wide range of constituents in groundwater and surface waters. These constituents include floating and suspended materials (branches, leaves, algal mats, soil particles), colloidal constituents (trace organic and inorganic constituents, clay, silt, pathogenic organisms, algae, other microorganisms), dissolved constituents (iron and manganese, hardness ions, organic compounds, tannic acids, inorganic salts, radionuclides), dissolved gases (carbon dioxide, hydrogen sulfide), and immiscible liquids (oils and grease) (Crittenden and Harza, 2005).

Conventional water treatment predominantly uses chemical means to destabilize particles for the removal of unwanted constituents from water (although physical and biological methods are also used in conjunction). This is in contrast to membrane technology, which predominantly uses a physical barrier to perform aqueous separations (although chemical and electrophysical barriers also play a role in some cases). Membrane technology has been shown to be more efficient and effective in traditional

treatments for both water and wastewater. Therefore, membranes have been used to supplement traditional treatment technologies, and in some cases completely replace the existing framework (Mulder, 1996).

Briefly, traditional water treatment follows a process train of sequential treatment as show in figure 2.1. In a traditional water treatment plant, the typical processes for raw water treatment follows this path: screening, coagulation, flocculation, sedimentation, granular media filtration, disinfection, stabilization, and distribution. Chemical and physical means of separations are combined throughout the process train. However, traditional water treatment hinges on the chemical destabilization of unwanted particles and colloids, i.e. coagulation, without which the physical separations would be ineffective. In conventional wastewater treatment, often the process is centered around biological processes. In both traditional water and wastewater treatment trains, membranes can be used to supplement, simplify, or supplant the traditional process (Crittenden and Harza, 2005).

Chemical treatments are used to remove and treat contaminants by the addition of various chemicals. Chemical processes include coagulation, chemical precipitation, chemical oxidation, chemical disinfection, and stabilization. Coagulation, the crux of traditional water treatment, destabilizes colloidal particles so that they aggregate to form large flocs during flocculation. Destabilization of suspended aqueous particles is brought about by the addition of chemicals such as ferric chloride, alum, and a variety of polymers. Chemical precipitation removes heavy metals and phosphorous through solid phase precipitation. Chemical oxidation processes, using chemically oxidizing compounds, are used to oxidize iron and manganese, humic compounds, pesticides, and chlorinated organic compounds. These oxidation processes can also be used to oxidize and degrade organic taste and odor causing agents. Following these oxidative processes, chemical disinfection is used to oxidize pathogenic organisms in water. This is done using chlorine, chlorinated compounds, or ozone (Crittenden and

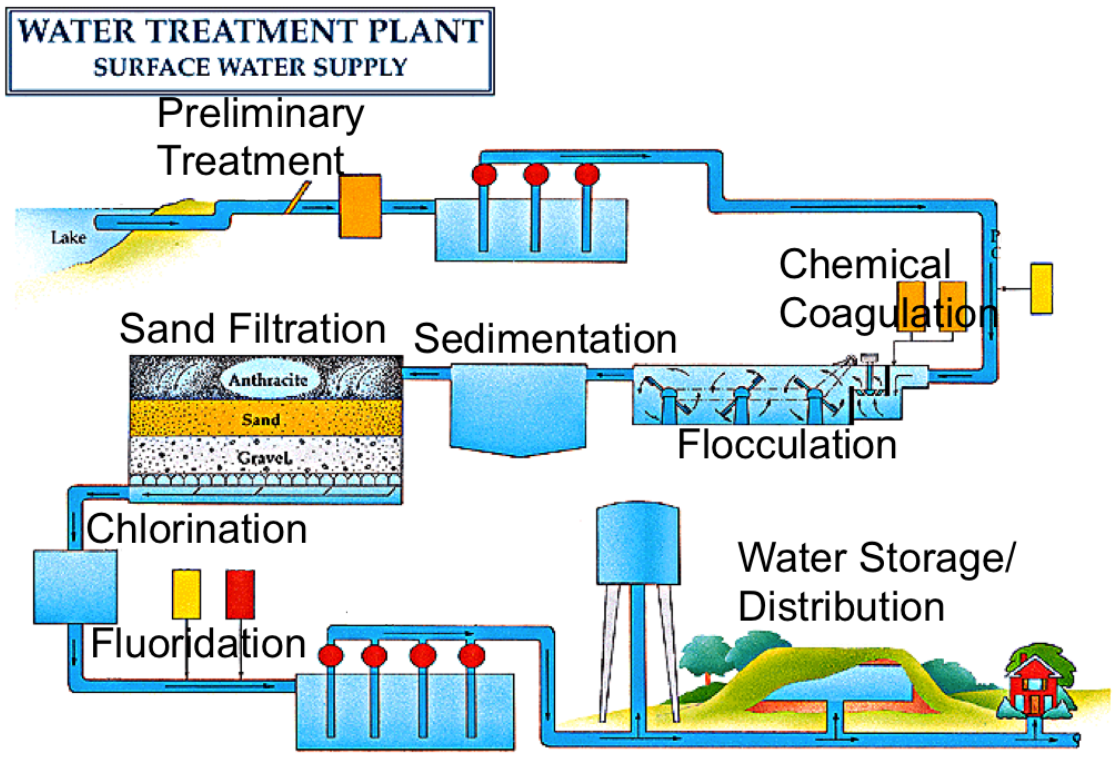

FIGURE 2.1: A typical process flow in a conventional water treatment system. The principle steps include chemical coagulation, flocculation, sedimentation, sand/granular separation, chlorination and fluoridation. The process hinges on the initial chemical destabilization of particles in solution by coagulation.

Harza, 2005). Membranes can be used to replace many if not all of these processes through physical separations.

Membrane filtration can span a variety of treatments from removal of turbidity, bacteria, and protozoa, (microfiltration (MF)) to the removal of humic acids, viruses, and organic compounds (ultrafiltration (UF)) down to the removal of salts and pesticides (reverse osmosis (RO)). MF and UF are used to replace traditional treatment processes of groundwater and surface waters, while RO is used to produce potable water from saline sources. The latter membrane process will be discussed in greater detail in the next section. Colloids and particles, bacteria and protozoa, organic compounds and humic acids, as well as viruses can all be separated by ultrafiltra-

tion membranes, a combination of MF and UF, or a combination of flocculants and MF or UF. A single process step of ultrafiltration can replace the majority of the chemical processes (coagulation, precipitation, oxidation, and disinfection) required in traditional water treatment. By supplanting these chemical processes, many of the physical processes become redundant. Physical processes such as flocculation, sedimentation or accelerated gravity separation, and flotation are all made superfluous by the lack of the corresponding chemical treatments. Flocculation, for example, aggregates particles that have been chemically destabilized during coagulation, so that they may be removed by other processes such as sedimentation or accelerated gravity separation (Crittenden and Harza, 2005). Without the chemical processes that necessitate the physical ones, both can be supplanted by membrane filtration (Mulder, 1996).

Certain traditional processes, however, are still necessary with the use of membranes. Importantly, while disinfection may be replaced by UF during water treatment, chemical disinfection during distribution is still used to protect against downstream, post-treated waters from bacterial and viral intrusions. In addition, before treated water enters into the distribution system it is chemically stabilized to prevent the formation of calcium carbonate scale. Stabilization occurs regardless of whether the water was treated by traditional methods or by advanced membrane techniques. Screening is also a necessary first step in both treatment methodologies. In several special cases, such as when dealing with the removal of gases such as radon, CO_2, H_2S, and VOCs, from groundwater, the physical process of aeration may be used. Aeration is used to oxygenate waters to promote the oxidation of iron and manganese. This occurs by contacting the liquid with air to encourage gas transfer either from the liquid to gas phase (gas stripping) or from gas to liquid phase (gas absorption) (Crittenden and Harza, 2005). It is important to note that while membrane processes are generally more efficient and often more effective than their chemical

and physical counterparts, the infrastructure for traditional treatment has been in place for many decades limiting the economic viability of replacing traditional water treatment plants in their entirety with membrane plants. As a result, membrane processes are often integrated within existing traditional frameworks to replace specific components of traditional water treatment trains. Further, membrane processes are not without their own problems and limitations. These are addressed in greater detail in later sections.

Membrane processes greatly simplify and ameliorate water treatment, but their advantages go beyond the simplification of the water treatment process and the improvement of product waters. Membrane processes are more cost effective, require less physical space, and have fewer negative environmental repercussions, positioning them overall as a more sustainable technology. Traditional treatments for disinfection, decontamination, and desalination can and have been used to confront some of the major problems with quality and supply, but they are less than ideal as they are chemically, energetically, and operationally intensive. The cost of chemicals in addition to regulations on allowable concentrations of chemicals limits traditional water treatment (Crittenden and Harza, 2005). Further, in many cases, waste contamination and salting are exasperated through the use of intensive chemical treatments (such as ammonia, chlorine compounds, hydrochloric acid, sodium hydroxide, ozone, permanganate, alum and ferric salts, coagulation and filtration aids, anti-scalants, corrosion control chemicals, and ion exchange resins and regenerants) and the residuals those treatments produce (Shannon et al., 2008). Finally, land requirements are very high for traditional treatment because surface loading rates are typically low. The cost of a large footprint for a treatment facility can be very high in certain parts of the world where land is scarce or in high demand (Crittenden and Harza, 2005). Finally, traditional treatment methods are inadequate to deal with many emerging contaminants that are entering natural water systems at increasing rates.

2.2.2 Traditional Desalination

Many techniques have been traditionally used to desalinate sea water to produce fresh water including distillation (multi-stage flash evaporation, MSF), electrodialysis, membrane distillation, freezing, and reverse osmosis. Among these, Multi-stage Flash Distillation is the most important technique traditionally used for desalination of sea water. However, reverse osmosis is being applied to a greater extent. As opposed to integration of membranes within the traditional separation system, as is possible with traditional ground water or surface water treatment, reverse osmosis is not integrated but rather completely supplants the existing traditional desalination infrastructure (Mulder, 1996).

Extensive pretreatment is required before sea water can contact reverse osmosis membranes to prevent fouling and membrane damage. Flocculants such as iron chloride ($FeCl_3$) or polyelectrolytes are added to remove the majority of suspended solids, followed by deep bed filters and/or UF membrane trains. However, scaling and biofouling remain serious problems for RO membranes (Mulder, 1996).

Scaling is the precipitation of salts on the membrane. Scaling occurs because the concentration of salts in the feed exceeds their solubility in solution. At these high concentrations, salts precipitate out of solution and accumulate on the surface of membranes. The precipitation of calcium salts ($CaSO_4$, $CaCO_3$) or silica (SiO_2) are of particular concern at the membrane surface and can cause significant reductions in transmembrane water flux. To reduce scaling, pH is often adjusted by the addition of acids. Calcium, barium, and magnesium salts will not precipitate at low pH values, while silica will not precipitate at high pHs. Following scaling prevention, biofouling must be prevented. Chlorines are used to remove bacteria and algae, however the most successful membrane material to date, polyamide (PA), is not resistant to free chlorine. As a result, treatment with sodium hydrogen sulphite ($NaHSO_3$)

is necessary to remove the chlorine after addition. All these pretreatment steps unfortunately incur energy, chemical, and operational costs, in addition to increased space requirements and capital costs (Mulder, 1996).

2.3 Membranes

2.3.1 Introduction to Membranes

Synthetic membranes offer a promising avenue for low cost, low footprint, energy efficient, sustainable, scalable, safe and chemically neutral water treatment. A membrane is a selective barrier between two phases. They are materials that enable the separation of an isomeric mixture under the application of an external force. This differential force is often in the form of a pressure difference between the initial mixture (the feed) and the product (the permeate). Other driving forces include externally applied thermal, concentration, and electromagnetic gradients (Mulder, 1996). In this dissertation, the focus is on pressure gradients as the primary driving force for separation.

There are many types of synthetic membranes, and they can be subdivided into organic (polymeric or liquid) and inorganic (ceramic and metal). In this dissertation, the focus is on nanocomposite organic membranes, i.e. membranes composed of polymers and nanoparticles. Another classification of membranes is based on morphology or structure. Membranes can either be symmetric or asymmetric, porous or dense. Symmetric membranes have a homogeneous structure throughout their cross-section, whereas asymmetric membranes are structurally heterogeneous with a dense top layer and a porous sublayer. These membranes combine the selectivity of dense membranes with the high permeation rate of very thin membranes and the mechanical strength of thick porous membranes. An example of an asymmetric membrane that was made during the research of this dissertation is shown in figure 2.2. Further, asymmetric membranes can have a thin dense skin on their toplayer.

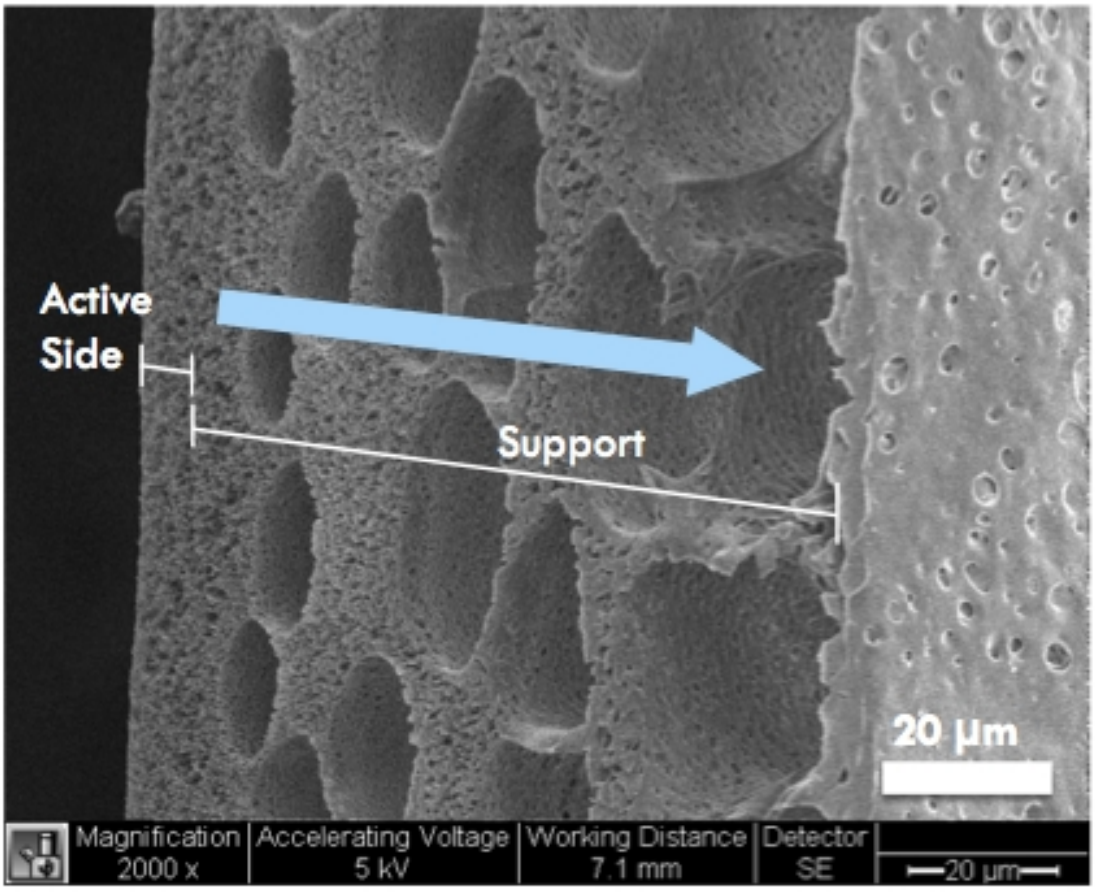

FIGURE 2.2: A cross-section of a typical asymmetric membrane that was made during this research. This cross-section clearly demonstrates the more densely packed polymeric configuration of the active side and the more porous structure of the support sublayer.

This toplayer is a different material than the sublayer so that each layer can be optimized independently. These membranes are called composite membranes (Mulder, 1996).

Membranes enable separations based on several material properties that allow the transport of one component from the feed mixture more readily than any other component(s). In aqueous separations, membranes act as a barrier to the flow of certain solutes. They selectively reject solutes based on the physical and/or chemical properties of the solutes and of the membrane. Membrane separation of solutes can

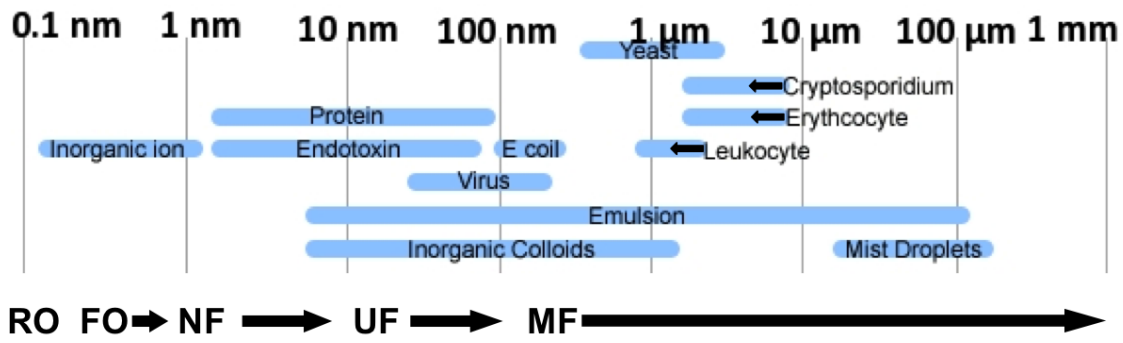

FIGURE 2.3: Membranes are categorized according to their selectivity. Microfiltration (MF) membranes are the most porous and are able to separate bacteria and large colloids. Ultrafiltration (UF) membranes have smaller pores and are able to separate viruses, proteins, and small colloids. Nanofiltration (NF), Reverse osmosis (RO), and forward osmosis (FO) membranes are dense membranes and can remove small organic molecules and ions.

be based on size, vapour pressure, affinity, charge, or chemical nature (Mulder, 1996).

For the separation of particles with diameters $> 100\,nm$, separation is often executed through size exclusion. Membranes with relatively porous structures subjected to low pressures are sufficient to separate these particles. This is termed microfiltration. To separate macromolecules with molecular weights in the range of 10 to $1000\,kDa$ from an aqueous solution, the membrane must be much more dense and the applied gradient must be greater. This separation is also based on size exclusion and is termed ultrafiltration. Low molecular weight components can be separated from aqueous solution, but often the components' size is on the order of that of water molecules. Highly dense membranes are required that favor the diffusion of water through their bulk over that of the solutes, and correspondingly high gradients are also required. In most of these cases, pressure gradients are used. An electric potential difference can only be used in the case that charged molecules of opposite charge are present (Mulder, 1996). The categorization of membranes according to their selectivity is graphically represented in figure 2.3.

Membrane processes separate the feed stream into two streams; 1. the retentate

or concentrate stream, and 2. the permeate stream. This implies that either the concentrate or the permeate stream is the product. If the goal is concentration, then the retentate is the product, but if the goal is purification, either the retentate or the permeate can be the desired product. The selectivity of the membrane is expressed as the retention factor, R. For dilute aqueous solutions, R is the retention towards the solute in the aqueous phase. The solute is completely retained when the solvent, water, passes freely through the membrane. Retention is given by:

$$R = \frac{(c_f - c_p)}{c_f} \tag{2.1}$$

where c_f is the solute concentration in the feed and c_p is the solute concentration in the permeate (Mulder, 1996).

The current state of the technology is such that there is great potential for improvement as current materials and methods are still far from the natural-law limits in their ability to separate compounds, remove deleterious pathogens and chemical agents, transport water molecules across boundaries and move ions against concentration gradients (Shannon et al., 2008).

Polymeric membranes have a wide applicability in diverse fields ranging from water purification plants, breweries, and the dairy industry, to the pharmaceutical and drug delivery world. As the costs and limitations associated with traditional separation techniques increases, membrane technology is currying favor with many industries. As a result, membrane processes are increasingly gaining prevalence in the production of potable water and in water reuse systems due to their ability to produce water of high quality (Geise et al., 2010).

Membranes can be easily integrated within the traditional process train, saving space and costs. To treat surface waters, microfiltration (MF) and/or ultrafiltration (UF) membrane modules take the place of coagulation mixers, flocculation

basins, sedimentation basins, and granular media filters. Membrane modules replace these stages, leaving only screen filters before the membrane modules and disinfection/oxidation processes after the membrane modules. In this way, the treatment train is greatly simplified and the overall plant footprint is greatly reduced. Further, the use of chemical coagulants is completely eliminated. In the case of water-softening, nanofiltration membranes also entirely replace flocculation basins, clarifiers, re-carbonation settling tanks, and granular media filters (Crittenden and Harza, 2005).

Membrane technology is very versatile. Membranes are not limited to environmental applications; they are used in pharmaceutical separations, gas separations, and industrial liquid processing, among many other applications. However, membranes can be used to great effect in water treatment, wastewater treatment as well as in desalination plants, as described above. This great versatility allows them not only to treat currently contaminated water sources, but also to increase the water supply in an energetically efficient manner.

2.3.2 Membrane Theory

A membrane is a layer of material serving as a selective barrier between two phases, remaining impermeable to specific particles, molecules, or substances when exposed to the action of a driving force (Geise et al., 2010). A membrane traditionally separates a feed stream into a permeate stream and a retentate stream. From Darcy's law, shown in 2.2

$$J = \nu = \frac{k\Delta P}{\ell} \tag{2.2}$$

the velocity of water passing from one side of the membrane to the other, v, which can also be thought of as the volumetric flux, J, is proportional to the difference in

pressure across the membrane, ΔP, and inversely proportional to the distance the water must travel, i.e. the thickness of the membrane.. It is imperative, therefore, to minimize the membrane thickness to maximize flux. For a given material, minimizing thickness occurs at the cost of membrane strength, and as the membrane is subject to high pressures it is perilous to weaken the membrane in this way. One way to maintain membrane strength while minimizing thickness is to add a thick support layer with a wide porous structure to the back of a very thin active membrane layer. This more porous support layer does not aid in the separation of solutes, and as such does not hinder the passage of water flow across the membrane. The support layer thus helps maintain a short water travel distance, and thus a high volumetric flux. Support layers, however, are polymeric themselves and can only resist so much mechanical stress. Despite the great mechanical stability provided by support layers, membranes especially hollow fibers, are prone to breakages during membrane operation. Another way to strengthen polymeric materials, whether they are thin membrane active layers or thicker, robust support layers, is with the addition of membrane additives for structural support. One such additive is carbon nanotubes (Wiesner et al., 2007).

A theoretical description of transport through membranes, both porous and non-porous, must account for two contributions to flux: diffusional flow (v) and convective flow (u). The flux component through a membrane can thus be described as the product of velocity and concentration. The velocity term, either diffusional flow or convective flow will dominate depending on whether the membrane is porous or non-porous.

$$J_i = c_i(v_i + u) \tag{2.3}$$

A description of transport through a porous membrane can based almost entirely

on convection, while transport through nonporous membranes are described mostly by diffusive flows. This can be explained by looking at the factors affecting diffusion. The driving force for diffusion is the difference in chemical potential and both applied pressure and the concentration of solutes contribute to this driving force. Since the concentration on either side of MF and UF membranes can be assumed to be equal, the pressure difference must be the only driving force for diffusion in this case. However, the effect of pressure on diffusive water flow is extremely small, indicating that the diffusive contribution to transport through porous membranes can be neglected. It can therefore be stated, that transport in porous membranes occurs by convection and in nonporous membranes by diffusion. However, this simplified division cannot be so easily be made for membranes in the intermediate regimes of dense UF and NF membranes. For these membranes, both convection and diffusion must be taken into account.

2.3.2.1 Porous Membranes

MF and UF membranes are porous structures, and can be thought of as parallel arrays of capillary tubes. Permeate flux can then be described by Poiseuille flow through many parallel cylinders. According to Poiseuille's formulation, (in which there is constant velocity, there are no net forces or no accelerations in a stationary reference frame, and the flows are all steady and laminar), the velocity is maximum at the center of each membrane pore and zero at the walls, a constraint known as the no-slip condition. This leads to a parabolic velocity profile. Poisseuille's equation as derived from the Navier-Stokes equation in cylindrical coordinates is shown in equation 2.4:

$$\nu_x = \frac{(P_o - P_L)}{4\,\mu L} R^2 \left(1 - (\frac{r}{R})^2\right) \tag{2.4}$$

Membranes filter particles through the action of a driving force. This driving force can be a pressure differential, a temperature gradient, a concentration gradient, or an electric potential. For polymeric membranes geared towards micro-, ultra-, nano-, and hyperfiltration (i.e. reverse osmosis) this gradient is most often delivered from pressure differences on the feed side of the membrane compared to the permeate side. From Darcy's law and the Hagen-Poiseuille equation, equation 2.5 can be derived for flux across a membrane

$$J = \frac{\Delta P}{\mu R_m} \tag{2.5}$$

where ΔP is the pressure drop across the membrane, μ is the absolute viscosity of the fluid, and R_m is the hydraulic resistance of the membrane, given as $R_m = A_{membrane} 8\theta\delta_m/(A_{pore} r_{pore}^2)$. A_{pore}/A_m is the ratio of the open pore area to the entire area of the membrane surface, θ is the pore tortuosity factor, and δ_m is the effective thickness of the membrane. This equation predicts that flux should decrease with the square of decreasing pore size and increases linearly with applied pressure (Wiesner et al., 2007). The driving force must be great enough to force water through the pores, but also to overcome existing gradients across the membrane. When filtering water with high solute concentrations, for example, there exists a large concentration gradient across the membrane. This gradient becomes even greater as solutes accumulate at the surface of the membrane. Locally, high solute concentrations accumulated at the surface of the membrane, cause high reverse gradients on the feed-side of the membrane. This gradient induces osmotic pressure, which encourages the flow of water against the externally applied driving force. This effect, known as concentration polarization, is of more concern for dense membranes, such as RO membranes, that filter smaller solutes.

2.3.2.2 Nonporous Membranes

RO membranes are nonporous membranes and as a result cannot be described by the convective Poisseuille flow equations as described above. Transport through a nonporous membranes can be described by a solution-diffusion model instead, in which each of the dissolved components dissolves into the membranes and diffuses through independently.

The diffusive, or non-convective, flux can be described by the product of the concentration and the velocity of the dissolved species in the solvent.

$$J_i = c_i v_i \tag{2.6}$$

The velocity of a solute in the membrane is determined by the driving force acting on it, namely the gradient of the chemical potential, $d\mu/dx$, and the frictional resistance exerted by the membrane, f_i, i.e.

$$v_i = \frac{d\mu}{dx}\frac{1}{f_i} \tag{2.7}$$

The frictional coefficient is related to the thermodynamic diffusion coefficient, D_T, so that equation 2.6 becomes

$$J_i = \frac{D_i c_i}{RT}\frac{d\mu_i}{dx} \tag{2.8}$$

The chemical potential can be written as

$$\mu_i = \mu_i^o + RTlna_i + V_i(P - P^o) \tag{2.9}$$

Substituting 2.9 into 2.8 gives

$$J_i = \frac{D_i c_i}{RT}\left[RT\frac{dlna_i}{dx} + V_i\frac{dP}{dx}\right] \tag{2.10}$$

If we assume that thermodynamic equilibrium exists at the membrane interface, i.e. that the chemical potential of the liquid at the feed/membrane interface is equal in both the feed and the membrane, and that the pressure inside the membrane is equal to the pressure on the feed side, then we can use these boundary conditions to solve for the chemical potential μ_i and activity (mole fraction), a_i, at the feed and permeate sides of the membrane. By substituting these equations for μ_i and a_i into equation 2.10 and further by integrating Fick's law,

$$J = -D\frac{dc}{dx} \tag{2.11}$$

across the membrane, we can turn equation 2.10 into an equation that can be used to determine fluxes for RO transport:

$$J_i = \frac{P_i}{\ell}\left(c^s_{i,1} - \alpha_i c^s_{i,2} exp\left[\frac{-V_i(P_1 - P_2)}{RT}\right]\right) \tag{2.12}$$

where the specific subscript 1 represents the feed interface, the subscript 2 represents the permeate interface, generally denoted by, n, the specific superscript s represents the aqueous (solution) phase and m represents the membrane phase, generally denoted by, x. Further $c^x_{i,n}$ is the mole fraction, (e.g. $c^s_{i,2}$ is the mole fraction in the solution (s) at the permeate phase (2)), P_1 and P_2 are the pressures at the permeate and the feed respectively, ℓ is the membrane thickness, V_i is the volume of solution, $P_i = K_{i,1}D_i$ and $\alpha_i = K_{i,2}/K_{i,1}$, in which $K_{i,n}$ is the ratio of the solution to membrane activity coefficients, $\gamma^x_{i,n}$, at the nth interface, and D_i is the diffusivity of the solute species, i. The above equation is the basic equation used to determine the diffusive transport of any membrane process. This equation can be used for RO, but is not limited to liquid phases on either side of the membrane. Equation 2.12 can be used to compare any membrane process that occurs by diffusive transport including gas separation and pervaporation (Mulder, 1996).

Reverse osmosis membranes are used to separate salts or low concentrations of organic solutes from aqueous solutions. These membranes are highly selective for salts, while allowing water to permeate through. The driving force for separation is a high pressure that must be applied to the liquid feed solution to allow water to pass through the membrane. This pressure must be greater than the osmotic pressure exerted by the dissolved salts in the feed side. When the applied pressure is less than the osmotic pressure, water flows from the dilute solution in the permeate (pure water) to the concentrated solution in the feed (salt water).

The total flux through the membrane is the sum of the water flux and the solute flux, but for highly selective RO membranes (and even for less selective dense membranes) the solute flux is negligible compared to the water flux and thus it can be ignored. Further simplifying equation 2.12, for small values of x, $1 - exp(-x) \approx -x$ and $K_w c^s_{w,1} = c^m_{w,1}$ equation 2.12 can then be written as:

$$J_w = \frac{D_w c^m_{w,1}}{\ell} \left(\frac{V_w(\Delta P - \Delta\pi)}{RT} \right) \tag{2.13}$$

which can be simplified to:

$$J_w = A_w(\Delta P - \Delta\pi) \tag{2.14}$$

Where A_w is called the permeability coefficient, and defined as,

$$A = \frac{D_w c_w V_w}{RT\ell} \tag{2.15}$$

Equation 2.14 is used for both RO and NF. RO membranes, however, are not completely semipermeable, allowing some of the solutes to pass through. A simple equation describing the solute flux can be derived from equation 2.12. With $\alpha = 1$ and the exponential term approximately unity, since $RT >> V_i \Delta P$ for relevant

pressures and volumes,

$$J_s = \frac{D_s K_s \Delta c}{\ell} = B\Delta c \tag{2.16}$$

where B is the solute permeability coefficient and Δc_s is the solute concentration difference across the membrane. The permeability coefficient is given by

$$B = \frac{D_s K_s}{\ell} \tag{2.17}$$

These equations demonstrate that the solute flux in RO is proportional to the concentration difference, while the water flux is proportional to the effective pressure difference.

Another revealing property of dense (RO and NF) membranes is how important the choice of material is for highly efficient separation. This can be shown mathematically by deriving the rejection coefficient, as follows. Assuming no solute can permeate through the membrane, the effective water flux across a reverse osmosis membrane is given in equation 2.14. (In practice, the membrane will be slightly permeable to molecular solutes so the real osmotic pressure difference is not $\Delta\pi$, but rather $\sigma\Delta\pi$ where σ is the reflection coefficient of the membrane towards a certain solute.) While water flux is dependent on the difference in applied pressure and osmotic pressure, solute flux, J_s is independent of pressure as shown in equation 2.16. It can be seen that in (2.14) flux increases linearly with pressure, while (2.16) is independent of pressure and only depends on the concentration gradient across the membrane. The driving force for solutes in reverse osmosis, therefore is limited to diffusion. As the pressure increases, the selectivity also increases because the solute concentration in the permeate decreases. This can be demonstrated by combining equations (2.1), (2.14), and (2.16) with $c_p = J_s/J_w$:

$$R = \frac{c_f - c_p}{c_f}$$

$$= \frac{\Delta c_s}{\Delta c_s + c_p}$$

$$= \frac{J_s/B}{J_s/B + J_s/J_w}$$

$$R = \frac{A(\Delta P - \Delta\pi)}{A(\Delta P - \Delta\pi) + B} \tag{2.18}$$

Since A and B are ideally independent of pressure, as $\Delta P \Rightarrow \infty$ then $R \Rightarrow 1$ and perfect separation of solutes from solvent occurs. Much higher pressures are used in RO (and NF) than for MF and UF. Since the rejection is entirely dependent on the parameters A and B, A should be maximized, while B should be minimized for optimal separation. This means that the membrane material must have a high affinity for the solvent, generally water, and a low affinity for the solute, generally salts. The choice of material, rather than pore size, dictates the choice of membrane in RO, as the material of the membrane determines the intrinsic membrane properties. This is in direct contrast to UF and MF membranes, where pore size is the most important factor for determining separations, while membrane material is chosen based on resistance to fouling and chemical and thermal stability.

2.3.3 Common Membrane Limitations and Strategies to Overcome Them

An ideal membrane has four characteristics: 1. high water flux, 2. high strength, 3. narrow pore-size distribution, and 4. high resistance to fouling (scale formation, cake layer formation, and biofouling) (Antony et al., 2011). These traits are directly related to material composition and structure. High water flux requires that the membrane pores are as numerous as possible and as straight and perpendicular to the membrane surface as possible. The lower the pore tortuosity, the higher the

water flux, and the greater the number of pores per surface area, the more routes the water has to flow from one side of the membrane to the other. Further, as previously mentioned, high water flux is inversely proportional to the thickness of the membrane. A thinner membrane produces higher fluxes. High strength, on the other hand is wholly dependent on the type and amount of membrane material. These first two requirements are often at odds. As the number of pores increases per surface area, and thereby the fraction of empty space within the membrane increases, membrane strength rapidly declines. Additionally, a thinner membrane is always less mechanically resistant. Strength is as much dependent on the type and amount of membrane material as it is on the formation of the pores within the membrane matrix.

The percentage of solutes of a given size that will be separated from the solution is directly proportional to the number of pores of a given size at the membrane surface. Thus the uniformity of pore dimension across the membrane is a critical parameter for effective separation. The more homogeneous the pore dimensions, the more precisely the size cut-off for the membrane. In polymeric membranes, this third criteria is governed by the pore formation mechanism of the membrane. This is associated with the thermodynamics of polymer, solute, and non-solvent systems involved in the formation of the membrane. Finally, low fouling is dependent on a number of factors including the hydrophobicity, surface morphology, surface chemistry and pore shape (Shannon et al., 2008). The more hydrophilic the membrane, the less likely it is for biofilms to grow on its surface, while flatter, smoother surfaces prevent accumulation of organic matter on the membrane surface. Other factors such as charged surfaces, antibacterial coatings, specialized surface chemistries, and novel polymer morphology can lead to good resistance against biofilm formation (Zularisam et al., 2006). Charging membrane surfaces as a method to prevent biofouling will be discussed in greater depth later.

2.3.3.1 Membrane Breakage

The main reason for MF and UF is for pathogen removal. Giardia ($\sim 6-20\,\mu m$) and Cryptosporidium ($\sim 4-6\,\mu m$) in particular are two microorganisms that need to be removed to high degree for public health and safety reasons. It is not practically feasible to remove 100% of all pathogens, but a UF membrane is a highly effective barrier against microorganisms, viruses and particles and thus the concentration of these aqueous components can be reduced by a factor of 10^5 from feed to permeate (Guo et al., 2010). Generally, the drinking water industry measures pathogen removal efficiency in terms of the log removal value, or the log reduction value (LRV). The LRV - log reduction value - is the amount by which these constituents are reduced in the permeate(Gijsbertsen-Abrahamse et al., 2006). LRV is defined as:

$$LRV = log_{10}\left(\frac{C_f}{C_p}\right) \tag{2.19}$$

where C_f is the concentration of the retained species in feed solution and C_p is the concentration of the species in permeate solution. Of course, a stated LRV is related to a particular particle size or particle size distribution. When there are membrane failures, the impact of a liquid leak on the retention can be calculated as:

$$\Delta LRV = LRV_1 - log_{10}\left(\frac{C_f V_T}{C_p V_p + C_f V_d}\right) \tag{2.20}$$

where LRV_1 is the LRV of the uncompromised portion of membranes, V_p is the feed volume passing through the uncompromised portion of the membrane, V_d is the feed volume passing through the defect and V_T is the total feed volume passing through the membrane. Here, it is assumed that the defect does not partially retain the considered species (Guo et al., 2010).

Leakage of feed water to the permeate side poses a problem to permeate water

quality and will allow pathogens to enter into the public water supply system. This can occur if the membrane system integrity is compromised. Leakages can be caused by mechanical failure of the O-rings and gaskets or the breaches in the hollow fibers themselves (Gijsbertsen-Abrahamse et al., 2006). Membrane failure either in sheets or in fibers results from four main factors: 1. damage by chemical corrosion, such as oxidation; 2. damage from faulty installation and maintenance, such as fiber compression; 3. membrane stress and strain from operating conditions, such as backwashing or excessive vibrations due to vigorous bubbling; and 4. damage by foreign objects incompletely removed by pretreatment(Guo et al., 2010) (Childress et al., 2005). Failure from oxidation is attributed to incompatibility between the chemicals in the feed water or the chemicals used to clean the membranes and the membrane material. Membrane stresses from operational conditions often occurs from vibrations, which can arise at start-up and shut-down of pressurized filtration and upon transition from clean rinsing water to viscous waste-water (Childress et al., 2005). These stresses are aggravated if membranes are fouled. Further, high local shear forces can arise when fibers or aggregates are forced through the membrane hollow fibers, and this build-up of pressure can strain membranes to the point of damage (Huisman and Williams, 2004). In these latter two cases, identification of the source of the membrane failure necessitates determining the load points and shear sources coupled with evaluating the modulus of elasticity of the membrane and the potting materials (Childress et al., 2005).

It is typically thought that mechanical properties are not important for membrane processes because the membrane is supported by spacers or potting material, however, hollow fibers are self-supporting (Childress et al., 2005) Mechanical strength of a fiber is defined by two parameters: Young's Modulus (elastic modulus, E) and the strength (σ). Young's Modulus is defined as the ratio of the stress applied to the fiber and the resulting deformation, or strain, of the material. This ratio represents

the stiffness of the material or its resistance to elastic strain. The strength on the other hand is simply the maximum stress (negative pressure) that a fiber can withstand before breakage. The strongest materials for UF membranes were shown to be PVDF and PAN, while some of the least resistant membranes were formed from PES and PSf/PVP mixtures. These membranes would benefit the greatest from additives for improved tensile strength (Gijsbertsen-Abrahamse et al., 2006). The mechanical properties of polymeric materials depend on both the molecular properties of the inherent and on the morphological properties of the resultant material. In other words, both the chemical structure and the supermolecular structure of the polymeric material affect its mechanical strength. The same molecular structure can yield many different morphological structures depending on the orientation of the polymer fibers. This potentially wide variety of orientation is due to differences in fabrication techniques, cooling rates, thermal history, and secondary crystallization. As a result, the mechanical strength of a polymer fiber cannot be assessed apriori; mechanical testing is a necessity (Childress et al., 2005).

Fiber failure rate was found to be between 1 and 100 fibers per million fibers. Most modules have approximately 3000 - 20 000 hollow fibers that are held in place by a resin, therefore on the higher end, this corresponds to two broken fibers in each module of the total membrane installation every year. Broken fibers are often found in the top and bottom pressure vessels and outer modules in the pressure vessels. This lack of random distribution of broken hollow fibers, points to consistent factors affecting membrane integrity. Frequently the potting material and its interaction with the polymer is a source of mechanical weakness and will be the location of breakage when an abnormal external stress is present. (Gijsbertsen-Abrahamse et al., 2006) (Childress et al., 2005). Some reported incidents that caused fiber failure include: metal strings of a strainer of the backwash installation broke into pieces and were blown into the installation during backwashing, which then perforated many of

the fibers. Another incident was the failure of the flocculant dosing, which rapidly increased the pressure. Other common incidents which cause fiber breakage include failures of micro-strainers resulting in sand grains entering the hollow fiber modules, scouring of particles in the feed water at the outside of the fibers, insufficient removal of mussel larvae resulting in growth in the system, insufficient removal of silica needles produced by algae, which may pierce the membrane (Gijsbertsen-Abrahamse et al., 2006) (Childress et al., 2005).

2.3.3.2 Biofouling

Membranes succumb to a number of stresses throughout their working lifetimes, but the most detrimental to their proper functioning is fouling. Biofouling in particular is a plight common to all membranes. Biofouling arises in combination with cake layer fouling, since microbes feed on the rich organic matter that accumulates on the surface of membranes during separation. As natural organic matter (NOM) is filtered from the feed solution, it collects on the membrane surface. The presence of NOM rich in nutrients encourages the growth of bacteria either on the spacers separating membranes as in spiral wound membrane systems, or on the membranes themselves as in the case of both spiral wound and hollow fiber membranes. As these bacteria consume the accumulated NOM, they multiply, secure themselves to advantageous surfaces, reproduce and form colonies, and form thick interconnections between genetically similar communities. This thick, stable, interconnected web of bacteria is called a biofilm. Microbe-generated extracellular substances such as polysaccharides and proteins are the primary constituent of biofilms and are the leading cause of fouling in membranes (Wiesner et al., 2007) (Zularisam et al., 2006) (Vrouwenvelder et al., 2009) (Mansouri et al., 2010).

Biofouling of polymer surfaces is a ubiquitous and costly problem. Biofouling occurs when bacteria grow on surfaces known as biofilms, which secrete a thick sticky

layer composed of extra-polymeric substances (EPS) (Davies et al., 1998) (Chen et al., 2004). Biofouling afflicts fields as widespread as medical equipment (prosthetics, IV tubing, and dialysis membranes), commercial and private boating (hulls and propellers), and industrial and municipal liquid treatment (orange juice concentration, protein separation, desalination, and wastewater treatment). The applications most beleaguered by biofilms are membrane-based desalination and wastewater treatment processes. These processes are challenged with conditions that are ideal for the rapid proliferation of bacterial colonies and the establishment of robust biofilms on the membrane surface. The confluence of high pressures concentrating an ideal nutrient balance onto rough organic surfaces contaminated with extremely high bacterial populations represents ideal biofouling conditions (Chen et al., 2004) (Herzberg and Elimelech, 2007).

As biofilms grow in thickness, they clog pores and reduce the water flux of the membranes. Thick biofilms formed on the surface of a membrane is shown in figure 2.4. As flux reduces, higher trans-membrane pressures are required, which creates more mechanical stress on the membrane and incurs greater energy costs (Zularisam et al., 2006). When fouling becomes too predominant on the membrane, membranes need to be cleaned with caustic chemical agents, which may damage the polymer membranes over time and have associated costs including the cost of temporarily ceasing filtering operation and the price of the chemicals themselves.

The problem of biofouling on membranes frequently stems from the materials used to make membranes. Porous membranes are often made from chemically and mechanically stable polymers. These polymers tend to be very hydrophobic, which makes them highly susceptible to organic foulant adsorption (Jucker and Clark, 1994). Caustic cleaning agents are employed to remove organic matter from membrane surfaces, but these treatments damage the membrane surface and reduce the membrane effectiveness (Wiesner et al., 2007) (Zularisam et al., 2006). Solving the

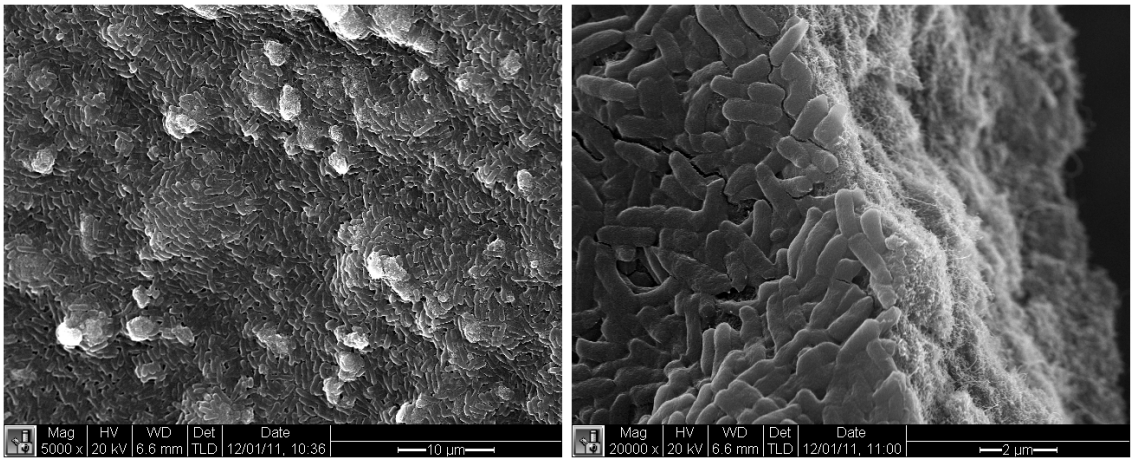

FIGURE 2.4: The attachment and multiplication of bacteria on a surface helps to reduce the flux through membranes. Biofilms are evident in this SEM image taken of membranes biofouled during membrane testing in this dissertation. On the left is a view of an area completely fouled by membranes. On the right is a cross-section of the same membrane showing the layer of biofilm on the surface of the membrane.

biofouling problem on polymer surfaces, in particular on membrane surfaces, is the holy grail of membrane materials research.

Proposed and attempted materials solutions for membranes can be divided into anti-adhesion and anti-microbial strategies. Anti-adhesion approaches include bulk polymer blending to alter polymer hydrophilicity, mixing inorganic additives to affect surface roughness and hydrophilicity, grafting anti-adhesion materials to the surface of membranes, and modifying surface chemistry of membranes with materials to change surface roughness and hydrophilicity (Van der Bruggen, 2009a). Anti-bacterial approaches include coating surfaces or mixing bulk polymers with organic and inorganic biocides, creating reactive surfaces, and modifying surfaces with bioactive compounds (Chen et al., 2010).

These strategies have varying success, but they all come with significant challenges. Polymer blends combine a matrix polymer (the base polymer used for the stable pore structure) with a functional polymer (the additive used for special tailored surface properties). If a macromolecular additive has high surface segregation

and coverage, the surface characteristics of the membrane can be changed with only minor influences on the bulk morphology and properties. Another advantage is that it is easily implemented at an industrial scale. The main problems with blending are the miscibility of polymer pairs and the stability of the induced modifications (Chen et al., 2010).

The addition of polyvinylpyrrolidone (PVP) and polyethylene glycol (PEG) has become a standard practice to improve the hydrophilicity of most polymer membranes (Boom et al., 1992). While they improve the hydrophilicity of the surface of membranes including PSf, PES, and PVDF, they can have adverse effects including changes in pore size and porosity of the membranes. These changes often increase the flux of the membrane at the expense of lower solute rejection and higher molecular weight cut-off (MWCO) (Chen et al., 2010).

Amphiphilic polymer additives also offer great opportunities for improving the anti-adhesive properties of membranes. Inspired by research on antifouling marine paints, amphiphilic polymers have been blended with membrane polymers to prevent biofouling. These additives have low surface energy and high hydrophilicity and are suspected to have long-lasting antifouling characteristics; their hydrophobic segment improves anchoring within the bulk polymer and their hydrophilic segment mostly remains at the surface and acts to combat biological adhesion (Zhao et al., 2008). Unfortunately, improving the hydrophilicity of the membrane is only one factor in combating adhesion of biosolids and only aids in reducing biofouling rather than permanently eliminating it (Chen et al., 2010).

Metal oxide nanoparticles have been incorporated into polymeric membranes for a variety of applications including anti-fouling and anti-adhesive improvements. These nanoparticles include SiO_2, Al_2O_3, and TiO_2. Titanium dioxide is particularly interesting for its high hydrophilicity, chemical stability, and antibacterial properties (Zhang et al., 2008). Unfortunately, TiO_2 requires UV irradiation to achieve its anti-

bacterial potential, which is highly impractical for currently manufactured membrane modules in industrial processes.

Graft polymerization of hydrophilic monomer chains on the membrane surface acts to reduce fouling by acting as a steric barrier to foulant adsorption. These chains have varying success in preventing fouling, but they are usually sensitive to cleaning agents. Further, these chains interfere with the membrane pores, partially blocking the flow of water across the membrane, thereby reducing membrane permeability and increasing cross-membrane pressure requirements (Pieracci et al., 2002). Additionally, graft polymerization is only a two-dimensional solution to an inherently three-dimensional problem, as the pores themselves remain hydrophobic and susceptible to biofouling (Shannon et al., 2008).

Grafting results in permanent modifications of membrane properties including permeability and pore size. Grafting density is difficult to control and results in significant reduction in pore size and flux, necessitating a balance between fouling control and membrane flux. Coating is a much more simple process than grafting and affects membrane hydrophilicity, roughness, and charge to give improved resistance to biofouling. Coatings include hydrophilic polyvinyl alcohol (PVA) and negatively charged polyacrylic acid (PAA). These coatings have shown some improvements in biofouling resistance, but their main disadvantage is that they affect the permeability of the membrane. Further, they are often sensitive to harsh chemical environments including caustic cleaning agents and may delaminate from the membrane surface (Chen et al., 2010). These strategies all focus on preventing bacterial adhesion and the rate of biofilm growth, but they fail in preventing long-term biofilm development and biofouling. For extended efficient membrane operation, it is imperative to find strategies that prevent biofilm formation for extended periods of membrane operation.

Anti-bacterial approach may provide membranes with long-term biofouling relief

by killing bacteria before they can adhere to the surface or before they multiply and form a biofilm. These approaches will not prevent fouling altogether, however, because dead bacteria will still accumulate on the surface and hinder trans-membrane flux.

Biocides can be embedded into membrane surfaces and slowly release from the polymeric material. They must be mobile so that they can migrate through the polymer film and across bacterial cell membranes to destroy bacteria. Silver and silver nanoparticles are common biocides that are added to membranes to prevent bacterial proliferation. Silver is a highly effective toxic agent and its use and mechanisms have been investigated in depth. Other biocides include copper, zinc, and quaternary ammonium compounds. Unfortunately, the activity of these biocides requires high mobility, but high mobility implies high water leaching. This can be avoided by designing a slow-release carrier such as a zeolite. Other biocidal agents that don't require release include chitosan. These molecules must be long enough to interfere with and damage the cellular membrane or cell wall of bacterial cells in contact with the surface (Tikhonov et al., 2006).

A new field that includes bioactive and reactive surfaces, has great potential in preventing biofouling on membranes. Several newly researched bioactive compounds can be added to membranes to disrupt biofilm development. Quorum sensing compounds, for example, can be used to disrupt signaling within the biofilms and antifouling enzymes can be used to degrade biofilm components (Paul et al., 2009) (Kristensen et al., 2008). Reactive surfaces or coatings that respond to various stimuli can provide tunable surface roughness and hydrophilicity. Certain polymers such as poly(N-isopropylacrylamide) (PNIPAAm) respond to temperature changes and alter their state from highly-hydrated brushes to hydrophobic surface layers (Berndt and Ulbricht, 2009).

2.3.3.3 Membrane Cleaning

During membrane operation, biofilms, cakes of particles, and crystallization of minerals and salts form on both the membranes and the polymer spacers used to separate one membrane from another. Bacteria attach themselves to either the spacers or the membranes and, as previously described, generate and excrete extracellular substances, which form thick films over the membrane surface. Back-flushing and cross-flow cleaning can be employed to dislodge those foulants that cause reversible fouling. Foulants that cause irreversible fouling, such as biofilms, resist back-flushing. They persist and grow, continually decreasing the permeate flux. At some point the membranes must be cleaned more aggressively to combat these foulants (Wiesner et al., 2007). The most common method to dispose of these films is through chemical cleaning using caustic chemical agents, which include hydrochloric acid (HCl), sodium hydroxide (NaOH), and sodium hypochlorite, also known as bleach (NaOCl) at concentrations as high as 2M. These chemicals destroy the bacterial membranes through reductive or oxidative processes, respectively, and help dislodge the biofilms from the spacer and membrane surfaces (Zularisam et al., 2006) (Maartens et al., 1998).

Highly effective at breaking down biofilms and hindering further microbial growth, these aggressive solutions cause damage to the polymeric membranes as well and are particularly detrimental to the membrane pore shape and size. By widening the pores and deforming their shape, membranes become less effective at segregating size classes of solutes, thereby reducing their selectivity. Chemical damage to the surface of the membranes may also create rougher surfaces that are more prone to fouling in the future. In addition, for membranes with sterically hindering grafted chains, cleaning solutions may have adverse effects on their conformation and therefore their efficacy at deterring biological growth and organic matter accumulation (Zularisam

et al., 2006) (Maartens et al., 1998). While caustic cleaning alleviates immediate fouling, prolonged use reduces both the membrane's separation efficacy and their future fouling resistance.

Biofouling in membrane separation processes necessitates extensive pretreatment that incurs additional costs (Flemming, 1997). Pretreatment includes chemical treatment (e.g. flocculation) and ultrafiltration (UF), which limit process efficiency and increase costs (Saad, 1992) (Elimelech and Phillip, 2011). Polyamide (PA) thin films are currently the state-of-the-art material for desalination and wastewater reclamation (Lee et al., 2011). A solution to biofouling on PA thin films could revolutionize the entire RO process train by reducing costs associated with pre-treatment, energy for high recoveries (Wilf and Klinko, 2001), and capital; by reducing the plant foot print through minimized pre-treatment; and by increasing membrane life-time through reduced chemical use and biofouling suppression. Finally, eliminating biofouling on these polymeric thin films would ease the environmental impact of RO by lessening carbon emissions and minimizing chemical waste (Lattemann and Hopner, 2008).

2.4 Polymers

2.4.1 Introduction to Polymers

Polymers are the primary constituents of most membranes. Many of the most common membranes are formed from linear, unbranched polymers (eg. PSf, PVDF, CA), but membranes can be made from all different types of polymers including cyclic polymers, branched polymers, network polymers, and even dendrimers. Linear chain polymers have many characteristics that describe them, but the three properties that define them well are: 1. molar mass, which is the mass of 1 mol of the polymer and usually quoted in units of g/mol or kg/mol. The molar mass is related to the degree of polymerization, x, which is the number of repeat units in the polymer chains by

the simple relation,

$$M = xM_0 \tag{2.21}$$

where M_0 is the molar mass of the repeat unit. 2. flexibility, which is determined by the number of benzene rings found along their chains, and 3. charge, which is the presence of charge carriers or charged functional groups along their chain length. Polymer length is well defined for a single polymeric chain, but with very few exception, polymers consist of an ensemble of macromolecules or network chains with a range of molar masses. The molar mass changes in quantized units of M_0, so the distribution is discontinuous. For most polymers, these intervals are very small in comparison to their total range of molar masses possible, and thus the distribution can be assumed to be continuous. This ensemble of macromolecule size is defined by the number-average molar mass, M_n, which is the product of the molar mass of each fraction of macromolecules of a given length scaled by the mole fraction that it represents within the ensemble.

$$\bar{M_n} = \sum X_i M_i \tag{2.22}$$

where X_i is the mole fraction of molecules of molar mass M_i and is given by the ratio of N_i to the total number of molecules. Thus

$$\bar{M_n} = \frac{\sum N_i M_i}{\sum N_i} \tag{2.23}$$

More conveniently, the distribution of polymers is often considered with respect to a weight fraction rathe than a mass fraction. The weight-average molar mass, $\bar{M_w}$ is defined as the sum of the products of the molar mass of each fraction multiplied by its weight fraction,

$$\bar{M}_w = \sum w_i M_i \tag{2.24}$$

where the weight fraction, w_i, is defined as the mass of molecules of molar mass, M_i divided by the total mass of all the molecules present,

$$w_i = \frac{N_i M_i}{\sum N_i M_i} \tag{2.25}$$

Combining equation 2.24 with equation 2.25 we can express the weight-average molar mass, $\bar{M}_w$ in terms of the number of molecules:

$$\bar{M}_w = \frac{\sum N_i M_i^2}{\sum N_i M_i} \tag{2.26}$$

The ratio of $\bar{M}_w/\bar{M}_n$ must be greater than unity for a non-uniform (polydisperse) polymer and is known as the dispersity ($\bar{D}$). Its value measures the breadth of molar mass distribution, though it is only representative and is not the exact distribution curve of molar masses and their representative fraction. A perfectly uniform (monodisperse) polymer would have a $\bar{D} = \bar{M}_w/\bar{M}_n = 1$. This distribution of polymer lengths in any given non-uniform macromolecular ensemble limits complete deterministic approaches to bulk property prediction, however these approximations to the distribution curves provides an initial starting point. Further complicating predictive ensemble description are the associated molecular morphology and charge of each polymer chain. Polymer morphology in solution is described in detail below, but detailed theoretical descriptions associated with charged groups on polymer chains is beyond the scope of this dissertation.

2.4.2 Polymer Theory and Immersion Precipitation

Polymeric membranes are formed from the spontaneous gelation of dissolved polymers in a non-solvent bath. This process is termed immersion precipitation. Poly-

mers can be dissolved in a number of solvents depending on specific chemistry, which is determined by their ability to form homogeneous mixtures. The requirement to form a solution is that the Gibbs free energy, G_{12}, of the mixture must be less than the sum of the Gibbs free energies, G_1 and G_2, of the pure components in isolation. This requirement is defined in the Gibbs free energy of mixing as shown in equation 2.27:

$$\Delta G_m = G_{12} - (G_1 + G_2) \tag{2.27}$$

which must be negative for a solution to form. Gibbs free energy is related to the enthalpy and the entropy of the mixture by the standard thermodynamic equation,

$$G = H - TS \tag{2.28}$$

so, a more useful expression for ΔG_m is

$$\Delta G_m = \Delta H_m - T\Delta S_m \tag{2.29}$$

where ΔH_m is the enthalpy of mixing and ΔS_m is the entropy of mixing. In order to determine whether a solution will form, one needs to determine the sign of the Gibbs free energy of mixing. There is no ideal equation to predict the solubility of all polymers, however as a first approximation, the Flory-Huggins Theory provides an adequate estimation of the energetics of mixing. The entropy of mixing can be derived to be equation 2.30:

$$\Delta S_m^{comb} = -R[n_1 ln\varphi_1 + n_2 ln\varphi_2] \tag{2.30}$$

where n1 and n2 are the number of moles of the solvent and solute respectively, and where $\varphi_1 = N_1/(N_1 + xN_2)$ and $\varphi_2 = xN_2/(N_1 + xN_2)$ are the volume fractions of the solvent and polymer respectively, in which N1 is the number of solvent molecules

and N_2 is the number of polymer molecules with x number of chain segments. The second half of the Flory-Huggins Theory is to calculate the term, which accounts for the effects of intermolecular interactions (Young and Lovell, 1991). The total Gibbs free energy of mixing in equation 2.31,

$$\begin{aligned} \Delta G_m^{contact} &= p_{12}\Delta g_{12} \\ &= p_{12}\left(g_{12} - \frac{1}{2}(g_{11} + g_{22})\right) \end{aligned} \tag{2.31}$$

can be shown to follow from the assumption that for every two solvent-segment contacts formed on mixing, one solvent-solvent and one segment-segment contact is lost, which affects the change in the Gibbs free energy for formation of a single solvent-segment contact, Δg_{12}. In this case, p_{12} is the total number of solvent-segment contacts in the solution. This total number of solvent-segment contacts is equal to the total number of lattice sites adjacent to each polymer molecule occupied by the solvent molecules, and is given by $N_1(z-2)\varphi_2$ (Young and Lovell, 1991). This gives equation 2.32,

$$\Delta G_m^{contact} = (z-2)N_1\varphi_2\Delta g_{12} \tag{2.32}$$

To simplify the end result, a lattice parameter is introduced known as the Flory-Huggins polymer solvent interaction parameter defined by equation 2.33.

$$\chi = (z-2)\frac{\Delta g_{12}}{kT} \tag{2.33}$$

To obtain the equation for the Gibbs free energy of mixing, one needs to combine equation 2.30 with equation 2.32 to produce

$$\Delta G_m = \Delta G_{contact}^m - T\Delta S_m^{comb} \tag{2.34}$$

This gives the final form the Flory-Huggins equation for the Gibbs free energy of mixing, which describes the equilibrium thermodynamic properties of polymer solutions, and thereby predicts whether a polymer and a solvent are miscible.

$$\Delta G_m = RT[n_1 ln\varphi_1 + n_2 ln\varphi_2 + n_1\varphi_2\chi] \tag{2.35}$$

This equation is able to predict general trends but cannot agree precisely with experimental data. Reasons for its shortcomings include the fact that it does not exclude the possibility of self-intersection chains and its use of a mean-field approximation, which restricts its use to high polymer concentrations. Finally the interaction parameter, χ, is not a simple parameter to calculate. Nevertheless, the Flory-Huggins lattice theory lays the ground-work for understanding the thermodynamics of polymer solutions (Young and Lovell, 1991).

Standing on this theory, many solvent-polymer pairs have been determined and elaborately described, but in most practical situations, all that is required is a guide to the miscibility of polymer-solvent systems. The ability of a solvent to dissolve a polymer is governed by a set of constraints described by the formal Hildebrand Solubility Parameters and more simply by the Hansen Solubility Parameters. The Hildebrand equation estimates the enthalpy of mixing for mixtures of liquids, as shown in equation 2.36:

$$\Delta H_m^{contact} = V_m\varphi_1\varphi_2(\delta_1 - \delta_2)^2 \tag{2.36}$$

where V_m is the molar volume of the mixture, and δ_1 and δ_2 are the solubility parameters of components 1 and 2 respectively. The solubility parameter, δ, of a liquid is the square root of the energy of vaporization per unit volume and is given by:

$$\delta = [(\Delta H_v - RT)/V]^{\frac{1}{2}} \tag{2.37}$$

where ΔH_v is its molar enthalpy of vaporization and V is its molar volume. From equation 2.36, enthalpy is only zero or positive. Mixing is more favorable as enthalpy becomes less positive (or closer to zero), which is the case if the solubility parameters of the polymer and the solvent are near to each other. This equation does not take into account hydrogen bonding and charge transfer interactions, which can lead to negative enthalpies. Solubility parameters of polymers can only be determined indirectly. Values of δ for a polymer are often taken as those associated with solvents that give the maximum intrinsic viscosity for soluble polymers. The solubility parameter method, therefore, can only act as a guide to determine miscibility. Since it does not take into account hydrogen-bonding interactions and other specific effects, the theory is limited to non-polar amorphous polymers with non-polar solvents. Finally, since the theory is based on liquid-liquid mixtures, it does not take into account the energy required to overcome the enthalpy of crystallization when dissolving crystalline polymers, such as polyvinyl alcohol (Young and Lovell, 1991).

Using this guide it is then possible to determine several possible solvents (used to dissolve polymers) and non-solvents (used to precipitate them) for most polymers of interest. Common ultra- and nano-filtration membranes are formed from polysulfone (PSf), which has been found to be soluble in several solvents including chloroform, dimethyl acetamide (DMAc), dimethyl formamide (DMF), and N-methyl perrolidone (NMP). Dissolved in this solvent, the polymer forms a viscous mixture, which precipitates in contact with non-solvents such as water and ethanol. Precipitation occurs for a critical amount of non-solvent added, as the solvents in the polymer mixture enter the non-solvent phase and leave a solid polymer behind, the kinetics of which are dependent on both thermodynamic and rheological properties.

2.4.3 Polymer Structure and Membrane Materials

Polymer precipitation kinetics affects the structural morphology of membranes. The greater the difference between the solubility parameters of the solvent and the non-solvent, the faster the kinetics and thus the more quickly the solvent will leave the polymer to enter the non-solvent phase. It is this rate that affects the pore frequency, size and structure. A high rate of precipitation causes small, frequent, and uniform pores across the membrane, which is ideal for tight ultra- and nanofiltration membrane fabrication.

In addition to membrane structure, surface chemistry of the membrane plays an important role in determining the efficiency of the membrane separation and the membrane's propensity to foul. Some of the most commonly used polymers for membrane fabrication are listed in Table 2.1. These polymers are used to make a wide range of membranes, ranging from microporous to nanoporous, and from hydrophilic to hydrophobic.

The relative hydrophobicity of a membrane is an important parameter for water treatment applications. For example, polysulfone (PSf) is an inherently hydrophobic material that has been used as a polymer for commercial microfiltration and ultrafiltration membranes. PSf is also regularly used as a support material for thin film composite nanofiltration and reverse osmosis membranes because it has an excellent balance of resistance to chemical, thermal, and mechanical stresses. However, its inherent hydrophobicity resists transmembrane water flow, which reduces flux efficiency. The ideal membrane for pressure-driven applications in water treatment is one that is hydrophilic for this reason, but also because natural organic matter preferentially sorbs to hydrophobic surfaces. PSf membranes can be modified to increase hydrophilicity by polymer chain modification (sulfonation, carboxylation), surface modification (plasma treatment, UV-induced grafting, pre-adsorption, plasma-

Table 2.1: Common polymers used for commercial membrane production modified from (Pinnau and Freeman, 2000)

Membrane Material	Membrane Process
Cellulose regenerated	D, UF, MF
Cellulose nitrate	MF
Cellulose acetate	GS, RO, D, UF, MF
Polyacrylonitrile	UF
Polyamide	RO, NF, D, UF, MF
Polysulfone/Sulfonated Polysulfone	GS, UF, MF
Poly(ether sulfone)	UF, MF
Polyetheretherketone	UF
Polycarbonate	GS
Poly(ether imide)	GS
Poly(2,6-dimethyl- 1,4 phenylene oxide)	UF, MF
Polyimide	GS, UF
Poly(vinylidene fluoride)	GS
Polytetrafluoroethylene	UF, MF
Polypropylene	MF
Poly(methyl methacrylate)	D, UF, MF
Poly(vinyl alcohol)	PV
polydimethylsiloxane	PV, GS
MF= microfiltration; UF= ultrafiltration; NF= nanofiltration; D= dialysis; PV= pervaporation; GS= gas separation	

induced grafting, grafting by ion beam irradiation, grafting after redox initiation), and polymer blending (Van der Bruggen, 2009a) (Ulbricht and Belfort, 1995)(Noshay and Robeson, 1976)(Nystrom and Jarvinen, 1991)(Han and Nam, 2002)(Kim et al., 2005)(Park et al., 2006). Polyvinylpyrrolidone (PVP) and polyethyleneglykol (PEG) are common polymer additives in PSf blends to increase its hydrophilicity (Ahmad et al., 2005).

Polymer molecules possess the ability to crystallize. In the formation of a solid polymer, long chains of polymers can align in localized regions packing side-by-side in one particular direction forming ordered crystal structures. The spatial arrangement of the atoms is controlled by the covalent bonding within a particular molecular segment and between polymer segments held together by van der Waals forces or

hydrogen bonding. These ordered arrangements are only localized, so polymers can only be semi-crystalline, but the degree to which they crystallize and the size and arrangements of the crystallites in a semi-crystalline polymer have profound effects on the physical and mechanical properties of the polymer. As expected therefore, polymer crystallinity plays a significant role in governing membrane characteristics (Young and Lovell, 2011).

Crystallization in polymers occurs either when the polymer cools down from the molten state past the melting temperature, or during gelation from solution. Crystallization occurs because of the favourable thermodynamics. To minimize the Gibb's free energy, $G = HTS$, either the difference in enthalpy must be negative, or the product of the temperature and entropy must be very large. A polymer melt is a highly entropic random assortment of entangled polymer chains. As the temperature decreases below the melting temperature, and crystallization occurs, the entropy decreases. The entropic contribution becomes less significant at lower temperatures, and this entropic penalty is offset by the large reduction in enthalpy that occurs during crystallization. Solid polymers formed from solution phase often demonstrate higher crystalline perfection than solid polymers formed from melts, because there is little to no entanglement in solutions (Young and Lovell, 2011).

Polymers with high crystallinity form membranes with low permeability. This is because domains of crystallinity are composed of tightly compacted, aligned polymer chains, which reduces free volume and thus limits diffusion of solutes through the membrane. Transport of solutes occurs mostly through the amorphous regions of the polymer membrane. Low amounts of crystallinity have little influence on diffusion resistance but as crystallinity increases, the resistance increases exponentially. This can be described in the following manner:

$$D_i = \frac{D_{i,0}(\psi_c^n)}{B} \tag{2.38}$$

where B is a constant, D_i is the diffusion coefficient, $D_{i,0}$ is the initial diffusion coefficient without crystalline regions, ψ is the fraction of crystalline material present, and n is an exponential factor ($n < 1$) (Mulder, 1996).

Crystallization of a polymer from solution occurs through the local alignment of small ordered polymer chain regions, in a process called nucleation. Crystal growth from these nuclei occurs by addition of more polymer chains. It is thought that in most cases, nucleation starts on foreign bodies, such as on dust particles or on the walls of the vessel containing the polymer (Young and Lovell, 2011).

In certain applications, such as desalination, high polymer crystallinity may be desirable for higher solute rejection, however in other applications, such as ultrafiltration, polymer crystallinity limits flux and transport across the membrane. Crystallinity can be altered to address these various needs through inclusion of additives into bulk polymer membranes. Microscopic additives act as seeds for crystal growth during immersion precipitation. The inclusion of more additives, encourages crystallization of the polymer throughout the bulk (Young and Lovell, 2011). Surprisingly, however, this is not always true for the addition of nanoscopic additives, as demonstrated in this dissertation.

The flux of water through a membrane is as important as its selectivity towards various kinds of solutes. As previously discussed, porous membranes for MF and UF require high porosity and uniform pore sizes for separation of solutes, while their material properties, i.e. the choice of polymer, is primarily based on surface chemistry such as charge and hydrophilicity to limit fouling. For reverse osmosis membranes, the polymer material of choice is important not only for its surface properties but it is also essential for its affinity to water (described by the water permeability coefficient,

A, defined in equation 2.15) and its selectivity towards certain solutes (described by the solute permeability coefficient, B, defined in equation 2.17) Mulder (1996).

Flux is oftentimes improved by reducing the thickness of the membranes, since flux is roughly inversely proportional to membrane thickness. With this in mind, all contemporary reverse osmosis membranes are asymmetric structures composed of a very thin dense toplayer ($\ell < 1\,\mu m$) supported by a thicker porous sublayer ($\Delta x \approx 50 - 250\,\mu m$). In this configuration, the vast majority of the resistance towards transport is governed by the dense top layer. The asymmetric structure of reverse osmosis membranes can take one of two forms a) integrally asymmetric membranes or b) composite membranes.

Integrally asymmetric membranes are composed in such a way that both the top dense layer and the porous support layer are formed from the same polymer. These membranes are made by the phase inversion technique similar to the way that UF membranes are made. The difference between UF and RO membranes formed in this way is the choice of polymer and the specific membrane formation parameters including the concentration of the polymer-solvent solution, the composition of the non-solvent bath, the presence or absence of pore forming additives for UF and RO membranes respectively, the temperature of the non-solvent bath, and the humidity content of the atmosphere during membrane formation. Each of these parameters plays a role in making membranes more or less porous and greatly effects the final membrane properties. However, the most important parameter is the choice of polymer in order to optimize the constants A and B. For desalination of seawater and brackish water, hydrophilic materials should be used with low solute permeability Mulder (1996).

Composite membranes are formed by covering a porous support membrane with a dense selective layer by one of a variety of coating methods. The membrane is thus composed of two (or more) different polymers, each of which can be optimized

independently. The porous support sublayer is often a traditional asymmetric UF membrane, while the dense toplayer is any number of specific polymers discussed later. The coating layers are applied by either dip coating, in-situ polymerization, interfacial polymerization, or plasma polymerization. Interfacial polymerizaiton is the most common method for forming composite RO or NF membranes. In this method, two very reactive different mult-functional monomers are reacted together. This is commonly done by soaking the asymmetric UF porous support membrane in an aqueous solution of one of the monomers and then exposing the wetted membrane to an organic solvent solution of the other reactive monomer. The reaction between the two reactive monomers occurs at the well defined water/organic solvent interface to form a polymeric network structure. The reaction only occurs at the interface resulting in a very thin film dense polymeric surface coating. The most successful monomer constituents to date are the building blocks of polyamide, trimesoyl chloride (TMC), and M-phenyl diamine (MPD). These two monomers react together in a 2:3 reactive network to create an interconnected polymeric barrier that is both highly permeable to water and highly selective to salts.

The two primary materials used for reverse osmosis membranes are the cellulose esters and aromatic polyamides. Cellulose esters, especially cellulose diacetate and cellulose triacetate are particularly suitable polymers because they have high permeability towards water and very low solubility towards salt. Unfortunately, these polymers are unstable in the face of chemicals, extreme temperatures, and most critically bacterial exposure. These membranes can generally only be operated within a pH range of 5 to 7 and at temperatures at or below $30^{\circ}C$. The most severe issue, however, is the rapid biological degradation of cellulose esters. Biological contaminants, especially bacteria, easily degrade cellulose esters. This poses a large problem since these membranes are also susceptible to chemical degradation. Finally, cellulose ester membranes have poor selectivity towards small organic molecules (other

than carbohydrates such as glucose or sucrose).

Aromatic polyamides are another class of polymers that show very high selectivity towards salts, however their flux is slightly lower than that of membranes composed from cellulose esters. Polyamides have the significant advantage that they can be operated over larger pH ranges from 5 to 9, which aids in preventing silica scaling. Polyamides do not degrade under bacterial exposure, however, they are susceptible to biofouling. One of the main drawbacks for polyamide RO membranes, is that chlorine cannot be used to combat biofouling. Free chlorine, Cl_2, degrades amide groups, thus any polymer with the general $-NH-CO$ group is highly susceptible to chlorine attack. As a result, less effective anti-biofouling pre-treatment strategies must be employed.

Other polymers used for RO membranes include polybenzimidazoles, polybenzimidazolones, polyamidehydrazides, and polyimides.

Some new research on novel polymers could be highly promising for decreasing the operational costs of wastewater treatment by significantly reducing the amount of membrane cleaning and replacement, while also increasing the process efficiency. Brush and comb copolymers with hydrophilic backbones and hydrophilic side chains have been designed such that they coat membrane surfaces and internal pores alike during the standard immersion precipitation process used in membrane manufacture. These combs provide complete resistance to irreversible fouling by three types of extracellular polymeric substances and thereby provide large longterm flux enhancements. But as mentioned previously, steric additions to membranes reduce flux, interfere with pore structure, and are highly susceptible to cleaning agents. Other membrane materials currently under investigation offer some similar advantages such as novel block copolymers, graft/comb copolymers, self-assembling biopolymers and lyotropic liquid crystals, and electrospun fibers (Shannon et al., 2008). Carbon nanotubes could potentially be greatly advantageous membrane additives. By altering

functionality, inclusion and reactions with polymers, one can govern hydrophilicity, strength, pore size, crystallinity, surface charge, and electrical conductivity.

2.5 A Brief Overview of Carbon Nanotubes and their Functionalization

Twenty-two years of intense research. Characterization. Modification. Application. Implication. The discovery of a new allotrope of carbon carbon nanotubes (CNTs) by Iijima in 1991 set off a flurry of unrelenting research (Iijima, 1991). From space elevators (Edwards, 2000) to fast single molecule information devices (Wada et al., 2000), from nano-diagnostics (Yue et al., 2002) to low energy desalination (Majumder et al., 2005), the unique properties of CNTs offered limitless possibilities.

Carbon nanotubes are an allotrope of carbon composed entirely of sp^2 hybridized carbon atoms in a hexagonal interconnected structure rolled into long tubes. Individual tubes are called single walled carbon nanotubes (SWCNTs), but these tubes can also be formed concentrically. Concentric tubes can be formed anywhere from two walls called double walled CNTs (DWCNTs) up to many walled or multi-walled CNTs (MWCNTs). Carbon nanotubes (CNTs), which measure between a few nanometers to several tens of nanometers in diameter and can be as long as several millimeters, exhibit amazing properties including extreme strength and high electrical and thermal conductance (Ruoff and Lorents, 1995)(Krishnan et al., 1998)(Ebbesen et al., 1996)(Yu et al., 2000). Carbon nanotubes can also vary from semi-conducting to highly conducting simply by altering the geometric bonding pattern of the carbon lattice. CNTs may be formed with variable number of walls and as such are named either single-walled (SWCNT), double-walled (DWCNT) or multi-walled carbon nanotubes (MWCNT), all of which exhibit these incredible properties to varying degrees. Unfortunately, the realization of these properties in applications is severely hampered by their tendency to tightly bundle due to the large van der

Waals interactions along their immense length (Sun et al., 2002). Their unique properties can only fully be exploited through uniform dispersion and alignment, which poses significant challenges. Alignment has been pursued through a plethora of novel methods ranging from magnetic alignment, unique deposition and growth techniques (Coluci et al., 2006)(Correa-Duarte et al., 2005)(Xie et al., 2005b), while considerable research has been directed to sidewall-functionalization and surface modification of carbon nanotubes to improve their dispersibility in various media (Sun et al., 2002) (Liu et al., 1998)(Ciofani et al., 2009)(Sun et al., 2001)(Qu et al., 2005)(Nakashima and Fujigaya, 2007)(Wang et al., 2005). The research group under Sun, for example, has developed a plethora of refined CNT functionalizations (Sun et al., 2002).

The dispersion of carbon nanotubes can be described by a set of solubility parameters called the Hansen solubility parameters, which include dispersion, intermolecular or polar, and hydrogen bonding. Solvents with high polar and hydrogen bonding such as water and dimethylformamide (DMF) induce hydrophobic bonding of CNTs and provoke tight bundling and precipitation (Coleman et al., 2006). Surface modification such as chemical functionalization allows homogeneous dispersion in these polar solvents. One of the most common functionalizations of carbon nanotubes is carboxylic acid functionalization. Broken hybrid carbon bonds on carbon nanotubes are susceptible to strong acids. By creating and exploiting existing defect sites, through exposure to acids, along the external wall of carbon nanotubes and at their capped ends, one can form carboxylic acid functional groups bonded to carbon nanotube sidewalls. This functionalization greatly increases their dispersibility in many common polar solvents (Liu et al., 1998). While many researchers subject carbon nanotubes to this functionalization, the degree to which the carbon nanotubes are functionalized, and subsequently how varying percent functionalizations affect CNTs and the materials to which they are added, is rarely determined.

2.6 The Incorporation of Carbon Nanotubes into Polymer Nanocomposite Membranes

2.6.1 Strength Enhanced Membranes

Much attention in the past decade has been given to polymer nanocomposites. The addition of small amounts of nanoparticles to polymer matrices as nanofillers has profound effects on the properties of these materials. These include increases in polymer nanocomposite stiffness (Kim et al., 2006), strength (Hou et al., 2009a), thermal stability (Han and Fina, 2011), barrier properties (Shawky et al., 2011a), and electrical properties (de Lannoy et al., 2012). The relative size of nanoparticles compared to polymer chains is important for understanding the effects of NPs on polymers due to the enormously larger chain-particle interface area in the case of nanocomposites compared to micro-composites (Jancar et al., 2010). Polymer nanocomposites formed from the addition of carbonaceous nanoparticles, specifically carbon nanotubes (CNTs), dominate much of recent research (Coleman et al., 2006)(Moniruzzaman and Winey, 2006)(Sahoo et al., 2010). The aim of CNT-polymer nanocomposites is to improve polymeric materials by capitalizing on the unique properties of CNTs, which include extremely efficient load transfer (Falvo et al., 1997) and resistance to shear (Ruoff and Lorents, 1995), as well as unparalleled electrical conductivity (Ebbesen et al., 1996). Several groups have shown great benefits from functionalized CNTs to some polymers primarily poly(vinyl alcohol) (PVA)(Shaffer and Windle, 1999)(Ni et al., 2006)(Lin et al., 2003)(Hou et al., 2009a) , polysulfone (PSf) (Xie et al., 2005b) (Sahoo et al., 2010) (Choi et al., 2006)(Lin et al., 2007), and polyethersulfone (Daraei et al., 2013). There are many proposed applications for such nanocomposites and membrane and thin film technology is among those that offer great promise (Daraei et al., 2013)(Vecitis et al., 2011a)(de Lannoy et al., 2013a).

Polysulfone (PSf) is one of the most widely used polymers to make ultrafiltration membranes; nevertheless it suffers from a few key negative characteristics (Geise et al., 2010)(Tweddle et al., 1983). PSf is a hydrophobic polymer with relatively low tensile strength. Hydrophobic membranes resist water permeability, which limits high water flux. Further, hydrophobic membranes are typically more susceptible to biofouling than hydrophilic membranes (Knoell et al., 1999)(Ostuni et al., 2001). Secondly, polymers with low tensile strength are susceptible to breakage from operational stresses including applied high pressures and vibrational shear stresses commonly found within hollow fiber modules (Gijsbertsen-Abrahamse et al., 2006)(Childress et al., 2005)(Tsai et al., 2001).

CNTs can potentially improve the properties of PSf membranes by incorporating them into PSf solutions as a composite. Even in quantities as low as 0.1% by weight of the final polymer membrane, functionalized or chemically tailored CNTs offer the opportunity to alter various membrane properties including surface chemistry (Choi et al., 2006), pore size (Celik et al., 2011), tensile strength (Hou et al., 2009a), solute rejection (Shawky et al., 2011a), and polymer crystallinity (de Lannoy et al., 2012). Of particular interest, Choi et al. prepared MWCNTs/PSf blend membranes by the immersion phase process. MWCNTs were surface functionalized using strong acids before blending them into the PSf polymer solution, using NMP as the solvent for the casting solutions. Due to the hydrophilic nature of the functionalized MWCNTs, the surface of the MWCNTs/PSf blend membranes appeared to be more hydrophilic than membranes made from PSf alone (Choi et al., 2006).

The state of dispersion of nanoparticles in the polymeric matrix has a large impact on the nanocomposite material. Forming uniform, stable dispersions of nanoparticles in polymer matrices is a difficult task and often results in wildly varying properties from systems composed of the same materials but formed in different ways (Jancar et al., 2010)(Akcora et al., 2009). The unique properties of CNTs, for example, are

most readily exploited when they are homogeneously dispersed throughout polymer mixtures (Xie et al., 2005a); a feat that provides significant challenges since CNTs bundle tightly and are highly insoluble due to the prevalent van der Waals interactions along their length. Research has been directed towards CNT dispersion in solvents and polymers (Lin et al., 2003)(Hu et al., 2007)(Grossiord et al., 2006) including sonication of CNTs prior to mixing with polymers (Huang et al., 2002) and chemical sidewall-functionalization of CNTs to encourage debundling and enhance hydrophilicity (Wang et al., 2005).

The most common and effective CNT functionalization is carboxylation (Liu et al., 1998). Carboxylic functionalization of CNTs begins with either breaking sp^2 hybrid carbon bonds along the sidewalls or capped ends of CNTs, or by exploiting existing broken bonds found thereon. Exposing broken hybridized carbon bonds to strong acids oxidizes them and forms carboxylic acid functional groups on CNTs. This functionalization greatly increases CNT dispersibility in many common polar solvents (Liu et al., 1998). The degree to which CNTs are functionalized is rarely determined, despite the prevalence with which many researchers subject CNTs to this functionalization. Subsequently, very little research investigates how varying the degree of functionalizations affects the properties of CNTs and their composites. Only recently, Fairbrother and others have thoroughly investigated the effect of different methods of carboxylation on CNTs (Wepasnick et al., 2011). Investigations are absent into the effects that greater or lesser degrees of carboxylation have on the properties of polymers, in particular on polymeric membranes.

2.6.2 Electrically Conductive Membranes

Electrically conducting polymers have potential to greatly enhance a wide variety of fields (Hall, 2003). Numerous applications including electrostatic materials, electromagnetic shielding (Angelopoulos, 2001), artificial nerves (Hadlock et al.,

1998), chemical/thermal/biochemical sensors (Janata and Josowicz, 2003)(Osada and De Rossi, 2000)(Adeloju and Wallace, 1996), organic solar cells (Nalwa, 2001), light emitting diodes (Pei et al., 1996), selective membranes (Price et al., 1999)(Biesheuvel and van der Wal, 2010), and bio-resistant coatings (Vecitis et al., 2011b), to name a few, can all be realized and greatly improved with conductive polymers. One area of research, in particular that can benefit significantly is membrane science.

Polymeric membranes are ubiquitous. They are central to a wide variety of fields that span the gamut from separation of pharmaceutical compounds to filtration of ions in reverse osmosis as described in detail above (Van der Bruggen et al., 2003)(Ulbricht, 2006). Despite their wide applicability, however, they are plagued by their tendency to foul due to the attachment and proliferation of bacteria (Chen et al., 2010). A long-active area of research in membrane science is the development of novel strategies to overcome biofouling (Lee et al., 2011). Solutions developed have included chemical (the use of caustic cleaning agents to destroy adhered biofilms), steric (Ulbricht and Belfort, 1996) and electrostatic (Reddy et al., 2003) (membrane surface modification to improve resistance to bacterial attachment) approaches, none of which are entirely effective (Chen et al., 2010).

It has been suggested that small, applied electrical potentials on electrically conductive surfaces can prevent the growth and proliferation of biofilms (Perez-Roa et al., 2006)(Liu et al., 2012) and it has been shown in several experiments than electrically charged surfaces can cause significant detrimental effects to bacteria and viruses, hindering their biofouling capability (van der Borden et al., 2004)(Shim et al., 2011). It has been further hypothesized that applying a positive bias creates an oxidizing environment for the bacteria, which increases bacterial surface mobility and prevents bacteria from attaching. A negative bias creates a repulsive electrostatic force between the similarly charged bacteria and the surface. Applying an alternating electrical potential to a surface efficiently prevents bacteria from forming a biofilm

(Hong et al., 2008). Thus, an electrically conducting membrane has the potential of solving the biofouling challenge. Bacterial attachment and biofilm formation are common in numerous applications outside of membrane science ranging from the use of medical implant devices to nautical shipping (Flemming, 2002)(Greenberg et al., 1999)(Matsunaga et al., 1998). The use of small, pulsed electric currents and/or voltage to prevent bio-attachment has been found to be efficacious in these applications (van der Borden et al., 2004)(Schoenbach et al., 1997)(Nakayama et al., 1998)(Yoon et al., 2011). Passing a current through a ship's hull or a metal cathode is simply achieved. The same approach has not been applied to polymeric MF, UF, NF or RO membranes due to the highly insulating nature of polymers.

Electrically conducting polymers have been proposed as potential materials for current-carrying water-treatment membranes (Price et al., 1999)(Ding et al., 2003)(Loh et al., 1990)(Mansouri and Burford, 1994). However, traditional conducting polymers, such as polypyrrole, are notoriously difficult to process; these polymers are not readily soluble in common solvents and their glass transition temperature is often much higher than their burning point. As a result, these polymers cannot be melt-processed, or easily stretched, molded, or precipitated into membranes as can be done with most other plastics (McCullough, 1998). Methods have been developed to overcome these limitations (Mansouri and Burford, 1994), but none are sufficiently satisfactory as the final membranes made from these materials suffer from low flux, poor separation characteristics, brittleness, and sometimes low conductivity (Price et al., 1999)(Ding et al., 2003)(Loh et al., 1990) (Mansouri and Burford, 1994) (McCullough, 1998) (Huang et al., 1989). Despite their highly conductive nature and some considerable advances, membranes made from these polymers to date appear to be relegated to niche applications (Wallace et al., 2003).

The electrical conductivity of carbon nanotubes suggests that these materials may be candidates to overcome the innate resistivity of polymers (Ebbesen et al.,

1996). Many CNT functionalizations have been developed to be specifically compatible with a wide variety of polymers (Lin et al., 2007). While polymeric materials suffused with sufficient CNTs to overcome the percolation threshold show reduced resistivity by several orders of magnitude, the conductivity of these composites is limited by the insulating nature of the polymers (Koning et al., 2006). Resistivities of polymer-carbon nanotube composites are frequently as high as $10^4 S/m$ (Winey and Moniruzzaman, 2006). Recently, it has been reported that electrically conducting carbon nanotubes (CNTs), deposited on a support layer in a dead-end configuration, are capable of bacterial inactivation once an electric bias is applied (Vecitis et al., 2011b)(Gao and Vecitis, 2011). CNTs have also been shown to have anti-bacterial properties, as demonstrated by Elimelech and others (Kang et al., 2008), which could have positive implications for membranes composed of CNT-polymer composites (Celik et al., 2011). The direct deposition of CNTs onto a support membrane avoids the insulating nature of polymers altogether by dry-depositing CNTs under pressure onto the surface of a support membrane (Vecitis et al., 2011a) to yield a highly conductive membrane. However, UF, NF, and RO membrane processes rely on a cross-flow, where feed water flows in parallel to the membrane surface. These carbon nanotubes are not bound in any way to the membrane surface. This deposited layer is thus highly unstable and will easily wash off the support in the cross-flow or during back-flushing. To the best of our knowledge, there is no report of any stable electrically conductive MF, UF, NF, or RO membranes composed of carbon nanotubes, let alone the application of these membranes to the successful prevention of biofilm formation.

In several of the primary membrane regimes - MF, UF, NF, and RO - CNTs can improve membrane performance, longevity, and efficacy through improved strength, higher permeability, control over membrane selectivity, and resistance to biofouling. With these perspectives, CNTs offer the potential for multiple improvements over

the current state of technology.

3

Methods

3.1 Methods for Fabricating Polyvinyl Alcohol - CNT Membranes

These methods describe the fabrication, characterization, and membrane testing of electrically conductive polyvinyl alcohol (PVA) carbon nanotube composite ultrafiltration thin film membranes.

3.1.1 Materials

Carboxylated multiwalled carbon nanotubes were purchased from www.cheaptubes.com (length $10 - 30\,\mu m$ and radius $< 8\,nm$) and were determined to be functionalised to 3.86 w/%. Polyvinyl alcohol was purchased from Fischer Scientific (M_w 100 000). Hydrochloric acid (36.5%–38%) and succinic acid (ACS $>$ 99.0%) were purchased from Sigma Aldrich. Cellulose nitrate (CN) membranes with pore size $0.1\,\mu m$ were purchased from Sartorius Inc.

3.1.2 Membrane Fabrication

Carboxylated multiwalled carbon nanotubes were thoroughly dispersed in DI water to a 1 w/% concentration through utlrasonication using an ultrasonicator probe

(Branson Ultrasonics, Danbury, CT) for 30 minutes with a power delivery equivalent to 70 W in solution. The carboxylation of the carbon nanotubes ensured that they remained homogeneously suspended in solution. 1 w/% PVA was dissolved in DI water for 6 hours at $90^{\circ}C$. The PVA was allowed to cool to room temperature, then $5\,mL$ of PVA was mixed with a certain amount of the carbon nanotube solution to achieve the desired weight percent of CNTs to PVA. For example, if 10% CNTs with respect to PVA was desired and $5\,mL$ of the 1% PVA solution was used, then $0.5\,mL$ of the 1% CNT solution would be added for a total of $5\,mg$ of CNTs in solution. The PVA-CNT mixture was then sonicated with a microtip for 1 minute with a power delivery equivalent to 26.2 W in solution in intervals of 2 seconds on and 5 seconds off to prevent the solution from foaming. Additionally, sonication was performed in an ice bath to avoid overheating. A solution of 0.1% succinic acid was made in DI water and enough succinic acid was added to the fully sonicated PVA-CNT mixture such that PVA cross-linking was maintained at 20% as computed using equation 4.1 found in Chapter 4. Subsequently, enough hydrochloric acid was added to the solution to achieve a concentration of 2 M in solution. HCl acted as a catalyst to the cross-linking reaction. This mixture was added to the top of a $47\,mm$ support cellulose nitrate membrane held in a glass vacuum filtration flask and allowed to react for at least 30 minutes. After reaction, the vacuum was turned on and the solution filtered through the membrane with all the CNTs retained on the surface while the excess PVA, all the HCl and water filtered through the membrane. This procedure ensured that the minimum amount of PVA remained on the surface of the membrane, and around the CNTs, to prevent them from being fully insulated by the PVA mixture. Further, this reduced the contact time of HCl with the membrane to minimize potential damage to its surface. The membrane was removed from the filtration flask, laid on a non-woven fabric taped to a glass plate and cured in an oven at $100^{\circ}C$ for varying amounts of time with the minimum optimal amount of

time being 15 minutes. The cross-linked PVA-CNT membranes were then removed from the oven, allowed to cool at room temperature and then soaked and washed in DI water over night before use.

3.1.3 Surface Imaging

Polymer samples were sputter coated with Pd/Au atoms to a thickness of $10\,nm$ using an Anatech Hummer 6.2 vacuum sputter system. The coated samples were then affixed to SEM stubs using copper tape and analyzed with a FEI XL30 SEM-FEG scanning electron microscope at $15\,kV$ and varying magnifications under both normal imaging mode and ultra-high resolution (UHR).

3.1.4 Electrical Conductivity

Conductivity of the membranes was measured in two ways. Firstly the membranes were cut into long thin strips with dimensions of 1 cm by 4 cm. The probe tips of a laboratory grade multimeter-voltage detector were placed at three different distances along the length of the membranes at 3, 2 and 1 cm apart. The resistance readings from the multimeter along with the membrane dimensions were used to calculate the resistivity of the membranes. These measurements were compared with more accurate measurements using a Signatone S–302–4 Four Point Resistivity Probe Station connected to a Keithley 4200–SCS Parametric Analyzer. The four-point probe calculates the resistivity between two points by accurate knowledge of the spacing between the probe tips and the thickness of the sample to be analyzed. The four-point probe slightly punctures the coatings it measures and takes a measurement across the entire cross-section of the film, effectively measuring an average cross-sectional electrical conductivity throughout the entire film thickness.

3.1.5 Surface Hydrophilicity

Contact angle measurements were performed with a Krss EasyDrop drop shape analysis system with digital goniometer and camera connected via DSA1 software. A minimum of 15 measurements was made per type of membrane and the highest and lowest values were discarded to account for error. Contact angle of more hydrophobic membrane films were measured using the sessile drop method, while for those membranes that were especially hydrophilic, captive bubble method was used to determine contact angle.

3.1.6 Flux and Rejection

Pure water flux was measured using a $250\,mL$ Strelitech stainless steel stirred cell. The membranes were compacted with $500\,mL$ of water over 1 hour at a pressure of $90\,psi$. Water flux testing was conducted under pressures of $20, 40, 60$ and $80\,psi$ and flux measurements at each pressure were conducted every ten seconds for 1 minute. The average of those six measurements was used to compute the flux at that one pressure.

Rejection experiments were performed with the same Strelitech stirred cell. $2000ppm$ PEG solutions of three different molecular weights were made for rejection experiments and $100\,mL$ of the total $250\,mL$ in the stirred cell was filtered through. The concentration of PEG in the permeate was measured using a Total Organic Carbon Analyzer (TOC).

3.1.7 Crystallinity

Crystallinity of the polymer was determined through x-ray diffraction (XRD) using a Panalytical XPert PRO MRD HR X-Ray Diffraction System. The polymer samples were mounted on a flat backing and crysallographic data was obtained with 2θ phase analysis.

3.1.8 Cross-Linking

Evidence for cross-linking between the polyvinyl alcohol and the carboxylated carbon nanotubes was gathered from FTIR spectra. The FTIR spectra of membrane films formed from pristine CNTs mixed with PVA were compared to the spectra of coatings formed from carboxylated CNTs mixed with PVA and reacted with HCl. The films that lacked cross-linking were predominantly composed of CNTs as the vast majority of the PVA filtered through the membrane, while those films that were cross-linked contained both CNTs and PVA and the corresponding distinctive and ubiquitous hydroxyl group on the chain of the PVA molecule. As cross-linking was controlled to 20% the PVA chains contained large amounts of hydroxyl groups.

3.2 Methods for Fabricating Polyamide-CNT Membranes

These methods describe the fabrication, characterization, and membrane testing performed for the highly electrically conductive tight NF thin film membranes composed from the reaction of the monomer constituents of polyamide (PA) with hydroxylated carbon nanotubes.

3.2.1 Membrane Fabrication

Electrically conducting tight NF membranes were fabricated from carboxylated multi-walled carbon nanotubes (CNTs) reacted with polyamide to form a highly salt-rejecting thin film. CNTs ($0.1\,mg/mL$) (www.cheaptubes.com, Brattleboro, VT; $< 8\,nm$ diameter; $10 - 30\,\mu m$ length, 3.8% carboxylation) were added to deionized water (DIW) together with sodium dodecylbenzene sulfonate ($1\,mg/mL$). This suspension was sonicated with a sonication probe (Branson Ultrasonics, Danbury, CT) for 5 minutes at 70 Watts, in 3 second pulses interspersed by 3 seconds. This was followed by 2 minutes of continuous sonication in a sonication bath to ensure that all the CNTs were well suspended. Once the CNTs were homogeneously suspended in

solution, $30\,mL$ of the CNT suspension was pressure filtered onto a polyethersulfone (PES) support membrane ($0.1\,\mu m$; Strelitech, Kent, WA, $47\,mm$ diameter coupons, $274 \pm 13\,mg$). The suspension of CNTs was deposited on the surface of the member so produce a deposited CNT layer with a final content of $3\,mg$ per membrane ($274 \pm 13\,mg$). This membrane surface contained remnant surfactant so DI water was pressure filtered through the deposited layer several times to wash the surface free of surfactant. To form the salt rejecting thin-film, we followed established PA thin film membrane forming techniques Cadotte et al. (1981), Abu Tarboush et al. (2008).

In short, the CNT covered PES support was immersed in a 2.0% (w/w) aqueous solution of m-phenylenediamine (MPD) for 30 seconds, slightly dried, and then immediately immersed in a 0.15% (w/w) solution of trimesoyl chloride (TMC) dissolved in hexane for 30 seconds. The membranes were then air-dried, cured in an oven, and stored in DIW until used. Plain PA membranes were formed in the same manner, without the CNT deposited layer. Control 3 membranes were formed in the same manner as highly conducting tight nanofiltration membranes, with added electrical resistivity to their surface. CNT deposition followed the same procedure as with ECPNC membranes, but soaking in MPD was done for 5 minutes instead of 30 seconds, followed by less rolling and wicking, and then immersion in TMC for 5 minutes, as opposed to 30 seconds. This longer immersion time formed a much thicker polyamide thin film on the surface of the membrane and as a result a much more electrically insulating surface.

3.2.2 Membrane Characterization

The membrane material was characterized by several methods. For Scanning Electron Microscopy (SEM; FEI XL30 SEM-FEG), bare membranes were dried in a desiccator and then coated with $5\,nm$ of gold particles in a vacuum sputter coater (Den-

ton Desk IV) before being analyzed under SEM. Transmission Electron Microscopy (TEM; FEI Tecnai G^2 Twin TEM) was used to analyze thin-film cross-sectional morphology. For TEM studies, membranes were cast in SPURR resin and then microtomed to 60 nm slices (Ultra Microtome, Ultracut). These thin cross-sections were mounted on TEM lacey copper grids and analyzed under TEM. Attenuated Total Reflectance Fourier Transformed Infrared Spectroscopy (ATR-FTIR; Bruker Tensor 27 spectrometer fitted with a Pike Technologies Single Reflection ATR accessory and a DTGS detector) was used to determine bonding behavior. ATR-FTIR Spectra of the membrane were recorded using 64 co-added scans and a mirror velocity of 10 kHz at a resolution of 4 cm^{-1}. Four-point conductivity probes (Signatone S–302–4) were utilized to measure electrical sheet resistance. Contact angle instrumentation (Krüss Easy Drop Shape Analysis System DSA25) was used to elucidate surface hydrophilicity.

3.2.3 Membrane Permeability and Salt Rejection

Salt rejection and membrane permeability experiments were conducted using the novel cross-flow cell shown in figure 3.1. Two electrical conditions were evaluated in all experiments no charge and a 1.5 V square wave that alternated potential between positive and negative signals applied for a period of 1 minute each ($\pm 1.5V$ at 16.7 mHz). Two NaCl solutions were used to evaluate rejection. The first solution was 1 g/L NaCl in DIW. The second solution used was a 10% Lysogeny broth (LB; 10 g/L tryptone, 5 g/L yeast extract, 10 g/L NaCl). In all cases the membranes were allowed to compress for 120 minutes with DIW at 100 psi. Following compression, the salt solutions were introduced to the membrane, also at 100 psi, with a flow rate of 100 mL/min. After 4 hours of operation, permeate conductivity was measured to determine salt rejection, and flux measurements were taken every 5 minutes for an hour.

3.3 Biofouling Testing

These methods describe the development of a cross-flow cell with electrical leads and the long-term testing of the anti-biofouling capabilities of the previously described electrically conductive tight NF thin film membranes, under the application of an external alternating potential.

3.3.1 Electrode Modified Cross-Flow Cell

A polycarbonate, custom built, cross-flow filtration unit was used to measure salt rejection and membrane permeability, and was employed for all biofouling experiments including all control experiments. The filtration unit was designed with built-in insulated steel electrodes capable of delivering an electric charge to the membrane thin film surface (effective membrane surface area was 21.6 cm^2) and to a counter nonreactive platinum electrode located at the top of the channel, 5 mm above the membrane surface, as shown in figure 3.1 During operation, a pressurized feed stream was passed over the membrane. This feed stream was separated into a permeate and a retentate stream. The former was collected to measure flux and rejection, while the latter was recycled to the feed stream.

3.3.2 Membrane Biofouling

All processes were kept sterile to avoid contamination, unless otherwise specified. *Pseudomonas Aeruginosa* (*P. Aeruginosa* strain PAO1 ATCC number 47085), model biofouling bacteria Herzberg and Elimelech (2008) were take from frozen stock (stored at $-80°C$) and spread on Petri dishes in three diluted tracks. Bacterial colonies were grown for 48 hours in an incubator at $35°C$. After 48 hours, a single colony was removed and added to a flask containing 100% LB media. Bacteria grew in this media for 48 hours at $35°C$. The bacterial concentration was measured by UV-Vis absorption. The absorption intensity value was compared against a standard curve

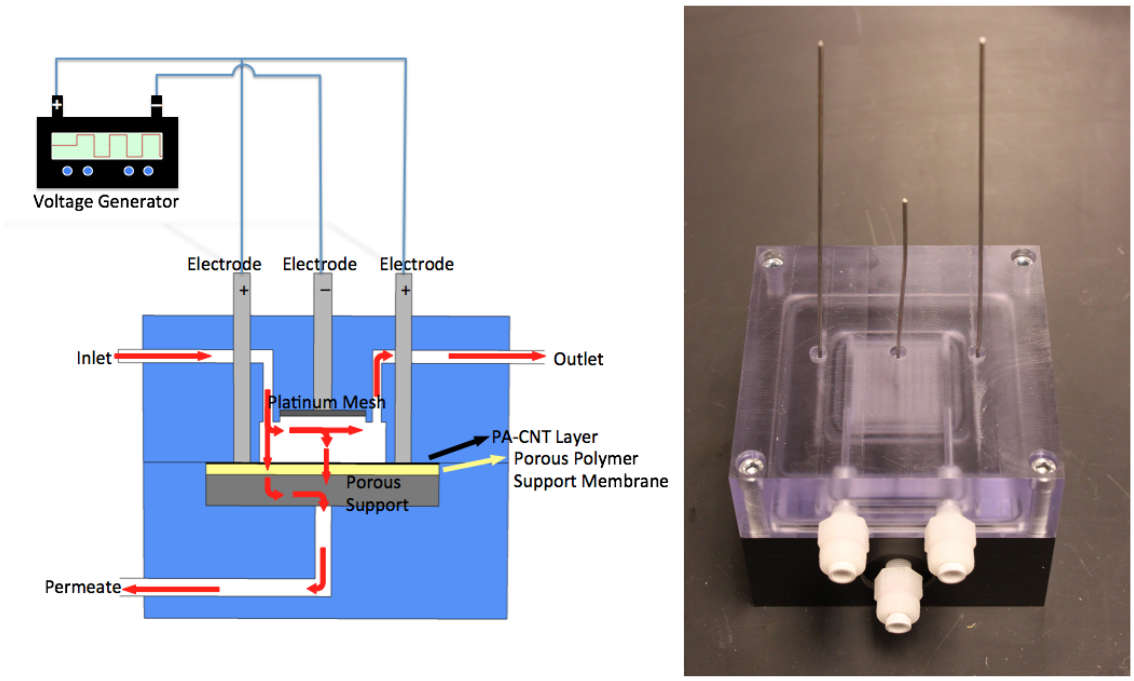

FIGURE 3.1: (Left) A schematic of the pressurized vessel showing the path of fluid flow. (Right) The cross-flow cell with insulated electrodes that connect the membrane to the voltage source.

that was developed from series plate counting. Absorption measurements were thus used to determine bacterial concentration in the flask of *P. Aeruginosa*.

Membranes in the modified cross-flow cell were compressed with DI water for 24 hours, followed by filtration of 10% LB media for a few hours. From the determined concentration measurements, the bacterial solution was diluted to 10^7 cells/mL in this 10% LB media. Filtration of this media across the membrane occurred immediately upon addition of the bacterial solution to the 10% LB media. In each biofouling experiment, feed-water containing 10^8 CFU/mL of *P. Aeruginosa* in 10% LB media was used to challenge the membrane. These bacterial concentrations are significantly larger than those found in traditional wastewater treatment plants and over three orders of magnitude greater than those typical found in environmental conditions. The retentate solution was recycled into the feed and the permeate was

collected to measure flux and salt rejection. The permeate was collected throughout the experiment and not recycled into the feed. Flux measurements were automated so that they were collected continuously throughout the experiment. Bacteria grew unchecked for the duration of the experiment so that final bacterial populations after several days growth were consistently higher than 10^{12} CFU/mL. Desalination of the feed was conducted up to 90% recovery over 3–6 days, with no feed dilution. This resulted in highly concentrated bacterial feed solutions, representing extreme operating conditions.

Highly conducting tight nanofiltration membranes were inserted into the novel cross-flow cell to simultaneously filter and desalinate bacterially contaminated waters to demonstrate the biofilm inhibition capabilities of these membranes when an external electric potential is applied. In addition, we conducted three different control experiments (all performed in triplicate) to desalinate these bacterially contaminated waters. Three control conditions were evaluated: 1. plain PA membranes without an applied potential, 2. ECPNC membranes without an applied potential, and 3. CNT-PA membranes formed with an electrically resistive surface layer with an applied potential. In each experiment and control, membranes were securely positioned in the cross-flow chamber ensuring that the insulated electrodes were in good contact with the membrane. In each biofouling experiment, membranes were exposed to a cross-flow of the previously described extreme conditions highly bacterially contaminated waters in LB media. The experiments were allowed to continue until the water flux had decreased by $45 \pm 3\%$ over the initial flux. At this point, a flushing procedure was carried out. Flushing of the membrane was done thusly: the flow across the membrane was turned off, which released the pressured across the membrane. The retentate valve was opened completely so that when the flow was increased again, there would be no external hydraulic pressure across the membrane and all the feed flow would go into the retentate (which was recycled back to the feed). In

this configuration the feed flow was increased to high velocities twice the velocity of that used during desalination of the feed and maintained at this high velocity for 1 minute. After this 1 minute of flushing, the flow across the membrane was turned off and the retentate valve was partially closed back to its original valve position so that when the feed flow was increased again, now there would be a pressure exerted across the membrane and resultant permeate flow. The feed flow was then turned up to the original velocity and desalination of the feed continued until once again the permeate flux declined to 45% of the original value. As shown in the controls, the flux decreased to 45% of the original value immediately. In this case, desalination was permitted to continue for approximately 2 hours and the flushing procedure was repeated. In the case of the electrically conducting nanocomposite membrane with the electrical potential applied, the flux decreased to 45% of its original value only after several days desalination. In total, this procedure was repeated three times consecutively for each membrane.

3.3.3 Biofilm Analysis

Membrane biofouling was quantified as irrecoverable loss-of-permeate flux and further characterized by SEM, fluorescence microscopy of the membrane surface, and PCR detection. Membranes used in biofouling experiments were gently washed in an indirect stream of DIW after the completion of the experiment. For SEM analysis, membranes were immobilized in a 15% gluteraldehyde solution for 24 hours, and then dehydrated in stages with increasing concentrations of ethanol before they were exposed to SEM. SEM was used to analyze surface morphology, bacterial colony distribution, and presence of EPS. For fluorescence microscopy, membranes were stained with DAPI stains and then imaged under fluorescence microscopy. DAPI stains bacterial DNA indicating the presence or absence of bacteria on the membrane. Biofilm growth on the membrane filter was verified as *P. Aeruginosa* through

PCR detection. We isolated bacterial DNA through standard methods from swabs of the biofilms. Primers VIC1 (5TTCCCTCGCAGAGAAAACATC 3) and VIC2 (5CCTGGTTGATCAGGTCGATCT 3) were used to target the GDP mannose dehydrogenase (algD) gene in *P. Aeruginosa* Da Silva et al. (1999). Reactions conditions were similar to Da Silva Filho, et al. with a thermocycler run of 5 min at $94°C$ followed by 30 cycles of $94°C$ for 60 s, $60°C$ for 60 s, and $72°C$ for 60 s, with a final extension of $72°C$ for seven minutes.

3.4 Methods for Fabricating Polysulfone-CNT Membranes

These methods describe the carboxylation of multiwalled carbon nanotubes, the fabrication, characterization, and membrane testing of bulk mixed polysulfone (PSf) carbon nanotube membranes, and the quantification of leaching and loss of CNTs from the membrane matrix.

3.4.1 Materials

Pristine multiwalled carbon nanotubes (pCNT) and 2.56% carboxylated CNTs were purchased from CheapTubes.com (www.cheaptubes.com) and used and functionalized without further purification ($> 95\,wt\%$). The diameter of these tubes was listed as $8-15\,nm$, and their length was listed as $100\,\mu m$. Polysulfone (PSf) and Polyvinyl pyrrolidone (PVP) were purchased from Sigma-Aldrich and had molecular weights of 35 kDa and 40 kDa respectively. Dimethyl formamide (DMF), purchased from Sigma-Aldrich as well, was used as a solvent for the polymers. De-ionized water (DIW) was used as the non-solvent in the immersion precipitation non-solvent bath. Trace metal grade nitric acid ($67-70\%HNO_3$) was purchased from Fischer Scientific, extra pure sulfuric acid ($96\%H_2SO_4$) was purchased from Acros Organics, hydrochloric acid was purchased from Sigma Aldrich ($36.5-38\%$ HCl), sodium hydroxide was purchased from Fischer Scientific (N/100, 0.0101–0.0099 N $NaOH$), and sodium

hypochlorite ($6.15\% NaOCl$) was purchased as standard household Clorox Bleach.

3.4.2 Carbon Nanotube Carboxylation

Carbon nanotubes were carboxylated to varying %-carboxylation following the traditional nitric and sulphuric oxidation process (Liu et al., 1998). Briefly, CNTs were heat refluxed for varying amounts of time in nitric and sulphuric acid. A dilute slurry was separated by centrifugation, and then dialyzed until the solution reached $pH 5.6 - 6$. The suspension of CNTs was then frozen at $80^{\circ}C$ and sublimated in a freeze drier (LabConco FreeZone 2.5 Plus).

3.4.3 Analysis of CNTs

Transmission electron microscope (TEM, FEI Tecnai G^2 Twin) images of pristine- and carboxylated-CNTs were taken to demonstrate the CNT debundling effects of functionalization. Samples were imaged on lacey carbon copper grids. X-Ray photoelectron spectrometer (XPS, Kratos Analytical Axis Ultra) spectra of pristine and functionalized CNTs were used to determine the number and type of oxygen bonds on the CNTs. From the percentage of oxygen on the CNT surface, the CNT %-carboxylation was determined.

3.4.4 Formation of Membranes

Polymer nanocomposite solutions for membrane formation were prepared in DMF with $17\, wt\%$ PSf and $6\, wt\%$ PVP with respect to the total volume of solution and $0.5\, wt\%$ CNTs with respect to the polymer constituents. Membranes containing either pCNTs or CNT-COOHs with a range of carboxylation amounts were suspended in DMF before dissolution of the polymers. CNTs were added to DMF, cooled in an ice bath to $8^{\circ}C$, then probe ultra-sonicated (Misonix Ultrasonic Liquid Processor) in intervals of 3 seconds interspersed by 3 seconds, to avoid localized heating, for a total of 1 hour at a power delivery of 70 Watts. Once fully suspended, PVP was added

to the CNT suspension and stirred for 30 minutes until fully dissolved. Mixing PVP with CNTs wraps CNTs in PVP. Following PVP wrapping, PSf was added to the CNT suspension. The mixture was heated to $60^{\circ}C$ and stirred continuously until the PSf was fully dissolved and the mixture was homogeneous. The final solution was then cast with a casting knife set to a distance of $250\,\mu m$ away from a glass plate. The cast solution was allowed to equilibrate and de-gas on the glass plate before immersion in a known volume of DIW, in which the membrane precipitated and released from the glass plate. The membrane stayed in the bath for 20 minutes, was then transferred to fresh DI water, stored at $4^{\circ}C$ for 24 hours, and then characterized and tested.

3.4.5 Characterization of Membranes

Membrane samples were prepared for Scanning electron microscope (SEM, FEI XL30 SEM-FEG) imaging by sputter coating (Hummer 6.2 Vacuum Sputter) with Au atoms to a thickness of $5\,nm$. SEM images were taken using several different magnifications and beam strengths.

Stress-strain measurements (TA Instruments RSA III Micro-Strain Analyzer) of strips of the polymer membranes were performed. At least 15 strips were measured for each polymer membrane composition to produce an average Youngs Modulus of that particular material. The highest and lowest values were discarded, and the remaining measurements were averaged.

A minimum of 15 contact angle (Krüss Easy Drop goniometer) measurements were performed and recorded for each membrane analyzed. The highest and lowest values were discarded and an average of the remaining angles was reported.

Flux measurements (Strelitech steel pressure dead-end cell) of all membranes were performed with DI water at a minimum of four different pressures ranging from $70\,kPa$ to $700\,kPa$.

UV-Vis measurements were used to analyze the CNT content of the non-solvent bath before and after membrane precipitation. UV-Vis background curves were generated for pure DI water, PVP dissolved in DI water, and diluted DMF in DI water. Control curves were produced for suspended CNTs at varying concentrations in both DI water and diluted solutions of DMF. CNTs do not have a specific absorbance peak in the wavelength range used ($900\,nm - 100\,nm$) however, by controlling for the absorbance signal from the background materials (PVP and DMF) it was possible to correlate the absorbance intensity from CNTs found in the non-solvent bath post-membrane precipitation, to the control curves of dilute CNT suspensions. After precipitation of the membranes, well-mixed samples of the non-solvent bath were analyzed using the UV-Vis spectrophotometer. Compared against the background and control curves, the absorption intensity of each sample obtained was used to determine the amount of CNTs in the non-solvent bath. These control curves area ll presented in Appendix B. UV-Vis intensity comparison was a direct method for detection of CNT concentration in the non-solvent bath. This method was also applied to membrane cleaning solutions of HCl, NaOH, and NaOCl. UV-Vis was used as opposed to TOC, because the organic solvent, DMF, was released during membrane precipitation. The amount of total carbon in the released solvent was several orders of magnitude higher than the amount of carbon from released CNTs. The TOC signal from the organic solvent completely quenched that from the CNTs.

3.5 Methods for Fabricating Sulfonated Polysulfone-CNT Membranes

3.5.1 Materials

Pristine multiwalled carbon nanotubes (pCNT), 3.86% carboxylated CNTs (CNT-COOH), 1.2% amine-functionalized CNTs (CNT-NH2), and 7.0% amine-functionalized CNTs were purchased from CheapTubes.com (www.cheaptubes.com) and used without further purification ($> 95\,wt\%$). The diameter of the pCNTs was listed as

$8 - 15\,nm$ and lengths of $10 - 50\,\mu m$, the diameter of the CNT-COOHs was listed as $< 8\,nm$ and lengths of $10 - 30\,\mu m$, the diameter of the $CNT - NH_2$s was listed as $< 20\,nm$, and lengths of $1 - 12\,\mu m$. Polysulfone (PSf) and Polyvinyl pyrrolidone (PVP) were purchased from Sigma-Aldrich and had molecular weights of 35 kDa and 40 kDa respectively. N-methyl Pyrrolidone (NMP), purchased from Sigma-Aldrich as well, was used as a solvent for the polymers. De-ionized water (DIW) was used as the non-solvent in the immersion precipitation non-solvent bath. Chloroform, purchased from EMD, trimethylsilyl chlorosulfonate, sodium methoxide, and ethanol, all three purchased from Sigma-Aldrich, were all used to sulfonate the polysulfone and were used as purchased.

3.5.2 Carbon Nanotubes

3.5.2.1 Analysis of CNTs

Transmission electron microscope (TEM, FEI Tecnai G2 Twin) images of pristine- and carboxylated-CNTs were taken to demonstrate the CNT debundling effects of functionalization. Samples were imaged on lacey carbon copper grids.

3.5.3 Polysulfone

3.5.3.1 Sulfonation of Polysulfone

The polymer, polysulfone (PSf), was sulfonated to a low degree to obtain sulfonated polysulfone (SPSf) in gel form. The sulfonation procedure was obtained from a combination of previous research found in the literature in (Lufrano et al., 2000) and (Baradie et al., 1998). Specifically, the PSf was dissolved in chloroform at room temperature then treated with the addition of trimethylsilyl chlorosulfonate into the polymer solution to produce a silyl sulfonate. The degree of sulfonation is controllable by varying the mole ratio of sulfonating agent and polymer repeat units as well as the rection time between the two components. A low degree of sulfonation was desired,

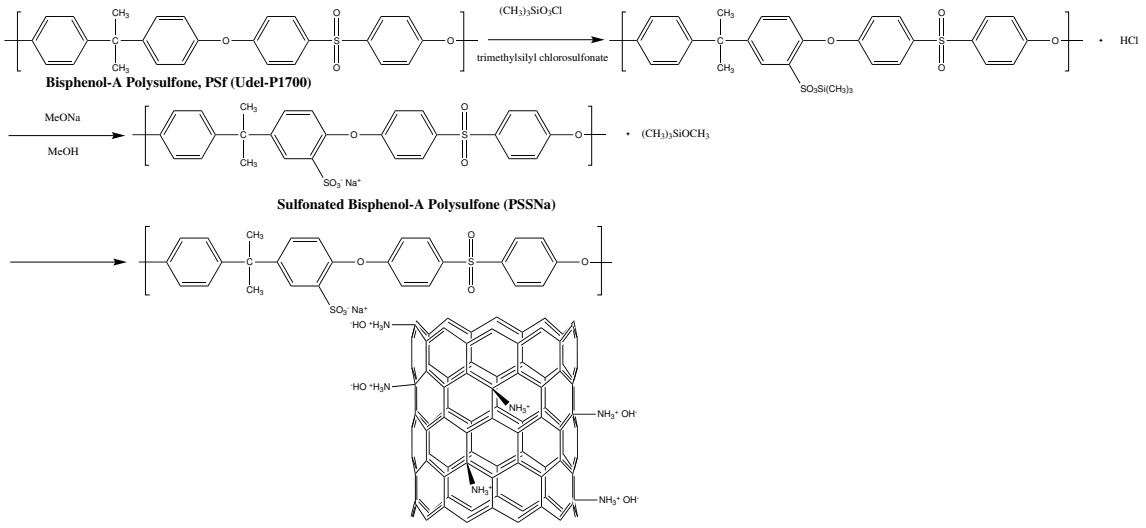

FIGURE 3.2: The reaction scheme for converting polysulfone to the sodium sulfonate form of sulfonated polysulfone. Further, the scheme also indicates the association of the negatively charged carrier groups of the sulfone on the SPSf chains with the positively charged carrier groups on amine-functionalized CNTs.

thus we chose a mole ratio of 0.7 and a reaction time of 24 hours. The reaction was carried out at room temperature. Following reaction, sodium methoxide was used to cleave the silyl sulfonate moieties. Sodium methoxide was added to the reaction vessel and was allowed to react with the solution for 1 hour to yield the final sodium sulfonate form of the sulfonated polysulfone product. This sulfonated polymer solution was added dropwise to a nonsolvent bath of ethanol to precipitate the final product. Thick clods of precipitated polymer were then sieved from the ethanol, washed at least three times in DI water and dried in an oven for at least 48 hours at $100^{\circ}C$ for complete removal of all the remaining solvents and non-solvents.

3.5.4 Membranes

3.5.4.1 Formation of Membranes

Polymer membrane solutions were prepared in NMP with $18\,wt\%$ SPSf and $6\,wt\%$ PVP with respect to the total volume of solution. Nanocomposite solutions for mem-

brane formation were prepared with the same constituents in the same ratios with the addition of carbon nanotubes added either at $0.5\,wt\%$ CNTs or 5.0% CNTs with respect to the polymer constituents. Membranes containing either pCNTs, carboxylated CNTs (functionalized to 3.86%), or amine-functionalized CNTs (functionalized to 1.2% and 7.0%) were dispersed in NMP before dissolution of the polymers. CNTs were added to NMP, cooled in an ice bath to $8^{\circ}C$, then probe ultra-sonicated (Misonix Ultrasonic Liquid Processor) in intervals of 3 seconds interspersed by 3 seconds of rest (to avoid localized heating), for a total of 1 hour at a power delivery of approximately 70 Watts. Once fully suspended, PVP was added to the CNT suspension and stirred for 30 minutes until fully dissolved. Following PVP dissolution, SPSf was added to the CNT suspension. The mixture was heated to $60^{\circ}C$ and stirred continuously until the SPSf was fully dissolved and the mixture was homogeneous. The final solution was then hand-cast with a casting knife set to a distance of $250\,\mu m$ away from a glass plate. The cast solution was allowed to equilibrate and de-gas on the glass plate before immersion in a known volume of DIW (1 L), in which the membrane precipitated and released from the glass plate. The membrane stayed in the non-solvent bath for at least 20 minutes, was then transferred to fresh DI water, stored at $4^{\circ}C$ for 24 hours, and then characterized and tested.

3.5.4.2 Characterization of Membranes

Membrane samples were prepared for Scanning electron microscope (SEM, FEI XL30 SEM-FEG) imaging by sputter coating (Hummer 6.2 Vacuum Sputter) with Au atoms to a thickness of $5\,nm$. SEM images were taken using several different magnifications and beam strengths. Stress-strain measurements (TA Instruments RSA III Micro-Strain Analyzer) of strips of the polymer membranes were performed. Stress-strain measurements were performed for each membrane through all regions of deformation, from linear elastic strain, to inelastic irreversible deformation, until mem-

brane failure and breakage. However, only the linear elastic region was analyzed. At least 15 strips were tested for each polymer membrane composition. The slopes of the linear region, ending at the beginning of the inelastic deformation region, were measured. The transition between elastic and inelastic regions was determined by the R_2 of the linear fit to the elastic region. Data points were included into the fit up until the R_2 dropped below $R_2 = 0.96$. Any data point that started to deviate from this linear fit criterion was deemed to be in the inelastic region of strain. The collection of at least 15 slopes from the linear region was calculated to produce an average Youngs Modulus of that particular material. The highest and lowest values were discarded, and the remaining measurements were averaged.

A minimum of 15 contact angle (Krüss Easy Drop goniometer) measurements were performed and recorded for each membrane analyzed. The highest and lowest values were discarded and an average of the remaining angles was reported.

Flux measurements (Strelitech steel pressure dead-end cell) of all membranes were performed with DI water at a minimum of four different pressures ranging from $70\,kPa$ to $700\,kPa$.

UV-Vis measurements were used to analyze the CNT content of the non-solvent bath before and after membrane precipitation. In an identical procedure as described above, UV-Vis background curves were generated for pure DI water, PVP dissolved in DI water, and diluted DMF in DI water. Control curves were produced for suspended CNTs at varying concentrations in both DI water and diluted solutions of DMF. All of the UV-Vis data is presented in Appendix C, with detailed explanations of the analysis given in there. CNTs do not have a specific absorbance peak in the wavelength range used ($900\,nm - 100\,nm$) however, by controlling for the absorbance signal from the background materials (PVP and DMF) it was possible to correlate the absorbance intensity from CNTs found in the non-solvent bath post-membrane precipitation, to the control curves of dilute CNT suspensions. After precipitation of

the membranes, well-mixed samples of the non-solvent bath were analyzed using the UV-Vis spectrophotometer. Compared against the background and control curves, the absorption intensity of each sample obtained was used to determine the amount of CNTs in the non-solvent bath. UV-Vis intensity comparison was a direct method for detection of CNT concentration in the non-solvent bath. This method was also applied to membrane cleaning solutions of HCl, NaOH, and NaOCl.

4

Results

4.1 Prelude to Findings and Discussions Thereon

4.1.1 Various Strategies for the Inclusion of CNTs within Polymer Matrices

Carbon nanotubes' exceptional properties suggest their advantage as additives to polymer materials. Optimally enhancing polymer materials with carbon nanotubes is a much sought after goal and has been studied by many research groups. Firstly, carbon nanotubes must be processed in one of several ways to get them from their bundled powder phase into a mixture with polymers. Conventionally this is done either by sonicating pristine CNTs in a solvent bath or by chemically functionalizing pristine CNTs in a number of different ways or a combination of the two. Sonicating pCNTs is not particularly effective, and most of the current research efforts focus on a plethora of chemical modifications to carbon nanotubes followed by their homogeneous dispersion in solvents through sonication.

Chemical modifications to CNTs for dispersion into polymers fall under two broad categories, both of which I explore in this dissertation: covalent functionalization and non-covalent exohedral functionalization. Covalent functionalizations are a group of modifications to CNTs that add chemical moieties to their sidewalls and end

groups. This can be achieved either by taking advantage of existing defects along the lengths of CNTs or by breaking select few $\pi - \pi$ bonds along their length. One can then add chemical functional groups at those defect sites, tailored to a specific purpose. Non-covalent exohedral functionalization encompasses any association of molecules with CNTs that does not necessitate breaking $\pi - \pi$ bonds and chemically modifying the CNT sidewalls or end-groups. This type of functionalization includes π-stacking, in which molecules containing localized groups of $\pi - \pi$ bonding can lie flat against CNT sidewalls. The attraction of their mutual π-bonds non-covalently binds these molecules to the sidewalls of CNTs. Another form of non-covalent exohedral functionalization is sidewall wrapping. This is achievable with long molecular chains, such as polymers, that can wrap around the lengths of CNTs.

CNTs, either pristine, covalently functionalized or non-covalently functionalized, can then be associated with polymers to form CNT-polymer nanocomposites, and in particular, nanocomposite membranes. This can be achieved in a number of ways, and three most common or effective ways of producing nanocomposite membranes will be introduced here and explored in detail in this dissertation. These three methods are: 1. covalent bonding of CNTs with polymers, 2. polymer wrapped non-covalent association of CNTs with polymers, and 3. ionic bonding of CNTs with polymers. The results of this dissertation are divided by these three methods of CNT-polymer associations to form three distinct types of nanocomposite membrane. This breakdown of the dissertation is pictorially demonstrated in figure 4.1.

Most simply, CNTs can be blended or bulk mixed with polymers. This can be done with pristine CNTs, in which pCNTs are mixed with solutions of polymers in a solvent(s). Alternatively, functionalized CNTs or polymer-wrapped CNTs can be suspended in solvents, to which polymers are then added. In this way, CNTs are more homogeneously distributed within the polymer. Functional groups can be chosen to suit a certain solvent or polymer system. For example, functional groups

can be added to CNTs that achieve high dispersibility within solvents to encourage the greatest homogeneous dispersion of CNTs within polymers. Additionally, CNT functional groups can be added to favor ionic bonding with existing charged groups on polymers. In this configuration, CNTs exist in small quantities with respect to the polymer, and act as additives to the bulk polymer. Once blended with the polymer, these composite mixtures can be cast as nanocomposite membranes. A second method of associating CNTs with polymers is to covalently cross-link or bind the polymers to the functional groups on the CNT sidewalls in solution. This is done by dispersing functionalized CNTs within a solvent, adding a soluble polymer to the suspension and then initiating a cross-linking reaction between the polymer and the CNTs. This can be achieved by a number of different cross-linking reactions, many of which may need catalysts to initiate them. In this way, the CNTs and the polymers are covalently bound to one another and form a intercalated network of polymers and CNTs. In this configuration, polymer chains are bound to the CNTs and all excess polymer chains can either be retained or discarded. Therefore the ratio of CNTs to polymers can be varied for specific applications. Finally, the third method discussed in this dissertation is the monomer growth of polymers from the sidewalls of CNTs. This polymer-CNT association can be achieved in a few different ways, but the methodology discussed in this dissertation is called interfacial polymerization. In this methodology, CNTs are suspended in aqueous suspensions of monomers of one type that bind to the CNT sidewalls. To the surface of this suspension is exposed a non-miscible solution of another type of monomer. When in contact, these two monomers bind to one another and polymerize at the interface of the solvents forming an interconnected network of polymers bound to CNTs. In this process, only those CNTs that exist at the interface between the two solvents will partake in the polymerization of the monomers. This process forms thin films and the monomer concentration can be varied to either include greater or fewer CNTs

into the thin film.

Each of these methods has their distinct advantages. CNTs that are covalently bound or ionically bound to the membrane matrix are stable and are linked to polymer chains within the polymer network. Their inherent stability prevents leaching into solution, however, binding CNTs to polymers affects the morphology, orientation, and mobility of polymer chains. This may have detrimental or unexpected effects and needs to be taken into consideration when forming nanocomposite membranes. Polymer wrapped, or non-covalent, non-ionic interactions, are less stable interactions, however the polymer chains are less hindered in their mobility or morphology, and thereby retain more bulk material structural properties than when bound to CNTs.

Moreover, each of these methods has their distinct uses. CNTs that are covalently bound to polymers either in cross-linked reticulations or bound within polymerized interfaces can be formed with limited amounts of polymers. These configurations can be formed in such a way as to minimize the amount of polymer surrounding the CNTs while still maintaining structural integrity due to the covalent interactions. In this way, the polymers act both as a glue to bind CNTs to each other, and as the active layer for separations. As a result, one can easily surpass the electrical percolation threshold to form highly electrically conductive nanocomposites. With the limited polymer content, however, these nanocomposites are structurally thin films rather than load bearing bulk membranes. In contrast, material structural enhancements are achievable with CNTs that are processed in the bulk of the polymers by blending. In this dissertation, these CNTs are added as structural reinforcing additives, and can interact with the polymer either through polymer wrapping or through ionic association. In this case, the predominant membrane characteristics come from the bulk polymer, with alterations to the base structure coming from the CNT additives.

This dissertation explores the three types of CNT-polymer associations described

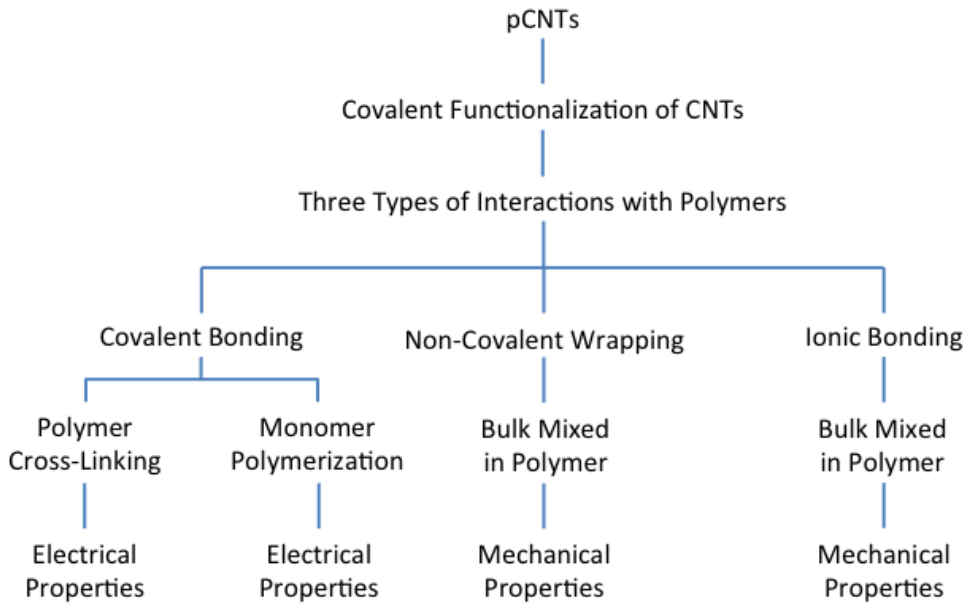

FIGURE 4.1: A flow-chart break-down of the research approach in this dissertation.

above and the dissertation results are divided along the lines of these three polymer-CNT interactions - covalently bound CNTs to polymers, polymer wrapped CNTs, and ionically bound CNTs to polymers. Further, the dissertation investigates and is organized by the two predominant property enhancements associated with CNTs in polymer membrane systems increased electrical conductivity and increased tensile strength. Therefore this dissertation is structured with respect to both the polymer-CNT interactions and their respective dominant property enhancement: Covalently bound interactions are used for electrical conductivity enhancement while polymer wrapped and ionically bound interactions are used for tensile strength enhancements. These two applications are briefly introduced below.

4.1.2 Covalent Binding of CNTs for Electrically Conductive Membrane Surfaces

Polymeric membranes are pivotal to a wide variety of fields, however, they are limited by several persistent problems. Some of these problems include inefficient means for charged particle separation and insufficient strategies for biofouling mitigation. Charged particles can be separated from solution through the application of a charge across a membrane. Depending on the sign of the applied charge, specific ions can be prevented from passing through the membrane through a process known as electrodialysis. Currently, Nafion, an expensive material that is limited in its application, dominates this technology (Strathmann, 2004). Other similar applications for charged particle separation include membrane capacitive deionization for desalination of brackish waters (Biesheuvel and van der Wal, 2010). The use of small, pulsed electric currents and/or voltage to prevent bio-attachment has been found to be efficacious in many applications. An electrically conductive membrane would, therefore, provide a non-destructive, chlorine-free, continuous and renewable strategy for the mitigation of biofouling as well as an efficient means to achieve a whole host of other applications including charged particle separation.

The covalent cross-linked and monomer grown interfacially polymerized systems described above are ideally suited to developing electrically conductive thin films on the surface of membranes. These thin films add electrically conductive functionality to the surface of existing polymer membranes. The thin films can be limited to electrical conductivity enhancements, but they can also add separation functionality. Separation characteristics can be controlled by a variety of parameters including the cross-linking density and the CNT concentration.

4.1.3 Polymer Wrapped and Ionically Bound CNTs for Membranes with Enhanced Tensile Strength

The optimal configuration for polymeric ultrafiltration membranes in industrial applications is as hollow fibers. Hollow fibers have a much higher packing density than spiral wound membranes and as such are highly favored. The major drawback for hollow fibers, however, is their resistance to tensile strength. Hollow fibers undergo a variety of stresses throughout their operational lifetime including variable pressures, vibrations to the modules during filtration, and stresses from air scouring. It is critical, therefore, to increase their tensile strength. This may be achieved through small additions of CNTs. Homogeneous distribution of functionalized CNTs throughout a polymer hollow fiber may increase the Young's Modulus while also positively affecting other membrane properties including permeability and surface chemistry. In bulk mixed nanocomposite membranes, it is important to investigate the stability of the CNTs within the polymer matrices. Loss or leaching of CNTs from polymer matrices will negatively effect the membrane properties, as well as potentially contaminating the waters these membranes are meant to treat.

4.2 Development and Application of Electrically Conductive Membranes Formed With Covalent Bonds Between Functionalized CNTs and Membrane Polymers

4.2.1 Properties of Electrically Conductive Ultrafiltration Membranes Formed from Carboxylated Carbon Nanotubes Covalently Cross-Linked with Poly(vinyl alcohol)

4.2.1.1 Proem: PVA-CNT Electrically Conductive UF Membrane Properties

In this study we demonstrate a simple method to create a highly conducting polymer-multiwalled carbon nanotube composite membrane. This membrane is highly flexible with resistivity many orders of magnitude lower than most polymer-carbon nanotube composites; similar to or several orders of magnitude higher than recently distinguished electrically conducting membranes such as poly(pyrrole) (Mcneill et al., 1963) and polythiophene (Shirakawa et al., 1977), or doped polyacetylene (Chiang et al., 1978). Poly(vinyl alcohol) (PVA) was covalently cross-linked with succinic acid (Peng et al., 2010) and carboxyl-functionalised multiwalled carbon nanotubes (CNT-COOHs, simplified in 4.2 as CNTs), and pressure filtered onto a polymeric support membrane. The effect of the degree of cross-linking and that of CNT concentration on the performance of these membranes was evaluated. These membranes demonstrated high pure water flux with good particle separation, high electrical conductivity, low polymer crystallinity, and low surface tensions. The properties of these membranes were optimized with respect to electrical resistivity, pure water flux, molecular weight cut-off, surface hydrophilicity, and crystallinity as a function of cross-linking curing time and CNT concentration as a fraction of PVA. Membranes formed with twenty minutes cross-linking curing times and 20 wt% CNT concentration showed electrical resistivity as low as $2.8 \times 10^{-4} \Omega - m$ (conductivities as high as $3.6 \times 10^{3} S/m$), pure water flux of $1440\, L/m^2 h$ at pressures of $550\, kPa$, and triple-point initial contact angles as low as 40° with high hysteresis.

4.2.1.2 Findings: PVA-CNT Electrically Conductive UF Membrane Properties

Cross-Linking Poly(vinyl alcohol) (PVA) membranes were formed by cross-linking PVA polymer with a dicarboxylic acid (succinic acid) and well-dispersed carboxylic acid-functionalised carbon nanotubes (CNT-COOH), with hydrochloric acid acting as the catalyst. Carbon nanotubes and succinic acid concentrations were selected to produce a theoretical cross-linking degree of 20 % as governed by the following equations:

$$\chi_{CL}[\%] = \chi_{CL,succinic} + \chi_{CL,CNT-COOH} \tag{4.1}$$

$$\chi_{CL,succinic} = \frac{W_{CL,succinic} \cdot MW_{PVAunit} \cdot 2}{W_{PVA} \cdot MW_{CL,succinic}} \times 100 \tag{4.2}$$

$$\chi_{CL,CNT-COOH} = \frac{W_{CL,CNT-COOH} \cdot MW_{PVAunit} \cdot \mu}{W_{PVA} \cdot MW_{FNCTunit}} \times 100 \tag{4.3}$$

Where $W_{CL,succinic}$, W_{PVA}, $W_{CL,CNT-COOH}$, $MW_{CL,succinic}$, $MW_{PVAunit}$, $MW_{FNCTunit}$, and μ are the weight of the succininc acid, the weight of the PVA, the weight of the carboxylated carbon nanotubes, the molecular weight of succinic acid, the molecular weight of one PVA unit ($-CHOH-CH_2-$), the molecular weight of one functional group on the carbon nanotube backbone ($-OOH-$), and the weight percent of functionalization of the carbon nanotubes.

The carboxylic acid functional groups on both the succinic acid and on the multiwalled carbon nanotubes were hypothesized to react with the hydroxyl groups on the poly(vinyl alcohol) as shown in figure 4.2. The reaction of the carbon nanotubes with the poly(vinyl alcohol) ensured their permanent immobilization within the polymer matrix as well as their homogeneous dispersion therein. Homogeneous dispersion of the CNTs is the most challenging aspect of such reactions and was deduced to be the major source of error and variance in membrane samples.

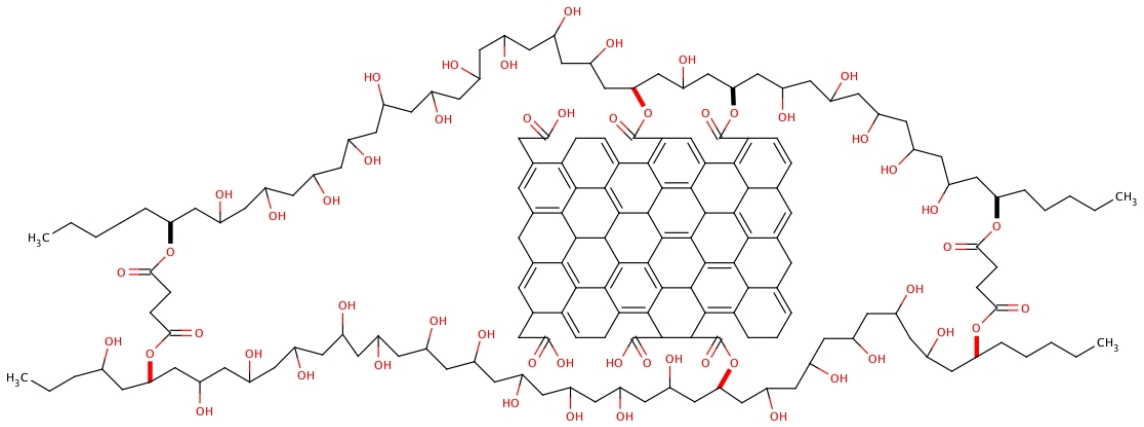

FIGURE 4.2: Poly(vinyl alcohol) (PVA) can be cross-linked through reaction with its hydroxyl groups. Di-carboxylic acids, such as succinic acid, can link one polymer strand to another. In this work, both succinic acid and carboxylated multi-walled carbon nanotubes have been used to cross-link PVA (cross-link bonds are covalent bonds shown in bold), immobilizing CNTs within the polymer and altering the spacing between polymer strands. This figure does not show the full extent of the CNTs used. Multi-walled carbon nanotubes are several orders of magnitude wider and significantly longer than PVA chains.

To demonstrate that the cross-linking reaction was occurring, two different membrane films were made: 1) a membrane with carboxylated carbon nanotubes cross-linked with polyvinyl alcohol under exposure to HCl, and 2) a control membrane formed with pristine carbon nanotubes mixed with polyvinyl alcohol, with no catalyst added. Both membranes were analyzed by FTIR to determine the presence or absence of PVA-CNT cross-linking. FTIR data is presented in figure 4.3 and shows clear differences in the spectral peak about $3700\,nm$. The FTIR spectrum of the control membrane, formed without the HCl catalyst, is shown in red. This spectrum lacks any distinctive peak. The FTIR spectrum of the PVA-CNT cross-linked membranes is shown in blue, and shows a large peak about $3700\,nm$. This peak is evidence of large numbers of hydroxyl groups. As is evident from the FTIR spectra of figure 4.3, the control membranes containing pristine CNTs and no cross-linking do not show any evidence of hydroxyl groups, while the membranes containing car-

boxylated CNTs cross-linked to PVA demonstrate high concentrations of hydroxyl groups. Hydroxyl groups are found predominantly on PVA chains and to a much lesser extent on the carboxylated CNTs.

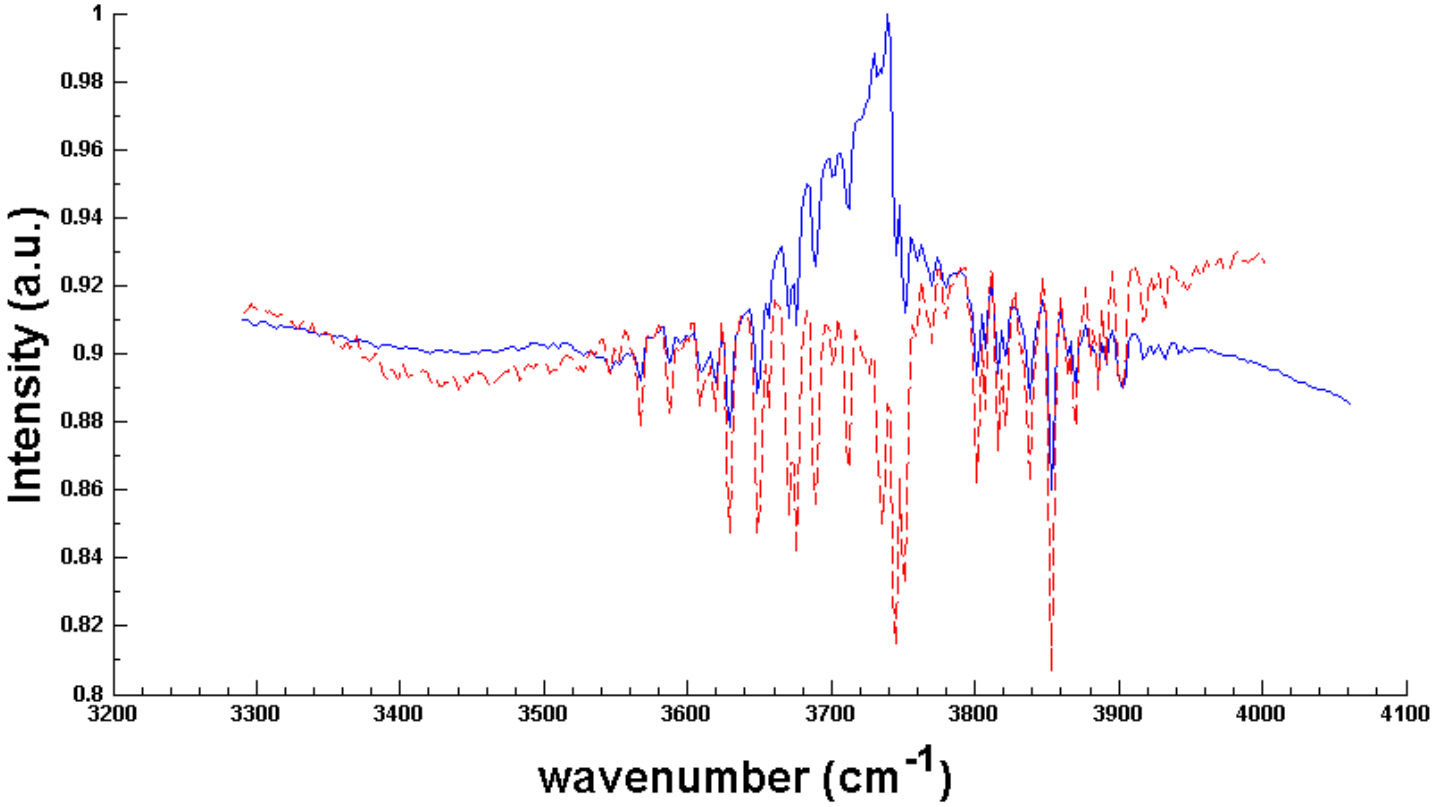

FIGURE 4.3: Films formed without cross-linking (shown in the dashed red line) are unstable and contain little to no polyvinyl alcohol as shown in the lack of distinctive hydroxyl peak in FTIR spectra at 3700 nm. Films formed with 20% cross-linking with polyvinyl alcohol are robust films and contain the hydroxyl group from the PVA. These films (show in the solid blue line) have a predominant peak at 3700 nm as can be seen from the FTIR spectrum in blue.

After reaction, the mixture was pressure filtered onto a support membrane and then cured in an oven at 100°C. Cellulose nitrate support membranes with 0.1 μm pore size were used as the support for the composite CNT-PVA-succinic acid film. These membranes were then thoroughly rinsed to remove excess reagents. The PVA membranes cross-linked with carboxylated carbon nanotubes and succinic acid were in this way securely attached to the support membrane. In contrast, carbon nanotubes pressure-filtered directly onto the membrane without the addition of PVA were unstable and washed off the support membrane when in contact with water. Moreover, unfunctionalized CNTs did not contribute to the cross-linking of PVA with succinic acid and were made even more unstable after curing. After curing the control membranes, CNTs could be easily removed from the support membrane. A comparison of the cross-linked membranes with the control membranes after curing is shown in figure 4.4. In addition, low curing times of less than 5 minutes produced unstable coatings that could be scratched off their support.

Surface Morphology Cross-linked, pressure-filtered PVA-CNT-COOH nanocomposite membranes exhibited remarkable electrical conductivity as well as good membrane characteristics in terms of surface hydrophilicity, surface roughness and pure water flux. The above-described procedure for membrane formation produced the optimal electrical conductivity as well as membrane stability and high water flux. Further optimization was possible by investigating the effects of curing time and carbon nanotube concentration. For the following analyses curing time was varied from 5 minutes to 40 minutes on membranes that contained 10 wt% CNTs with respect to PVA, and concentration of carbon nanotubes was varied at 0.1 wt%, 2.0 wt%, 5.0 wt%, 10 wt% and 20 wt% with respect to PVA and then cured for a minimum of 20 minutes.

The thickness and surface morphology of the pressure-deposited PVA-CNT mem-

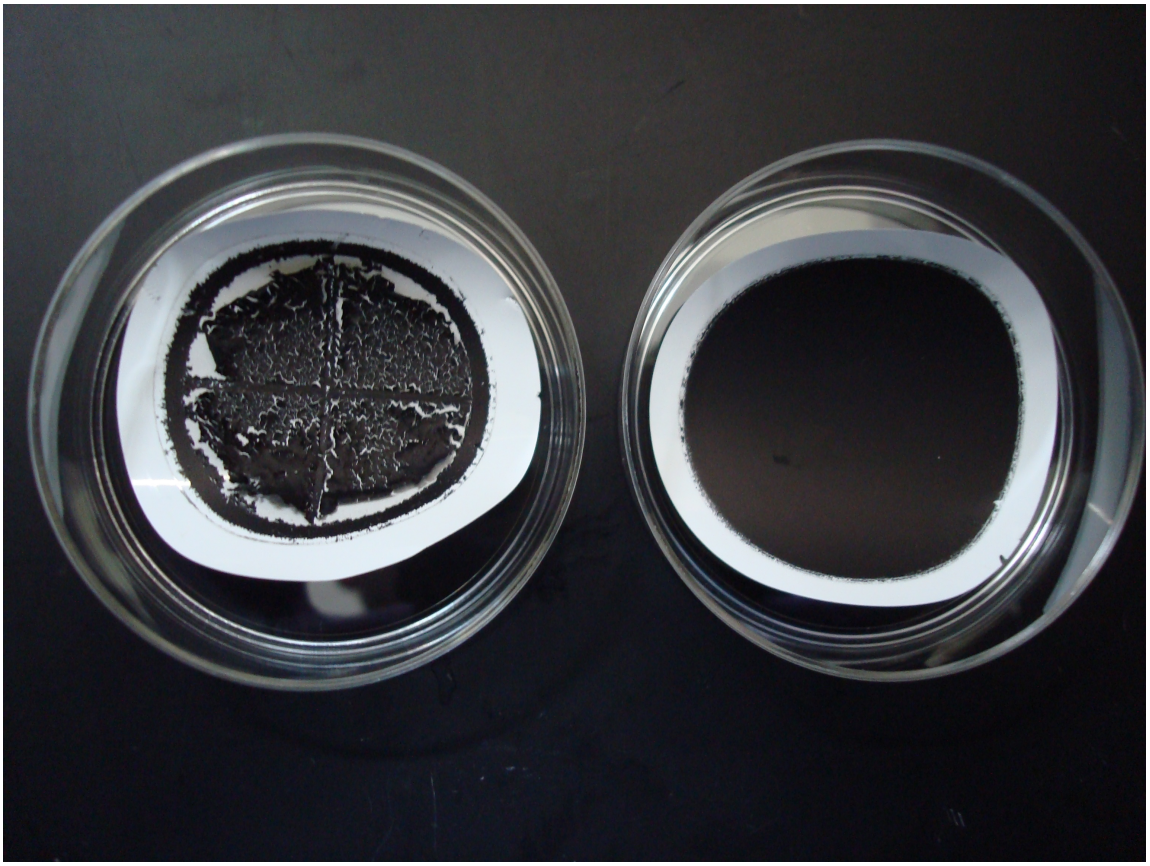

FIGURE 4.4: Directly pressure-filtering CNTs onto a support membrane without cross-linking with PVA produced unstable layers in which CNTs flaked off easily, as shown in the membrane on the left. This type of membrane is unusable for filtration applications. The membrane on the right has been successfully cross-linked with PVA to form a smooth, well-bound, highly conductive active layer.

brane layer was investigated by ultra-high resolution scanning electron microscopy (UHR-SEM). The carboxylated carbon nanotubes were visibly enmeshed with PVA and uniformly coated the membrane support (figure 4.5). As greater concentrations of carbon nanotubes were pressure-filtered onto the support surface, a slightly thicker conductive layer was formed, although the difference in thickness from one membrane coating to another was within $0.5\,\mu m$. The coating thickness was measured from UHR-SEM cross-sections an example of which is shown in figure 4.5. No difference in conductive layer thickness was observed by changing the curing times.

Further, no evidence of damage to the surface of the support membrane was observed.

Electrical Conductivity Most importantly, the CNT-PVA active layers exhibited high electrical conductivity (conversely their resistivities were very low). The most electrically conductive membranes that we measured had conductivities more than 20 orders of magnitude higher than plain PVA membranes. With conductivities as high as graphite or amorphous carbon, these polymer-composite membranes are the most conductive polymer membranes currently known.

Increasing the curing time slightly increased the conductivity (decreased the resistivity) of the membranes as can be seen in figure 4.6 a). Curing times of less than 10 minutes had lower electrical conductivity, with curing times of 5 minutes producing membranes with electrical conductivities as low as $825.4\,S/m$. Membranes cured for longer times of 20 and 40 minutes had statistically significant greater electrical conductivities. Membranes formed from 10 wt% CNTs with respect to PVA and cured for 40 minutes demonstrated electrical conductivities as high as $1593\,S/m$. Furthermore, the greater the percentage of CNTs on the surface of the membrane with respect to a constant amount of PVA, the higher was the conductivity. This was shown by varying the concentration of CNTs on the surface while keeping the curing time constant at 20 minutes. At the highest concentration of 20 wt% CNTs, the conductivity was approximately $3597\,S/m$. Higher concentrations of CNTs were not analyzed because of difficulties associated with uniform dispersion. Figure 4.6 b) shows that the conductivity increases as a function of increasing carbon nanotube concentration.

Surface Hydrophilicity Membrane surfaces showed considerable affinity to water. The initial advancing contact angle was measured for all membrane surfaces, but contact angle hysteresis was significant enough for some membranes, such that within several

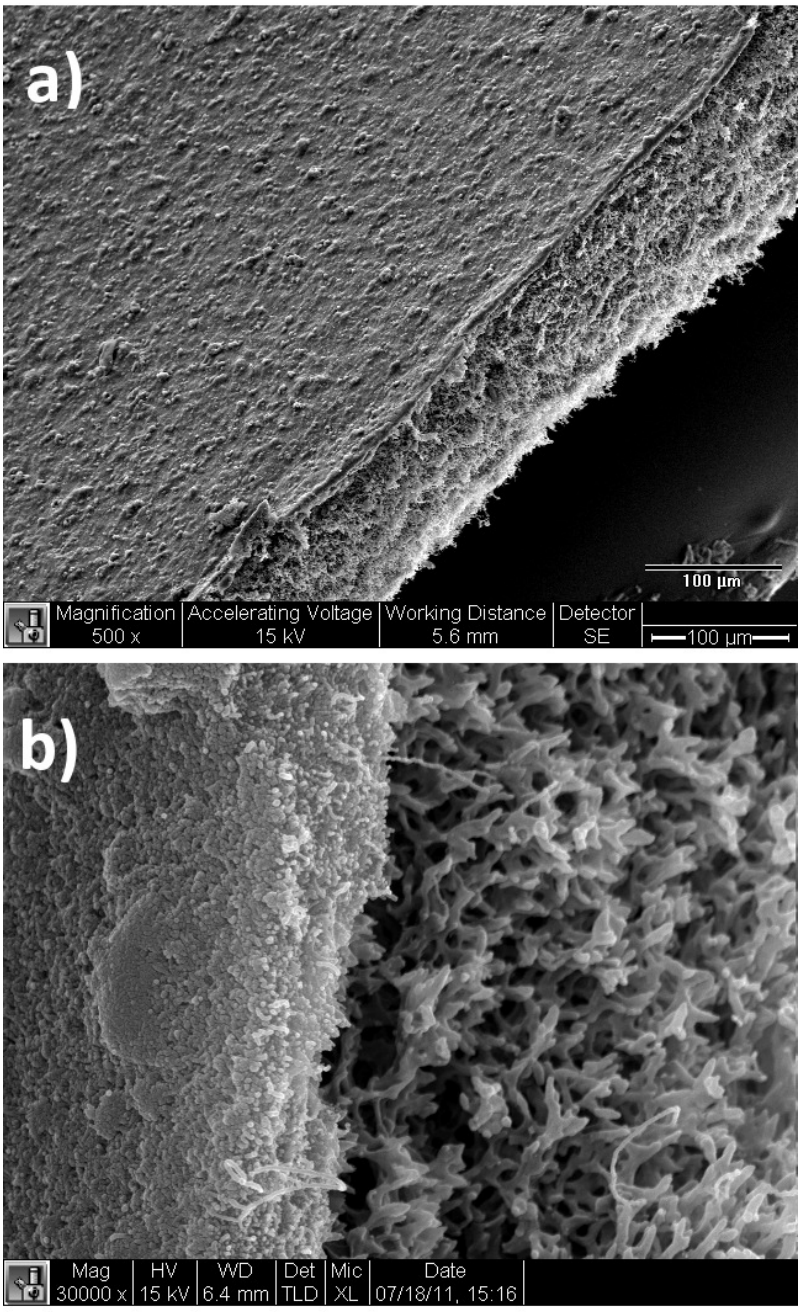

FIGURE 4.5: The top image is a cross-section of a pressure-filtered PVA-CNT membrane containing 5 wt% CNT with respect to PVA. The thickness of this surface coating is significantly less than that of the cellulose nitrate support membrane. On the bottom is a magnified image of the surface coating of a pressure-filtered membrane containing 10 wt% CNTs with respect to PVA. The thickness of this surface coating is approximately $1.0\,\mu m$.

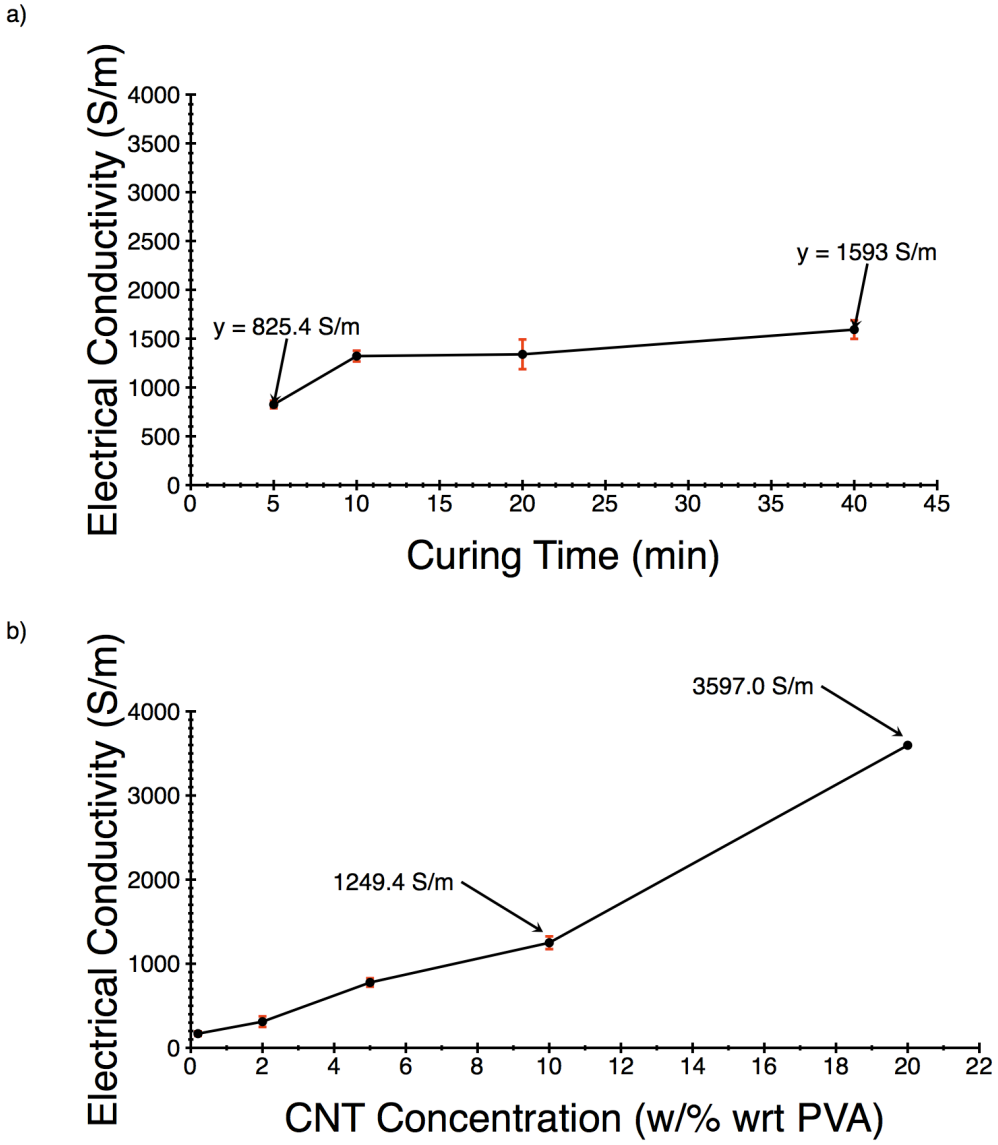

FIGURE 4.6: The conductivity of the PVA-CNT membranes is found to be very high on the order of $4 \times 10^3\, S/m$ on the same order of magnitude as graphite. In a) membranes made with 10% CNT with respect to PVA and cured for differing lengths of time show greater conductivity for greater curing times as more CNTs are securely cross-linked to the polymer. Most evidently, curing times less than 5 minutes show weak binding to the support membrane and lower conductivity overall. In b) the conductivity of the membranes increases with greater CNT concentration. Increasing CNT concentrations over 10 wt% with respect to PVA drastically effects the conductivity of the membranes.

minutes the retreating contact angle was found to be zero. Initial advancing contact angles showed no dependence on changes in membrane curing time, but varied significantly with changes in carbon nanotube concentration (figure 4.7). For low carbon nanotube concentrations, the positive hysteresis was so great, that no reasonable angle could be measured within the amount of time needed to setup the goniometer. In this case, to avoid reporting a zero value for contact angle, captive bubble measurements were performed. Captive bubble measurements were then taken for all CNT concentrations in order to verify those measured using the sessile drop method. Figure 4.7 is therefore compiled data demonstrating the decreasing affinity for water with greater amounts of CNTs incorporated into the film. In this figure, the trend of increasing contact angle with increasing CNT concentration can readily be observed. Contact angles vary from 28° to 48° for membranes composed of 0.5 wt% CNTs to 20 wt% CNTs.

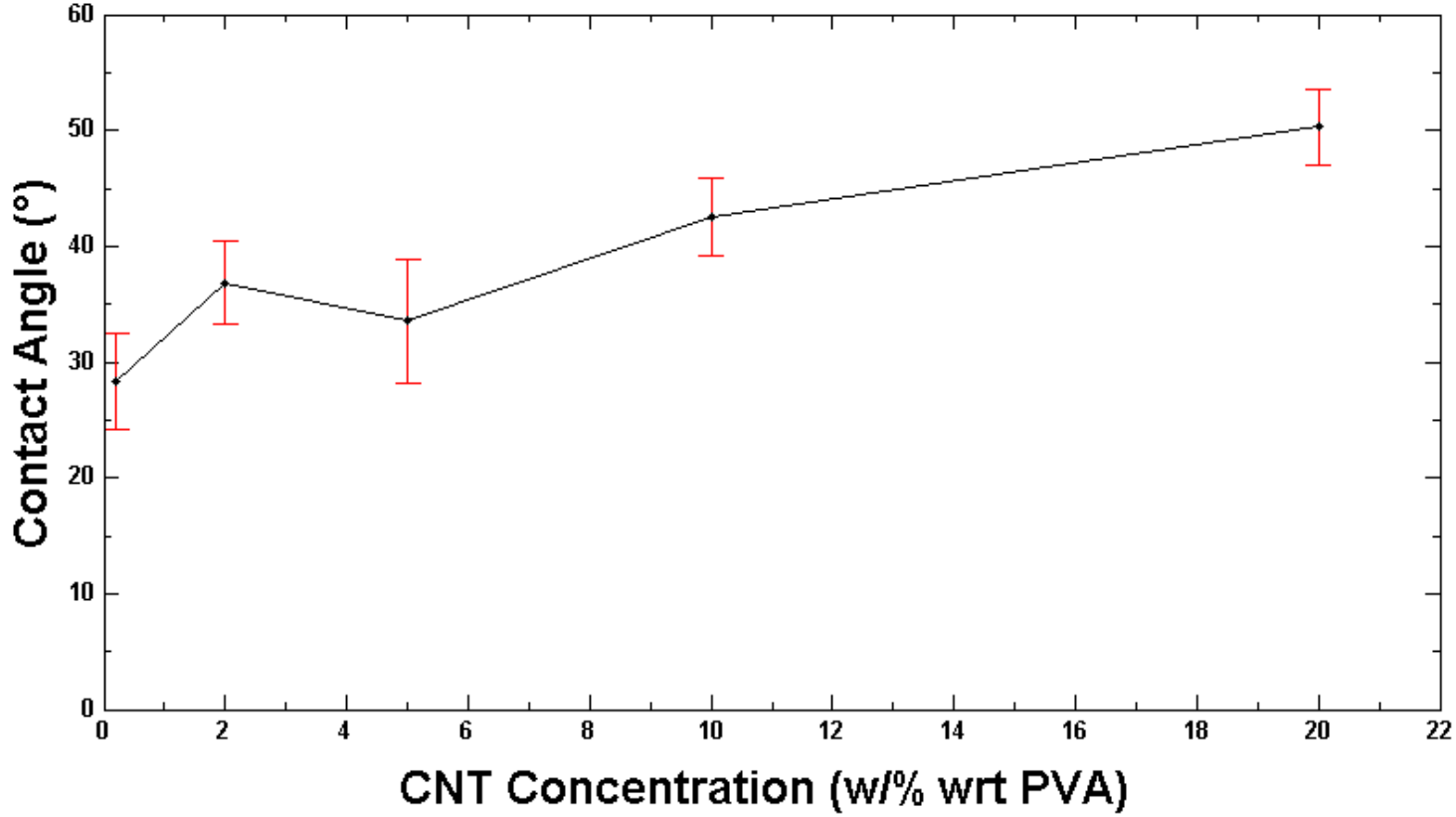

FIGURE 4.7: Contact angle of the polymer composite membranes as measured by the initial advancing contact angle of the triple point between the membrane surface, water and an air bubble placed on the surface. A lower contact angle implies a more hydrophilic surface. The hydrophobicity of the membrane increases with increasing CNT concentration.

Pure Water Flux and Crystallinity Pure water permeate flux through these membranes corresponded to a range of membrane resistance typical of an ultrafiltration membrane. Membrane resistance varied greatly as a function of both curing time and CNT concentration with higher concentrations of CNTs producing less resistant permeate flux (figure 4.8). Membranes with low CNT contents (2.0 wt%) showed the highest resistance to water flow close to $1.0\,kPa \cdot m^2h/L$, while membranes formed with the highest CNT contents (20 wt%) demonstrated low resistance to water flow of $0.4\,kPa \cdot m^2h/L$.

A decrease in membrane resistance with an increase in CNT content was suspected to be attributed to changes in PVA crystallinity. PVA is a semi-crystalline polymer and it was hypothesized that CNTs cross-linked to PVA caused disruptions to this semi-crystalline structure. Disruption of the PVA crystallinity was confirmed by x-ray diffraction (XRD) (figure 4.9). Membranes formed with PVA-CNTs of varying CNT content produced XRD spectra with wide peaks with broad shoulders. Contrasted with these broad spectra, membranes formed with pure PVA and no CNT content, produced XRD data with sharp peaks and an absence of shoulders. Sharp peaks in XRD data are associated with material crystallinity, while broad peaks n the XRD data are evidence of a lack of crystallinity.

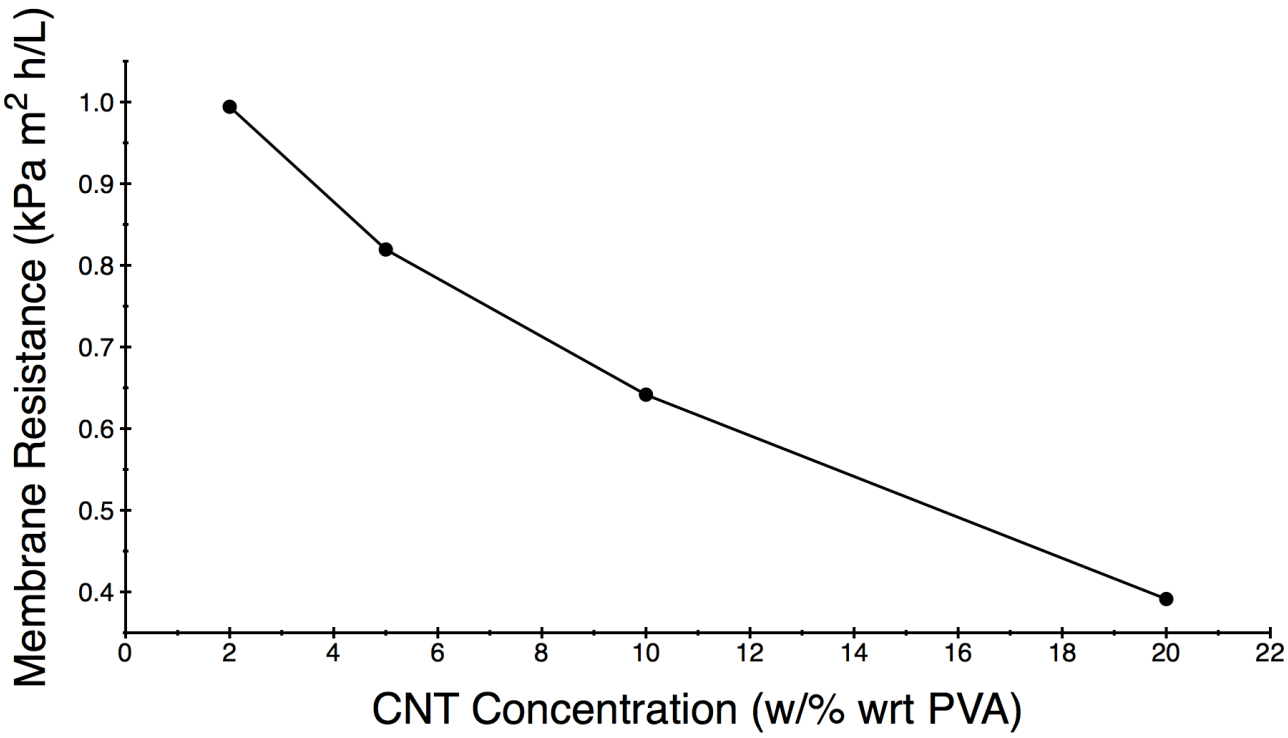

FIGURE 4.8: Pure water flux through PVA-CNT membranes show very high fluxes as high as $1400\,L/m^2h$ within a range of pressures $130550\,kPa$ $(20-80\,psi)$ suitable for ultrafiltration membranes. Fluxes increase for greater concentrations of CNTs as the spacing between cross-linked PVA chains increases creating more porous membranes. The membrane resistances were computed for these four concentrations of carbon nanotubes and plotted above. The highest concentration of carbon nanotubes used (20 wt% with respect to PVA) exhibits membrane resistances as low as $0.39\,kPa \cdot m^2h/L$.

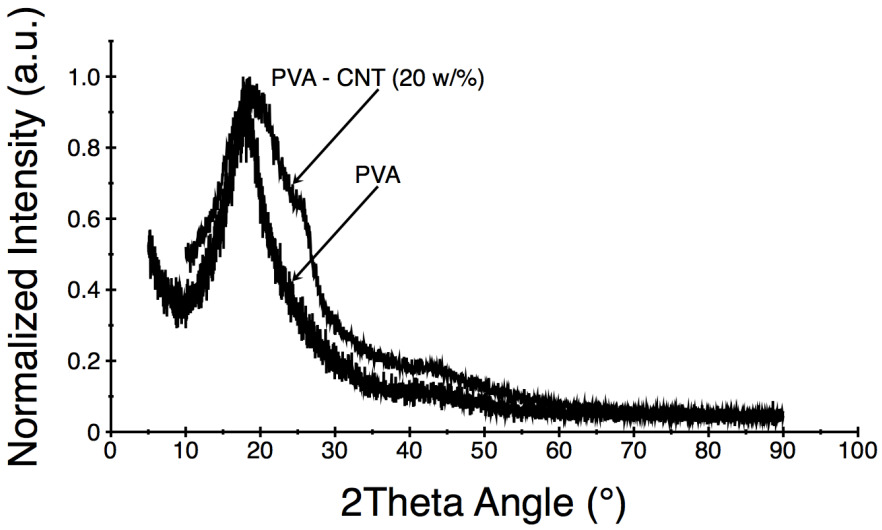

FIGURE 4.9: X-ray diffraction data for plain PVA membranes and PVA-CNT membranes. The narrow prominent peak for PVA is indicative of semi-crystallinity within the polymer, while the broad diffuse peak found for PVA-CNT membranes is evidence of amorphous carbon and a lack of crystallinity.

Separation Characteristics An increase in membrane permeability with CNT addition is achieved at the expense of the separation characteristics of the membrane. Measurements of the rejection of $100\,kDa$ polyethylene oxide (PEO) are consistent with the permeate flux (membrane resistance) data. Membranes with the lowest amount of carbon nanotubes with respect to the PVA (and thus the least amount of disruption to the polymer crystallinity) showed the highest rejection of PEO, at values of over 90% (figure 4.10). Membranes with the highest concentrations of carbon nanotubes, which demonstrated the highest fluxes, by contrast showed molecular weight cutoff (MWCO) similar to the support membranes. The support membranes used in this experiment had $0.1\,\mu m$ pore sizes. The rejection data for PEO of higher molecular weights ($600\,kDa$ and $1\,MDa$) are shown in A.

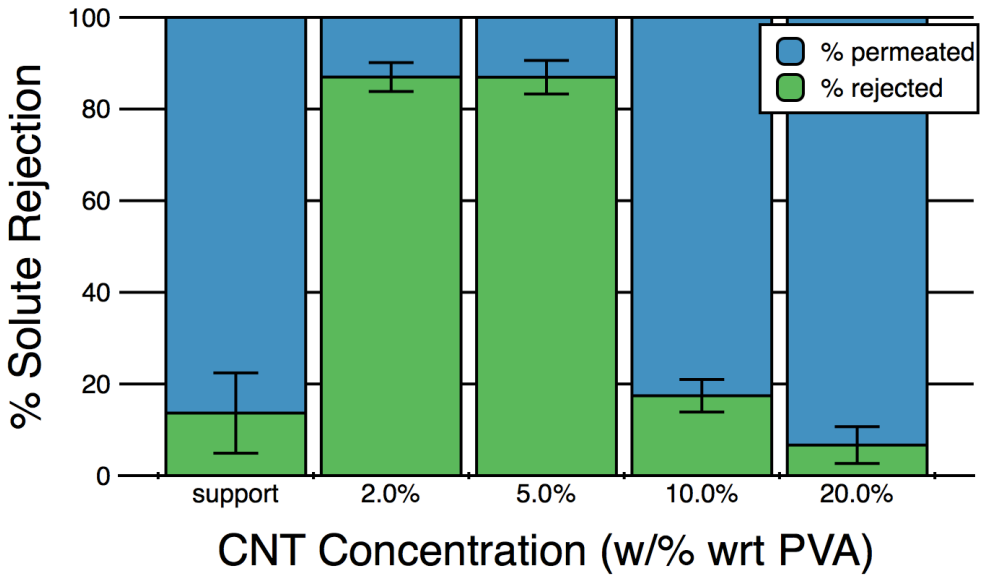

FIGURE 4.10: Rejection experiments performed on these membranes demonstrate the change in polymer ordering within the membrane. As greater amounts of carbon nanotubes are incorporated into the membrane, crystallinity of the polymer decreases and membrane permeability increases as measured by pure water flux and PEO rejection.

4.2.1.3 Discussion: PVA-CNT Electrically Conductive UF Membrane Properties

Cross-Linking PVA-CNT Films Structurally stable, electrically conductive thin films were hypothesized to be formed by cross-linking carboxylated CNTs with PVA, catalyzed by the addition of HCl. The hypothesized scheme for this cross-linking reaction is visualized in figure 4.2, which shows that the carboxylic functional groups on the sidewalls of the CNTs interacts with the hydroxyl groups on the PVA backbone. Under the addition of HCl, it is hypothesized that a hydrolysis reaction occurs to form a covalent bond between these two moieties. In this way, carboxylated CNTs cross-link adjacent PVA chains. In addition, succinic acid is added, simultaneously with the carboxylated CNTs, to further cross-link PVA chains. To demonstrate that cross-linking was occurring, CNT-PVA cross-linked membranes were compared with

control membranes formed from pristine CNTs mixed with PVA without the HCl catalyst. FTIR data of these two membranes was compared and presented in figure 4.3, which shows a large peak at 3700 nm for the cross-linked membranes, and an absence of that peak for control membranes. This peak is indicative of large numbers of hydroxyl groups. In both suspension mixtures, hydroxyl groups were present predominantly on PVA chains and to a much lesser extent on carboxylated CNTs. The control films contained pristine CNTs and uncrosslinked PVA, which would have a high density of hydroxyl groups. However, membranes were formed by pressure depositing the reaction mixture on porous support membranes. Control membranes, which lacked cross-linking, did not contain any PVA chains, and thus lacked hydroxyl groups, as the vast majority of the PVA filtered through the support membrane, leaving a film of unreacted pristine CNTs. In contrast, those films that were formed from the cross-linking reaction of PVA with carboxylated CNTs contained considerable amounts of PVA and as such contained high amounts of the ubiquitous hydroxyl groups. Cross-linking was limited to 20%, thus the PVA chains that were immobilized about the CNTs contained large amounts of hydroxyl groups. In figure 4.3, the blue line, representing the cross-linked films, shows a strong peak about 3700 nm demonstrating a predominance of hydroxyl groups, while the red line, representing films that lack cross-linking, and therefore lack PVA altogether, demonstrates an lack of a peak and thus an absence of hydroxyl groups.

This comparison is made even more clear by comparing the films after curing at 100°C, shown in figure 4.4. Curing binds the cross-linked CNT-PVA film to the support membrane and produced stable, flexible composite membranes. In contrast, curing the control films without cross-linking, and thus without PVA, produced unstable flaky films. A lack of PVA prevents binding to the support membrane during curing. Further, a lack of cross-linking prevents stability of the CNTs, which is aggravated during curing. The end result is a highly unstable film that is easily washed

off the support membrane. In addition, low curing times of less than 5 minutes, for either membrane (control or cross-linked) did not thoroughly bind the polymer to the support membrane and produced surface coatings that could be scratched off their support.

Morphology and Electrical Conductivity of PVA-CNT Films Thin films of cross-linked CNT-PVA deposited on support membranes showed thicknesses on the order of $0.5 - 1.0\,\mu m$. Greater concentrations of CNTs formed thicker thin films, while lesser concentrations formed thinner films, as expected. The surface morphology of the thin films was relatively rough across all thicknesses, however, which necessitates optimization of the solution mixture and deposition technique. We hypothesize that the hillocks that are found on the surface are caused by aggregated CNTs bound by PVA chains. During sonication of the CNTs, some small aggregates may still remain, which may react with PVA during the cross-linking step to form larger aggregates. These small clusters may be the cause of the surface roughness.

Curing time affected the surface electrical conductivity of the thin films because it affected both the degree to which the carbon nanotubes cross-linked with PVA and the degree to which this cross-linked network bonded with the support membrane. With short curing times of less than 10 minutes, fewer CNTs were covalently bonded to the matrix polymer and to the support. This was evident because CNTs could be dislodged from the surface either when the membrane was thoroughly washed after curing or simply by scratching the surface of the membrane. As all membranes were washed thoroughly after curing, CNTs that were not well bonded to the support membrane may have been lost from the surface. The loss of CNTs from the surface would adversely affect the membrane conductivity. Membranes formed with longer curing times, in comparison, contained CNTs that were strongly attached to the support surface. These CNTs could only be removed by destroying the support.

Concentration of CNTs had an even greater effect on surface electrical conductivity, as expected. By maintaining the concentration of PVA constant, and varying the concentration of CNTs, it was possible to produce thin films with very high electrical conductivity on the order of $4^3 S/m$. A greater concentration of CNTs in the thin film is equivalent to fewer polymer chains per CNT. Fewer polymer chains implies less resistance in the thin film and therefore a greater electrical conductivity. In the limit of no polymer chains, or a thin film composed entirely of CNTs, the electrical conductivity of the thin film would be maximized. However, without the polymer chains to cross-link the CNTs, the membrane would be highly unstable as demonstrated above. Further, interesting membrane properties such as flux and rejection would not be possible without the cross-linked polymer CNT network.

Flux and Separation Characteristics of PVA-CNT Underivatized carbon nanotubes are very hydrophobic and the addition of pristine CNTs into membranes increases the hydrophobicity of the surface. In these PVA-CNT thin films, the carbon nanotubes are carboxylated, which increases their hydrophilicity. Increasing the content of carboxylated CNTs in these thin films also increased the hydrophobicity of the membranes. However, the increased hydrophilicity associated with carboxylation tempered the increases in surface hydrophobicity. PVA-CNT thin film contact angle measured in all cases was less than 90° and never exceeded 55°. In addition to the hydrophilic functional groups on the sidewalls of carboxylated CNTs, PVA is highly hydrophilic due to its hydroxyl-saturated chains. These two complementary factors explain the hydrophilicity of the membrane surfaces, a trait that tends to favor high water flux and potentially reduced fouling due to adsorption of organic matter.

Flux increased with increasing CNT content in the PVA-CNT films. This unexpected trend - a decrease in membrane resistance with an increase in CNT content - is attributed to the way in which the PVA membranes were cross-linked. Membranes

composed of polymer chains of poly(vinyl alcohol) cross-linked with succinic acid are densely packed into semi-crystalline regions, which restrict water flow. In the CNT-PVA membranes the cross-linking with succinic acid is partially substituted by carbon nanotubes that covalently bonded to the polymer chains. The rigidity of the CNTs and their large size disparity compared with PVA chains and succinic acid (CNTs are several orders of magnitude wider than succinic acids and PVA molecules) creates much larger separation distances between PVA chains, and thus a more porous structure, while also disrupting the crystallinity of the polymer. The disruption of the polymer crystallinity is conceptually depicted in figure 4.2. Figure 4.2 is not to scale, as multi-walled carbon nanotubes are several orders of magnitude wider and significantly longer than PVA chains, and thus, the crystalline disruption and porous domains may be more exaggerated than presented in the figure. This change in crystallinity was evidenced in figure 4.9. The XRD data contrasts the wide peaked and broad shouldered spectra produced by the PVA-CNT films with the narrow peaked spectra produced by the pure PVA films. The former spectra indicate amorphous carbon dominating the polymer structure, and suggests a lack of long-range order, which would be indicative of crystallinity. The latter spectra, the sharp peaks produced by the pure PVA membrane, suggests semi-crystallinity among the long ordered chains of PVA macromolecules.

The reduction in crystallinity with increasing CNT content explains the increases in pure water permeability (or decreases in membrane resistivity). It is also associated with changes in selectivity. Greater CNT content, and thus less PVA crystallinity, is associated with larger pore sizes and thus a larger MWCO. While pure semi-crystalline PVA membranes are frequently used to create nanofiltration thin film composite membranes, the larger porous structure of the CNT-PVA composite membranes corresponds to a membrane in the ultra- or micro-filtration range. With greater disruptions to the polymer crystallinity, pore sizes increase between polymer

chains reducing their separation capabilities. This is evident in figure 4.10, in which membranes with low CNT content reject 100 kDa PEO to greater than 90%, while membranes formed with greater CNT contents have much lower rejections. These data suggest that the carbon nanotubes create large openings between adjacent PVA chains and that the CNT content can be used to control MWCO.

4.2.1.4 Conspectus: PVA-CNT Electrically Conductive UF Membrane Properties

These CNT-PVA composite membranes exhibit high electrical conductivity, high permeate flux, and a hydrophilic surface. The molecular structure of the membrane can be tailored to a specific permeate flux and associated solute rejection by altering the carbon nanotube concentration and, it is hypothesized, by changing the cross-linking degree. The electrically conductive properties of these membranes suggests a wide range of possible advantages and applications that include biofouling-resistant membranes, addressable membrane assemblies for sensing and monitoring, reactive membranes, and electrical potential-based separations. Further, coatings of such material have the potential to be used in a whole suite of biomedical applications in which biofouling is a persistent and detrimental factor.

4.2.2 Properties of Electrically Conductive Tight Nanofiltration Membranes Formed from Interfacially Polymerized Polyamide on Hydroxylated Carbon Nanotubes

4.2.2.1 Proem: PA-CNT Electrically Conductive Nanofiltration Membrane Properties

We have created a novel modification of PA thin film composites by covalently bonding the monomer constituents of polyamide with carboxylated multi-walled carbon nanotubes. CNTs imbue these thin films with electrical conductivity 20 orders of magnitude greater than the base polymer. This modification of the traditional polyamide membrane provides high electrical conductivity to the thin film without sacrificing either the requisite rejection or permeation properties of traditional

PA membrane. A simple route to the creation and application of these polyamide-carbon nanotube thin films is reported. These thin films were characterized with SEM and TEM as well as FTIR to demonstrate that the carbon nanotubes are embedded within the polyamide and form ester bonds with trimesoyl chloride, one of the monomers of polyamide. These polymer nanocomposite thin film materials boast high electrical conductivity ($\sim 400\,S/m$), good NaCl rejection ($> 95\%$), and high water permeability.

4.2.2.2 Findings: PA-CNT Electrically Conductive Nanofiltration Membrane Properties

Thin Film Surface Morphology The electrically conductive thin film PA-CNT membrane is shown in figure 4.11 a) as compared to the pure PA membrane shown in figure 4.11 b). The black surface is due to the presence of the CNTs in the PA matrix. The white rim around the black ECPNC membrane is the $0.1\,\mu m$ polyethersulfone (PES) support membrane. SEM images of the membrane show a thin layer of PA-CNT composite formed on the PES support (Figure 4.11 c). The PA-CNT thin film appears morphologically similar, but not identical, to other PA thin films reported in the literature (Liu et al., 2011) (Lee et al., 2011) and presented in figure 4.11 d). The combination of MPD, TMC and CNTs forms a covalently bonded thin-film (demonstrated in FTIR measurements) atop the PES support, in which the CNTs are an integral part of the active membrane layer.

Contact angle measurements of the membrane material gave a value of $77^\circ \pm 3^\circ$. This value is slightly higher than contact angles typically observed on PA membranes ($60^\circ - 70^\circ$).

Thin Film Surface Electrical Conductivity A TEM image of the cross-section of the microtomed resin-encapsulated ECPNC membranes is shown in figure 4.12. Three distinct layers are evident the PES support, a CNT layer, and a thin filamentous

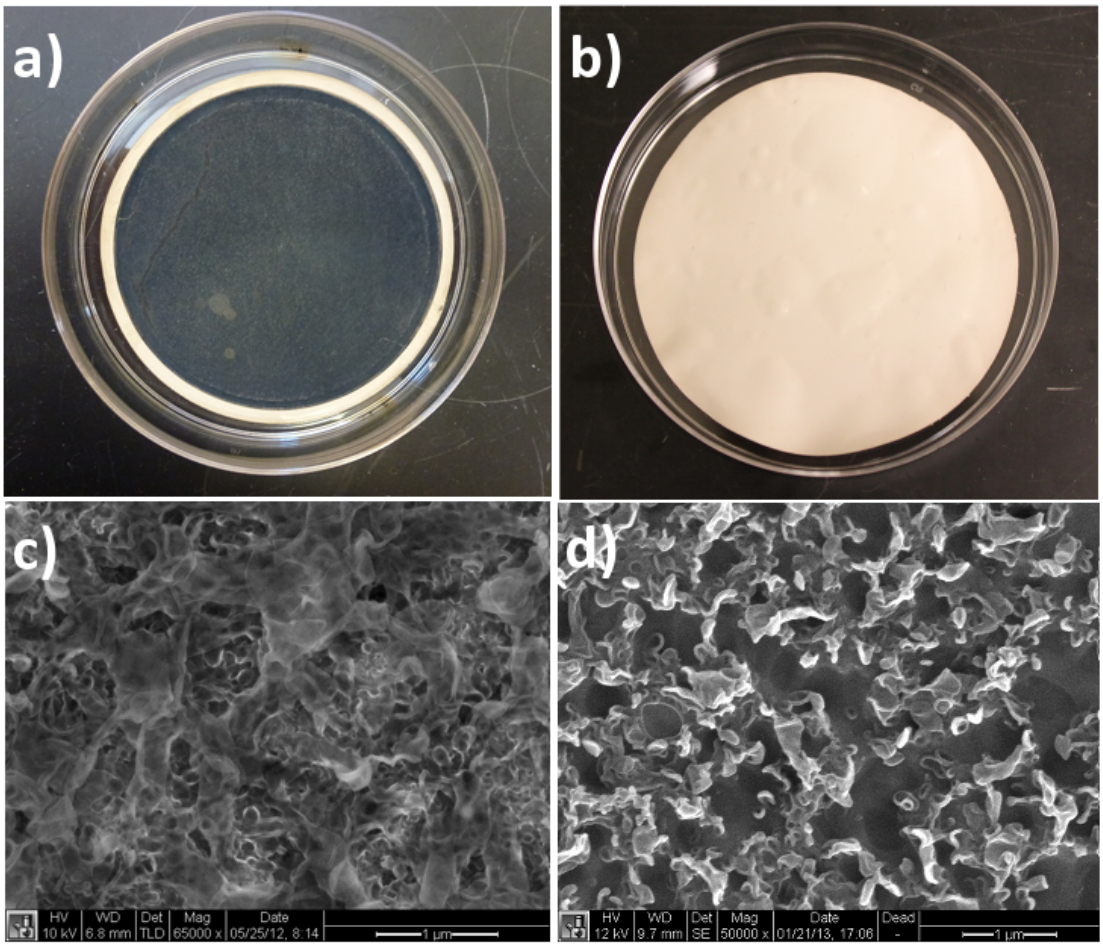

FIGURE 4.11: a) ECPNC NF membrane, the black surface shows the CNTs which have been reacted onto the white PES support, b) a plain PA membrane, c) SEM image showing the top surface of the PA-CNT ECPNC thin film morphology, d) SEM image showing the top surface of the plain PA thin film. While not identical, there are similar noodle-like structures found on both surfaces.

PA-CNT layer (Figure 4.12 a)). The PA-CNT layer is the active rejection layer that comes in contact with the salt solution. A few CNTs were visible within the PA matrix and although they were difficult to pinpoint, figure A.19 provided in Appendix A show CNTs within this thin-film. From the TEM images, the CNT layer was measured to be approximately 400 nm thick. The filamentous upper layer was measured to be approximately 100 nm thick.

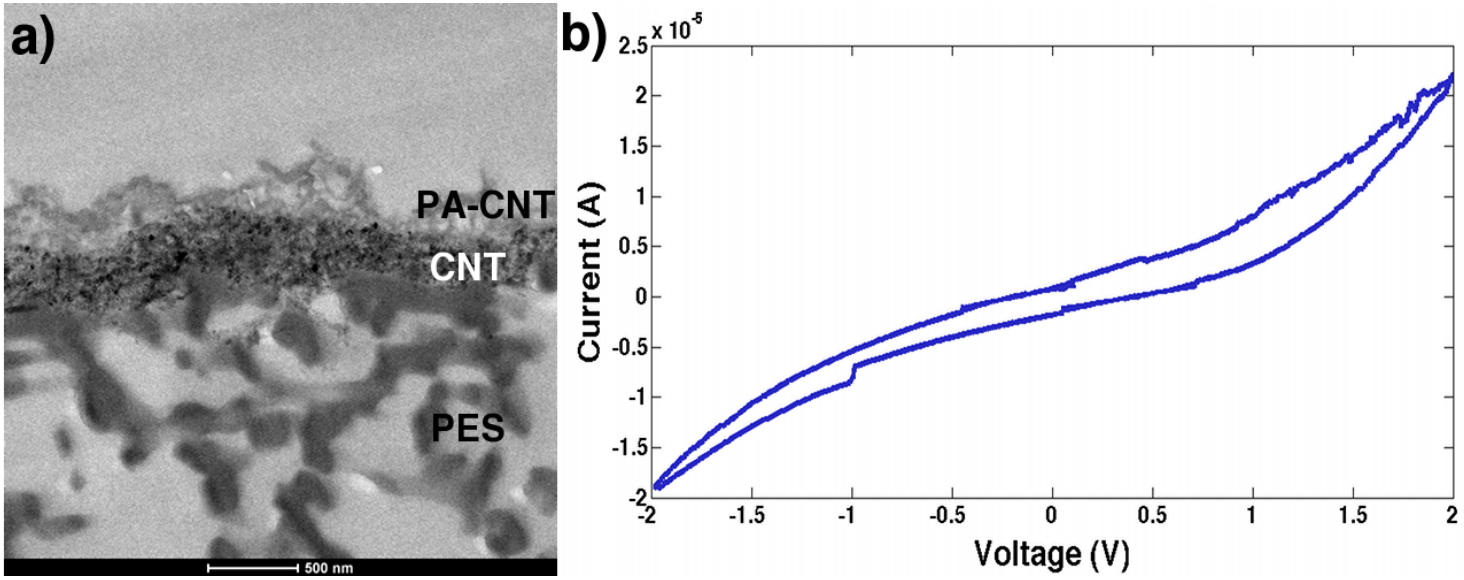

FIGURE 4.12: TEM image of the ECPNC PA-CNT membrane. Three layers are evident in a), the PES support, the deposited CNT layer, and the PA-CNT composite layer. In b) cyclic voltammetry data of the electrically conductive ECPNC surface reveals a linear relationship between $-0.9\,V$ and $0.9\,V$.

The measured sheet resistance of the ECPNC thin film surface was 6436 $\pm$ 336 Ω/sq. This is slightly higher than the sheet resistance of pure buckypaper, (2001000 Ω/sq, depending on film thickness) (De et al., 2009). Assuming a CNT thickness of $400\,nm$ as measured from the TEM images (figure 4.12), the membrane has an electrical conductivity of $\sim 400\,S/m$, which is nearly 2 orders of magnitude greater than seawater ($4.8\,S/m$). Cyclic Voltammetry was performed on the surface of the ECPNC membrane, in 1 M NaCl with an Ag/AgCl reference electrode with 4M KCl. Current to Voltage is linear from $-0.9\,V$ to $0.9\,V$ (figure 4.12 b)).

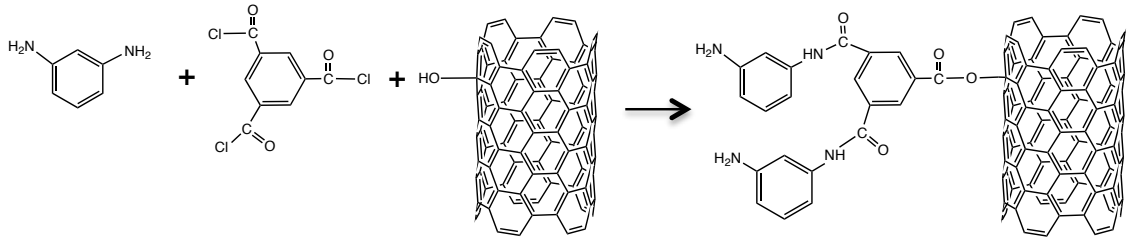

FIGURE 4.13: Condensation reaction between TMC, MPD and hydroxyl group on CNT sidewall leading to the incorporation of the CNTs into the membrane matrix.

ECPNC Chemical Bonding The CNTs used in this study were sold as carboxylated CNTs, with a carboxyl group content of 3.86%. To carboxylate the CNTs, the manufacturer refluxed the material with a mixture of sulfuric and nitric acid. It is known that refluxing CNTs in this mixture of strong acids adds both carboxyl (Datsyuk et al., 2008) (Geng et al., 2007) and hydroxyl side groups (Geng et al., 2007) (Hamon et al., 2002) to varying proportions depending on the ratio of the acids (Wepasnick et al., 2011).

The addition of carboxylated/hydroxylated CNTs to the PA matrix is evident by the appearance of the FTIR peak at $1725\,cm^{-1}$ (Figure 4.14) that is associated with the C=O stretching mode. Other peaks typically associated with PA, such as the C=O stretching of the amide bond ($1643\,cm^{-1}$), C=C ring stretching of the aromatic

amide ($1610\,cm^{-1}$), and N-H in-plane bending and N-C stretching vibration of the -CO-NH- group in the amide ($1543\,cm^{-1}$), are also evident (Figure 4.14).

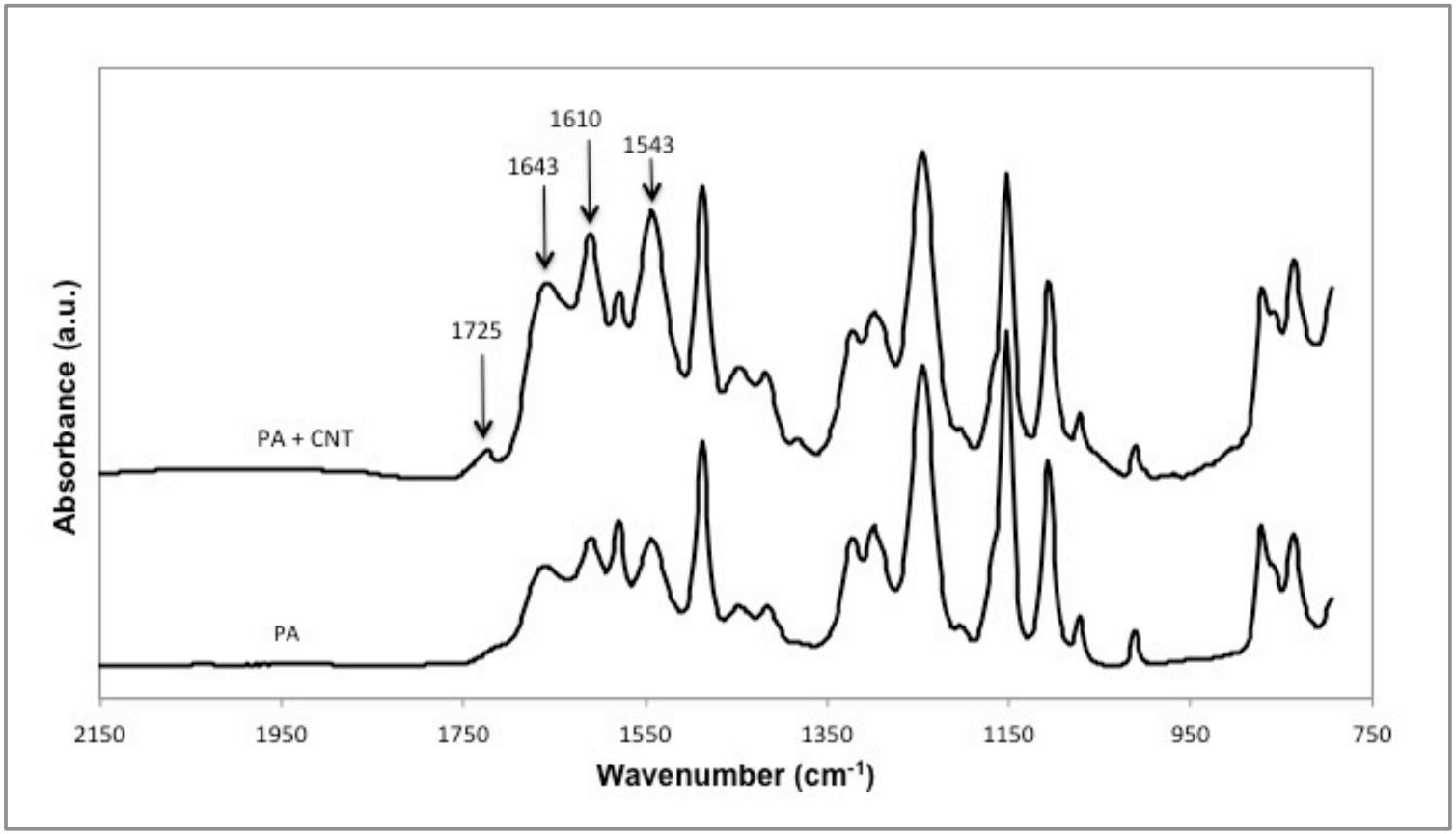

FIGURE 4.14: ATR-FTIR spectra of the membranes used in the study. The top curve is the PA+CNT polymer, while the bottom curve is the plain PA membrane.

Table 4.1: Salt rejection characteristics of electrically conducting tight NF membrane

Solution	Potential (V)	Salt Rejection
DIW + NaCl ($1\,g/L$)	1.5	$92.1 \pm 1.3\%$
DIW + NaCl ($1\,g/L$)	0	$91.3 \pm 0.9\%$
LB ($1\,g/L$ NaCl)	1.5	$93.4 \pm 2.1\%$
LB ($1\,g/L$ NaCl)	0	$95.2 \pm 1.6\%$

Salt Rejection and Permeability with and without Applied Potential NaCl rejection, measured as changes in conductivity, exceeded 90% in all cases (Table 4.1). Pure water permeability was assessed in the presence and absence of an applied voltage (1.5 V bloc current). Water permeability was measured at $8.8 \pm 1.0 \times 10^{-12}\,m/Pa \cdot s$ and $9.2 \pm 1.3 \times 10^{-12}\,m/Pa \cdot s$ ($3.2 \pm 0.4\,L/m^2 \cdot h \cdot bar$ and $3.3 \pm 0.5\,L/m^2 \cdot h \cdot bar$) with and without an applied voltage, respectively. In-house prepared plain PA membranes had water permeability of $1.3 \pm 0.2 \times 10^{-12}\,m/Pa \cdot s$ ($0.48 \pm 0.06\,L/m^2 \cdot h \cdot bar$) and NaCl rejection of 91.3%. Commercially available tight NF membranes achieve water permeability typically in the range of $1.58 \pm 0.11 \times 10^{-11}\,m/Pa \cdot s$ and $3.19 \pm 0.08 \times 10^{-11}\,m/Pa \cdot s$ ($5.7 \pm 0.4\,L/m^2 \cdot h \cdot bar$ and $11.5 \pm 0.3\,L/m^2 \cdot h \cdot bar$, respectively) and respectively their NaCl rejecting abilities at relatively low concentrations of $0.1\,g/L$ vary greatly from 66% to 99% (Plakas and Karabelas, 2008). The membrane material described in this work achieves a rejection value near the top of this range, with a permeability that is slightly lower.

4.2.2.3 Discussion: PA-CNT Electrically Conductive Nanofiltration Membrane Properties

Thin Film Surface Morphology Thin films formed from pure PA show the typical noodle-like structure that is widely reported in the literature. This structure is a result of the polymerization that occurs at the interface between the aqueous phase and the hexane phase. The TMC monomers in the aqueous phase polymerizes with the MPD monomers in the hexane phase by seeping into the hexane phase. The

interfacial polymerization and mixing that occurs results in the noodle structure. When hydroxylated CNTs are included into the MPD aqueous solution they may hinder the mobility of the MPD monomers and compete for reaction with TMC at the hexane interface. These two factors affect the surface morphology of the resultant membranes and forms a surface that is more wispy than noodle-like, as shown in figure 4.11. In addition, changes to surface hydrophilicity is likely the result of the addition of hydrophobic CNTs to the polymer matrix (Ghosh et al., 2008) (Jeong et al., 2007). CNTs are highly hydrophobic and while hydroxylated CNTs are more hydrophilic than their pristine form, these functional sites were assumed to be entirely consumed by reaction with TMC. The pristine, unfunctionalized sections of the CNT sidewalls were exposed at the surface of the CNT-imbued thin films, therefore, producing membranes with slightly higher surface contact angles.

Thin Film Surface Electrical Conductivity These thin films have been shown to be highly electrically conductive, however they are noticeably less conductive than films formed entirely of CNTs, i.e. buckypaper. The PA-CNT films are slightly less electrically conductive probably due to the insulating properties of the PA matrix. The polymer surrounding and grown from the CNT sidewalls partially hinders the electrical conductivity. However, for the application of an electric potential to the surface of the thin films for water treatment purposes as discussed above, the electrical conductivity of the PA-CNT composite tight NF membrane is more than sufficient. In order to preferentially allow the flow of electrons through the surface of the membrane, the electrical conductivity of the surface of the membrane must be significantly larger than that of the bulk of the solution. This is the case, the surface electrical conductivity is close to 2 orders of magnitude higher than that of sea water.

CNT-PA Chemical Bonding There are two possible reactions that may occur between CNTs and the TMC monomer constituent of PA. The first is that the acyl chloride group on the TMC molecule can react with the hydroxyl side group on the surface of the CNT to form an ester bond (figure 4.13) (**?**). The second is that the acyl chloride can react with the carboxyl groups on the CNTs. However, the resulting anhydride in the latter reaction is not stable in water and the bond is quickly hydrolyzed. Therefore, the most likely reaction is the reaction with hydroxyl groups on the CNT sidewalls. This is shown in the FTIR data presented in figure 4.14. The peak at $1725\,cm^{-1}$, indicative of the C=O stretching mode, is a result of the ester bond formed from the condensation reaction between the acyl chloride group on the TMC and the hydroxyl group on the CNT (Qin et al., 2003).

Salt Rejection and Permeability As was demonstrated in table 4.1, these electrically conductive thin films have high salt rejection, greater than 90%. This level of salt rejection indicates that the membranes are suitable for reverse osmosis or tight nanofiltration desalination applications, although improvements to the rejection capabilities are desirable. Under the application of a $1.5\,V$ alternating potential, the membranes did not show any statistically significant difference in salt rejection or flux. This similarity implies that applying an electrical potential to the membrane does not change its transport properties.

Commercial NF membranes often undergo several post fabrication processing steps, such as chlorine treatment, that increase their permeability. The membranes described here did not undergo any such treatments, and therefore, it is reasonable to expect that their permeability could be increased significantly. Further, commercial RO membranes have similar permeability to those of our ECPNC membranes, with higher salt rejection. With greater optimization of the CNT-PA layer, it is reasonable to expect higher salt rejections in the future, making ECPNC membranes more

comparable to commercial RO membranes.

4.2.2.4 Conspectus: PA-CNT Electrically Conductive Nanofiltration Membrane Properties

The development of a novel electrically conductive, salt rejecting, high-flux thin film composite provides exciting possibilities for efficient nanofiltration and reverse osmosis operations. The conductive properties of the membrane material create an electrically conductive surface that can be utilized in multiple applications Importantly, incorporating CNTs into the membrane matrix to allow electrical conductivity does not significantly sacrifice two of the most important properties crucial for NF processes, namely salt rejection and water permeability. Based on current CNT costs, imparting electrical conductivity to NF membranes would add $\$2.5/m^2$ in material costs representing only a 1.5% increase in the total price of traditional tight NF membrane modules. A more detailed long-term economic analysis is provided in the Appendix A.

4.2.3 Preventing Aquatic Biofouling on the Surface of Electrically Conductive Polyamide - Carbon Nanotube Nanofiltration Membranes

4.2.3.1 Proem: Preventing Aquatic Biofouling on the Surface of Electrically Conductive Membranes

Electrically conductive polymer-nanocomposite (ECPNC) tight nanofiltration (NF) thin film membranes were demonstrated to have biofilm-preventing capabilities under extreme bacteria and organic material loadings. We report here on the prevention of long-term biofilm growth achieved using a novel, highly electrically conductive polymer nanocomposite (ECPNC) tight NF membrane. This is made possible by the development of a simple route to the creation and application of new polymer nanocomposite membranes and a modification of the traditional cross-flow system that, taken together, eliminates the need for aquatic bacterial disinfection.

To demonstrate these membranes' biofouling capabilities, we designed a cross-flow water filtration vessel with insulated electrical leads connecting the ECPNC membranes to an arbitrary waveform generator. In all experiments, conducted in highly bacterially contaminated LB media, flux tests were run until fluxes decreased by $45 \pm 3\%$ over initial flux. Biofilm-induced, non-reversible flux decline was observed in all control experiments and a cross-flow rinse with the feed solution failed to induce flux recovery. In contrast, flux decrease for the ECPNC membranes with an electric potential applied to their surface was only caused by deposition of bacteria rather than bacterial attachment, and flux was fully recoverable following a short rinse with the feed solution and no added cleaning agents. The prevention of biofilm formation on the ECPNC membranes was a long-term effect, did not decrease with use, and was highly reproducible.

4.2.3.2 Findings: Preventing Aquatic Biofouling on the Surface of Electrically Conductive Membranes

Biofilm Development and Biofouling Prevention In this study we demonstrated the ability of ECPNC membranes to prevent biofilm development, and thus biofouling, during filtration and desalination of bacterially contaminated saline waters. Despite the extreme conditions to which we subjected these membranes, biofouling prevention was consistently and repeatedly confirmed. Robust controls done in triplicate were performed to verify these findings.

Biofouling Control Experiments As shown in figure 4.15, all control experiment fluxes decreased over time. In all control experiments, there was no significant (less than 15%) or lasting (less than 20 minutes) flux recovery due to cross-flow flushing, as shown in the supplementary data. Continued cross-flow desalination of the feed caused rapidly decreasing water flux, as shown in figure 4.15 and supporting information. In each control, a rapid decline in flux followed immediately after the flushing

procedure. Several flushing procedures were performed for the control experiments (orange and blue dotted lines) shown in figure 4.15 (red circles represent flushing points). Flushing for control type 2 occurred after 22 hours, and three flushing procedures were performed for control type 3, which occurred after 30, 32.5, and 35 hours. As can be seen in figure 4.15, none of these flushing procedures had any lasting effect on the permeate flux of the membrane. Control 1 demonstrated the characteristic biofouling behavior of PA RO membranes without pretreatment. CNTs have been shown to have some anti-bacterial activity, as demonstrated by others (Kang et al., 2008), but control 2 demonstrated that the potential anti-bacterial properties of CNTs in the ECPNC membranes were not effective in preventing biofilm formation when exposed over time to highly concentrated suspensions of bacteria (figure 4.15 blue hashed line). Control 3 eliminated the possibility of either Joule heating or electrical discharge from the electrodes as a factor in preventing surface biofilm formation (figure 4.15 orange dotted line).

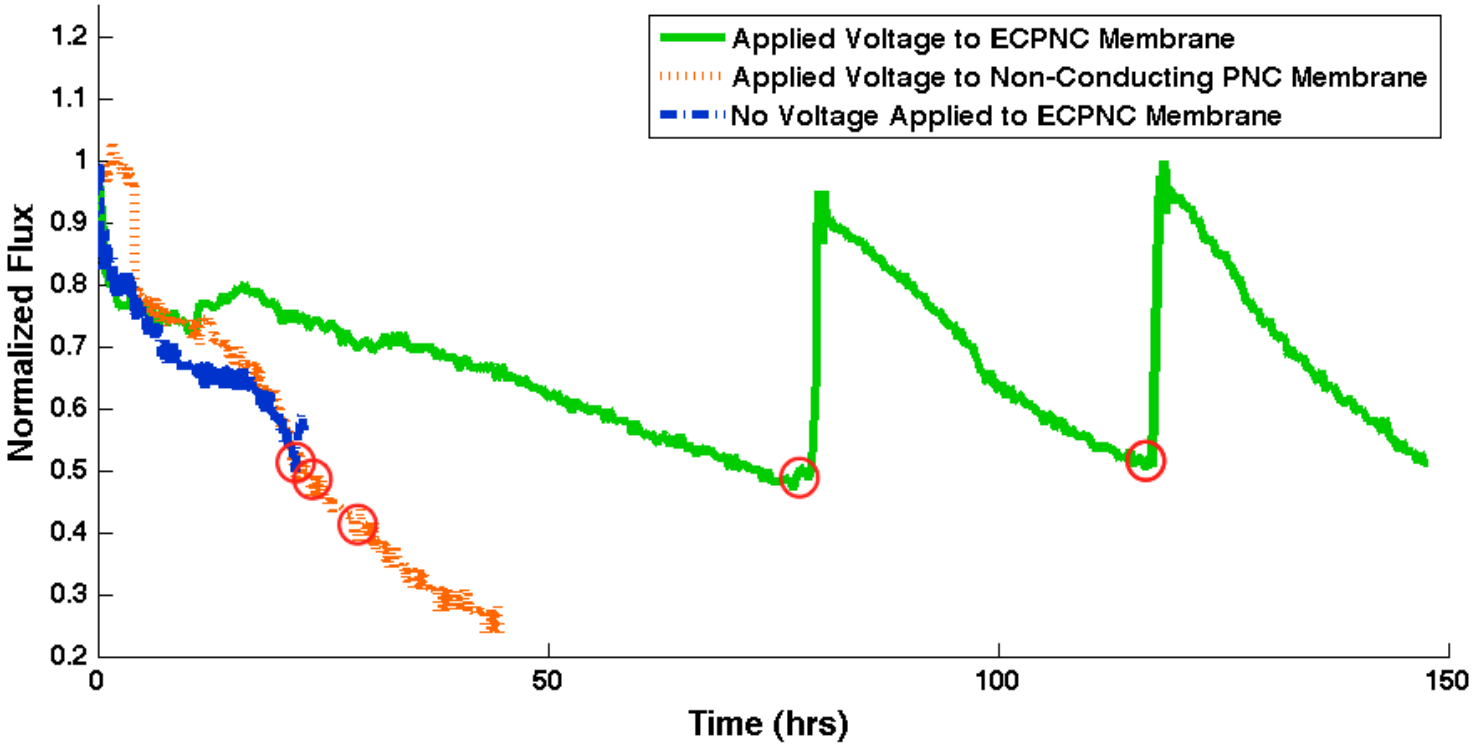

FIGURE 4.15: Control experiments without applied voltage and with highly resistive membranes with applied voltage suffered from irrecoverable biofouling. ECPNC membranes, with applied voltage, demonstrated much longer resistance to flux decline and flux was completely recoverable with one minute of cross-flow flushing. Red circles represent membrane flushing points. Bacteria grew continuously throughout all experiments so that bacterial concentrations increased as a function of time. Further, permeate was collected at high recoveries without feed recycling, so that feed concentrations increased throughout the experiment.

Table 4.2: Salt Rejection of ECPNC Membranes Before and After Cross-Flow Flushing

Salt Rejection	Control w/o V	Experiment w/V
Initial	$93.2 \pm 1.6\%$	$96.7 \pm 4.0\%$
Before Flushing	$89.4 \pm 2.6\%$	$95.6 \pm 6.1\%$
After Flushing	$90.0 \pm 2.0\%$	$94.6 \pm 4.6\%$

Biofouling Prevention with Electrically Charged ECPNC In the case of ECPNC membranes connected to the voltage generator ($1.5\,V$ square wave, $16.7\,mHz$), the flux reduction and recovery behavior were significantly different. A comparison of the controls with the ECPNC membranes is shown in figure 4.15. While flux loss did occur for the electrically charged ECPNC membranes, the rate of flux decline was up to three times lower than in the control experiments, with a 45% flux decline observed only after 80 hours, compared to 22 and 30 hours in experiments for control types 2 and 3, respectively. Further, after performing the pressure reduction and 1 minute of cross-flow flushing (with no cleaning agents), followed by continued desalination at high pressures, water flux was consistently and reproducibly recovered from 92% up to 100% of the initial flux. Flux recovery of such magnitude was reproducible throughout continued desalination of the feed and over triplicate experiments (figure 4.15 and supplemental information). In figure 4.15, these flushing procedures and their resultant flux recoveries can be clearly seen to occur after 80 hours and again after 118 hours (red circles). Salt rejection was monitored in all experiments (Table 4.2). Salt rejection was identical immediately before and after cross-flow flushing, demonstrating that flux recovery in the ECPNC membranes with applied voltage was not attributed to structural damage. The variations within the salt rejection data are statistically insignificant both throughout each experiment and between experiments and controls.

Membrane autopsies were performed post experiment and then prepared for imag-

ing under high resolution SEM. Images of the membrane surface show that control membranes were fouled with dense biofilms, while ECPNC membranes with applied voltage show clean and compressed surfaces lacking any evidence of bacterial attachment or EPS (Figure 4.16). As additional support for this claim, DAPI staining of the membranes was performed. Control membranes showed bright, homogeneous staining throughout the membrane, indicating large amounts of bacterial DNA located on the membrane surface. In comparison, ECPNC membranes with applied voltage showed insignificant amounts of bacterial DNA, suggesting a significant dearth of attached bacteria and an absence of biofilms.

4.2.3.3 Discussion: Preventing Aquatic Biofouling on the Surface of Electrically Conductive Membranes

Evidence for Biofilm Growth Prevention The results of these long-term experiments are explained in terms of biofilm development versus deposited organic matter. If the reduction in flux could be attributed solely to pressure deposited organic matter, including bacteria, unpressurized cross-flow flushing would remove the deposited organic matter, returning flux to its initial value (within some error, due to incomplete removal). However, if a biofilm formed, cross-flow flushing would not remove the EPS-bound biofilm. It has been shown in the literature that biofilms formed from the deposition of EPS are exceedingly difficult to remove (Ahmad et al., 2005). Neither back flushing of membranes, nor increased cross-flow velocities are effective in the removal of established biofilms. In the case that flux could not be recovered by increased cross-flow velocity, the loss of flux is wholly attributed to biofouling and EPS deposition, rather than to deposited organic matter. The control experiments demonstrate traditional biofilm formation, as evidenced by irrecoverable water flux, SEM images of biofilms, and DAPI staining of bacterial DNA. In stark contrast is the highly recoverable flux behavior of the electrically charged ECPNC membranes

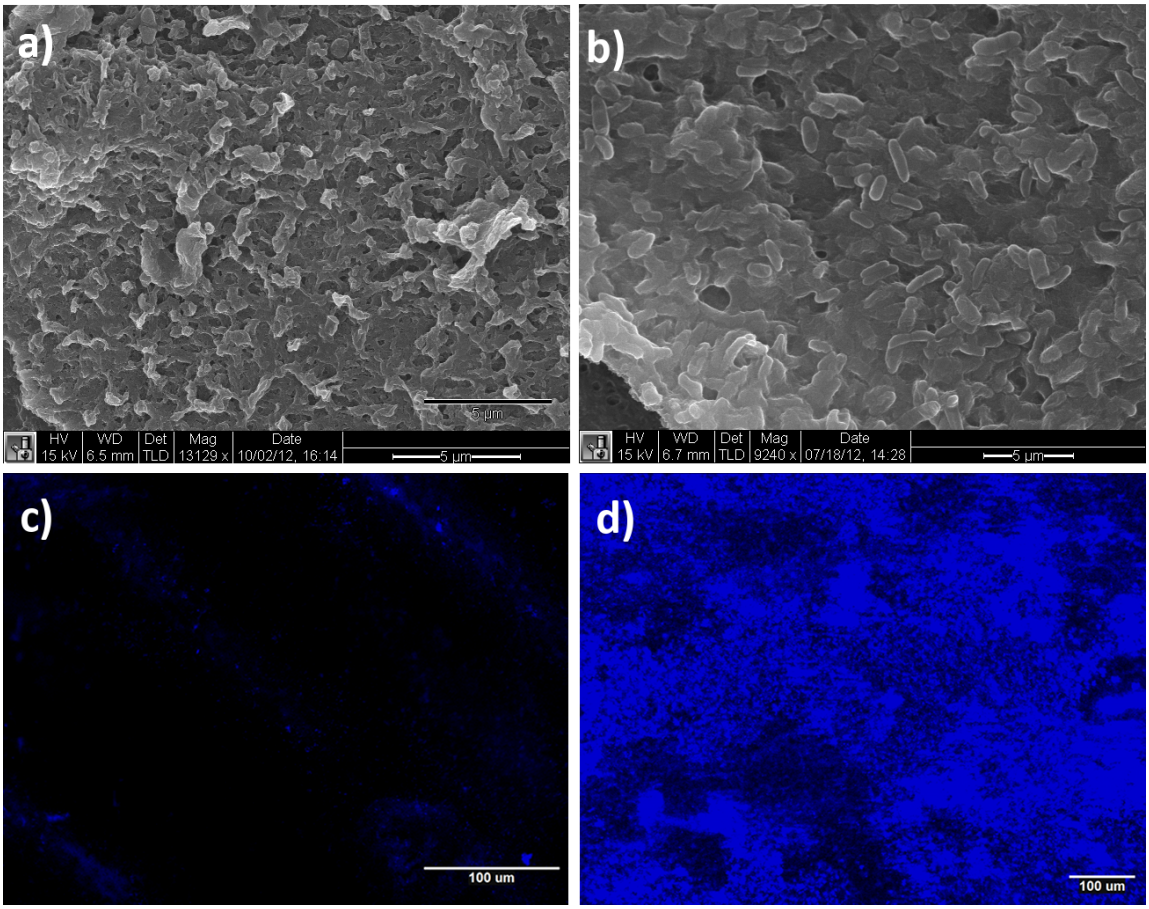

FIGURE 4.16: Membrane surfaces after desalination of *P. Aeruginosa* in LB media (same scale). In a) the SEM image shows a clean ECPNC surfaces devoid of biofilms after 6 days of continuous desalination of *P. Aeruginosa* in LB media. The rough surface is typical of compressed polyamide surfaces. In b) the SEM image shows the control membrane surface completely fouled with bacteria after 2 days of continuous desalination of *P. Aeruginosa* in LB media. EPS layers forming the biofilm are evident showing smooth interconnections between bacteria. In c) DAPI staining of the ECPNC membrane surfaces shows a small amount of bacterial DNA located in thin strips. In d) DAPI staining of the control membrane indicates large amounts of bacterial DNA throughout the membrane surface.

connected to a voltage source as well as the biofilm-free surfaces in the SEM and fluorescence images. The flux reduction in this case is solely due to deposition of organic matter from the applied pressures, rather than from biofilm formation.

Biofilm Growth Prevention Mechanism The mechanism for the prevention of biofilm formation through applied alternating electrical potential is currently not fully understood, but it is hypothesized to occur for a number of reasons. We hypothesize that an alternating electrical potential causes instabilities in the local pH and to the electrical double layer (EDL). These non-equilibrium conditions at the membrane surface create non-ideal environments for bacteria, obstructing the production of EPS. Further, during times of negative applied potential, it has been shown that bacteria are repelled by like-charge electrostatic interactions (Hong et al., 2008). Under positive applied potential, bacteria discharge the surface of the ECPNC membrane, causing oxidizing conditions, which have been shown to lead to cell lysis and cell death (Shim et al., 2011). Finally, given the cyclic voltammetry measurements (linearity between $\pm 0.9\,V$) and the applied potential ($1.5\,V$), hydrolysis may occur at the ECPNC surface. However, the over-potential for hydrolysis is only attained very near to the electrode contact point. As a result, hydrolysis that occurs within the flow cell would only have minimal effect on the overall biofouling resistance of the membrane. The composite effects occurring with environmentally relevant bacterial populations under realistic high-pressure conditions have not been explored.

4.2.3.4 Conspectus: Preventing Aquatic Biofouling on the Surface of Electrically Conductive Membranes

Highly electrically conductive tight NF membranes with the application of an external electric potential have been shown here to completely resist the development and proliferation of biofilms during the longterm desalination of bacterially contaminated feed waters. Despite some unanswered mechanistic questions surrounding this pro-

cess, the development of a novel electrically conductive, salt rejecting, high-flux thin film composite provides exciting possibilities for biofouling resistant salt separations. This novel electrically conductive tight nanofiltration membrane been shown here to completely prevent biofouling. By completely preventing biofilm formation and thus providing continued water flux recovery, ECPNC membranes offer a potential means to greatly reduce expensive and environmentally costly RO pre-treatments. With these improvements in current practices, RO can become an efficient alternative to other water treatment technologies, and can provide a cost-effective and environmentally benign way to fill the growing water needs of the world.

4.3 Development and Application of Membranes Formed with Polymer Wrapped CNTs Embedded in Membrane Polymers

4.3.1 Leaching of Functionalized Carbon Nanotubes from Polysulfone Ultrafiltration Membranes

4.3.1.1 Proem: CNT Dispersion in and Leaching form PSf Ultrafiltration Membranes

In this study, we have carboxylated CNTs at a range of weight percentages (0-10.55%), fabricated polysulfone ultrafiltration nanocomposite membranes with these CNTs, and investigated the changes in the tensile strength, hydrophilicity, and water flux of these membranes as a function of increasing carboxylation. In so doing we discovered that the change in membrane properties was not solely caused by the increasing dispersion due to greater functionalization, but that the stability of the CNTs within the polymer matrix played a crucial role. Higher degrees of functionalization caused greater loss of CNTs from the polymer membrane during formation and showed a greater tendency to leach CNTs from the membranes during membrane cleaning. This is of great import as there is concern that nanoparticles and CNTs, in particular, may have negative effects to humans and environmental ecosystems (Xia et al., 2006). Although their possible toxicological effects remain a topic of active investigation, it is prudent to minimize their release into the environment both from an environmental, practical, and economic perspective. No papers to date have investigated the potential for CNTs to leach from their polymeric membranes in which they are suspended. We have quantified the loss and/or leaching of CNTs during membrane production, use, and membrane cleaning as a function of %-carboxylation. In this way, we are able to identify the optimal %-carboxylation of CNTs for inclusion into PSf membranes. Finally, we propose ways in which CNTs can be maximally incorporated into polymeric matrices.

4.3.1.2 Findings: CNT Dispersion in and Leaching from PSf Ultrafiltration Membranes

Multiwalled CNTs were functionalized with carboxylic acids on their end caps and sidewalls as described briefly in section 3.4.2. Varying the acid conditions to which the CNTs were exposed controlled the degree to which CNTs were functionalized. The degree of carboxylation was measured as a weight percentage. This weight percentage was related to the relative atomic molar mass of carbon as compared to the atomic molar mass of the carboxyl group, i.e. 12 g/mol for carbon compared with 33 g/mol for the carboxyl group. The value of the weight percent of carboxylation of CNTs is thus the total amount of mass that is composed of oxygen and hydrogen in any measured amount of CNTs. For example, in a $10\,g$ sample of 2.56 wt% carboxylated CNTs, $0.256\,g$ of -OOH and $9.744\,g$ of C are present in the sample. Dividing by their molar masses, we determine that there are 0.007758 moles of -OOH and 0.812 moles of C in this $10\,g$ sample of CNTs. Further, these CNTs have a carboxylation of 0.946 mole %, which imples there is approximately 1 carboxyl group for every 100 C atoms. We are using multiwalled carbon nanotubes, thus only the outer walls are functionalized. If one assumes approximately 10 walls per tube, the carboxyl groups occupy approximately 10 % of the surface of the tube. CNTs were carboxylated between 0% and 10.55% by weight. After functionalization and purification, these modified CNTs were suspended in DMF, which then acted as the solvent for PVP and PSf. The degree to which CNTs were functionalized affected not only their intrinsic properties, but also the properties of the final polymer-CNT nanocomposite material.

CNT Functionalization MWCNTs were mixed with a 3:1 sulphuric to nitric acid mixture to form an aggressively oxidizing environment. By varying either the reaction time or the concentration of acids, it was possible to control the degree to which

Table 4.3: The reaction conditions that were used to achieve varying carboxylation of MWCNTs.

Carboxylation Degree (wt%)	0%	6.53%	6.94%	7.97%	8.29%	9.91%	10.55%
Reaction Time (hrs)	0	1	2	4	4	8	8
Volume of Acids to Mass of CNTs (mL/g)	0	150	150	75	150	150	75

CNTs were functionalised. In Table 4.3, the achieved weight %- carboxylation of CNTs is correlated to the various reaction conditions used.

The degree of carboxylation was determined from XPS. It is known that functionalization in this acid mixture is not limited entirely to carboxylation; there are significant amounts of hydroxyl and carbonyl functional groups added as well. The ratio of each of these three functional groups remains constant if the sulphuric to nitric acid ratio is kept constant, and is not affected by either the reaction time or the acid concentration (Wepasnick et al., 2011). As the ratio of sulphuric to nitric acid was the same for each CNT functionalization experiment, it was sufficient to determine the change in CNT carboxylation degree in order to investigate the effect that increasing acid functionalization would have on the properties of the final polymer nano-composite. XPS was used to determine the weight percent of single and double bonded oxygen to carbon on the CNTs, shown in figure 4.17. As the reaction time increased, and as the concentration of acids increased, an increase in the concentration of covalently bonded oxygen on the MWCNT was observed.

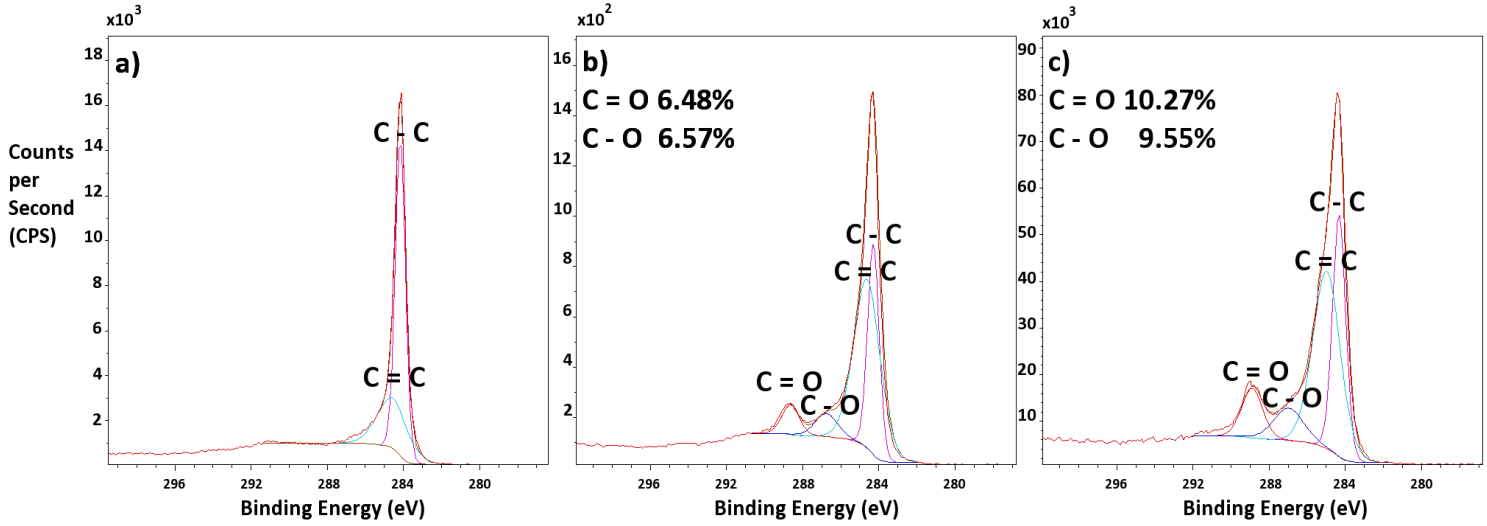

FIGURE 4.17: XPS data showing the main carbon bonding (C-C) peak and the small peaks representing the carboxyl, hydroxyl, and carbene groups formed on the CNTs. In a) pCNTs with no carboxylation show a lack of secondary and tertiary peaks about the main C-C bonding peak. In b) CNTs carboxylated to 6.53% show a small peaks about the main carbon peak indicating single- and doubly-bonded carbon to oxygen (C-O and C=O). In c) CNTs that have been carboxylated to 9.91% demonstrate more prominent peaks about the C-O and C=O bonds.

CNT Dispersion in PSf-PVP Membranes In order to thoroughly disperse CNTs in the polymer solutions, CNTs were sonicated in DMF prior to dissolution of the polymer. Suspension by sonication was much more effective for CNT-COOHs than for pCNTs, as expected. After sonication, carboxylated CNTs stayed in suspension indefinitely, while pCNTs precipitated out of solution within hours. To contend with this difficulty, PVP and PSf were added sequentially to the solvent-CNT suspension immediately after sonication. The final mixture was black, viscous, and homogeneous suggested by the lack of macroscopic aggregates in the mixtures. The viscous solution was then cast on a glass plate and precipitated in DIW. For each membrane, the original polymer nanocomposite solution contained 0.5 wt% CNTs with respect to the polymer constituents. SEM images of formed membranes are shown in figure 4.18 a) and b). Membranes made with pCNTs contained large aggregates found predominantly within the membranes as seen from cross-sections, while individual CNT fibers were uncommon. Membranes formed with CNT-COOHs of all functionalization weight percentages show more uniformly dispersed and individualized CNTs within the bulk membrane, with no apparent aggregates. No discernible difference was found between the internal and external morphologies of the formed membranes analyzed in SEM. Any physical, qualitative differences were assumed to be random variations due to the stochastic thermodynamic process of immersion precipitation.

Carbon Nanotube-Polymer Compatibility Ultrafiltration membranes undergo specific stresses throughout their life cycle, which may reduce the stability of CNT additives. We hypothesized that such processes could significantly affect the stability of CNTs within polymer membranes during membrane use. The stability of CNTs within polymer matrices affects key membrane characteristics and has implications for environmental release. Furthermore, we hypothesized that while theoretically, greater carboxylation of CNTs should provide greater benefits to the final polymer nanocom-

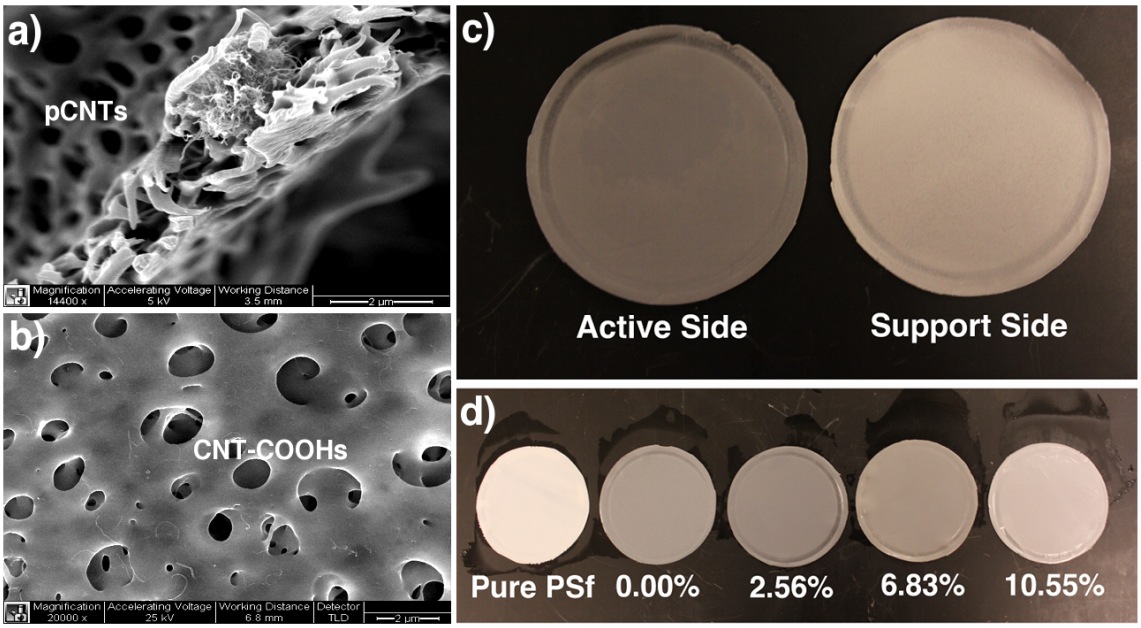

FIGURE 4.18: In a) aggregated pristine (unfunctionalized) MWCNT are found within the cross-section of a PSf membrane. In b) well-dispersed, functionalized CNT-COOHs (here functionalized to 7.97%) are seen spread evenly throughout the polymer membrane. In c) the active side of the CNT-COOH membrane is darker than the support side. In d) the color of the membrane surface is evidence of the compatibility of PSf with CNTs of various degrees of carboxylation. The membrane on the far left is composed entirely of PSf and PVP, while the other four membranes from left to right were made with polymer nanocomposite solutions with starting CNT concentrations of 0.5 wt% CNTs. The percentages indicate the degree to which the CNTs within those membranes were carboxylated.

posite membrane, highly carboxylated CNTs may have limitations with regards to stability and long-term compatibility, undermining their expected benefits.

Loss During Precipitation Immersion in Membrane Fabrication During immersion precipitation of the PSf-PVP-MWCNT solution, several phenomena were observed: 1) Small black plumes were noticed emanating from the membrane as the polymer system precipitated, 2) these black plumes were more evident for membranes composed of CNTs that were more heavily carboxylated, 3) the active side of the membrane was observed to be darker than the support side of the membrane, as shown in fig-

ure 4.18 c), 4) membranes containing CNTs with higher degrees of carboxylation were generally lighter in color than those with lower degrees of carboxylation, as evidenced in figure 4.18 d). UV-Vis absorption of the post-precipitation non-solvent bath was measured (explained in section 3.4.5 and used to identify the quantity of CNTs found in each precipitation bath from each type of membrane. The results of some of these measurements are shown in figure 4.19. The greater the amount of carboxylation, the greater the amount of CNTs found in the non-solvent bath.

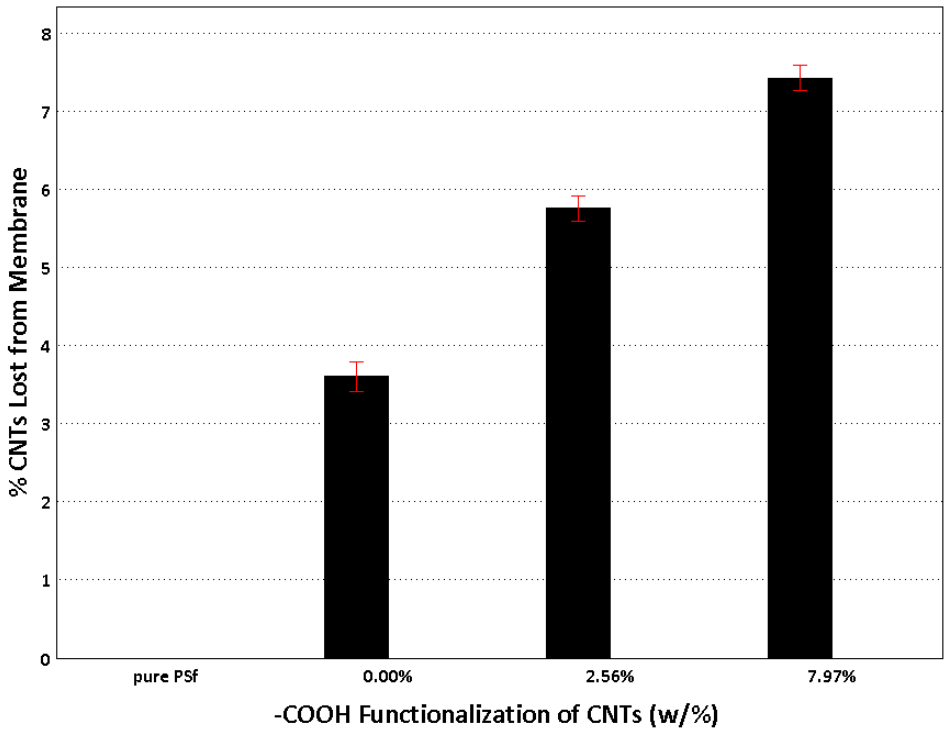

FIGURE 4.19: The loss of CNTs from polymer membranes during precipitation immersion in DIW. Membranes containing MWCNTs with higher degrees of carboxylation experienced greater losses of CNTs, while membranes formed with lesser degrees or no carboxylation, were shown to better resist the loss of CNTs from their polymer matrices.

Leaching During Caustic Cleaning of Membranes Microfiltration (MF) and ultrafiltration (UF) membranes are regularly exposed to harsh caustic and oxidizing (NaOH,

NaOCl) and sometimes reducing chemicals (HCl), during their operational lifetime to remove foulants and combat biofilms (Porcelli and Judd, 2010). PSf-PVP-CNT membranes containing CNTs of different carboxylation degrees were exposed to each of these chemicals for 2 hours to simulate a chemical cleaning regime. The chemical solutions were tested for the presence of CNTs after treatment of membranes and it was found that significant leaching of CNTs occurred. Figure 4.20 shows the fraction of CNTs released from the membranes during a single 2-hour exposure. CNT leaching from the membranes was observed to be greater with higher degrees of CNT carboxylation.

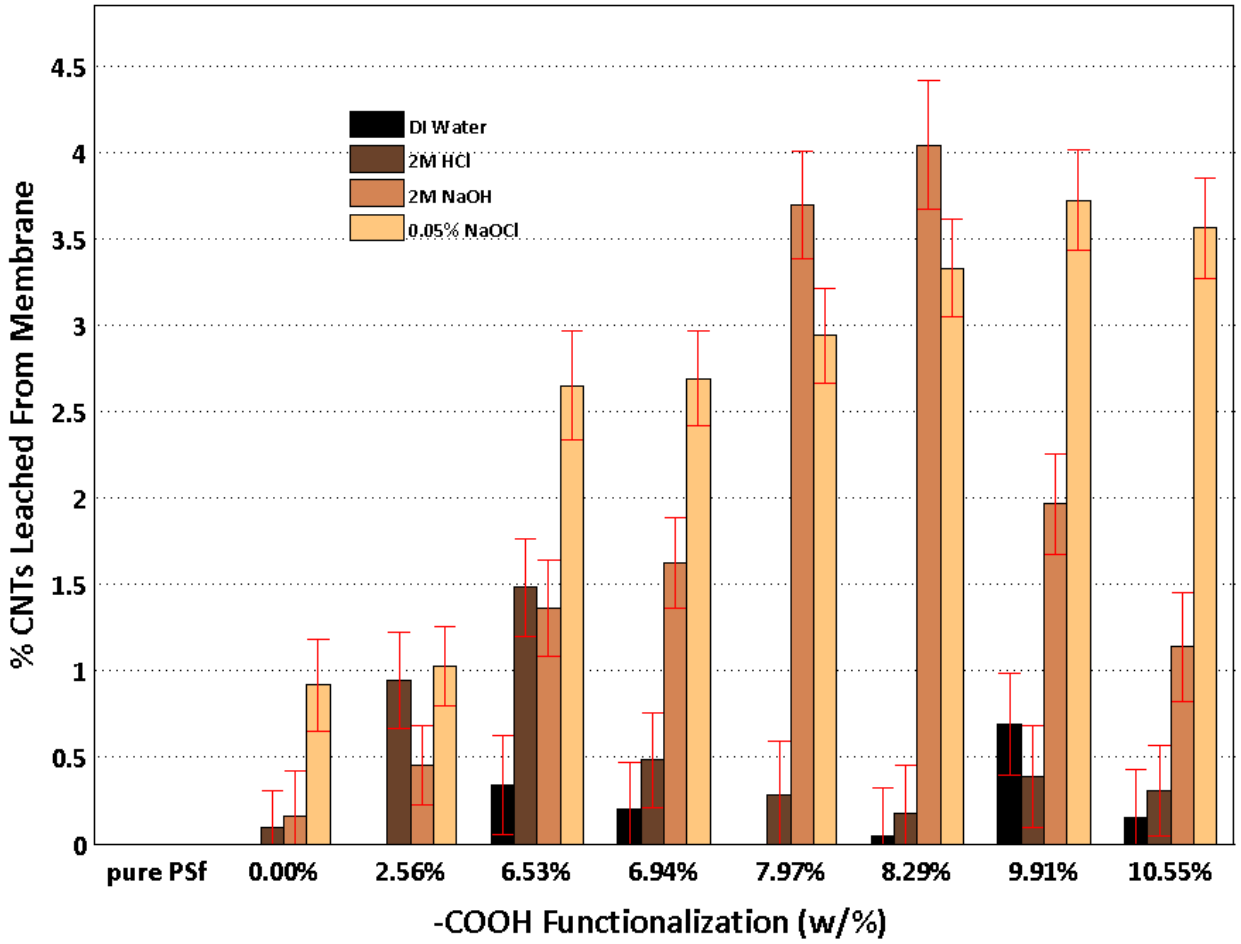

FIGURE 4.20: Leaching of CNTs from polymer membranes during membrane cleaning with three different caustic solutions: NaOH, NaOCl, and HCl. Membranes containing MWCNTs with higher degrees of carboxylation experienced greater leaching of CNTs during exposure to cleaning solution.

4.3.1.3 Discussion: CNT Dispersion in and Leaching from PSf Ultrafiltration Membranes

CNT Dispersion in PSf-PVP Membranes CNTs must be individualized rather than aggregated to exploit the desirable properties of CNTs most fully. Uniform dispersions within composites are also of paramount importance to capitalize on their properties. In this study, polymer nanocomposites were formed using solution chemistry, thus CNT dispersion within solvents was necessary, and achieving this required overcoming the intense van der Waals forces between individual nanotubes (Nakashima and Fujigaya, 2007). In this study this was realized through CNT sidewall and endcap carboxylation. As can be seen in figure 4.18 a) and b) (as well as in figure B.2 and figure B.3 in Appendix B), carboxylation greatly improved the dispersion and homogeneous distribution of CNTs throughout polymer matrices over that of pCNTs. CNTs offer greater material improvements when they are homogeneously distributed throughout the polymer matrix.

Stability of CNTs within PSf Membranes Stability of the CNTs within polymer composites is necessary. Stability implies that CNTs do not leach out during either material fabrication or the appropriate use and treatment of the product throughout its operational lifetime. Stability has varied implications at all stages of membrane life from industrial manufacturing, to membrane operation, from use, to disposal. For industrial membrane manufacturing, stability is important to reduce waste during production and to avoid environmental and workplace penalties associated with leached nanomaterials. Membrane operations is concerned with optimized nanocomposite membrane performance, which relies on the stability of CNTs within polymer matrices. For both the consumer and the environment during use and disposal, stability is critical to ensure minimized exposure routes and downstream risks associated with leached CNTs.

Water treatment membranes undergo many stresses throughout their lifetime: during membrane formation immersion precipitation causes major changes in the polymer-nanoparticle orientation (Kim and Lloyd, 1992); during membrane operation high pressures, turbulent cross-flows, and flushing and scouring can cause mechanical stresses (Childress et al., 2005); and during membrane cleaning in order to combat fouling, chemical oxidation and reduction can cause damage to the membrane (Porcelli and Judd, 2010). Loss and leaching of CNTs may occur at each of these stages.

In this study, precipitation immersion caused significant changes to the polymer nanocomposite solution (Kim and Lloyd, 1992). The carboxylated CNTs were well dispersed in the organic solvent, DMF, but they were less compatible with PSf (CNTs were not chemically bound within the polymer matrix). Using water as a non-solvent introduced a preferential phase for CNT-COOHs. As DMF diffused through the polymer solution during precipitation, CNTs preferentially segregated towards the side of the membrane initially in contact with water, i.e. the active side. This was observed by the darker color of the active side (figure 4.18 c). Migration to the active side was followed by escape into the non-solvent bath, evidenced by the changes in membrane color (figure 4.18 d) and the observed black plumes that emanated in the non-solvent bath during precipitation immersion. This loss during membrane formation was quantified with UV-Vis spectroscopy (figure 4.19). It was shown that CNTs with a greater degree of carboxylation were more susceptible to loss from the precipitating membrane, as a result of increased affinity for the polar non-solvent. This was evident both in the lighter coloration of the membrane surface (figure 4.18 d) and in the UV-Vis spectra (figure 4.19). The effective yield of CNTs placed in the composite, therefore was reduced. From a practical consideration, this material loss has associated economic costs as well as implications linked with an additional waste stream that must be treated, and the potential for workplace exposure.

During pure water flux testing of these membranes, no measurable amount of CNTs were observed to have leached from the polymer matrix into the permeate. This indicates that mechanical stresses, such as pressures, did not disturb CNT distribution within the polymer matrix once the polymer had been precipitated into its gelled state.

However, during membrane chemical cleaning some leaching of CNTs was detected (figure 4.20). Membranes were separately exposed to three different cleaning agents: HCl, NaOH, and NaOCl. In each case, CNT leaching was observed. As was true for CNT loss during membrane precipitation, it was found that with exposure to cleaning agents, in general membranes that contained CNTs with greater degrees of carboxylation showed greater leaching of CNTs from their matrices. With greater carboxylation, CNTs were more hydrophilic, and thermodynamically preferred to exist in a polar solution over a hydrophobic polymer matrix. Caustic cleaning agents are known to oxidize or reduce the surface of membranes, causing polymer chain reordering and sometimes breakage. This may have enabled more CNTs to leach from the polymer matrix. Leaching of CNTs during membrane cleaning was significantly lower than the loss of the CNTs during membrane precipitation.

It was observed that high CNT functionalization lead to lower final CNT yields within membranes and greater potential for creating nano-wastes. Releases were significantly smaller for lower functionalizations, but in all cases low functionalization did not prevent losses and leaching.

4.3.1.4 Conspectus: CNT Dispersion in and Leaching from PSF Ultrafiltration Membranes

Stability of CNTs within polymer matrices is an important parameter to consider when developing polymer nanocomposites from a manufacturing, use, and disposal perspective. It was shown that high CNT functionalization lead to high instabil-

ity within the membrane nanocomposites. This instability was observed both during membrane production (immersions precipitation) and during membrane surface cleaning (treatment with caustic chemicals). Releases were small for lower functionalizations, but losses can be reduced further and potentially eliminated altogether by increasing the affinity of CNTs for the polymer.

Stability of CNTs within polymer matrices is not only crucial for the long-term use of the product, but also to avoid the potentially harmful results of leached CNTs to the environment. The environmental repercussions of CNT contamination are not well known, and leached CNTs from products, such as membranes, could contaminate the waters they are meant to remediate. This loss also has the adverse effect of reducing the beneficial properties associated with CNTs. Finally, loss of CNTs is a manufacturing expense that should be avoided for economic reasons. To this end, it would behoove manufacturers of nanocomposite materials to look towards chemistries that permanently bind nanoparticles to their host materials in order to maximize their effectiveness within polymers, prevent economically expensive nanoparticle waste during manufacturing, and safeguard against contamination of the environment during production and use.

4.3.2 Properties of Ultrafiltration Membranes Formed from Polymer Wrapped Functionalized Carbon Nanotubes Embedded in Polysulfone

4.3.2.1 Proem: PSf-CNT Ultrafiltration Membrane Properties

Membrane properties including Young's Modulus, surface hydrophilicity, and pure water flux were investigated with respect to greater functionalization of CNTs. These properties were viewed in light of both a greater degree of dispersion within the polymer, and a lower overall quantity and quality of CNTs due to loss and sidewall damage, respectively, caused by functionalization.

4.3.2.2 Findings: PSf-CNT Ultrafiltration Membrane Properties

Young's Modulus and Stress Under applied stress, PSf undergoes linear, elastic non-deformation (reversible) and then inelastic deformation (irreversible) with increased applied stress, before eventually reaching material failure and breakage. During normal membrane operation, stresses that cause irreversible deformation of the membrane material create conditions that make the membrane unusable (Childress et al., 2005). Therefore inelastic deformation is equivalent to membrane failure for the purposes of industrial membrane operation. In this study, membranes were stretched under constant stress throughout their elastic, inelastic, and breakage regions. To analyze Young's Moduli, the elastic region was investigated, until the point of inelastic deformation. It should be noted that all polymer nanocomposite solutions used to form the final membranes contained 0.5 wt% CNTs with respect to the polymer constituents, regardless of the CNT functionalization degree. However the final amount of CNTs within the membranes differed as a result of loss of CNTs from the membranes during immersion precipitation (figure 4.19). In figure 4.21, Young's Modulus, therefore, is plotted against the increase in carboxylation of CNTs multiplied by the percentage of CNTs remaining in the membrane after immersion precipitation. This accounts for the final content of the CNTs within the membranes as well as the dispersion of the CNTs. The Young's Modulus of the nanocomposite membranes is compared to that of unmodified PSf-PVP polymer membranes, whose Young's Modulus does the orange line represent.

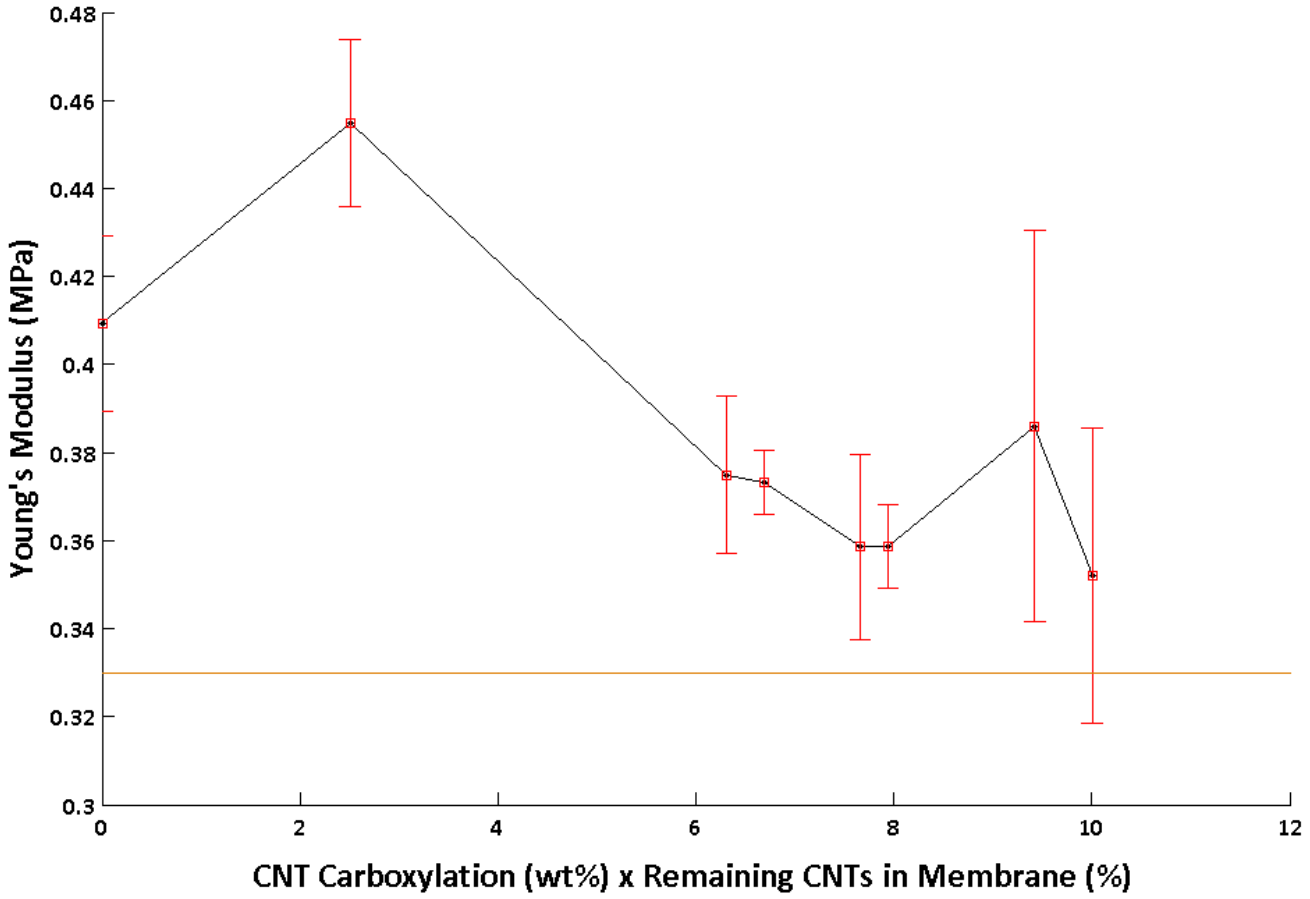

FIGURE 4.21: PSf membranes containing CNTs of varying degrees of carboxylation were strained under increasing amounts of stress. The Young's Modulus of these membranes is plotted against the varying degrees of CNT carboxylation. Increased carboxylation leads to an increased Young's Modulus initially, followed by a decrease. PSf membranes containing 0.5 wt% CNTs of all carboxylation showed improved Young's Moduli over pure PSf membranes (orange line).

Surface Hydrophilicity Surface hydrophilicity was determined through measurement of the triple point surface contact angle of a water drop in contact with the surface of the membrane in air. It should be noted, as in all of these experiments, that the initial CNT content of 0.5 wt% was the same for each of the membrane solutions, however the final quantity of CNTs in each of the solid membranes varied due to the loss of CNTs from the polymers to the non-solvent bath, during membrane fabrication in the precipitation step. Surface contact angle, and thus the hydrophilicity, of PSf membranes containing CNTs is therefore plotted against the degree to which the CNTs contained in the PSf membranes were carboxylated multiplied by the percentage of CNTs remaining in the membrane after immersion precipitation (figure 4.22). The surface hydrophilicity of the nanocomposite membranes is compared to that of unmodified PSf-PVP polymer membranes, whose contact angle does the orange line represent.

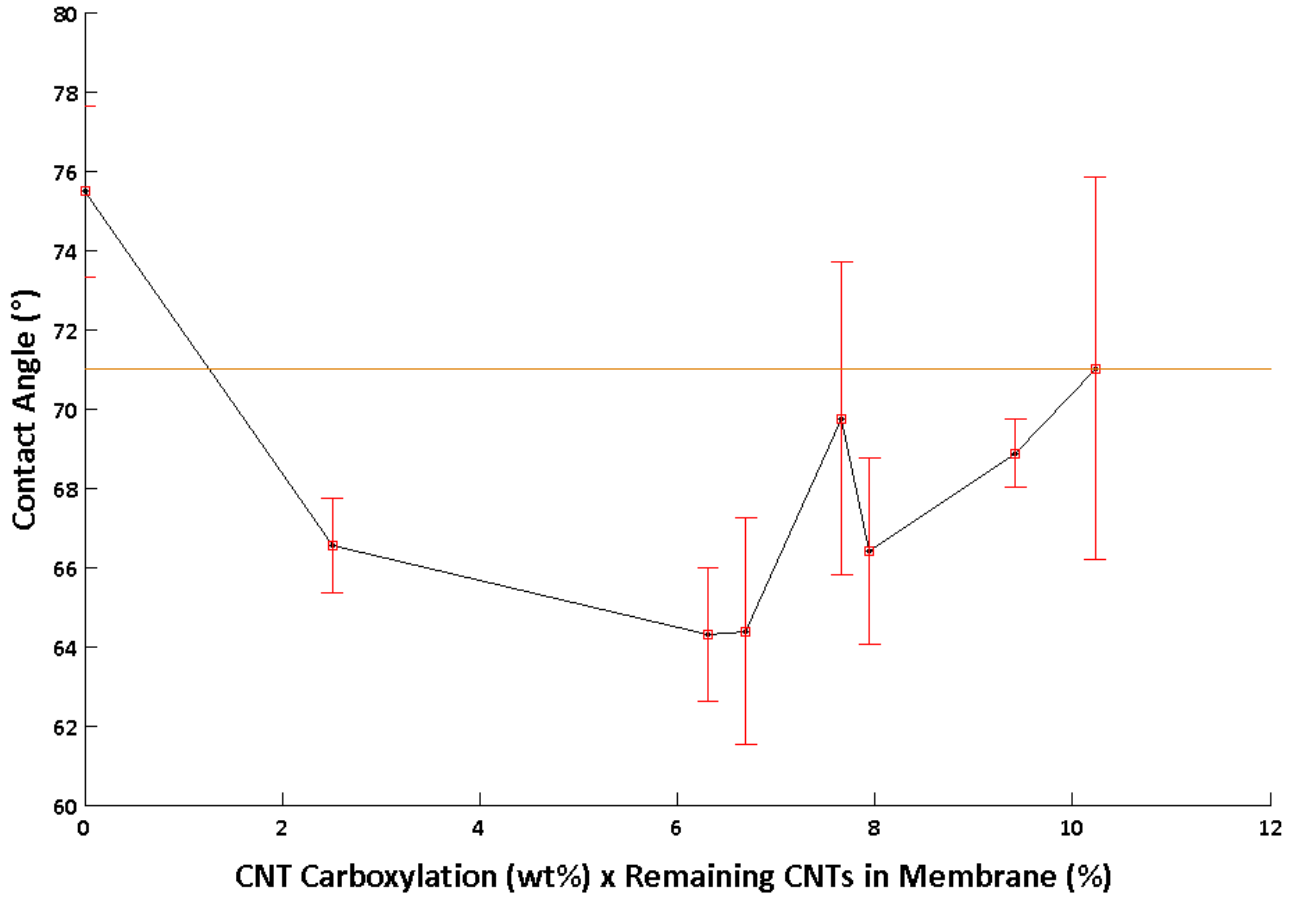

FIGURE 4.22: Surface contact angle of PSf membranes containing CNTs is plotted against the degree to which the CNTs were carboxylated. A decrease in contact angle implies a more hydrophilic surface. As carboxylation increases, the surface hydrophilicity increases initially, and then decreases with further carboxylation. The surface hydrophilicity for pure PSf membranes is shown in orange.

Pure Water Permeability Pure water flux was measured for all membranes in a dead-end filtration configuration. Pressures used ranged from $70\,kPa$ to $700\,kPa$. Flux measurements were performed in triplicate for each type of membrane, converted to permeability, and then averaged over all runs. As shown in figure 4.23, permeability of the membranes was higher for those that contained CNTs with greater degrees of carboxylation. Membranes composed from CNTs with greater carboxylation also experience, in general, much greater variation in their permeability, as evidenced by the significant error bars.

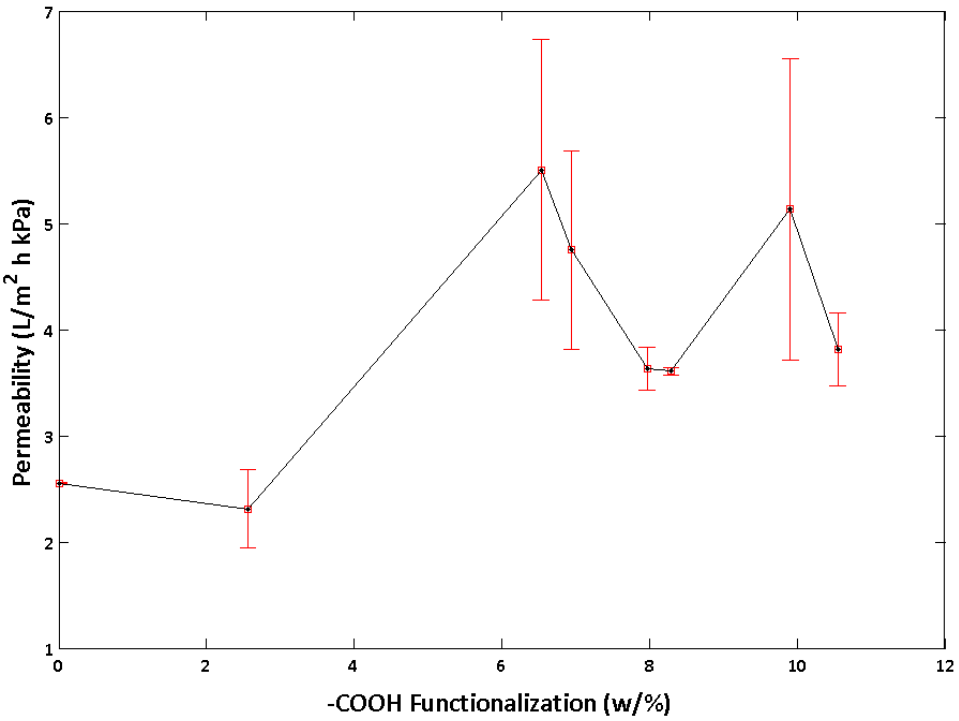

FIGURE 4.23: Permeability of the membranes was higher for those that contained CNTs with greater carboxylation. Membranes that showed greater permeability generally experienced greater variability in permeability as compared with membranes formed from lower or no carboxylation.

4.3.2.3 Discussion: PSf-CNT Ultrafiltration Membranes Properties

Stability of Functionalized CNTs in Polymers The more homogeneously CNTs are distributed, the more fully their properties and benefits can be exploited in polymer nanocomposites. Functionalization helps realize this goal, however, functionalization breaks pi-pi double bonds of which CNTs are entirely composed. The continuum $\pi - \pi$ bonding structure is wholly responsible for the unique properties of CNTs and creating defects on the surface dampens CNT properties (Sun et al., 2002). Further, increased functionalization reduces the stability and compatibility of CNTs within the polymer matrix. With greater carboxylation, therefore, CNTs are not only more dispersible, but they have reduced inherent properties and are more hydrophilic. Moreover, increased hydrophilicity means they are less likely to be permanently embedded within a hydrophobic polymer system. Loss of CNTs from the membrane results in a smaller gain in beneficial properties. There exists a balance, therefore, between increased functionalization for homogeneous dispersion, and minimal functionalization for greater stability and for the preservation of CNT properties.

Effect of CNT Functionalization on Young's Modulus This effect was shown in three experiments. In figure 4.21, Young's Modulus varied as a function of carboxylation degree scaled by the percentage of CNTs remaining within the membrane. This graph demonstrated an atypical trend: all membranes formed with pCNTs and CNT-COOHs demonstrated higher Young's moduli than pure polymer membranes, but membranes formed with CNT-COOHs only improved Young's moduli over that of pCNTs when the CNT carboxylation was low (2.56%). At greater carboxylation degrees of CNTs, the membrane had reduced physical strain properties compared with membranes formed with pCNTs. This can be explained by considering the balance between load bearing through distribution within the polymer matrix, reduced

$\pi - \pi$ bonding due to oxidative damage, and CNT loss. Pristine CNTs only provided tensile strength improvements in localized areas with inefficient load bearing, and thus limited increases in Young's Modulus. CNT carboxylation improved the homogeneous dispersion of CNTs within polymer solutions and thus improved the load bearing of the membrane. This improved homogeneous load bearing, however, was counter-balanced by two detrimental factors: a reduction in the tensile strength of the individual CNTs, and fewer CNTs present in the membranes. Increasing CNT carboxylation amplified the effects from both of these factors within the membrane, until the advantages of carboxylation were outweighed by the drawbacks. While the loss of CNTs from the membrane was accounted for in the x-axis of figure 4.21, the loss of CNTs was unevenly distributed throughout the membrane (figure 4.18). It is hypothesized that more CNTs were lost from the surface of the membranes than from the bulk. The uneven distribution of CNTs throughout the membrane greatly reduces the bulk load bearing ability. In addition, the uneven redistribution of CNTs during membrane gelation could have caused detrimental changes to the structural stability of the polymer matrix. Further, loss of CNTs from the membrane was coupled with the decrease in strength of each individual CNT from sidewall functionalization. As CNTs were further weakened and lost from the polymer matrix through increased carboxylation, the Young's Modulus of the membranes was reduced.

Effect of CNT Functionalization on Surface Chemistry This trend was also observed in the surface hydrophilicity of the membranes (figure 4.22). Pristine CNTs added to the membranes created surfaces with greater hydrophobicity over the plain polymer membranes, as expected, while carboxylated CNTs produced membranes with more hydrophilic surfaces. Greater carboxylation of the CNTs produced a more hydrophilic surface, due to the increase in carboxyl groups located at the surface of the membrane. Increasing carboxylation caused increasing surface hydrophilicity, up to

a point. Greater carboxylation also caused greater loss of CNTs during membrane formation. With fewer CNTs in the membranes, and therefore fewer carboxyl groups located on the surface, the surface hydrophilicity decreased. The bulk loss of CNTs from the polymer matrix was accounted for in the x-axis of figure 4.22, however, this did not reflect the loss of CNT-COOHs from the surface of the membranes. The majority of the CNTs lost from the membrane originated from the surface, because they were in closest proximity to the non-polar solvent during gelation. Loss of CNTs during membrane precipitation detracted from the advantages associated with carboxylation.

Effect of CNT Functionalization on Membrane Permeability Finally, water permeability increased for membranes composed of CNTs with higher degrees of carboxylation (figure 4.23). Greater surface hydrophilicity associated with increased carboxylation could only account for some of this trend. As demonstrated in figure 4.22, hydrophilicity decreased with greater loss of CNTs during membrane formation. We hypothesize that this loss of CNTs may have created structural changes to the polymer matrices, including variability in distribution of pore sizes, permitting greater flux through the membrane. Further, the thermodynamically driven motions and loss of CNTs during membrane precipitation may have caused great variability in the structure and shape of internally formed void spaces. The effects of these variable disruptions to the membrane porous structure were suggested by the large errors associated with the permeability of membranes containing CNTs with greater carboxylation. The detailed effects of CNT-leaching on porous polymer structure warrant further investigation.

4.3.2.4 Conspectus: PSf-CNT Ultrafiltration Membranes Properties

Carboxylation is a common functionalization for CNTs and has been used recently to disperse CNTs in a number of materials. Water filtration membranes, in particular, have been investigated for enhancement through the inclusion of CNTs. In this study, it was shown that intermediate functionalizations were associated with better product performance as well as greater stability. While it was found that CNTs of all functionalizations generally provide significant advantages to the materials to which they are added, it is important to consider the stability of the CNTs within their host materials. The compatibility of CNTs with polymers will determine both the optimal exploitation of CNT properties and also the longevity of CNTs within that material. The factors that drive low waste generation and optimized performance lead to conditions of reduced leaching, however greater gains in property enhancement is hypothesized to occur with more optimized functionalizations. This study of property change as a function of CNT functionalization, and thus of stability, suggests that novel strategies are required to increase the stability of CNTs within polymer matrices. These include tuning CNT functionalizations for affinity to polymer matrices as opposed to solvent systems. Further, ionic or covalent bonding between polymer chains and CNTs would be highly beneficial for material optimization and stability.

4.4 Development and Application of Membranes Formed With Charge Association Between Functionalized CNTs and Membrane Polymers

4.4.1 Leaching Prevention of Functionalized Carbon Nanotubes from Sulfonated Polysulfone Microfiltration Membranes

4.4.1.1 Proem: CNT Dispersion in and Leaching from SPSf Microfiltration Membranes

In bulk materials, where CNTs are used either for their mechanically re-enforcing, thermally conductive, or electrically conductive enhancing properties, much care is put into their functionalization, dispersion/suspension, and sometimes their alignment. The main concern for most researchers and engineers is to achieve the desired material properties in the most efficient and effective manner [ref]. In most of this research, unfortunately, rarely is the products' lifetimes or its end-of-use scenario considered. As a result, there is often little focus given to the long-term stability of CNTs within the material matrices to which they are added. Some researchers determine the local stability of CNTs within their formed nanocomposites, but these studies are few and far between [ref].

CNTs of various functionalizations are often blend mixed into polymer solutions for mechanical reinforcement [ref]. This is done for a variety of materials, including polymer ultrafiltration membranes used in water filtration. In the previous subsection, we have demonstrated that CNTs leach from these nanocomposite polymer matrices throughout their product lifetime. Initially, and most significantly, CNTs are lost from polymer matrices during immersion precipitation used to gel the nanocomposite solutions. Further, leaching of CNTs occurs during exposure of nanocomposite membranes to caustic chemical agents — a common membrane cleaning procedure. Loss of CNTs from the polymer solutions is highly dependent on the CNT functionalization, but occurs for pristine CNTs as well, albeit to a lesser degree. This implies

that blend mixing CNTs within polymer matrices produces nanocomposite materials that are inherently unstable. It is suspected that many nanocomposite materials are inherently unstable especially in long-term use.

In the literature, there is scant research devoted to the potential loss and leaching of CNTs from nanocomposite materials. In addition, researchers that produce nanocomposite materials often fail to address consideration for the potential repercussions that CNT loss and leaching may cause to human health, the environment, and to the nanocomposite long-term effectiveness itself. It is important, for these reasons, to develop nanocomposite materials in safe and responsible ways that minimize potential material repercussions and downstream effects. One simple way to do this is to design composites in which CNTs are permanently bound within the polymer matrix. In this way, we can minimize or potentially eliminate loss and leaching of CNTs from composites at all stages of the material lifetime from manufacture through to use until disposal.

This goal has benefits beyond human health and environmental concerns. Eliminating the loss and leaching of CNTs is also beneficial from a practical materials perspective. Minimizing loss during the nanocomposite material-manufacturing process greatly improves the engineering efficiency of material production. Additionally, minimizing leaching during use prolongs the nanocomposite material properties. It is therefore both responsible and practical to develop nanocomposite materials with stable and permanently bound nanoparticles.

In this chapter, we address the problem presented by bulk mixed CNT-polymer ultrafiltration membranes by modifying membrane polymers with charge carriers to bind CNTs functionalized with oppositely charged functional groups.

4.4.1.2 Findings: CNT Dispersion in and Leaching from SPSf Microfiltration Membranes

Various types of functionalized CNTs were added as fillers at different concentrations into SPSf membranes. Polymer-CNT nanocomposite membranes were then evaluated for various membrane properties, as well as investigations into their morphological differences and the compatibility of CNTs with SPSf.

CNT Dispersion in SPSf-PVP Membranes CNTs can provide polymer membranes with several enhancements including strength improvements. For maximal strength providing enhancements, CNTs need to be uniformly distributed throughout the polymer matrix. The greatest load bearing is achieved by individualized, non-aggregated (or unbundled) CNTs. In order to achieve this optimal configuration, CNTs must be dispersed evenly throughout the membrane. This was achieved through probe sonication. CNTs were added to the solvent, NMP, at either 0.5 wt% or 5.0 wt% with respect to the final polymer mass and then subjected to intermittent ultrasonication. After sonication, carboxylated CNTs were well dispersed and stayed in suspension indefinitely, while surprisingly, amine-functionalized CNTs precipitated out of solution after only several hours and as expected, pristine CNTs precipitated out of solution similarly, after only a few hours. To overcome this, PVP and SPSf were added to the suspended CNTs in NMP immediately after sonication was completed. After mixing for 24 hours at $60^{\circ}C$ under continuous stirring with a magnetic stir bar, the final solution for all CNT functionalizations and at all concentrations, were opaque black, viscous, and homogeneous, indicated by the lack of aggregates in the polymer-CNT mixtures. This viscous solution was then hand-cast onto a glass plate and precipitated in DIW. Each nanocomposite membrane either contained 0.5% or 5.0% CNTs with respect to the polymer constituents. Photographs and SEM images of the formed membranes are shown in 4.24.

These images show white pure SPSf-PVP membranes compared to black SPSf-PVP membranes that contain CNTs of various types: 0.5 wt% and 5.0 wt% pCNTs, 1.0 wt% CNT-COOHs (3.86%), 0.5 wt% and 5.0 wt% $CNT - NH_2$s (1.2%), and 0.5 wt% and 5.0 wt% $CNT - NH_2$s (7.0%). SEM images show well dispersed and individualized CNTs dispersed within the filamentous bulk polymer matrix.

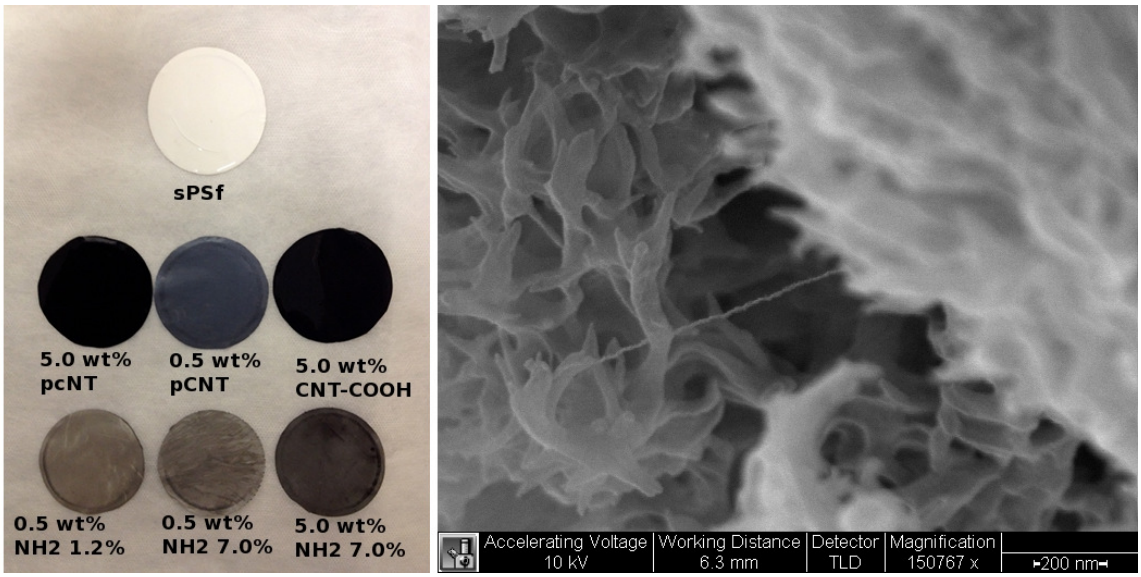

FIGURE 4.24: Photographs compare SPSf-PVP and SPSf-PVP-CNT membranes. The white membrane is a pure SPSf membrane, black membranes contain CNTs of different types. Starting from the top row on the left: 5.0 wt% pCNT, 0.5 wt% pCNTs, 1.0 wt% CNT-COOHs (3.86%), 0.5 wt% $CNT - NH_2$s (1.2%), 0.5 wt% $CNT - NH_2$s (7.0%), and 5.0 wt% $CNT - NH_2$s (7.0%). SEM images show well dispersed CNTs within the filamentous polymer structure.

Membrane Morphology Revealingly, there seems to be differences evident in both the cross-subsection morphology and the surface topography of the membranes containing CNTs compare to pure SPSf membranes. The internal morphology of pure SPSf membranes is highly filamentous. The internal structure of membranes containing CNTs is less filamentous and more sponge-like. Further, in some cases there seems to be large void-like structures present that are not evident in the pure SPSf membranes. These cross-section morphological differences are shown in figure 4.25.

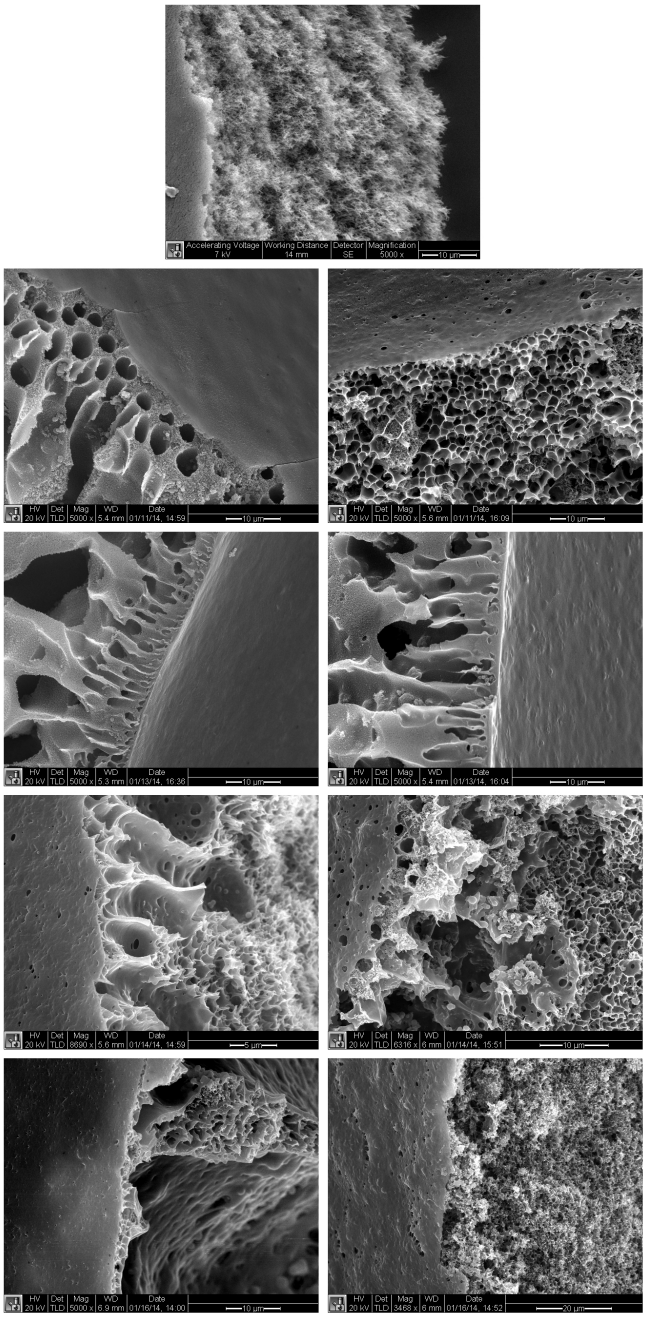

FIGURE 4.25: SEM images of membrane cross-subsections show the filamentous, internal structure of pure SPSf membranes in from top to bottom and left to right the membranes are composed of pure SPSf, SPSf-pCNT 0.5 wt%, SPSf-pCNT 5.0 wt%, SPSf-CNT-COOH (3.86%) 0.5 wt%, SPSf-CNT-COOH (3.86%) 5.0 wt%, SPSf-CNT-NH_2 (1.2 %) 0.5 wt%, SPSf-CNT-NH_2 (1.2 %) 5.0 wt%, SPSf-CNT-NH_2 (7.0%) 0.5 wt%, and SPSf-CNT-NH_2 (7.0%) 5.0 wt%.

Further, membranes formed with CNTs in their bulk also demonstrate significant void-like formations. Cross-section morphology differences are evident between SPSf and SPSf with $CNT - NH_2$s. No significant difference exists between morphologies of membranes formed with higher and lower CNT concentrations. However, surfaces seem to follow increasing roughness with greater addition of CNTs. Pure SPSf membranes are highly smooth as are membranes that contain CNT-COOHs. However, with the inclusion of $CNT - NH_2$s at low concentrations (0.5 wt%), the surface is slightly rougher. Most evident, however, is the topography changes that occur with inclusion of high concentrations (5.0 wt%) of $CNT - NH_2$s. These surfaces are notably rougher. Moreover, these surfaces seem to be much more porous than membranes composed of other CNT contents. Regardless of CNT content, membrane surfaces are all highly porous and contain large pores.

Loss of CNTs from Membranes During Gelation In the previous similar study of nanocomposite membranes formed from polysulfone (PSf), PVP, and carboxylated CNTs of varying functionalization percentages it was observed that CNTs were lost from the polymer solutions when membranes underwent immersion precipitation in the non-solvent bath. The loss of CNTs from polymer solutions was greater for membranes that contained more highly carboxylated CNTs. In the worst cases, CNT losses were greater than 10% for the most highly carboxylated CNTs (11% carboxylation). This loss was attributed to the highly hydrophilic nature of the carboxyl functional moieties coupled with a lack of CNT to polymer bonding.

The stability of CNTs within polymer matrices affects membrane characteristics. In particular, fewer CNTs in the final polymer-nanocomposite membrane was shown to adversely affect the strength enhancement of the membrane. Young's moduli were lower than expected, and the surface hydrophilicity and permeability of the membranes deviated from the expected trends with greater losses of CNTs. In addition,

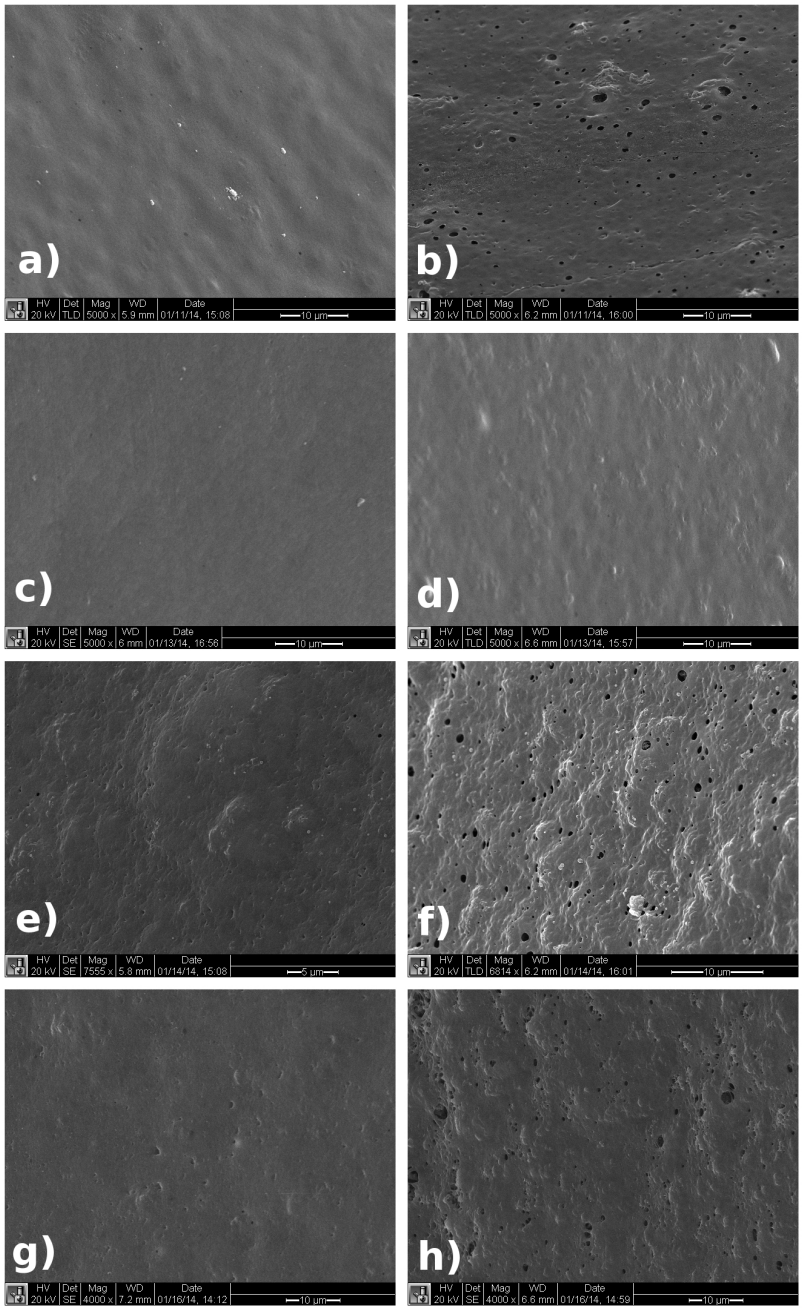

FIGURE 4.26: SEM images of the membrane surface show highly porous skins. The images in order show, a) 0.5 wt% pCNT, b) 5.0 wt% pCNT, c) 0.5 wt% CNT-COOH (3.86%) d) 5.0 wt% CNT-COOH (3.86%), e) 0.5 wt% $CNT - NH_2$ (1.2%) f) 5.0 wt% $CNT - NH_2$ (1.2%) g) 0.5 wt% $CNT - NH_2$ (7.0%), and h) 5.0 wt% $CNT - NH_2$ (7.0%). The surfaces become more rough and porous with the additions of $CNT - NH_2$ and with greater CNT content.

loss of CNTs from the membranes has environmental implications when one considers the potential for nanomaterials to release during membrane use. Furthermore, while greater carboxylation of CNTs should provide greater benefits to the final polymer nanocomposite membrane due to better dispersion of CNTs within the polymer solution and greater hydrophilic moieties present on the membrane surface, highly carboxylated CNTs were shown to have significant issues with regards to stability and long-term compatibility, undermining their expected benefits.

The main purpose of the present investigation was to determine whether ionic bonding of polymer chains with CNT functional groups could prevent the loss of CNTs from the polymer solution during membrane gelation in the non-solvent. Polysulfone was sulfonated to add a positive ionic charge to the polymer chains. It was hypothesized that this added charge would help bind CNTs to the polymer matrix through interaction with the charged functional groups present on the sidewalls of the CNTs.

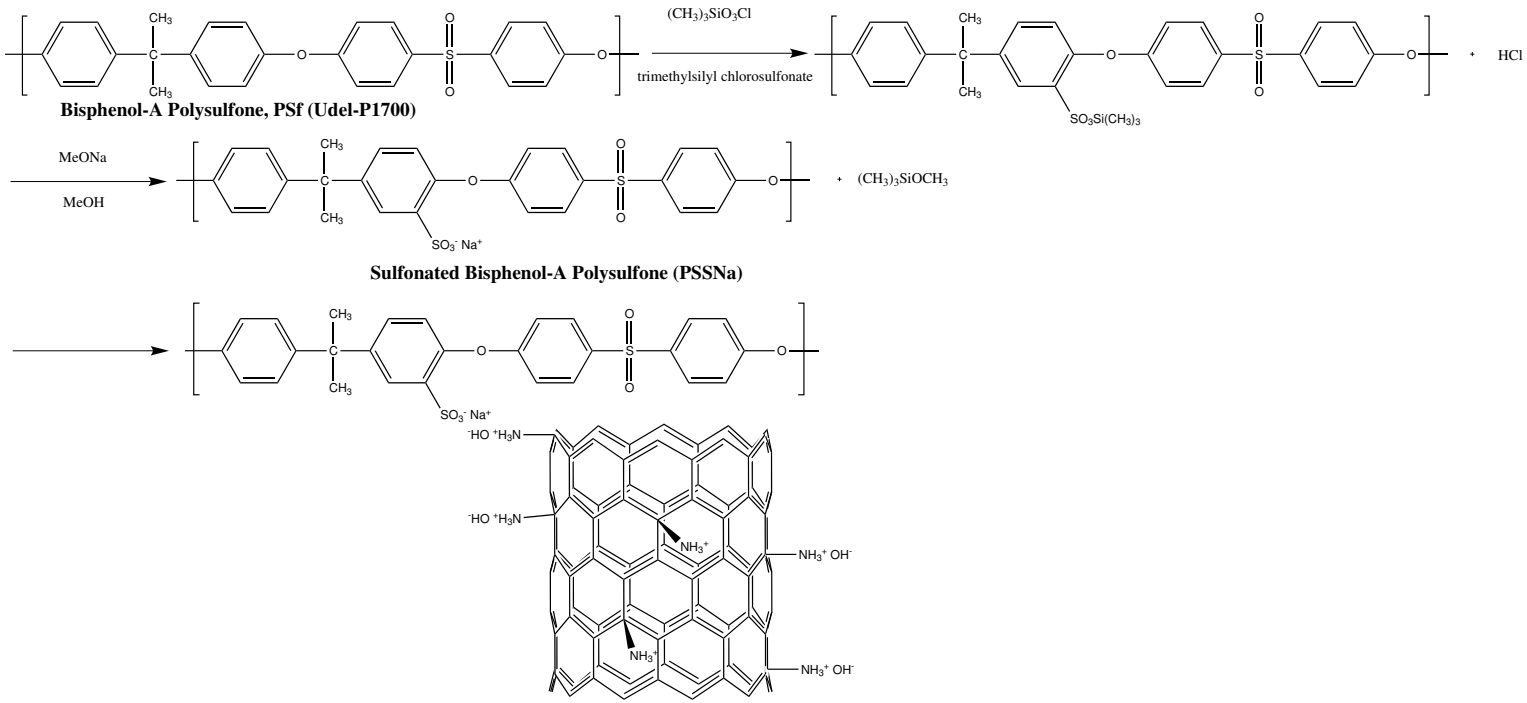

FIGURE 4.27: This scheme shows the sulfonation of polysulfone and the charge association between the charged moieties on the polymer chain and the charged functional groups on amine-functionalized CNTs.

UV-Vis absorption of the post-precipitation non-solvent bath was measured (explained in detail in subsection 2.3.2) and used to identify the quantity of CNTs found in each precipitation bath from each type of membrane. Figure 4.28, shows the results of these experiments. Precipitated membranes composed of SPSf, PVP, and $CNT - NH_2$s did not demonstrate any leaching within the detection limit of the UV-Vis instrument. Membranes that contained CNT-COOHs showed some leaching, up to 3.5%. Notable, this was the same amount of CNT loss from PSf membranes reported in our previous paper. $CNT - NH_2$s were stable in SPSf polymer matrices at both low and high concentrations, 0.5 wt% and 5.0 wt% respectively, as well as for lightly and strongly functionalized sidewalls, 1.2% and 7.0% amine-functionalization.

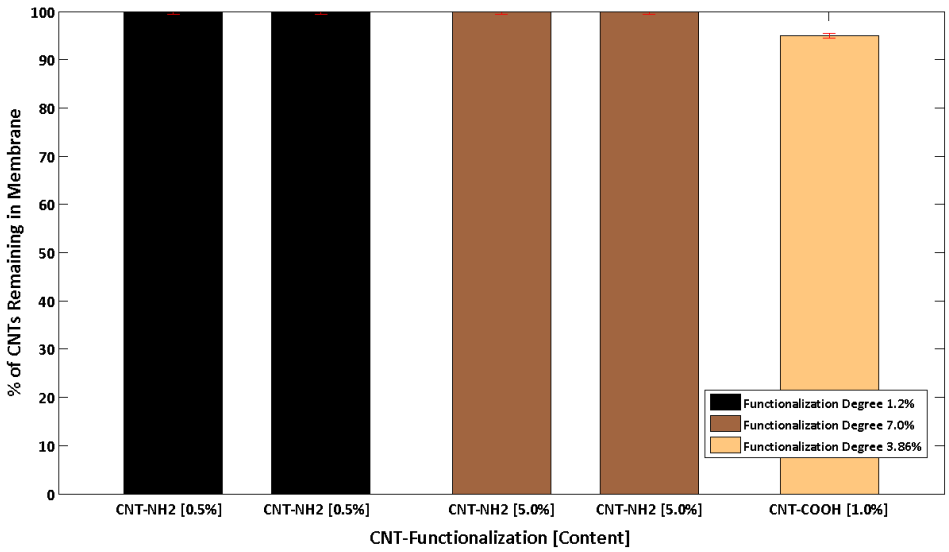

FIGURE 4.28: Loss of CNTs from the polymer nanocomposite SPSf-PVP-CNT membranes occurred for membranes containing CNT-COOHs, but was entirely absent (within the detection limit of the UV-Vis instrument used) for membranes containing $CNT - NH_2$. The stability of $CNT - NH_2$s was observed for both low (0.5 wt%) and high (5.0 wt%) concentrations of CNTs as well as for lightly (1.2%) and strongly (7.0%) functionalized CNT sidewalls.

4.4.1.3 Discussion: CNT Dispersion in and Leaching from SPSf Microfiltration Membranes

CNT Dispersion in SPSf-PVP Membranes CNTs that are functionalized show uniform dispersion within polymer matrices. There were no evident differences in the homogeneous dispersibility between low and high functionalized CNTs or between carboxylated or amine-functionalized CNTs. However, as demonstrated in much previous research, bundled and aggregated CNTs are found in membranes containing pristine unfunctionalized CNTs.

Membrane Morphology As demonstrated in figure 4.25, the functionalized CNTs are homogeneously dispersed throughout the SPSf polymer matrix. Both carboxylated and amine-functionalized CNTs were individualized throughout the membrane matrix. Functionalization of CNT sidewalls disaggregates CNTs from each other in solution. In previous studies, including our own, functionalized CNTs were found to be well dispersed in polymer matrices, so their dispersion within SPSf membranes was expected.

The bulk morphology of the membranes was altered by the addition of functionalized CNTs. Pure SPSf membranes demonstrate a very fine filamentous internal structure, while membranes that contain CNTs show slight differences to that formation. Membranes formed with CNT-COOHs have internal structures that are filamentous, with much longer and straighter filaments. In contrast, membranes formed with $CNT-NH_2$s show internal structures that are more dense and sponge-like. Moreover, large macrovoids are evident in the cross-subsections of membranes containing $CNT-NH_2$s. The differences in internal structure over pure SPSf membranes are entirely caused by the addition of CNTs. The high surface area of CNTs may encourage the adhesion of polymer chains onto CNTs. Further the CNT surface charge probably plays a significant role in the gelation of the polymer chains

during immersion precipitation. The carboxylic groups on CNT-COOHs are negatively charged and repel the negatively charged sulfonation groups on the polysulfone chains, whereas the positive charge of the amine groups on $CNT-NH_2$s attract the sulfonation groups of the SPSf chains. This major difference probably accounts for the significant changes in internal structure. As seeds for nucleation and aggregation, positively charged, high surface area $CNT-NH_2$s may encourage local adhesion of polymer chains to the carbon nanotubes during gelation. This attractive interaction may be responsible for the densely intertwined sponge-like structure.

The addition of functionalized CNTs into SPSf membranes also has a significant affect on the surface topography, i.e. the local roughness, the surface flatness, and the presence of large macro-pores. Membranes composed of pure SPSf are smooth and contain few surface defects. Macro-pores on the surface are not prevalent. The addition of CNT-COOHs did not seem to affect the surface structure of the membrane to any great degree. The addition of amine functionalized CNTs to the SPSf membranes, however, causes significant increases in porosity, roughness, and irregularity. Large macro-pores arise with the addition of CNTs in SPSf membranes. Greater concentrations of CNTs also cause more significant changes in membrane surface porosity. As is shown in 4.26 c) and e), membranes with 0.5 wt% $CNT-NH_2$s seem to have only minimal changes to their pore size and structure. A few macro-pores are evident on the surface, which are not evident in pure SPSf membrane, but overall no significant changes are evident. In figure 4.26 d) and f), membranes with 5.0 wt% $CNT-NH_2$s are highly porous. These membranes are also visually not as smooth as membranes formed from pure SPSf. Membrane surfaces become more rough as the concentration of CNTs increases, which is evident when comparing figure 4.26 c) with d) and comparing e) with f). As the concentration of $CNT-NH_2$s increases from 0.5 wt% to 5.0 wt%, the surface roughness visibly increases.

As in the case of internal morphology discussed above, both the presence of

CNTs and their charge affects the polymer gelation and the resultant membrane surface topography. No visible changes are evident with the addition of the negatively charged CNT-COOHs, however, the addition of the positively charged $CNT-NH_2$s leads to significant surface changes. Further, a greater concentration of $CNT-NH_2$s in the polymer membranes causes greater structural changes. The high surface area of positively charged CNTs encourages greater adhesion of negatively charged polymer chains to the CNT surface. As is expected based on this explanation, this polymer-CNT interaction is most evident with high concentrations (5.0 wt%) of CNTs. Membranes formed with high concentrations of CNTs are highly porous and very rough.

Stability of CNTs within SPSf Membranes The stability of CNTs in polymer matrices is a major concern and was the primary motivation of this study. In our previous research dealing with carboxylic functionalized CNTs in polysulfone (PSf) membranes, we showed that CNTs are lost from polymer solutions during immersion precipitation and leach from membranes during membrane cleaning with caustic chemicals. The majority of the CNT loss occurred during membrane gelation. This loss was greater for CNTs with higher degrees of carboxylation than for CNTs with low degrees of carboxylation and for pristine CNTs. It was hypothesized that the reason for this loss was the lack of bonding that existed between the CNTs and the polymer, in addition to the hydrophilic attraction of the carboxylic functional groups on the sidewalls of the CNTs for the aqueous phase. To investigate this loss mechanism further, and to determine ways to prevent loss and leaching of CNTs, it PSf was sulfonated to form SPSf, and thereby provide negative charges to the polymer chains within the membrane. These negative charges would serve as the basis for attraction to positively charged CNTs, and in this way prevent the loss of CNTs during immersion precipitation of the membrane.

We compared the stability of CNTs within SPSf membranes using several different concentrations of variously functionalized CNTs. In figure 4.28, loss of CNTs was undetectable from all membranes containing amine-functionalized CNTs, regardless of functionalization degree (1.2% or 7.0%) or CNT content (0.5 wt% or 5.0 wt%). This is significant as there is no increase in leaching of CNTs with higher degrees of functionalization, as was the case for carboxylated CNTs in the previous study. In addition, figure 4.28 indicates that CNT-COOHs were lost from the polymer membranes during membrane gelation. Moreover, the amount that was lost, 3.5% of the initial CNT content, was equivalent to the amount that was lost in our previous study for the same CNT carboxylation degree.

It is hypothesized that $CNT - NH_2$s did not leach from the SPSf membranes because of the charge attraction that existed between these positively charged CNTs and the negatively charged polymer chains. This attraction was also likely responsible for the morphological changes as discussed previously. Revealingly, the CNT-COOHs were not prevented from leaving the membrane composed of negatively charged polymer chains. This is to be expected, as there was a lack of charge attraction between CNT-COOHs and the SPSf chains.

4.4.1.4 Conspectus: CNT Dispersion in and Leaching from SPSf Microfiltration Membranes

The stability of CNTs has been shown to be greatly improved within polymer matrices when there is an ionic association between the sidewalls of the CNTs and the polymer chains of the bulk polymer matrix. This is evident in the lack of detectable loss of CNTs from the polymer matrix for CNTs functionalized with the positively charged amine groups, which are ionically bonded to the negatively charged moieties of the SPSf polymer chains. This stability is contrasted with the loss of carboxylated CNTs from the SPSf polymer matrix. CNT-COOHs are less stable because of their

negatively charged functional groups, which do not bond with the polymer chains. While charge associations between the CNTs and the polymer chains increases the stability of the CNTs, it affects the internal membrane structure and surface morphology. Membrane surfaces containing ionically bound CNTs demonstrate significant structural defects including large surface pores and highly sponge-like internal structures.

Membranes were fabricated from SPSf (a polymer with negatively charged functional groups) and various types and contents of CNTs, in an attempt to prevent loss and leaching of CNTs from the polymer matrix during membrane immersion precipitation. The addition of oppositely charged CNTs (functionalized with positively charged amine functional groups) had significant effects on the surface morphology and internal structure of the membrane. The addition of high concentrations of amine-functionalized CNTs to SPSf formed membranes with very high porosity and high surface roughness, in comparison to pure SPSf membranes and SPSf membranes formed from both pristine CNTs and carboxylated CNTs. Amine-functionalized CNTs were not lost from the SPSf membrane matrix during immersion precipitation. The charge association between the negatively charged polymer chains and the positively charged functional groups on the CNTs increased the CNT stability within the SPSf matrix. Unlike amine-functionalized CNTs, carboxylated CNTs leached from the membranes during immersion precipitation. Therefore, while ionic association between the polymer chains and the CNT sidewalls increases CNT stability within the polymer, this bonding has significant effects on the polymer gelation kinetics and the resultant surface and internal membrane morphology.

4.4.2 Properties of Microfiltration Membranes Formed from Amine Functionalized Carbon Nanotubes Ionically Bound to and Embedded in Sulfonated Polysulfone

4.4.2.1 Proem: Effect of CNT Amine Functionalization on SPSf Membrane Properties

Membrane properties including Young's Modulus, surface hydrophilicity, and pure water flux were investigated with respect to functionalization degree and content of CNTs. These properties were viewed in light of both a greater degree of dispersion within the polymer due to functionalization and the structural changes to the membrane caused by ionic bonding between the CNTs and the polymer chains.

Membrane properties that were tested include material strength properties of stress, strain, and Young's Modulus, surface hydrophilicity, and pure water flux. We investigated the effects of different concentrations of CNTs on these membrane properties, as well as the effects of variations in functionalization type and degree. In particular, amine-functionalization was compared with either pristine CNTs or carboxylated CNTs to demonstrate their effect on membrane properties.

4.4.2.2 Findings: Effect of CNT Amine Functionalization on SPSf Membrane Properties

Young's Modulus and Stress Polymer and polymer-nanocomposite membranes that are subjected to external stresses initially undergo elastic reversible strain, followed by inelastic irreversible deformation, and finally material failure and breakage upon increased applied stress. During normal membrane operation, membranes may experience all three of these mechanical strains. Stresses that cause irreversible deformations render the membrane unusable, as pore size, integrity, and structural stability are all compromised. Therefore, and as detailed in our previous research, inelastic deformation is equivalent to breakage for the purposes of practical application.

To analyze membrane strength, stress-strain measurements were performed until

breakage, however only the linear elastic region was analyzed. The details of how this analysis was done are explained in section 3.5.4.2 . It was observed that for most of the membranes that contained CNTs, the Young's Modulus increased. The only exception to this trend were the membranes that contained 0.5 wt% of $CNT - NH_2$ 7.0% functionalization. In this case, membranes showed a slight decrease ($< 5\%$) in the Young's Modulus over pure SPSf membranes. Maximum change in Young's Modulus was observed for 5.0 wt% of $CNT - NH_2$ 7.0% functionalization, with greater than 25% increase in Young's Modulus over pure SPSf membranes. It should be noted, also that the membranes containing CNT-COOH do not contain the entirety of the 1.0 wt% initially added to the membrane, but 3.5% less than this amount, i.e. 0.975 wt%. However, for simplicity, these membranes are identified as CNT-COOH [1.0%] in all subsequent graphs.

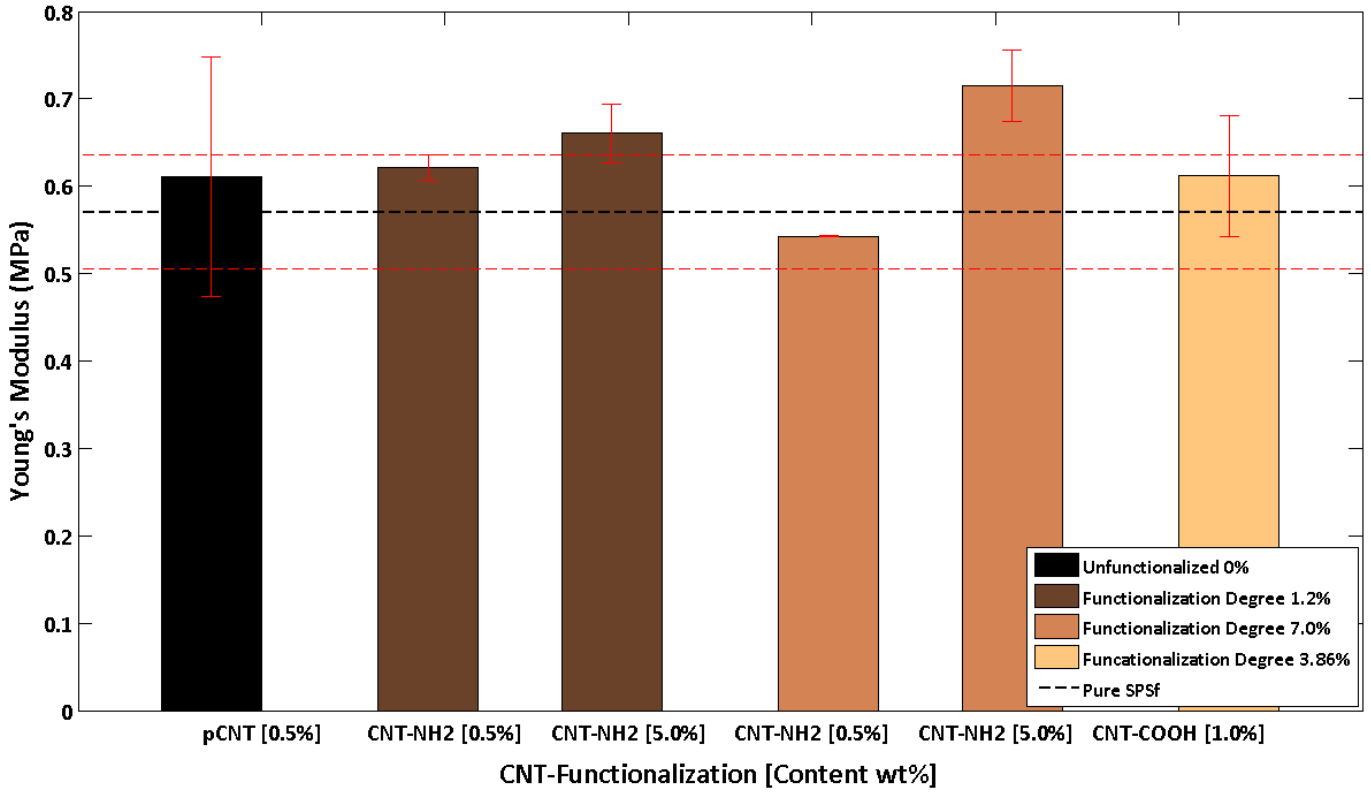

FIGURE 4.29: The Young's Modulus of SPSf membranes compared with the that of membranes containing different types of CNTs. Amine-functionalized CNTs provide the greatest improvement in membrane strength at concentrations of 5.0 wt%. At low concentrations of 0.5 wt%, 1.2% amine-functionalized CNTs demonstrated greater improvement in Young's Modulus over 0.5 wt% pCNTs and 1.0 wt% carboxylated CNTs. Unexpectedly, the inclusion of low amounts of 7.0% amine-functionalized CNTs reduced the Young's Modulus of the resultant membrane over membranes composed of pure SPSf.

Surface Hydrophilicity Surface hydrophilicity was determined through measurement of the triple point surface contact angle of a water drop in contact with the membrane surface in air. The contact angle of the surface of the membranes is a measure of the hydrophilicity of the membrane surface. This is compared to that of pure SPSf, which is shown on the graph by a black dotted line. In previous studies, it was shown that pCNTs increase the hydrophobicity (increase the contact angle) of the membrane surface, while the inclusion of functionalized CNTs reduces the surface hydrophobicity (reduces the contact angle). In all but one case, the surface hydrophilicity of the membranes containing functionalized CNTs is greater than that of the pure SPSf membranes, i.e. the contact angle is lower for all but one membrane containing functionalized CNTs. The one exception to this trend is the inclusion of 5.0 wt% $CNT-NH_2$ 1.2% functionalization. These membranes show slight increases in surface contact angle. Further, it can be observed that with greater inclusion of CNTs into the polymer membrane from 0.5 wt% to 5.0 wt%, the hydrophobicity consistently increases.

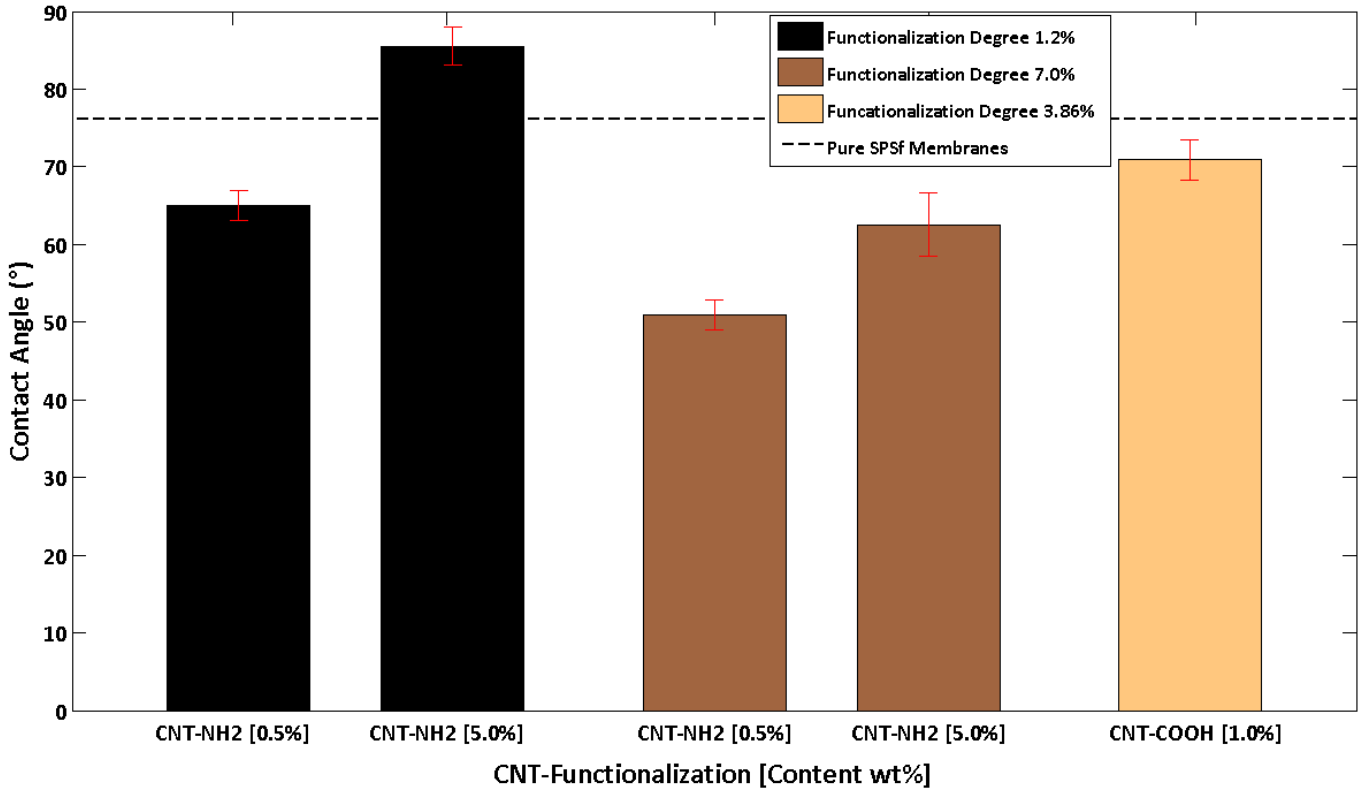

FIGURE 4.30: Contact Angle of a water-drop on the surface of the polymer nanocomposite membranes. In general the inclusion of functionalized CNTs decreases the contact angle making the membrane surface more hydrophilic. Greater concentration of CNTs, however, increases the hydrophobicity of the membrane. Comparing the amine-functionalized CNTs, greater functionalization degree creates membrane surfaces that are more hydrophilic.

Pure Water Permeability Pure water flux was measured for all membranes in a dead-end filtration configuration. The range of pressures used was between 70 kPa and 800 kPa. Flux measurements were performed in duplicate at four different pressure values within the given pressure range for all membranes. We performed linear regression on the flux results and from the resultant slope we determined the membrane permeability. Presented in figure 4.31 is the maximum water permeability attained for each membrane. This is compared to the maximum water permeability that was obtained for pure SPSf membranes, shown as a dotted black line. As can be seen in figure 4.31, the inclusion of small amounts of CNTs (0.5 wt%) into the membranes increases the membrane permeability over that of pure SPSf, while large amounts of CNTs (5.0 wt%) decreases the water permeability of the membrane compared to that of pure SPSf membranes. Furthermore, membranes containing $CNT - NH_2$s functionalized to a higher degree (7.0%) have higher water permeability than those that contain $CNT - NH_2$s functionalized to a lesser degree (1.2%), and in general membranes containing amine-functionalized CNTs have greater permeability than those containing pristine CNTs. The only exception to this latter trend is membranes that contain 5.0 wt% $CNT - NH_2$ 1.2% functionalization. In membranes that contain these CNTs, there is a slight decrease in permeability over membranes containing the same concentration of pCNTs.

4.4.2.3 Discussion: Effect of CNT Amine Functionalization on SPSf Membrane Properties

Effect of functionalized CNTs on Young's Modulus The addition of CNTs into SPSf membranes generally increased the Young's Modulus of the polymer membranes. From figure 4.29 one of the main findings was that higher functionalization of CNTs caused greater increases in Young's Modulus than lower degrees of functionalization. Specifically, the membranes with the highest Young's Modulus were the those that

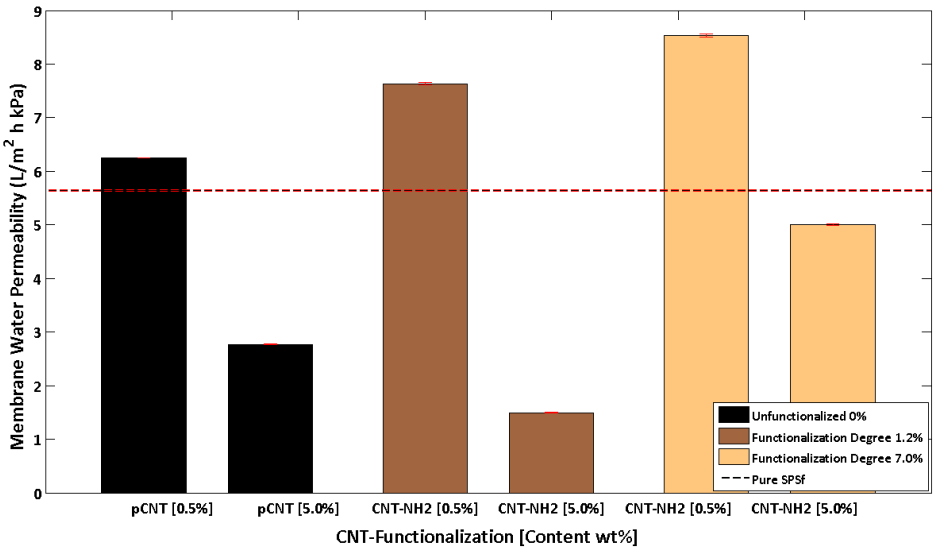

FIGURE 4.31: Maximum measured membrane permeability of the membranes was measured by pure water flux testing. The results indicate that low CNT loading increase membrane permeability, while high CNT loading reduces it. Membranes containing mine-functionalized CNTs have higher permeability than membranes formed with the same concentration of pristine CNTs. Moreover, greater degree of functionalization leads to greater permeability.

contained 5.0 wt% $CNT-NH_2$s functionalized to 7.0%. These membranes contained both the highest concentration of CNTs and the greatest functionalization degree. These membranes achieved an increase in Young's Modulus of over 25%. While this is a significant increase, it is significantly lower than strength increases found for equivalent concentrations of CNTs in other polymer matrices. Of note, this was a lesser increase than that found for 0.5 wt% additions of CNT-COOHs in PSf membranes from our previous study (de Lannoy et al., 2013b). The greatest increase in Young's Modulus from these membranes was expected as the dispersion of these CNTs was assumed to be the highest. A greater dispersion of CNTs throughout the polymer matrix implies a more homogeneous distribution of CNTs in the membrane, which is associated with a greater load bearing capacity of these membranes, as the CNTs are completely distributed across the entire system for optimal strength

enhancement.

Another finding shown in figure 4.29 was, expectedly, that increasing CNT concentration increased the membranes strength. Comparing membranes containing 0.5 wt% $CNT-NH_2$s with membranes containing 5.0 wt% $CNT-NH_2$s, Young's Modulus values were greater for the latter over the former in all cases. A greater concentration of CNTs in the membranes would allow for greater load bearing, as more CNTs are present to resist stresses.

The addition of pristine CNTs into the SPSf membrane matrix produced highly variable results, as evidenced by the large standard deviations in figure 4.29. This is also to be expected, as these CNTs were the least dispersed throughout the polymer network. Inhomogeneous distribution of CNTs causes some areas of the membrane to be reinforced while others are neglected. This uneven spread in load bearing is reflected in the high uncertainty or high variability of the data.

Unusually, the addition of low amounts of highly functionalized (7.0%) $CNT-NH_2$s caused a slight decrease in the Young's Modulus of the membranes. Compared to the addition of low amounts of lightly functionalized (1.2%) $CNT-NH_2$s, highly functionalized $CNT-NH_2$s may have had a greater disruptive effect on the polymer orientation due to greater interaction with the positively charged functional groups on the CNT sidewalls. Finally, it should be noticed that the variability in Young's Modulus for the CNT-COOHs was also relatively high. This is attributed to the fact that, although these CNTs were highly dispersed within the polymer matrix, there was measurable loss of these CNTs from the polymer matrices as described above. The dynamic process of loss of CNTs from the membrane matrix is assumed to cause significant changes to membranes and is hypothesized to cause variability in membrane properties.

Effect of functionalized CNTs on Surface Contact Angle The effect of adding functionalized CNTs into SPSf membranes is, generally, to increase the hydrophilicity of SPSf membranes, as shown in figure 4.30. This effect is found in both membranes containing $CNT-NH_2$s and CNT-COOHs. The only exception to this is the addition of high concentrations (5.0 wt%) of lightly functionalized (1.2%) $CNT-NH_2$s. Further, as expected, more highly functionalized CNTs lower the contact angle more than CNTs containing lower functionalization degrees. Figure 4.30 clearly shows that $CNT-NH_2$s functionalized to 7.0% reduce the hydrophilicity to a greater degree than $CNT-NH_2$s functionalized to 1.2%. Amine functionalization adds hydrophilic charged functional groups to the sidewalls of CNTs, which has an effect on the surface hydrophilicity of the membranes. Local changes from exposed functional groups acts to reduce the surface energy of the membrane, despite the largely hydrophobic nature of the CNTs. This result implies that CNT functional groups may, to an extent, be exposed on the surface.

From this figure, it is also observed that while the addition of small amounts of CNTs into the membranes lowers the contact angle, additions of CNTs in greater concentration increases the contact angle. Therefore, sidewall functionalization is not solely responsible for the change in surface contact angle. A balance may exist between greater functional group surface exposure and greater hydrophobic CNT exposure. In addition, the addition of CNTs into the membranes causes surface changes to the membrane surface, as detailed in previous subsections. These changes may account for altered surface hydrophilicity, but increased CNT content increases the hydrophobicity of the membranes due to the largely hydrophobic nature of the CNTs. Therefore, while hydrophilic CNT functional groups exposed on the surface of the membrane reduce the surface energy of the membrane, there is a threshold for this influence as more CNTs are added to the polymer system.

Effect of CNTs on Membrane Water Permeability Pure water membrane permeability data is shown in figure 4.31. Only the maximum values of permeability are shown here, while the full data is shown in the Appendix C. In this figure, it is clear that increased functionalization of CNTs causes greater permeability, thus the permeability of CNT containing membranes follows pCNTs $< CNT-NH_2$s 1.2% $< CNT-NH_2$s 7.0%. In all cases, 1.2% $CNT-NH_2$ had lower permeability than 7.0% $CNT-NH_2$, while membranes containing pCNTs at low concentrations had a lower permeability than both the membranes containing functionalized CNTs. (The only exception was 5.0 wt% pCNTs, which had a slightly higher permeability than the 5.0 wt% $CNT-NH_2$ 1.2%). This follows from the contact angle measurements, in which greater functionalization produced membrane surfaces with greater hydrophilicity. A greater membrane surface hydrophilicity leads to greater membrane permeability.

It is also observed, in general, that the addition of small amounts (0.5 wt%) of CNTs causes increases in pure water permeability, while the addition of large amounts (5.0 wt%) of CNTs reduces the permeability. Membranes that contained higher amounts of CNTs showed higher surface hydrophobicity, rougher surfaces, and a more dense internal structure. This factors combines could restrict flux through the membranes and cause lower pure water permeability.

4.4.2.4 Conspectus: Effect of CNT Amine Functionalization on SPSf Membrane Properties

Changes in Young's Modulus and surface hydrophilicity with the addition of more highly functionalized CNTs followed expected trends. Membranes formed with CNT functionalized to a higher degree of amine-functionalization caused a more homogeneous dispersion of CNTs throughout the polymer matrix which improved load bearing across the membrane. Further, membranes with higher concentrations of $CNT-NH_2$s had higher Young's Moduli, than membranes with lower concentra-

tions of $CNT - NH_2$s or none at all. However, the increases in Young's Modulus overall was less than expected compared with previous studies that bulk mixed CNTs into polymers without ionic association. A higher degree of amine-functionalization increased the CNT hydrophilicity, which in turn increased the surface hydrophilicity of the membranes compared to membranes formed with CNTs of lesser degrees of functionalization or none at all. Further, higher concentrations of CNTs produced membranes with higher surface hydrophobicity. These changes in surface hydrophilicity can be partially attributed to changes in CNT chemistry, but the large surface morphological changes of the polymer have a significant effect as well. The trends in surface contact angle are mirrored in the trends in permeability. Membranes containing CNTs with high amounts of amine-functionalization show greater water permeability than membranes formed with CNTs of low amine-functionalization. Generally, membranes containing high concentrations of CNTs had lower permeabilities than membranes containing low concentrations of CNTs. To conclude, while membranes formed with charge associations between the polymer chains and the CNT sidewalls prevents loss of CNTs during membrane gelation, this ionic bonding causes significant morphological changes to the membrane, which in turn greatly affects the membrane properties including surface chemistry and water permeability.

5

Conclusions

This dissertation delves into the ways in which carbon nanotubes can enhance polymeric membranes and explores some of the possible advanced applications. Six primary conclusions on three broad topics can be formed from the discoveries therein. These conclusions relate three ways in which CNTs can be reacted with polymers either through covalent interactions, through charge sharing associations, or through non-covalent polymer wrapping interactions. Within these three broad topics, there are six conclusions on specific topics: cross-linked nanocomposite networks; interfacially polymerized nanocomposite networks; applications of covalently bound nanocomposite networks to preventing biofouling; leaching of CNTs from polymer nanocomposites; polymer wrapped nanocomposites; and ionically bound nanocomposites. The details of these conclusions follow.

5.1 Covalent Bonding Between CNTs and Polymers

In this dissertation it was found that binding functionalized CNTs to linear polymer chains or polymerizing the monomer constituents of polymers from the sidewalls of functionalized CNTs creates mechanically (and under certain conditions, chemically)

stable nanocomposites. Moreover, by minimizing the polymer component within the nanocomposite, while still maintaining a sufficient density of covalent bonds between the CNTs and the polymers, it is possible to form a highly electrically conductive nanocomposite with mechanical (and under certain conditions, chemical) stability. Further, these stable, electrically conductive nanocomposites can be formed into highly functional thin film membranes. These membranes can be made with good flux and separation abilities and can be formed in a range of selectivities that spans from microfiltration to ultrafiltration to nanofiltration to reverse osmosis. Stable, electrically conductive membranes have the potential to radically improve separations by preventing surface biofouling, limiting surface scaling, and serving as a functional template for electro-catalytic degradations.

5.1.1 Cross-Linked Nanocomposite Networks

Linear polymers can be cross-linked by functionalized CNTs. A cross-linked polymer-CNT nanocomposite network is physically stable and can be bound to a polymer surface by thermal curing. By minimizing the amount of free polymer within this network, it can be made highly electrically conductive. The most electrically conductive thin film that remains stable, therefore, occurs theoretically when CNTs are minimally cross-linked by polymer chains. This is theoretically realized for,

$$n_{poly} = n_{CNT} - 1, n_{CNT} \geqslant 2 \tag{5.1}$$

where n_{poly} is the number of polymer chains in solution and n_{CNT} is the number of CNTs in the solution. A cross-linked polymer-CNT network demonstrates good membrane properties of flux and separation. These properties can be manipulated by changing the cross-linking density between CNTs and polymer chains. This can be achieved either by changing the concentration of CNTs or by adding cross-linking additives, such as succinic acid. In the case of PVA, an increase in the concentra-

tion of CNTs both increases the potential cross-linking density and causes greater disruptions to the semi-crystalline nature of the polymer, thereby simultaneously increasing the transmembrane flux and reducing the rejection characteristics of the thin film. PVA-CNT cross-linked thin film networks demonstrate good stability, controllable flux and rejection characteristics. With these unique characteristics, CNT cross-linked polymer thin films can serve as the template for customizable membranes. Furthermore, these networks are highly electrically conductive and have the potential to act as anti-fouling coatings and surfaces, as well as the scaffold for multi-functional electro-catalysis.

5.1.2 Interfacially Polymerized Nanocomposite Networks

The monomer constituents of polymers can be covalently bonded to functional groups on the sidewalls of CNTs and then polymerized to form a covalently bound polymer-CNT network. A polymerized covalently bound polymer-CNT nanocomposite network is physically stable and can be bound to a polymer surface by thermal curing. The polymer component can be minimized by polymerizing the monomers at an interface between two immiscible liquids, such as at the interface of water and hexane. Limiting the reaction to an interface allows a very thin film of bound polymer-CNTs to form. In this way, this network can be made highly electrically conductive. Electrical conductivity of the network is increased for shorter chain lengths of the grown polymers and for fewer grown polymer chains with respect to the CNTs. These parameters can be controlled. An interfacially polymerized polymer-CNT network demonstrates dense membrane properties akin to tight NF or RO membranes. The permeability and salt rejection properties are affected by the concentration of CNTs in the membrane. Thin films produced from m-phenylenediamine, trimesoyl chloride, and hydroxylated CNTs, in particular, form tight NF membranes with good flux properties and high electrical conductivity. These electrically conductive poly-

mer nanocomposite networks have high potential to resist biofouling, prevent surface scaling, and electro-oxidatively degrade organic molecules, while simultaneously performing aqueous separations.

5.1.3 Biofouling Prevention

The application of an alternating electric potential to the surface of an electrically conductive membrane prevents the attachment and proliferation of bacteria, and resists the development of biofilms on its surface. Generating an alternating electric field across a solution heavily contaminated with active biofilm producing bacteria prevents their attachment to the source or sink of the electric field lines. Specifically, an alternating square wave at an over-potential of ± 1.5 V was shown to be highly effective over the course of 35-185 hours to prevent the attachment of bacteria to the electrically conducting membrane surface. The application of this potential did not prevent the complete decreases in flux, although it did reduce the rate of flux decline. The surface of the membrane was entirely cleaned of any flux reducing entities and the transmembrane flux restored to greater than 90% of the original flux by increasing the speed of the cross-flow feed solution and changing the direction of its flow. The application of such a square-wave electric potential in no way affects the salt rejection of the electrically conductive membranes. Further, the transmembrane flux of pure water or saline waters is not detectably affected by the application of this over-potential. The highly effective anti-fouling effects of applied electric potential suggests that these membrane could be used to great affect in a variety of membrane systems that struggle with biofouling. This includes membrane bioreactors, ultrafiltration separations, and desalination systems. With regards to the latter application, pretreatment can be significantly reduced if electrically conductive membranes are used in place of conventional polyamide membranes. Further, the economics are such that the cost of the new electrically conductive material can be recovered if

pretreatment were reduced by 3.4% or more. Pretreatment could be reduced by significantly more than this, implying the potential for tremendous economic gains with the use of electrically conductive membranes for surface biofouling prevention. The mechanisms for the highly effective, long-term biofouling prevention are as of yet unconfirmed, but it is suspected that a combination of bacterial oxidative stress, electrostatic repulsion, and bacterial stress due to the disruption of the ionic and pH equilibria on the surface of the membrane are the primary causes.

5.2 Non-Covalent Polymer Wrapping of CNTs

In this dissertation it was found that non-covalent, polymer wrapped CNTs have low stability in polymer matrices and leach from them under certain conditions. Both pristine and functionalized CNTs were found to exhibit low stability in polymer matrices, with greater instability occurring for greater functionalization. Despite their instability and proclivity to leach, polymer wrapped CNTs added to polymer membranes enhance a range of membrane properties. The benefits of adding functionalized CNTs into polymer matrices include increased Young's Modulus, increased resistance to tensile stress, and increased surface hydrophilicity. Minimizing the CNT instability within polymer matrices helps maximize the benefits to the polymer membranes from the CNTs. Well stabilized CNTs in polymer matrices could significantly improve membrane structural stability, among other properties, allowing membranes to be used in more severe conditions and increasing their operational lifetime, which is economically beneficial.

5.2.1 CNT Leaching from Nanocomposite Polymer Matrices

Pristine or sidewall-functionalized CNTs leach from polymer matrices to which they are added, in the absence of chemical binding between the CNTs and the polymer chains of the bulk polymer matrix. This represents an instability of the CNTs within

their polymer surroundings. Loss of CNTs occurs for membrane production, specifically during the gelation of the membranes during immersion precipitation. Leaching of CNTs also occurs during caustic chemical cleaning of the membrane surfaces. No leaching of CNTs was observed during pressurized filtration. The loss of CNTs from the polymer matrices is aggravated by CNT sidewall functionalization. CNTs that are functionalized to a higher degree are lost from the polymer matrices to a greater degree. Specifically, carboxylated CNTs have greater affinity for solvents than they do for the membrane polymers to which they are added and as a result are susceptible to loss and leaching from polymer matrices when they are unbound to the polymer chains of the bulk polymer matrix. The loss of carboxylated CNTs is greatest during immersion precipitation. The dynamic re-orientation of the polymer matrices and the exchange of solvents and non-solvents during immersion precipitation encourages mixing of functionalized CNTs. Their increased mobility during this process as well as the kinetic solvent/non-solvent exchange process accounts for their high degree of loss from polymer solutions during membrane formation. Polymer CNT membranes were used as a template for nanocomposite materials. Leaching of chemically unbound CNTs, both pristine and functionalized, occurs with high probability from all polymer systems to varying degrees. To safeguard against environmental contamination, potential impacts to human health, and poor material performance, nanocomposite manufacturers must be aware of CNT loss and leaching and develop strategies to limit or eliminate it throughout the nanomaterial's life-cycle.

5.2.2 Property Enhanced Nanocomposite Polymer Matrices

Functionalized CNTs that are minimally lost and leached from polymer nanocomposites optimally enhance the properties of membranes. This includes improvements to Young's Modulus, tensile strength, and surface hydrophilicity. However, loss and leaching of CNTs from polymer nanocomposite membranes reduces the total amount

of CNTs from those matrices and causes significant deviations from the expected material properties associated with the addition of CNTs. Expected increases in Young's Modulus and tensile strength, for example, are not realized with highly carboxylated CNTs, as these functionalized CNTs are lost from the membrane matrix to a high degree and do not contribute to the load bearing properties of the membrane. Furthermore, the dynamic loss of CNTs during membrane gelation through immersion precipitation affects the membrane morphology. This causes increased membrane permeability and reduced selectivity as well as a loss in pore size uniformity. Overall, CNT leaching from membranes causes membranes to be formed in inconsistent ways with properties that have low reproducibility. Membranes with low loss and leaching of functionalized CNTs, on the other hand, showed strong membrane property enhancements and more consistent properties across multiple membranes. Nevertheless, loss and leaching of chemically unbound CNTs is unavoidable, even for CNTs with low degrees of carboxylation, albeit to a lesser degree than for highly functionalized CNTs. Chemical strategies, therefore, must be developed to stably bind CNTs to polymer matrices. Chemically unbound CNTs will be lost and leached from polymer composites, which is unacceptable both from an environmental and health risk perspective as well as from a manufacturing and economic viability perspective. CNTs, therefore, must be bound to polymer chains in all nanocomposites.

5.3 Ionic Bonding Between CNTs and Polymers

In this dissertation it was found that binding CNTs ionically to polymer chains greatly improves the stability of CNTs within the polymer matrices and eliminates the loss and leaching of CNTs from membranes. Stabilizing CNTs within polymer matrices in this way is beneficial from both an environmental sustainability and economic viability perspective. The polymer chains of the nanocomposite membranes formed in this way, however, are affected by the ionic bonding to the CNTs. This

charge association between CNTs and polymer chains alters the final membrane morphology and structure in negative ways.

5.3.1 Ionically Bound Nanocomposite Polymer Matrices

Ionic bonds between CNTs and polymer chains eliminates the loss of functionalized CNTs from polymer nanocomposites. Specifically, CNTs functionalized with positively charged amine functional groups bind to negatively charged polymer chains through charge association. This binding eliminates the loss of the functionalized CNTs from the polymer solutions during the membrane gelation process undertaken with immersion precipitation. However, the ionic bonds formed between the polymer chains and the functionalized CNTs altered the way in which the polymers formed the final membrane structure. Under normal immersion precipitation the restricted polymer mobility causes large structural changes including highly porous surfaces which affects the flux and rejection characteristics of the resultant membranes. Despite changes to structural morphology, ionically bound CNTs within polymer membranes increase the membrane's Young's Modulus and tensile strength. CNTs covalently or ionically bound to polymer chains add functionality and enhanced properties to the resultant polymer nanocomposite, while also preventing leaching and loss of CNTs from the polymer matrix. The production of these materials, however, is affected by the bonding and changes to the material fabrication and processing steps are necessary to achieve optimized products. Membranes formed with highly stable CNTs and limited impacts to membrane morphology would have great impacts on hollow fiber operation and longevity. These membranes would be able to resist greater pressures, endure more harsh conditions, and maintain their structural integrity for longer, increasing their operational lifetimes.

5.4 Overall Conclusions of this Dissertation

Carbon Nanotubes have the potential to significantly improve polymeric materials. In this dissertation, in particular, CNTs have been shown to add functionality and enhance polymer membranes' properties in a variety of ways. CNTs can be used to alter pore size and therefore affect membrane selectivity and flux; they can add electrical conductivity to membrane surfaces and therefore prevent biofouling; and they can enhance the tensile strength of bulk membranes thereby increasing membrane longevity. To achieve these enhanced properties, different material and chemical bonding configurations between CNTs and polymers must be employed. Given a desired functionality, CNTs can be manipulated in specific ways to achieve it. Chemical bonding, fabrication process, and CNT type and content must be selected based on this desired functionality. In all cases, chemical binding of the CNTs to the polymer chains is imperative to prevent loss and leaching of CNTs from polymer nanocomposites. Mechanical and chemically stable polymer nanocomposites are critical in order to produce materials that are highly functional, provide expected property enhancements, and pose little or no risk to natural environments and humans. Carbon nanotube polymer composites have been demonstrated to enhance membrane properties in various ways, but there exists further potential for these composites. Notably, electrically conductive membrane surfaces have the potential to also prevent surface scaling as well as biofouling. These membranes can also act as surfaces for electro-degradation of environmental contaminants. Moreover, electrically conductive porous surfaces can act as templates for catalyst grafting, and can then be engaged in various environmental, chemical, and pharmaceutical catalytic processes including catalytic degradation of trace environmental contaminants, resource recovery, chemical catalysis, and pharmaceutical production. The potential for CNT-polymer nanocomposite membranes is an exciting area of research that has

much future potential.

Appendix A

Supplementary Data for Covalently Bound CNT-Polymer Membranes

A.1 Supplementary Data for PVA-CNT Membrane Properties

A.1.1 Additional Details on PVA-CNT Membrane Surface Morphology and Cross-Sections

TEM images of sonicated carboxylated CNTs show that CNTs are well dispersed in solution after sonication. Homo-aggregation is therefore not a factor in film formation limitations.

Below are cross-sectional and surface images of the surface coated membranes. Surface coating thickness was measured from these SEM images. Thickness increased with greater amount of CNTs used. In all images, the support membrane was cellulose nitrate, but other support membranes were also investigated including polysulfone and polyethersulfone.

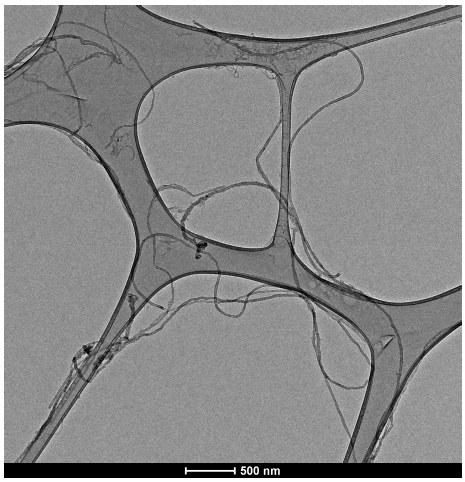

FIGURE A.1: TEM image of sonicated carboxylated CNTs. This image shows well dispersed CNTs post sonication in aqueous solution.

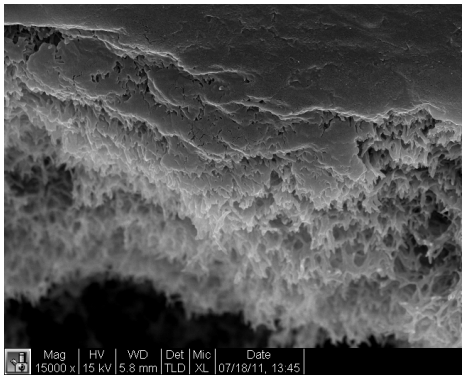

FIGURE A.2: Cross-section image of a pressure filtered membrane with 0.1 wt% carboxylated multi-walled carbon nanotubes with respect to PVA.

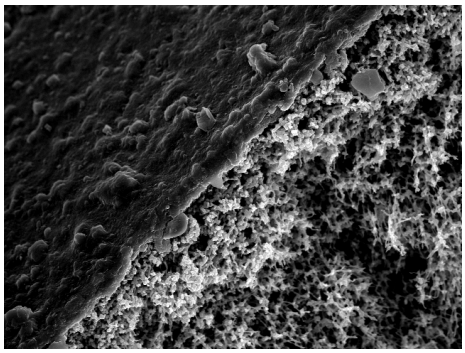

FIGURE A.3: Cross-section image of a pressure filtered membrane with 10 wt% carboxylated multi-walled carbon nanotubes with respect to PVA.

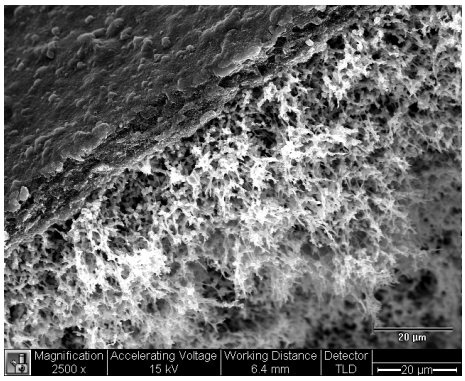

FIGURE A.4: Cross-section image of a pressure filtered membrane with 20 wt% carboxylated multi-walled carbon nanotubes with respect to PVA.

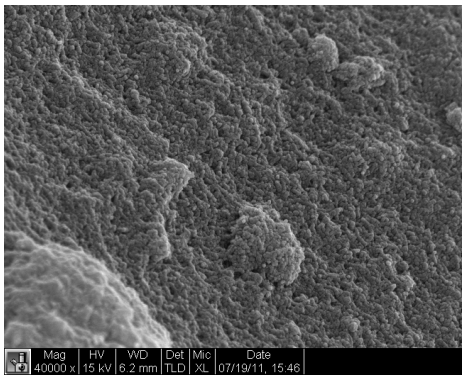

FIGURE A.5: Surface image of a pressure-filtered membrane with a carbon nanotube content of 20 wt% with respect to PVA.

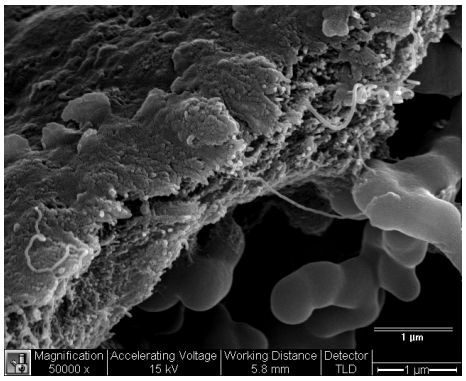

FIGURE A.6: A highly magnified image of the pressure-filtered surface coating with 5 wt% carboxylated multi-walled carbon nanotubes with respect to PVA. The nanotubes are clearly seen in this image intertwined with the PVA and sitting on top of the cellulose nitrate support membrane.

A.1.2 Additional Details on PVA-CNT Membrane Properties

Electrical resistivity measured in Ωm (the reciprocal of electrical conductivity measured in S/m) was plotted for all analysed types of membranes. The effect of curing time on the electrical resistivity of a membrane with 10 wt% carboxylated multi-walled carbon nanotubes with respect to PVA is shown in figure 4.6 a). The electrical resistivity does not change significantly with greater than 10 minutes curing time. However, less than this amount of curing time increases the electrical resistivity and weakens the affinity of the surface coating for the support membrane. In figure 4.6 b) the effect of CNT concentration on electrical resistivity is shown. In this case, all membrane were cured for a minimum of 20 minutes to ensure minimal resistivity and maximally binding with the support membrane.

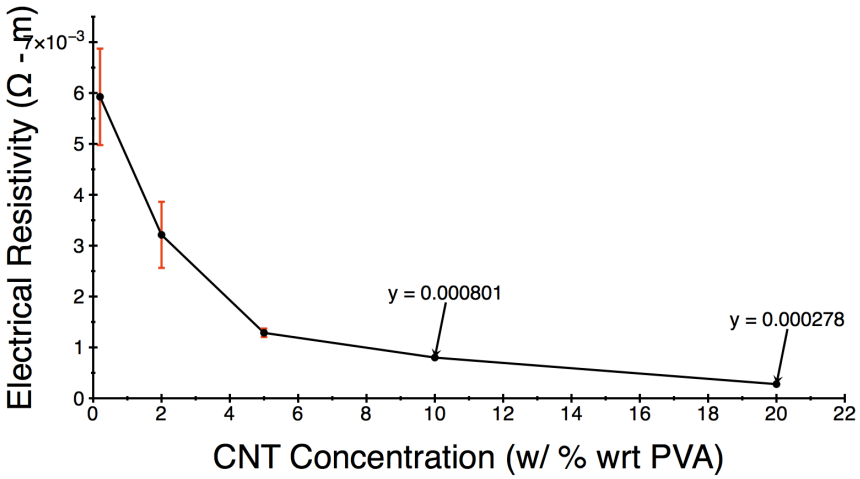

FIGURE A.7: The electrical resistance of membranes with varying amounts of carbon nanotubes and cured for at least 20 minutes was measured. Greater amounts of carbon nanotubes significantly reduces the electrical resistivity of the membranes.

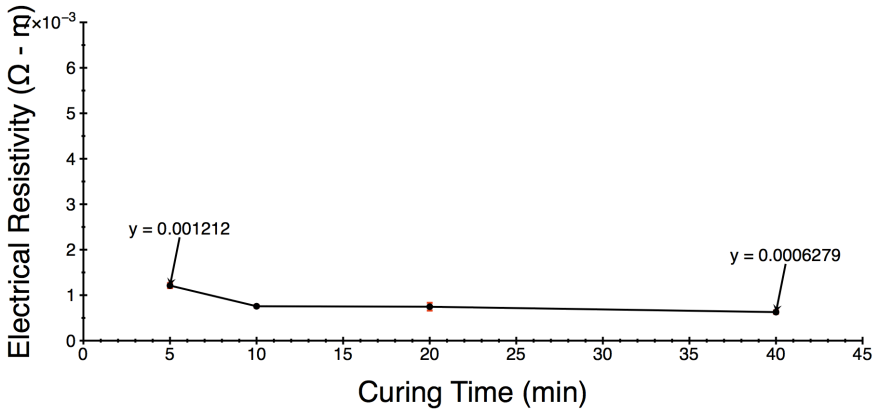

FIGURE A.8: Membranes with 10 wt% carboxylated multi-walled carbon nanotubes with respect to PVA were cured for varying amounts of time. Electrical resistivity does not vary significantly with curing time, however with curing times less than 10 minutes the resistivity is not as low as with longer curing times.

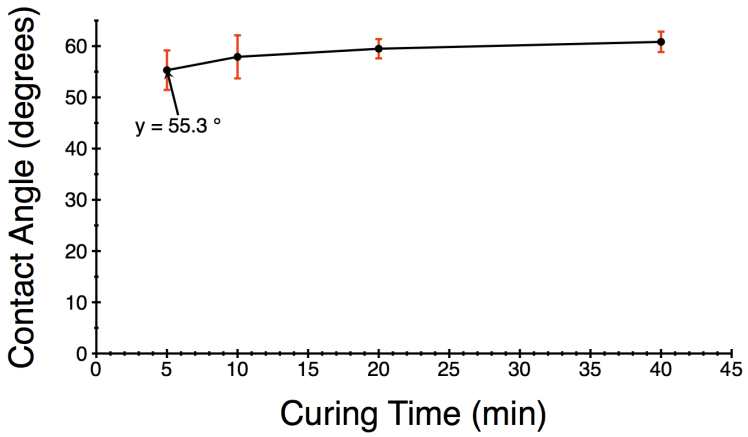

FIGURE A.9: Membranes with 10 wt% carboxylated multiwalled carbon nanotubes with respect to PVA were cured for various amounts of time. Their surface contact angle does not statistically change with different curing times. Regardless, the surface is still very hydrophilic considering most of these ultrafiltration membranes had a contact angle of approximately 55°.

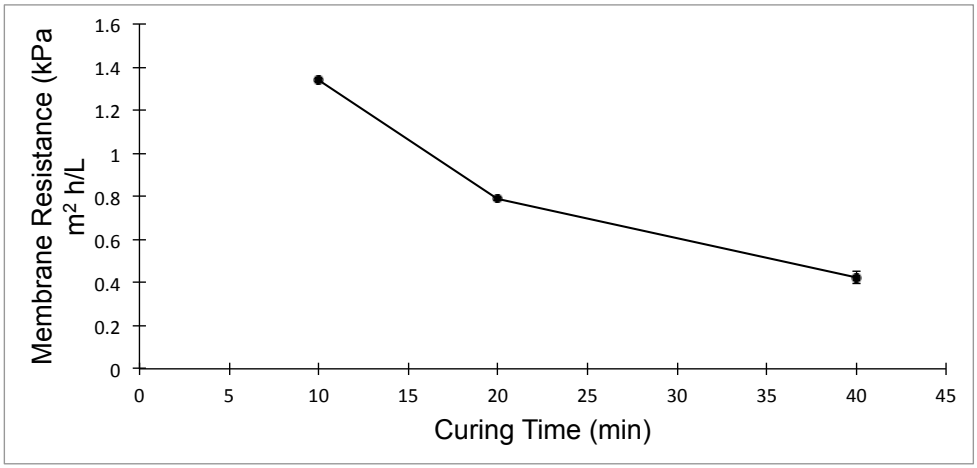

FIGURE A.10: The membrane resistance was computed from the inverse slope of the fluxes of each of the membranes formed with 10 wt% CNTs with respect to PVA and cured to three different curing times, 10 min, 20 min, and 40 min. In this graph one can see that longer curing times causes lower membrane resistances and thus higher fluxes.

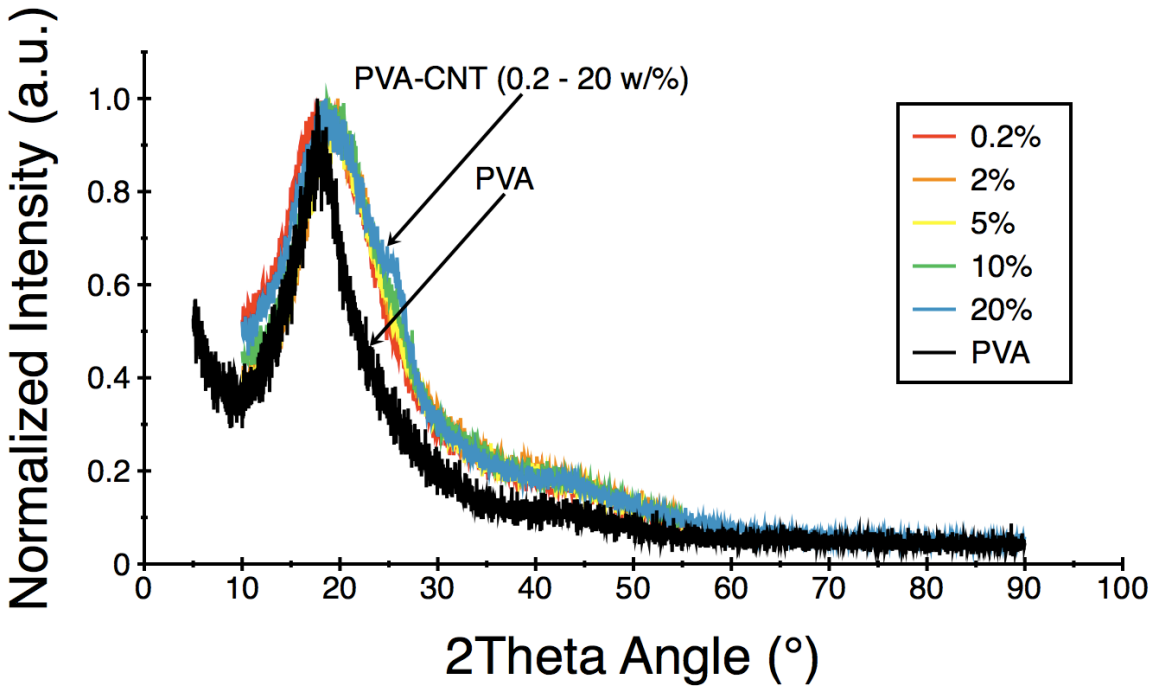

FIGURE A.11: The crystallinity of the conductive polymer coating is compared with that of the pure PVA membrane. CNTs covalently cross-linked to PVA chains disrupt the semi-ordered alignment of the PVA molecules as shown with XRD. The narrow peak of the PVA (in black) is evidence of carbon ordering within the matrix, while the broad diffuse coloured peaks (red = 0.2 wt%, orange = 2 wt%, yellow = 5 wt%, green = 10 wt%, blue = 20 wt%) indicate a lack of ordering among the polymer chains caused by the large, stiff carbon nanotubes.

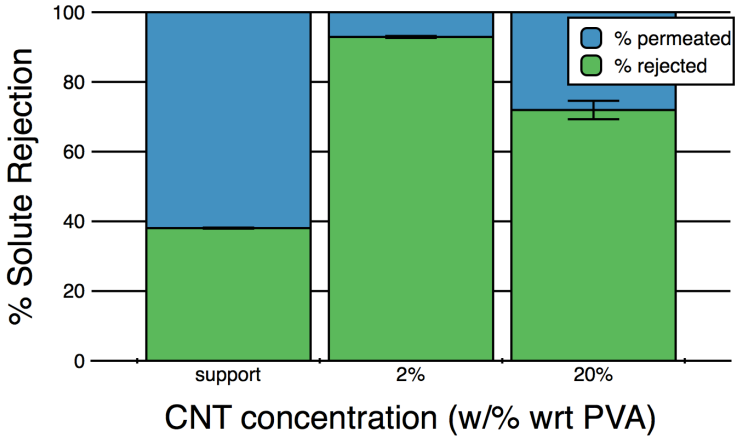

FIGURE A.12: Polyethylene oxide (PEO), with molecular weights 600 kDa, was used to analyse the separation characteristics of highly conductive cross-linked carbon nanotube membranes. Membranes formed with higher concentrations of carbon nanotubes with the same cross-linking density showed lower rejection of polyethylene oxide. Membranes formed with 2 wt% CNTs, for example, had over 90% rejection of PEO 600 kDa, while those with 20 wt% had just over 70% rejection. Membranes formed with lower amounts of CNTs had higher rejection rates (not shown). Rejection in all cases was higher than that of the support.

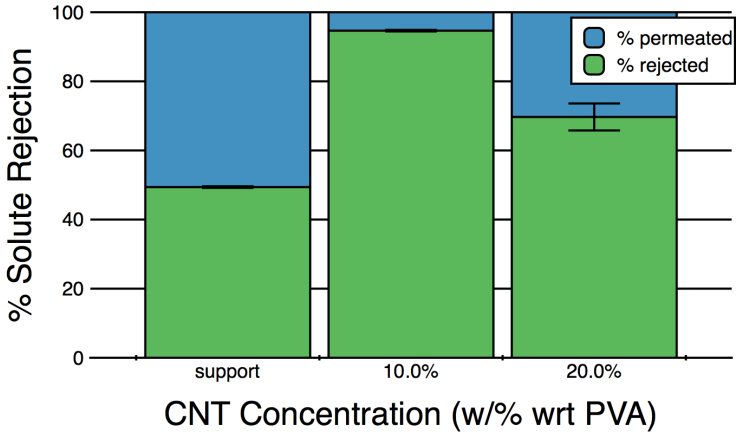

FIGURE A.13: Polyethylene oxide (PEO), with molecular weights 1 MDa, was used to analyse the separation characteristics of highly conductive cross-linked carbon nanotube membranes. Membranes formed with higher concentrations of carbon nanotubes with the same cross-linking density showed lower rejection of polyethylene oxide. Membranes formed with 10 wt% CNTs, for example, had over 95% rejection of PEO 1 MDa, while those with 20 wt% had approximately 70% rejection. Membranes formed with lower amounts of CNTs had higher rejection rates (not shown). Rejection in all cases was higher than that of the support.

A.2 Supplementary Data for PA-CNT Membrane Properties

A.2.1 Detailed Description of Control 3 Material Fabrication

Control 3 membranes were formed in the same manner as highly conducting ECPNC membranes, with added electrical resistivity to their surface. CNT deposition followed the same procedure as with ECPNC membranes, but soaking in MPD was done for 5 minutes instead of 30 seconds, followed by less rolling and wicking, and then immersion in TMC for 5 minutes, as opposed to 30 seconds. This longer immersion time formed a much thicker polyamide thin film on the surface of the membrane and as a result a much more electrically insulating surface.

A.2.2 Additional Details on PA-CNT Membrane Properties

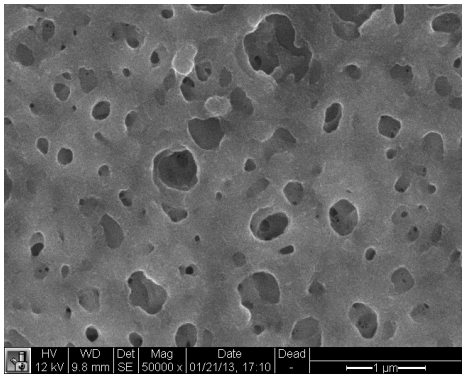

FIGURE A.14: The underside of a plain PA membrane, showing that only one side of the PA membrane has a thin film, while the other remains porous.

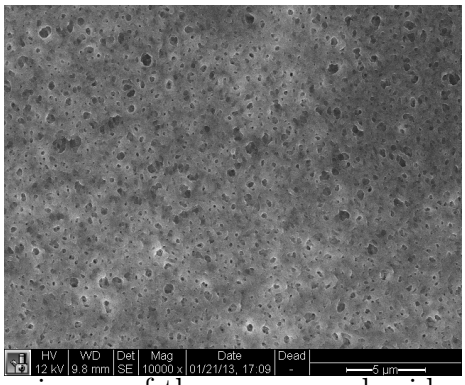

FIGURE A.15: A closer image of the porous underside of the PA membrane.

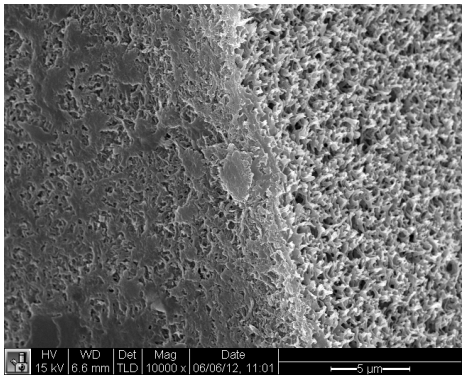

FIGURE A.16: PA-CNT ECPNC RO membrane cross-section showing the support PES membrane on the right.

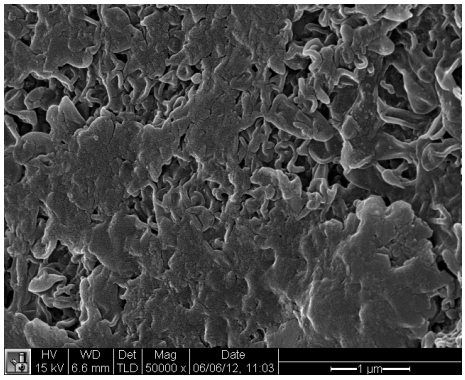

FIGURE A.17: Surface image of an ECPNC RO membrane. The typical PA surface morphology is clearly visible.

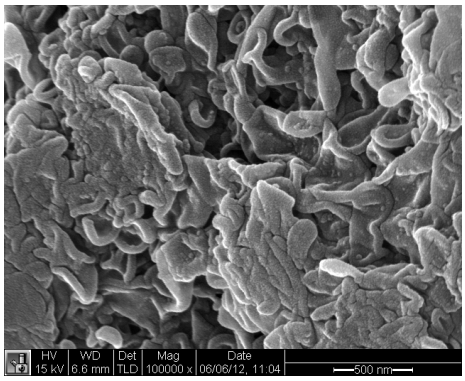

FIGURE A.18: The same membrane as in A.17, focusing on the PA-CNT surface morphology.

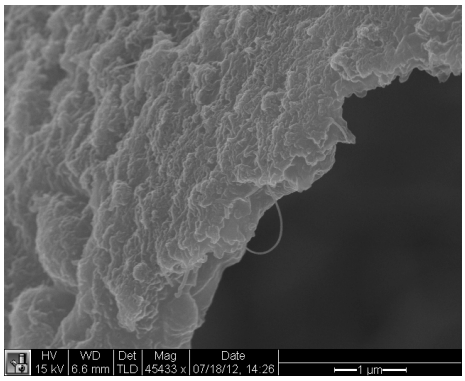

FIGURE A.19: Cross-section of the ECPNC membrane, showing CNTs emerging from the surface.

A.3 Supplementary Data for Biofouling Prevention on Electrically Conductive Surfaces

A.3.1 Additional Details on Biofouling Prevention on Electrically Conductive Surfaces

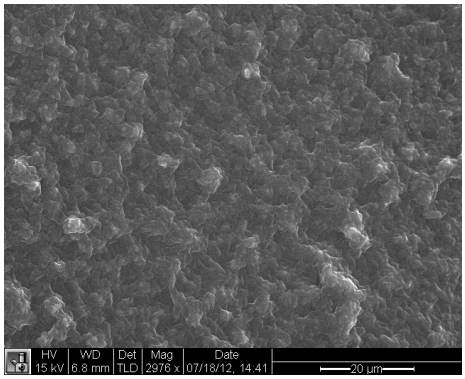

FIGURE A.20: The surface of an ECPNC membrane post experiment with applied alternating potential. The surface topology is rough and irregular but devoid of live bacteria.

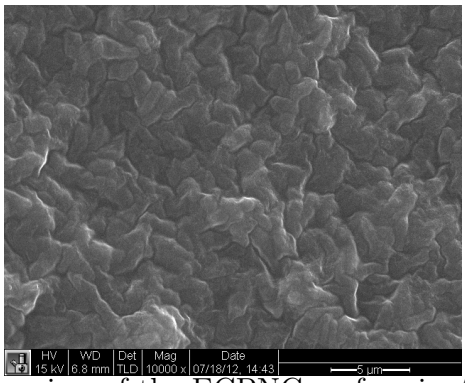

FIGURE A.21: A closer view of the ECPNC surface in A.20 post-experiment.

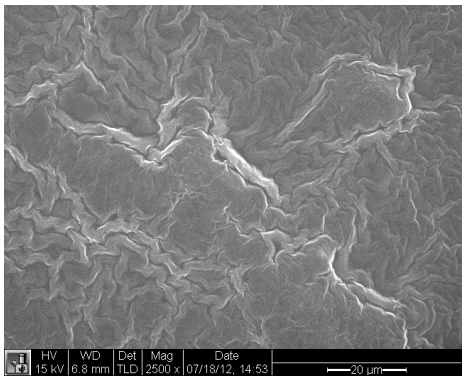

FIGURE A.22: Another ECPNC membrane post experiment with applied alternating potential. Surface is contorted but devoid of bacteria.

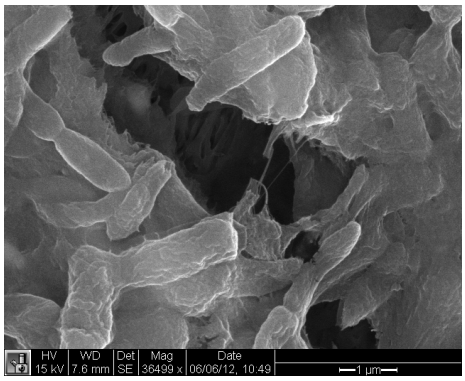

FIGURE A.23: Image of a biofilm formed on a fouled ECPNC membrane showing both P. Aeruginosa and the biofilm. This membrane is from a control experiment using an ECPNC membrane without applied voltage.

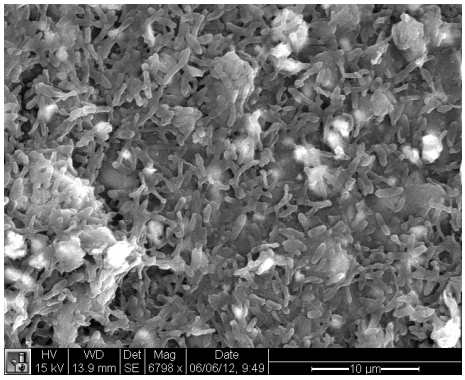

FIGURE A.24: Fouled ECPNC membrane of the same control experiment as in A.23 - a control experiment without an applied voltage.

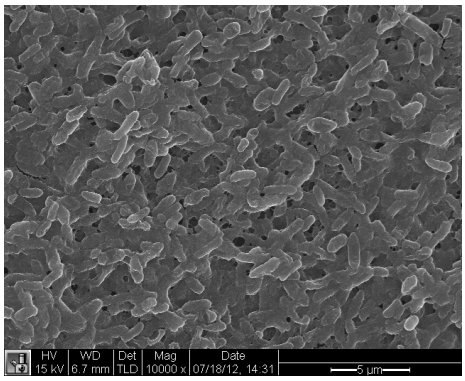

FIGURE A.25: Image of a membrane fouled by bacteria. This membrane is from a control experiment using a highly resistive PA-CNT membrane with applied voltage.

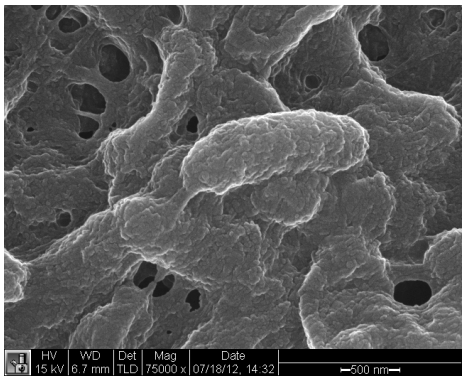

FIGURE A.26: Closer view of the P. Aeruginosa seen in figure A.25 from the same control experiment.

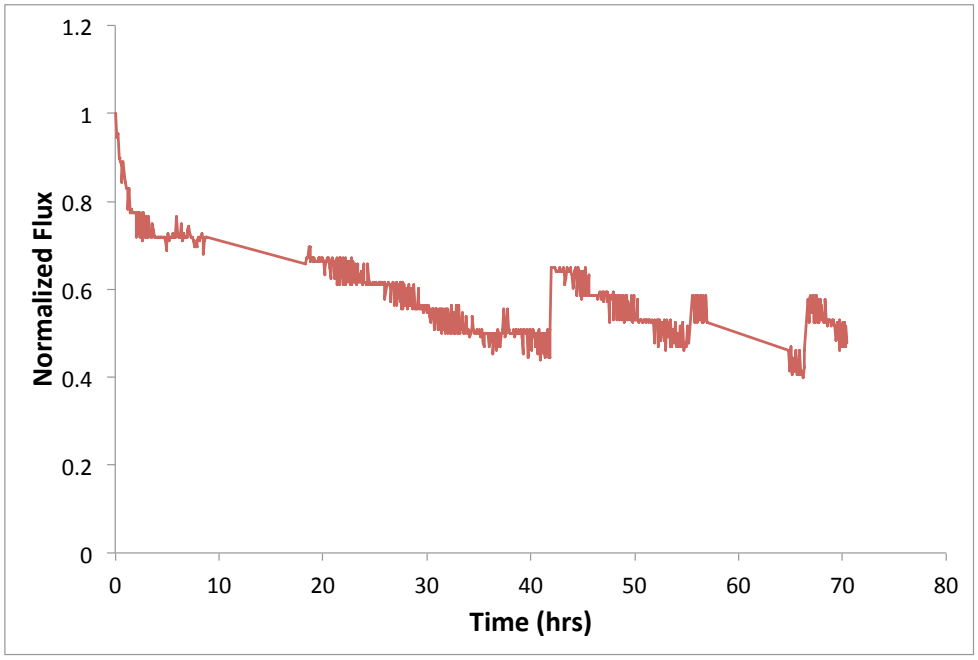

FIGURE A.27: Control 2 ECPNC membrane with no applied potential showing a maximum of 15% recovery after flushing.

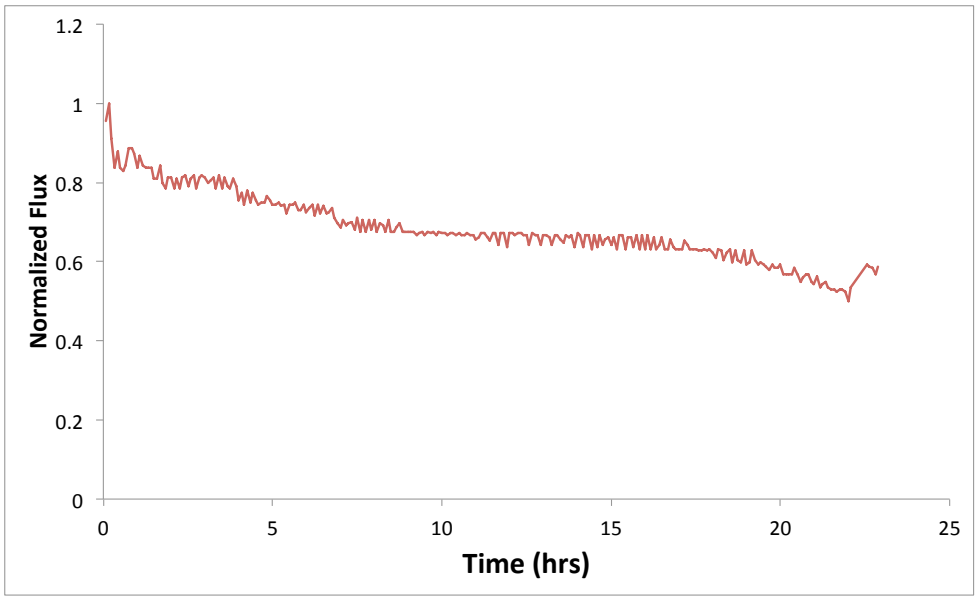

FIGURE A.28: Control 3 ECPNC membrane with no applied voltage. Very low flux recovery upon cross-flow flushing.

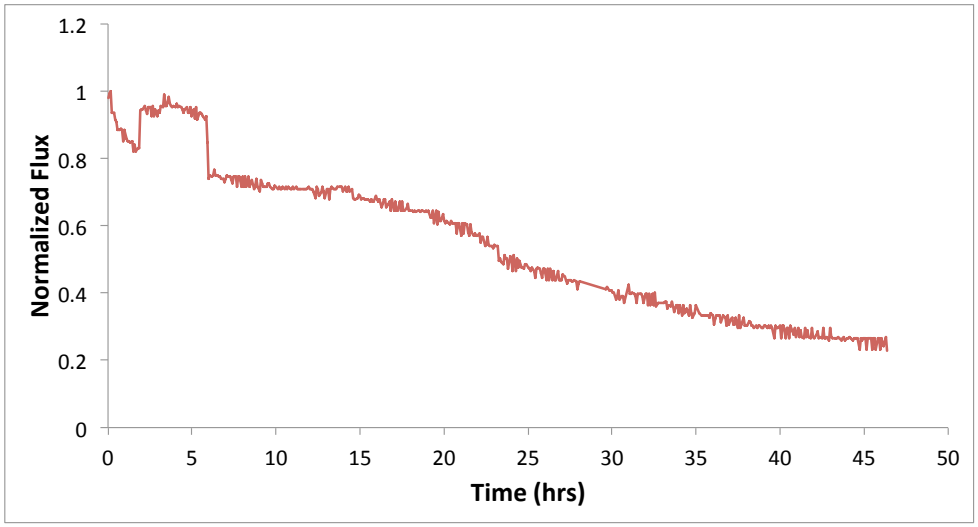

FIGURE A.29: Control 4 ECPNC membrane with no applied voltage. Very low and temporary flux recovery upon each of the three cross-flow flushings.

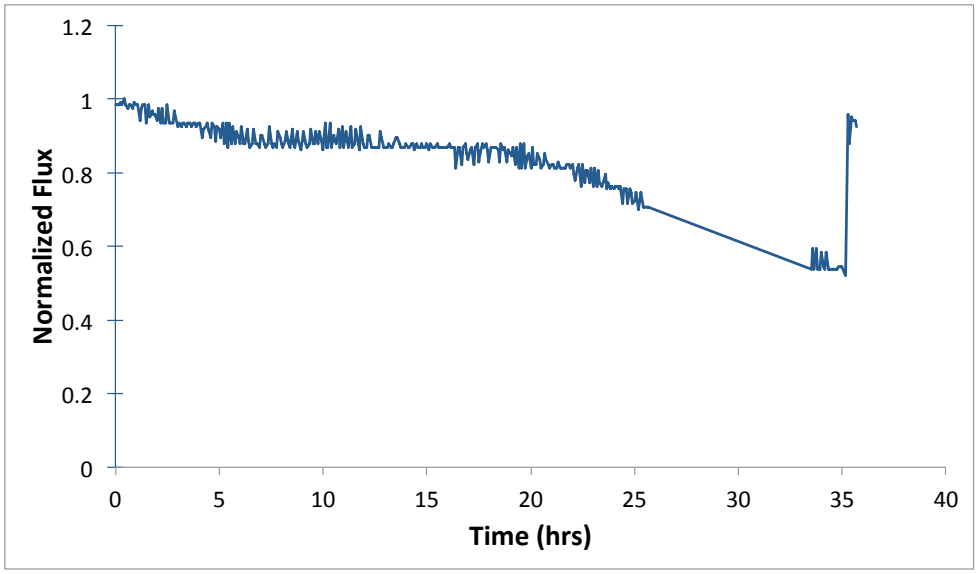

FIGURE A.30: Experiment 1 ECPNC membranes with applied voltage. Greater than 90% flux recovery is achieved.

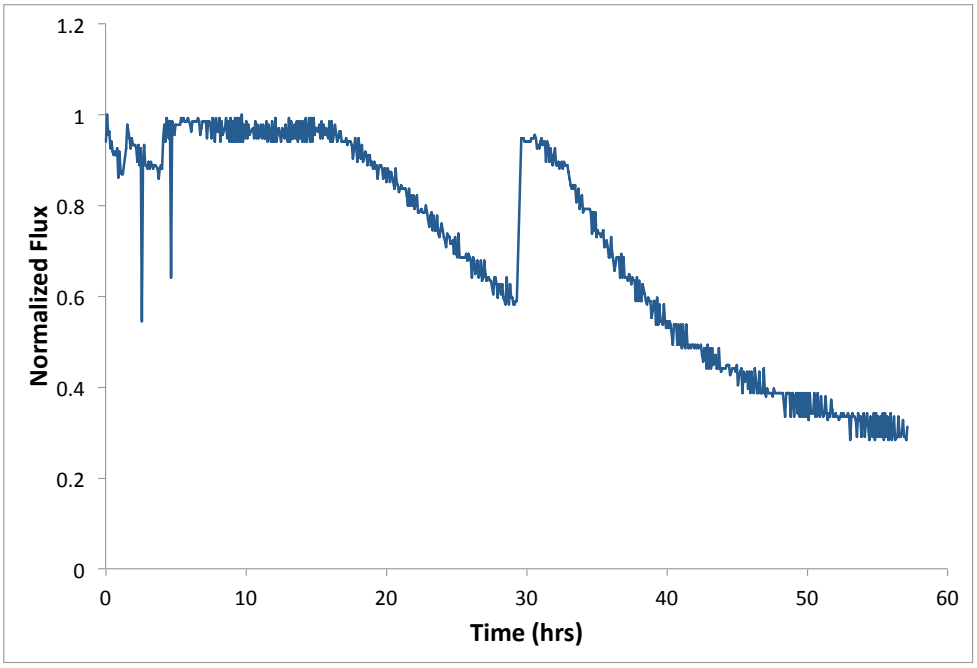

FIGURE A.31: Experiment 2 ECPNC with voltage applied showing close to 100% flux recovery after 45% flux decline from pressure-deposited matter.

A.3.2 Detailed Analysis for the Economic Viability of Electrically Charged Membrane Surfaces

The potential economic benefits of utilizing electrically conducting membranes in water treatment processes come from lower operating costs and reduced initial capital expenditure. The amortized initial cost of a pretreatment system for a typical reverse osmosis membrane facility with a water production capacity of $74000\,m^3$/day is $202US$/day and $143US$/day for an ultrafiltration (UF) or coagulation/sand filtration system, respectively. This is the equivalent to an amortized investment cost of $0.00273US$/m^3$ and $0.00193US$/m^3$ of water produced, respectively for a reverse osmosis plant that has an expected lifetime of 25 years. This represents approximately 20% and 15%, respectively, of the total investment cost for such systems (Fritzmann et al., 2007). The operating costs (chemicals, replacement UF filters, if such filters are used, and replacement spare parts) associated with pre-treatment processes are 0.1027 US$/$m^3$ and 0.0925 US$/$m^3$ for a UF or coagulation/sand filtration system, respectively (Fritzmann et al., 2007). A large membrane-based water reuse facility, such as the water reclamation facility in Orange County, CA, which uses a combination of MF and RO to treat 272,000 m^3/day, would incur a daily cost of $28677 in chemicals, replacement parts and amortized investments. The measured current density at $1.5\,V$ was 14.2 $\mu A/cm^2$. Using the Orange County Water Reclamation facility as an example, with its $584,000\,m^2$ of membrane area, the energy required to power the electrified membranes, if the entire plant was converted, comes out to be $2977\,kWh$, or $595.40/day, using 2012 electricity prices. Thus, if the pretreatment costs can be reduced by as little as 2.1% or more, then savings can be realized. These savings do not include the additional benefit that electrically conductive membranes offer, which is increased membrane lifetime. By avoiding biofouling and the use of caustic chemicals, membranes will degrade at a slower rate and last for longer during operation.

Appendix B

Supplementary Data for Polymer Wrapped CNT-Polymer Membranes

B.1 Details of CNT Functionalization and Suspension

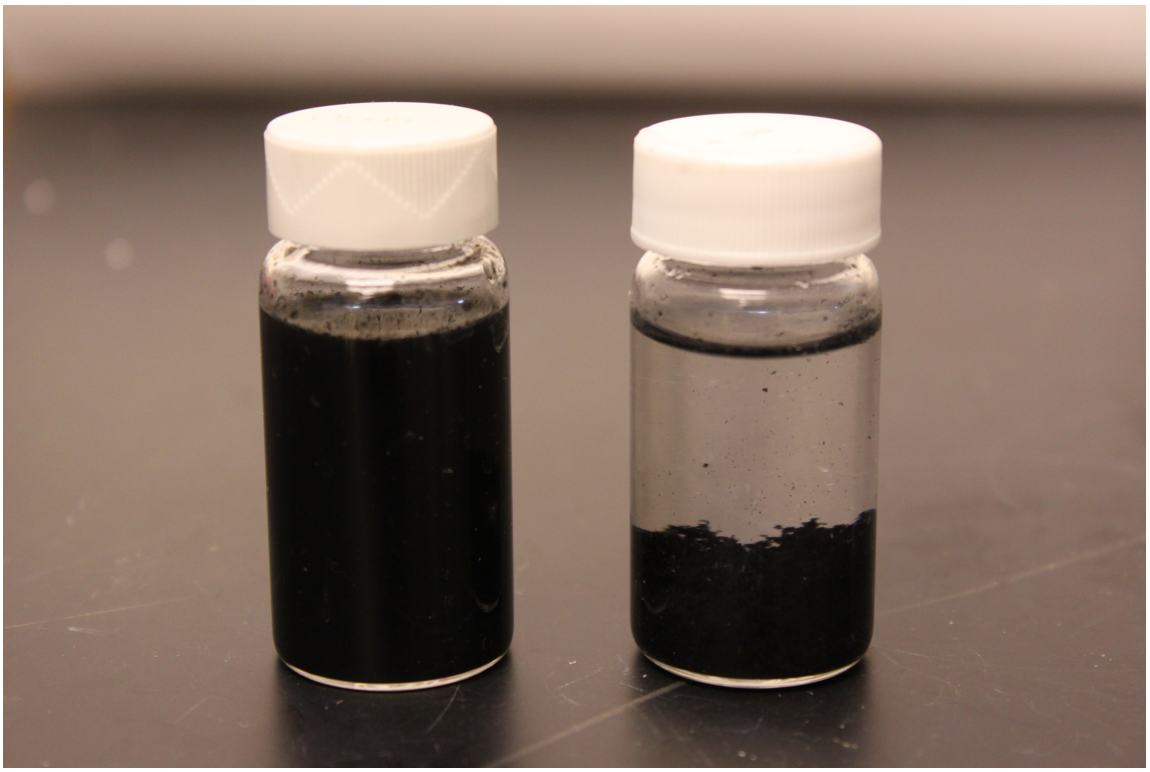

FIGURE B.1: Carboxylated CNTs in the left stay suspended indefinitely, while pristine (pCNTs) aggregate and sediment out of solution within hours after ultrasonication. In order to form membranes from these materials, it is necessary to dissolve the polymer in the CNT-solvent suspension immediately after sonication.

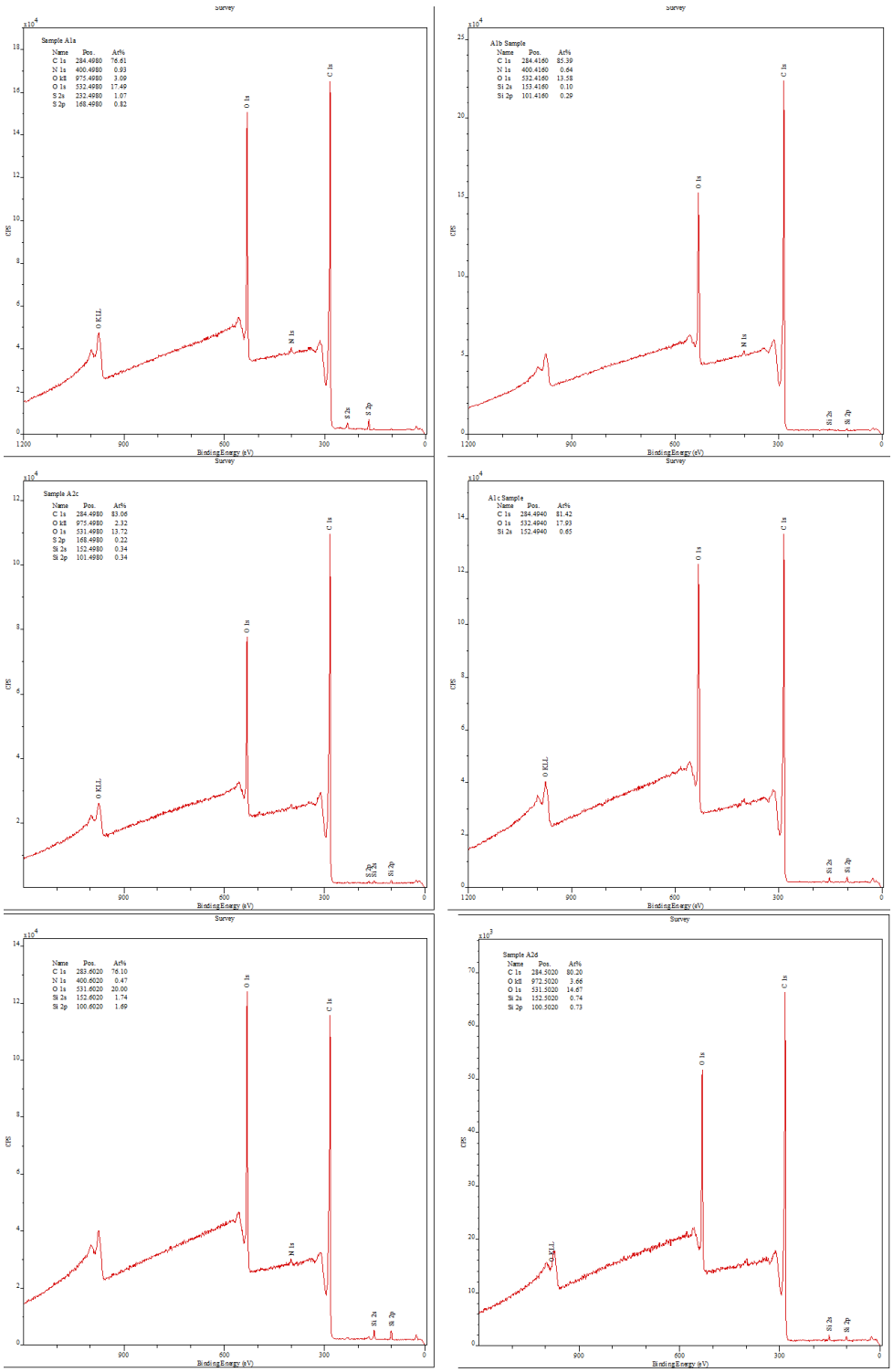

FIGURE B.2: XPS survey data of pCNTs and CNT-COOHs used in the experiments.

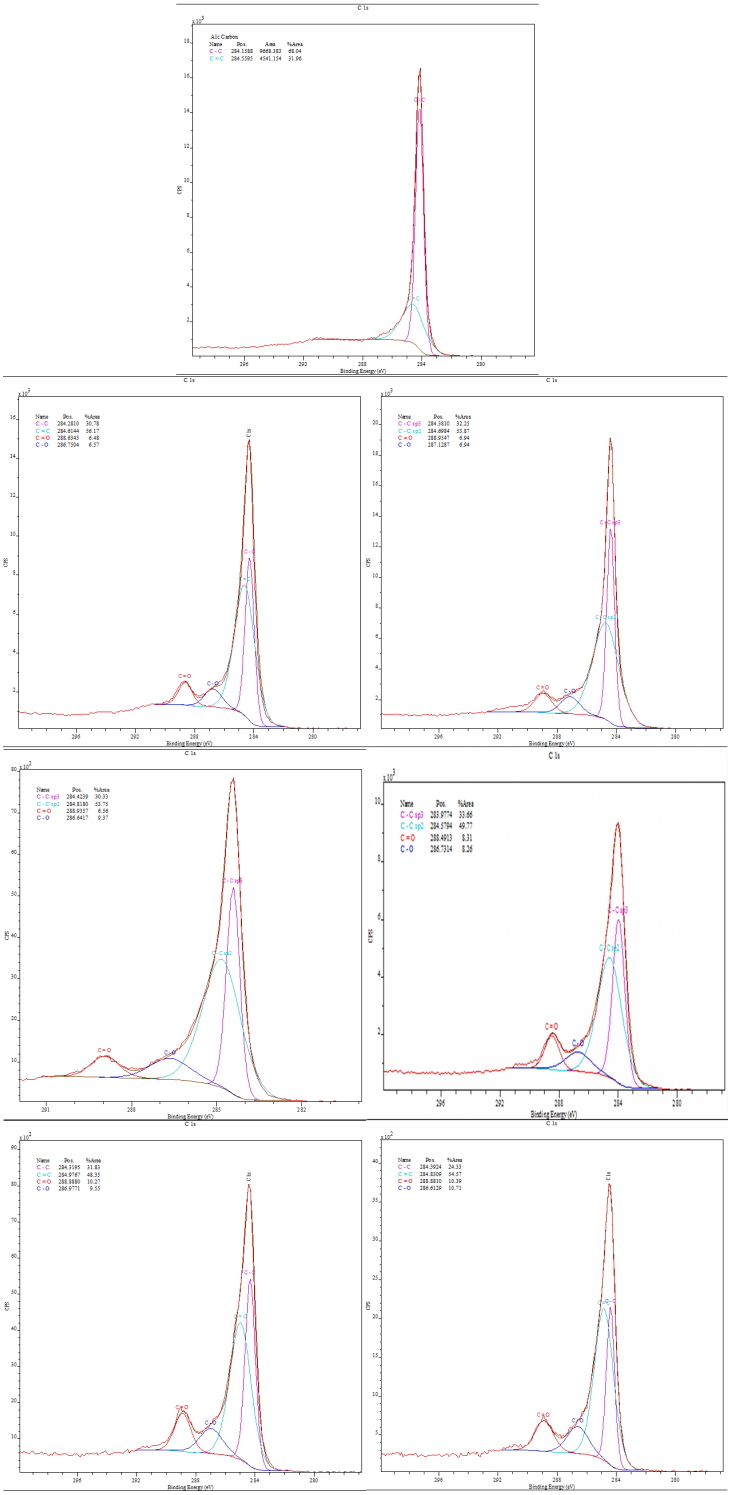

FIGURE B.3: XPS data around the carbon peak of pCNTs and CNT-COOHs used in the experiment. XPS graphs show C-C, C-O, and C=O bonding in the CNT samples. From the proportions of oxygen bonds, the functional content of the CNTs was elucidated.

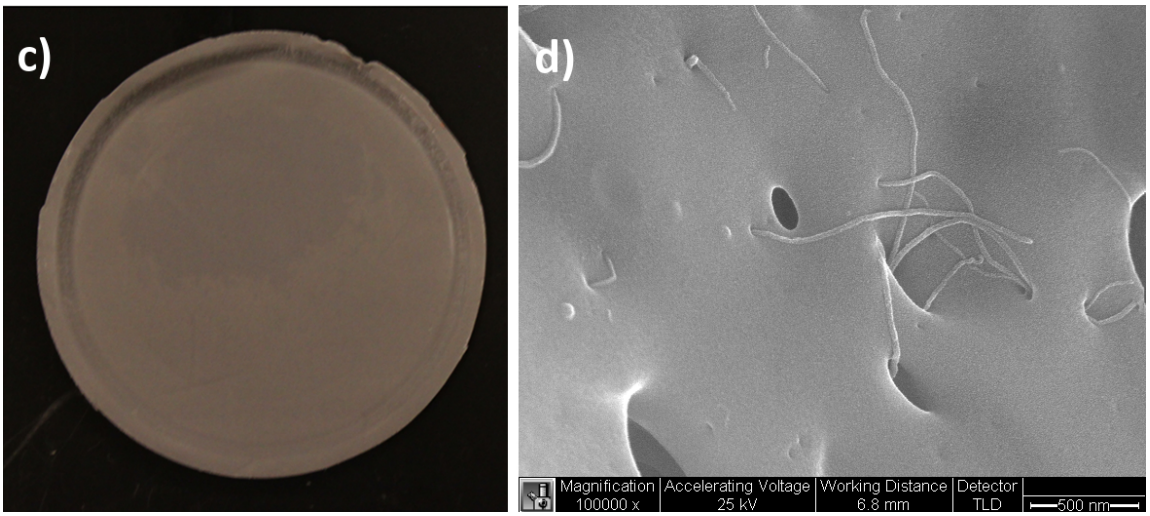

FIGURE B.4: In a) the surface of a PSf-PVP-CNT membrane containing 0.5% CNT-COOHs. In b) an SEM image of the surface of the membrane showing the well-dispersed CNTs throughout the polymer matrix.

B.2 Details of Stress-Strain Measurements

Stress-strain measurements were performed for all membranes by cutting each membrane sheet into rectangular strips approximately 10 cm in length and 1 cm in width. These strips were then clamped and strained by an MSA stress-strain measurement instrument. Membrane strips were strained over the entire spectrum of their deformation from elastic strain, through to inelastic strain, to membrane failure and breakage. This full spectrum of strain is shown in figure B.5. Only the elastic region was analyzed, however, the entire spectrum was measured.

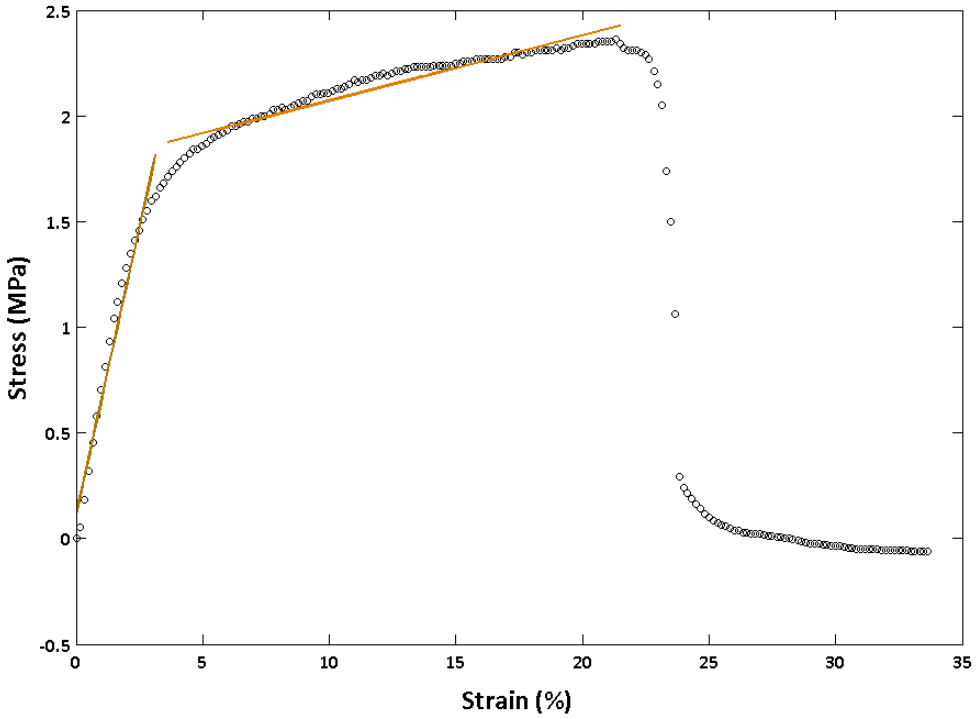

FIGURE B.5: Polysulfone membranes containing carboxylated CNTs were strained under increasing stress at a constant rate. The polymer nanocomposite membrane underwent elastic and inelastic deformation until breakage was induced. Only the elastic region was analyzed for determination of its Youngs Modulus. This is an example of the stress-strain curves that were analyzed. 15 independent stress-strain measurements were performed for each of the 8 membranes developed (pure PSf, pCNT-PSf, and 7 carboxylated CNT-PSf membranes) for a total of 120 measurements. This is one example of those curves.

B.3 Detailed UV-Vis Procedure and Measurements

UV-Vis measurements were taken to determine the leaching and loss of CNTs from polymer membrane matrices. The data revealed the absorbance intensity of solutions taken from the immersion precipitation non-solvent bath post membrane gelation. The amount of absorbed light is a measure of the darkness of the well-mixed non-solvent bath, which is a direct measure of the concentration of CNTs in the non-solvent bath. In order to determine the concentration of CNTs in solution that correlates with the absorbance intensity measured, we had to control for background signals and then compare the measured results to known concentrations. We made known concentrations of suspensions of CNT in DIW and DMF, which were then serially diluted from 42.5 mg/L down to 0.425 mg/L. A linear regression was then performed to determine the best fit for the data. This linear regression is shown in Figure B.6. We could then determine CNT concentrations in solution by comparing the intensity measured from the post-immersion precipitation non-solvent bath to this linearized data set.

Before we could make a direct comparison, however, a series of control experiments were performed to determine the intensity solely associated with CNTs, controlling for all the other non-solvent bath constituents including the background signal for water; the released solvent, DMF; any potentially leached membrane additive, PVP; and any un-gelled oligomer or monomer constituents of the original polymer solution. Representative control UV-Vis data for DIW and non-solvent bath solution obtained from PSf-PVP membranes formed without CNTs is shown in Figure C.10. Once the background signal was eliminated, absorbance intensities were compared to the linear regressions generated previously.

UV-Vis spectra were measured of non-solvent solutions obtained from immersion precipitation baths in which various CNT-PSf-PVP membranes were gelled. These

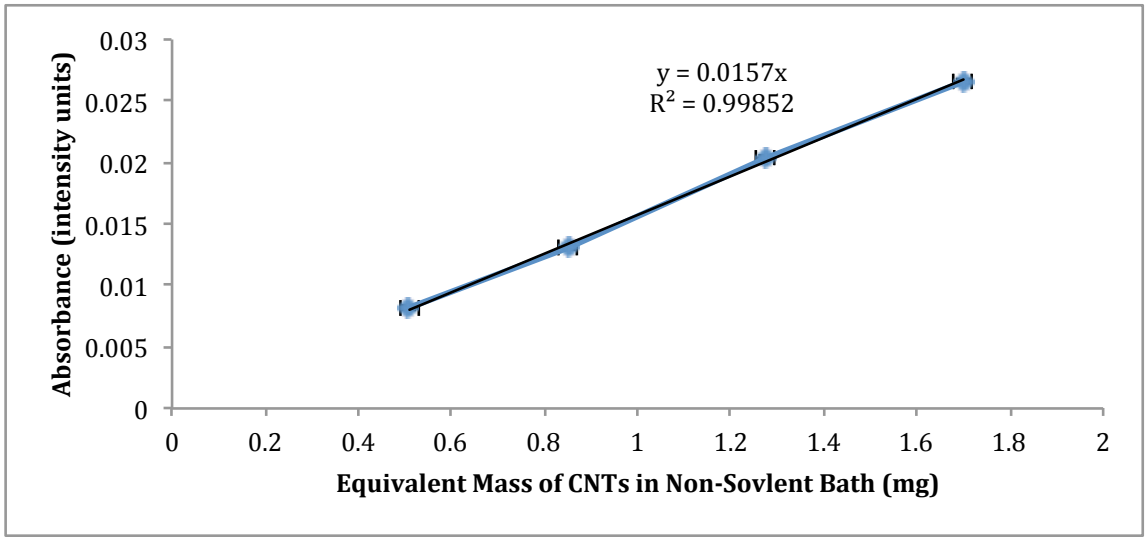

FIGURE B.6: The linear correlation between the absorbance intensity from UV-Vis measurements and the mass of CNTs in a standard volume of 1200 mL non-solvent bath. Using the linear regression equation, one can determine, for any intensity within the approximate range represented, the mass of CNTs that would be found in 1200 mL of DIW.

membranes had a constant initial concentration of CNTs of 0.5 wt% with respect to the polymer consitutents, PSf and PVP. The membranes varied in the types of CNTs impregnated within their matrices. Membranes analysed for CNT loss during immersion precipitation contained either pristine CNTs, CNTs carboxylated to 2.56% or CNTs carboxylated to 7.97%. During the immersion precipitation of each of these membranes, loss of CNTs was observed and UV-Vis spectra were obtained to quantify the amount of loss that occurred from the membranes. The UV-Vis curves of these solutions are shown in Figure B.8.

The average intensity values between 800 nm and 820 nm of each spectra were calculated. The values obtained for the control experiments were subtracted from those of the CNT loss experiments, which were then compared to the linearized regressions of the diluted concentrations discussed above. From these values, the mass of lossed CNTs was determined.

Each membrane was dried and weighed. The dry mass of the membranes and the

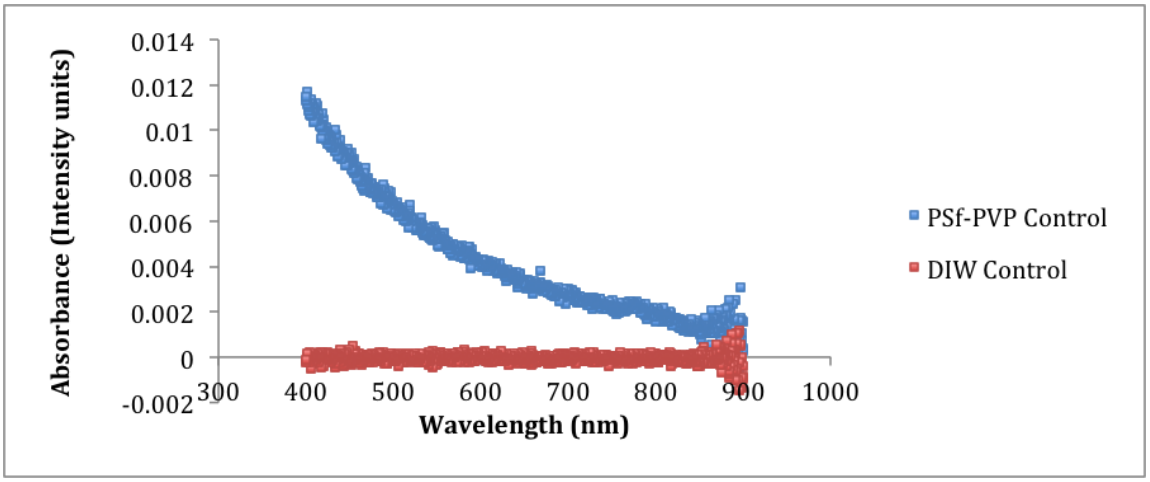

FIGURE B.7: Control UV-Vis signals for pure DIW (red) and non-solvent solution obtained from an immersion precipitiation bath in which pure PSf-PVP membranes (lacking any CNTs) were gelled (blue). Both UV-Vis spectra were obtained after controlling for the background signal associated with DIW, thus the constant zero signal for the DIW control.

mass of lost CNTs in the non-solvent solution were used to determine the percentage of CNTs that were lost from the membrane. This percentage was reported and compared across that of different membranes.

CNTs were observed to leach from membranes during causting cleaning with common membrane cleaning chemicals including HCl, NaOH, and NaOCl. The method to determine the percentage of leached CNTs from the membranes during cleaning, followed the same procedure as described above. Control experiments performed for this investigation included the spectra of DIW, diluted HCl, diluted NaOH, and diluted NaOCl, as shown in Figure B.9. The UV-Vis measurements of leached CNTs from the membrane matrices is shown in Figure B.10.

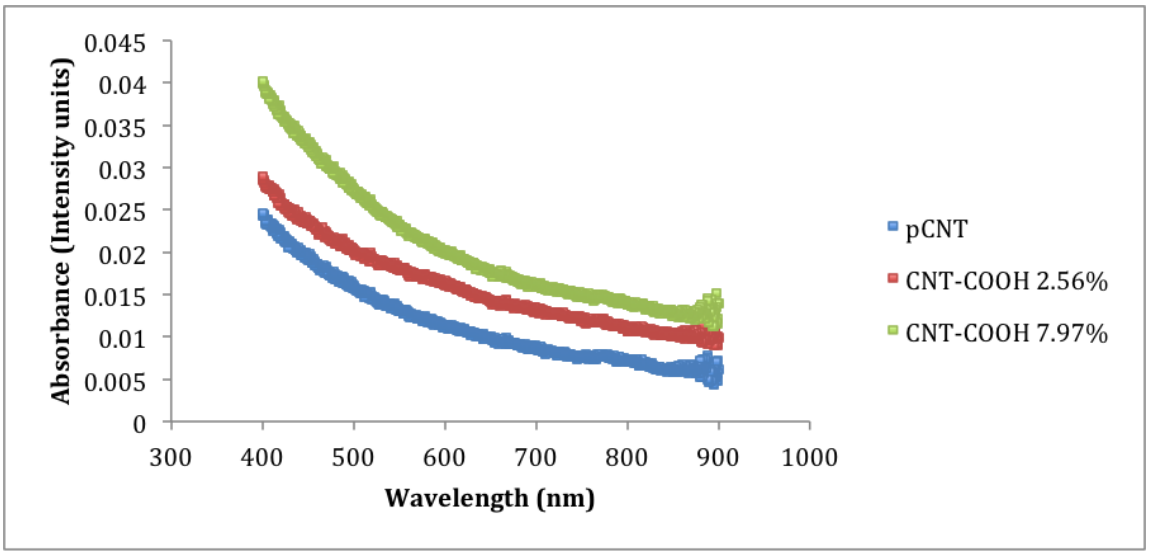

FIGURE B.8: UV-Vis signals from the non-solvent bath solution post immersion precipitation of three CNT-PSf-PVP membranes with identical initial CNT concentrations but different types of CNTs: pCNT (blue), CNT-COOH 2.56% (red), and CNT-COOH 7.97% (green).

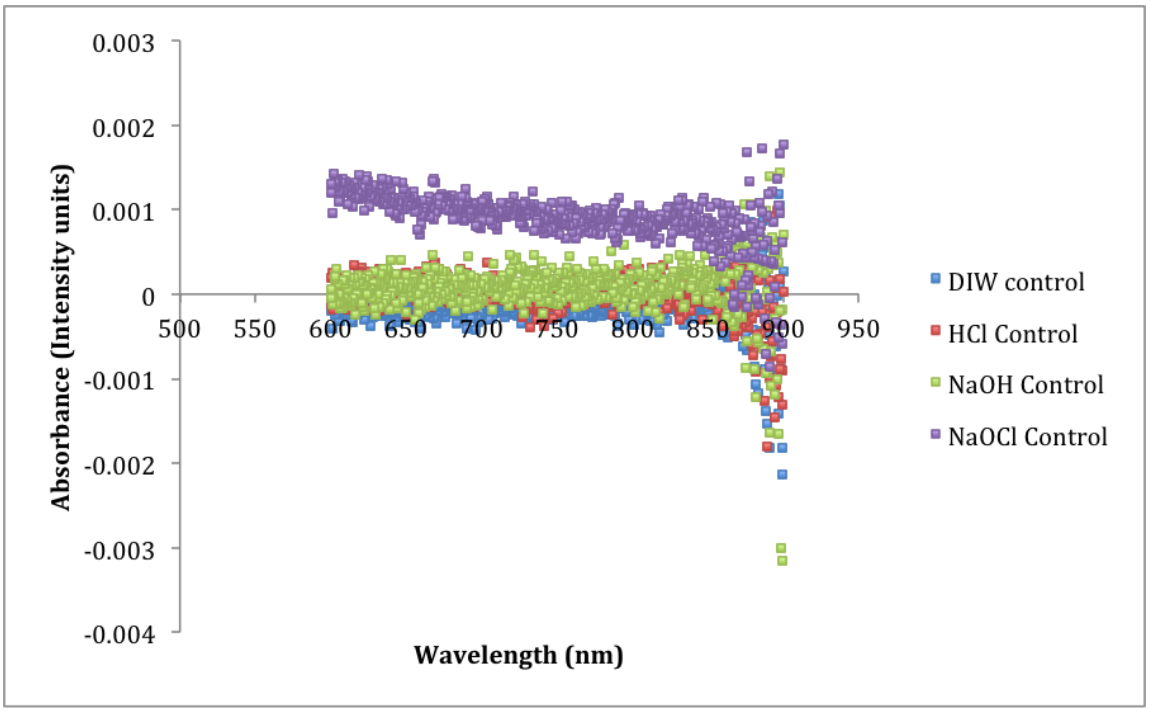

FIGURE B.9: UV-Vis background spectra of caustic cleaning agents use to clean membranes: Hydrochloric acid, HCl (red), sodium hydroxide, NaOH (green), and sodium hypochlorite, NaOCl (purple).

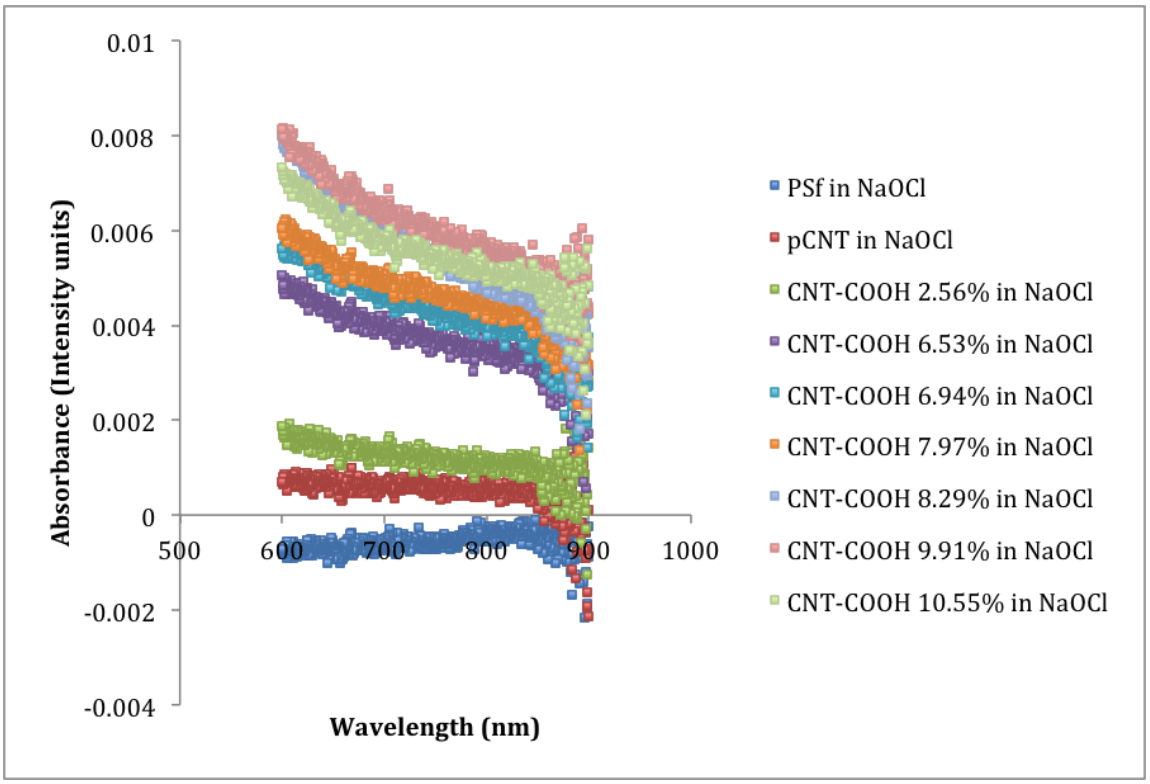

FIGURE B.10: UV-Vis spectra measured from the solution and leachate of various membranes cleaned with NaOCl for 2 hours. These spectra have not been controlled for the background spectra, thus the presence of some negative intensity units.

Appendix C

Supplementary Data for Ionically Bound CNT-Polymer Membranes

C.1 Supplementary Data for Ionically Bound CNT-Polymer Membrane Properties

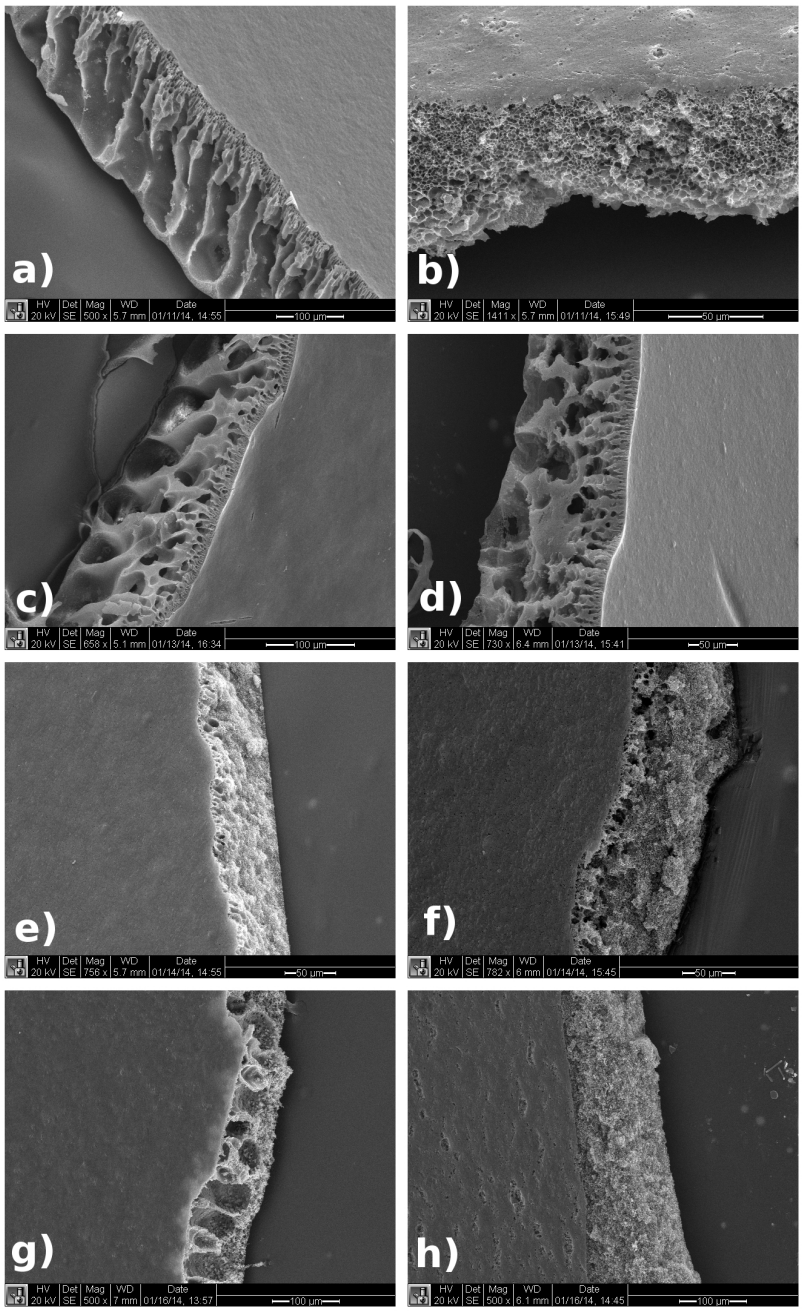

FIGURE C.1: The cross-sections of SPSf membranes formed with CNTs of varying functionalizations and contents. In a) SPSf-pCNT 0.5 wt%, b) SPSf-pCNT 5.0 wt%, c) SPSf-CNT-COOH (3.86%) 0.5 wt%, d) SPSf-CNT-COOH (3.86%) 5.0 wt%, e) SPSf-CNT-NH_2 (1.2%) 0.5 wt%, f) SPSf-CNT-NH_2 (1.2%) 5.0 wt%, g) SPSf-CNT-NH_2 (7.0%) 0.5 wt%, h) CNT-NH_2 (7.0%) 5.0 wt%. What is evident from these cross-sections is how the addition of small amounts of CNTs can greatly change the cross-section morphology of these membranes. Membranes with 5.0 wt% of CNTs show significantly greater morphological differences.

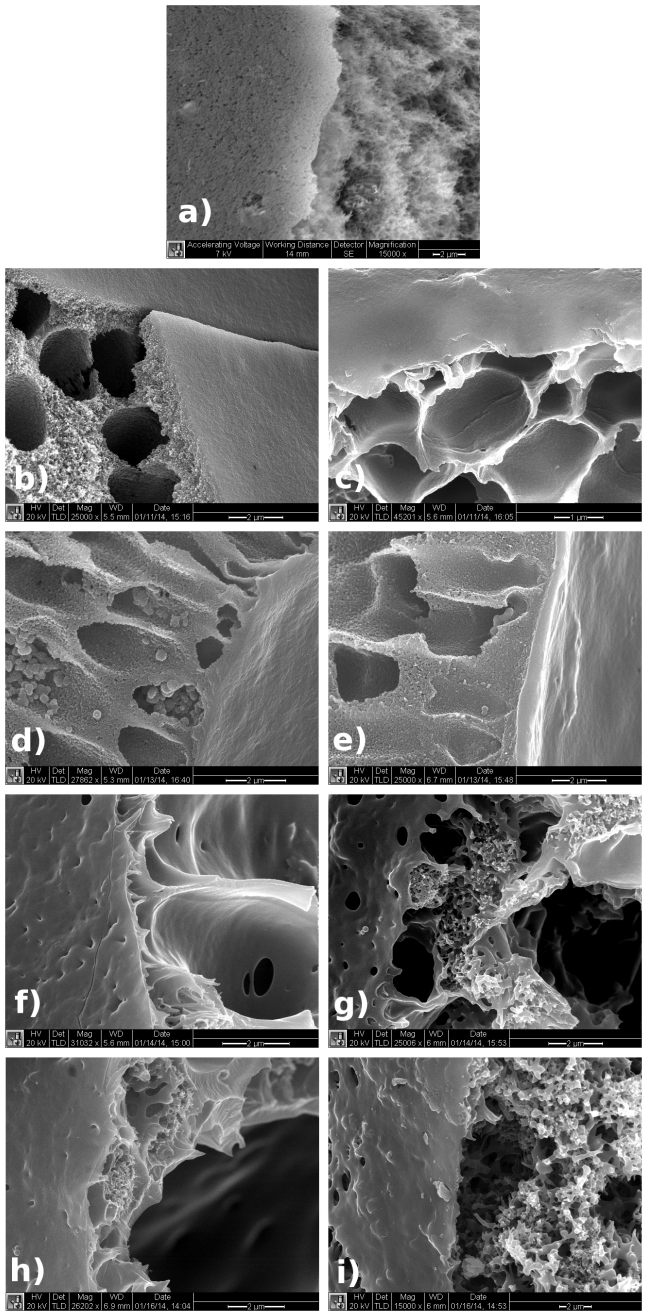

FIGURE C.2: Detailed cross-sections of SPSf membranes formed with CNTs of varying functionalizations and contents. In a) pure SPSf, b) SPSf-pCNT 0.5 wt%, c) SPSf-pCNT 5.0 wt%, d) SPSf-CNT-COOH (3.86%) 0.5 wt%, e) SPSf-CNT-COOH (3.86%) 5.0 wt%, f) SPSf-CNT-NH_2 (1.2%) 0.5 wt%, g) SPSf-CNT-NH_2 (1.2%) 5.0 wt%, h) SPSf-CNT-NH_2 (7.0%) 0.5 wt%, i) CNT-NH_2 (7.0%) 5.0 wt%. Closer views fo the cross-sections demonstate clearly the great morphological differences caused by the addition of CNTs. Membranes are significantly affected by the addition of CNT-NH_2. Membranes g) and i) in particular show significant disruptions to the smooth low-tortuosity formations evident in d) and e).

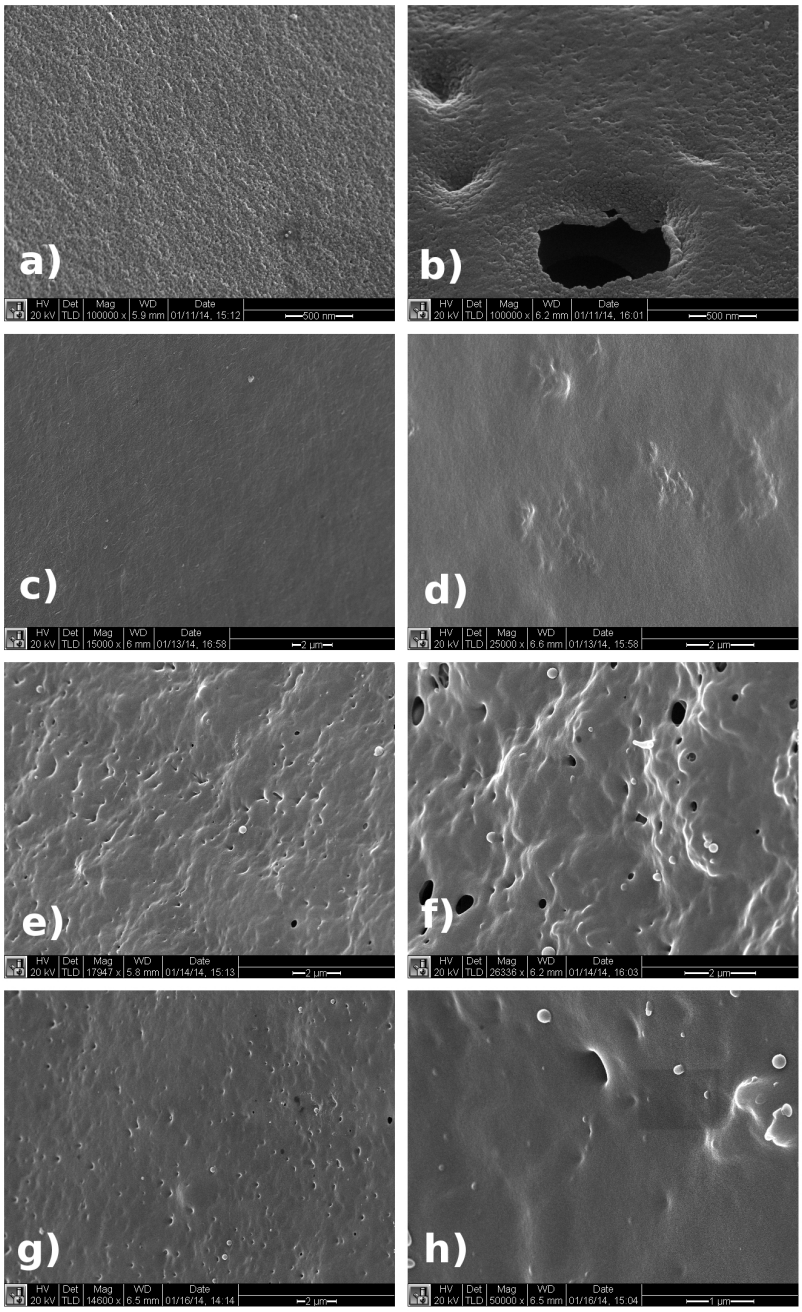

FIGURE C.3: The surface images of SPSf membranes formed with CNTs of varying functionalizations and contents. In a) SPSf-pCNT 0.5 wt%, b) SPSf-pCNT 5.0 wt%, c) SPSf-CNT-COOH (3.86%) 0.5 wt%, d) SPSf-CNT-COOH (3.86%) 5.0 wt%, e) SPSf-CNT-NH_2 (1.2%) 0.5 wt%, f) SPSf-CNT-NH_2 (1.2%) 5.0 wt%, g) SPSf-CNT-NH_2 (7.0%) 0.5 wt%, h) CNT-NH_2 (7.0%) 5.0 wt%. The combination of CNT-NH_2s with SPSf causes large pores to form on the surface of the membranes. This is clearly evident with higher concentrations of CNTs as in f) and h). These rough surfaces are contrasted with smooth membrane surfaces formed from pCNTs and CNT-COOHs as in a) - b)

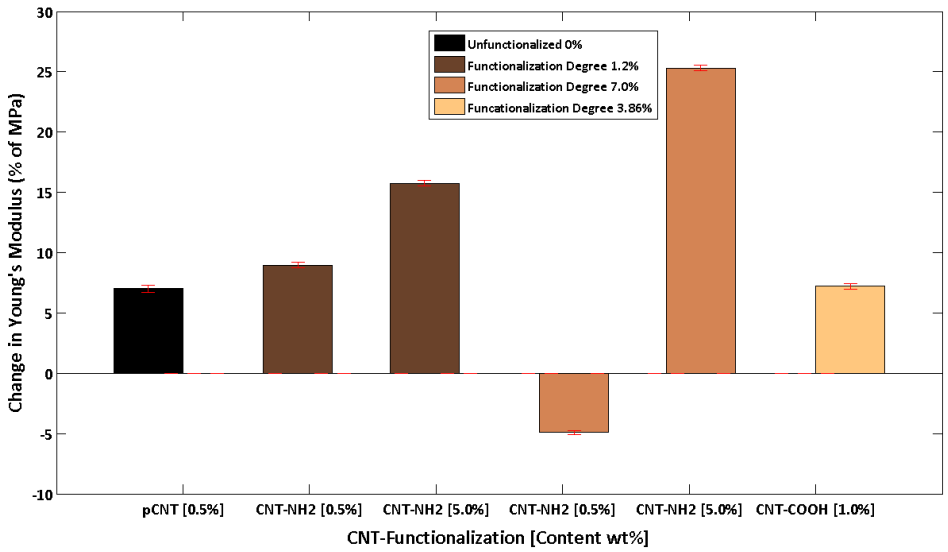

FIGURE C.4: The change in Youngs Modulus of SPSf membranes containing various types and concentrations of CNTs over pure SPSf membranes. Amine-functionalized CNTs provide the greatest improvement in membrane strength at concentrations of 5.0 wt%. The largest increase in Young's Modulus was an increase of 25% demonstrated by 5.0 wt% of 7.0% amine-functionalized CNTs. At lower concentrations of 0.5 wt%, 1.2% amine-functionalized CNTs demonstrated greater improvement in Youngs Modulus over 0.5 wt% pCNTs and 1.0 wt% carboxylated CNTs. Unexpectedly, the inclusion of 0.5 wt% of 7.0% amine-functionalized CNTs reduced the Youngs Modulus of the resultant membrane over membranes composed of pure SPSf.

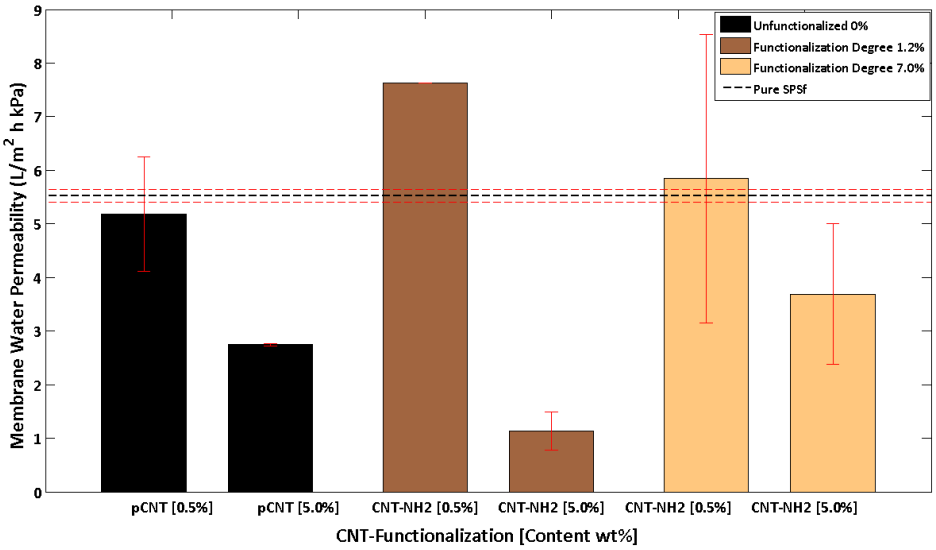

FIGURE C.5: The average values of all permeability data of SPSf membranes containing various types and concentrations of CNTs. Trends are identical to the maximum permeability data, but standard deviations in the data, represented by the error bars, are significantly larger.

C.2 Detailed UV-Vis Measurements

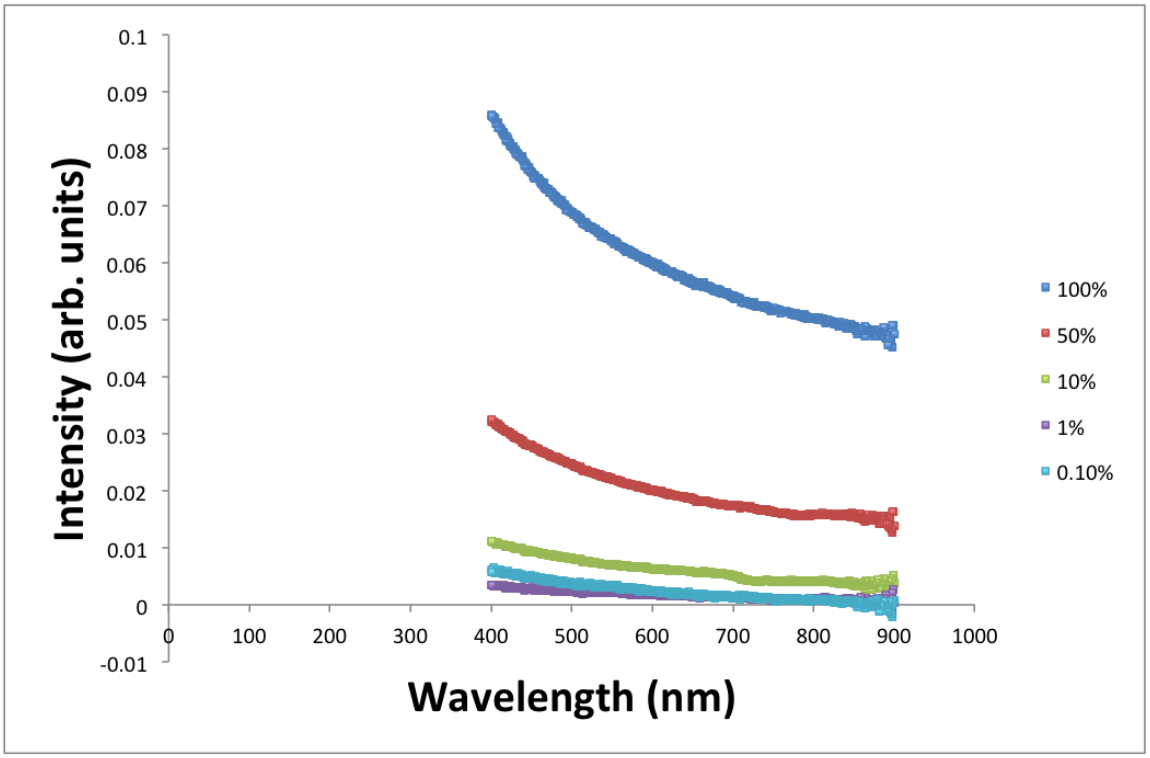

FIGURE C.6: UV-Vis spectra of suspensions of pristine CNTs in the non-solvent bath. These suspensions were diluted four times from stock to 50%, 10%, 1%, and 0.1% and the spectra of each dilution is presented in the figure. From these UV-Vis spectra extrapolations of pristine CNT concentration are determined in unknown aqueous suspensions.

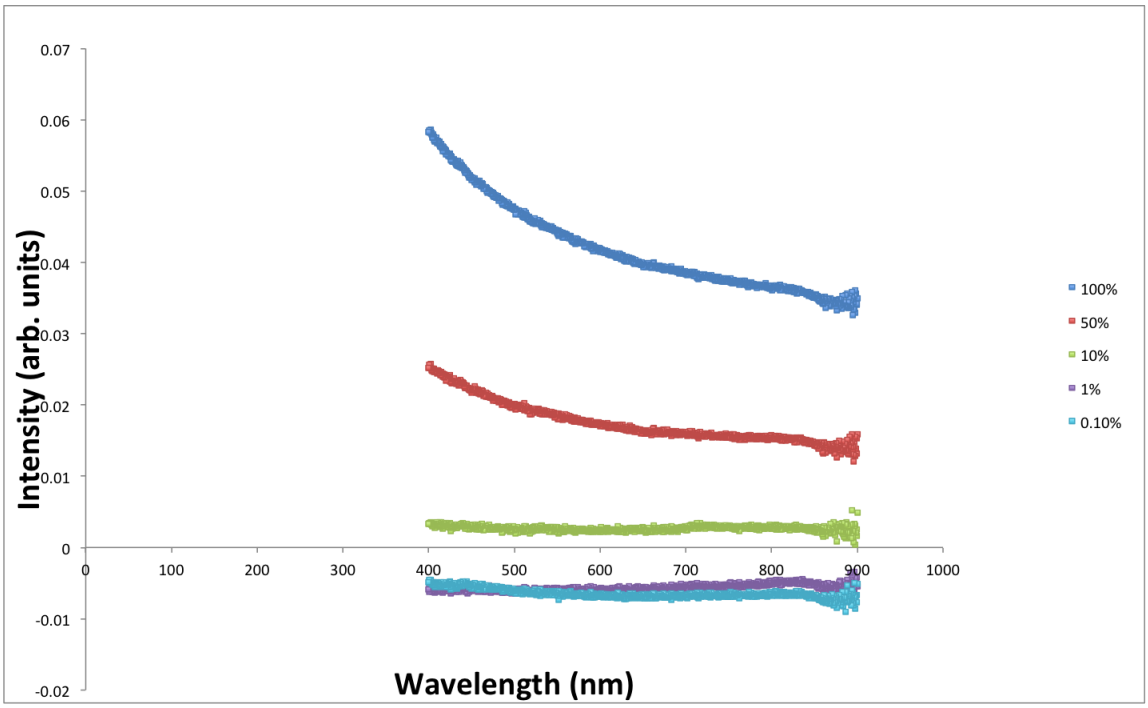

FIGURE C.7: UV-Vis spectra of suspensions of carboxylated CNTs in the non-solvent bath. These suspensions were diluted four times from stock to 50%, 10%, 1%, and 0.1%, the spectra of each dilution is presented in the figure. From these UV-Vis spectra extrapolations of CNT-COOH concentration are determined in unknown aqueous suspensions.

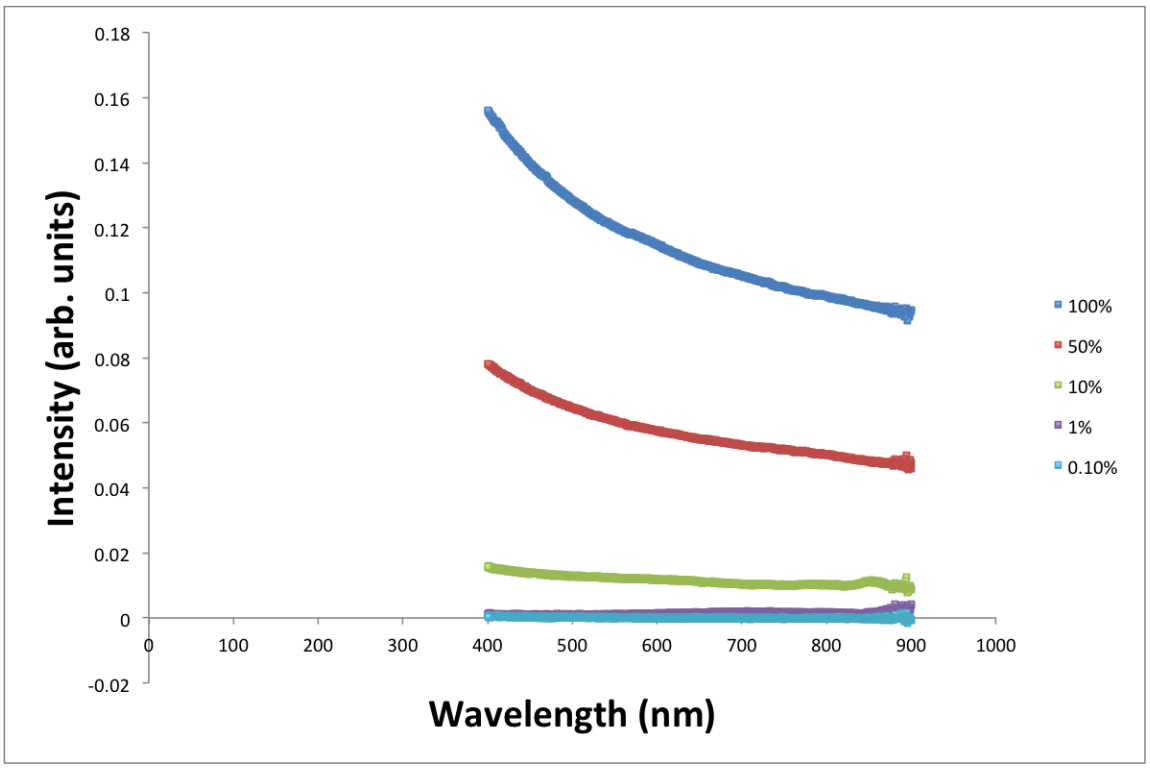

FIGURE C.8: UV-Vis spectra of suspensions of CNTs functionalized with amine groups to 1.2 wt% in the non-solvent bath. These suspensions were diluted four times from stock to 50%, 10%, 1%, and 0.1%, the spectra of each dilution is presented in the figure. From these UV-Vis spectra extrapolations of $CNT - NH_2$ functionalized to 1.2 wt% concentration are determined in unknown aqueous suspensions.

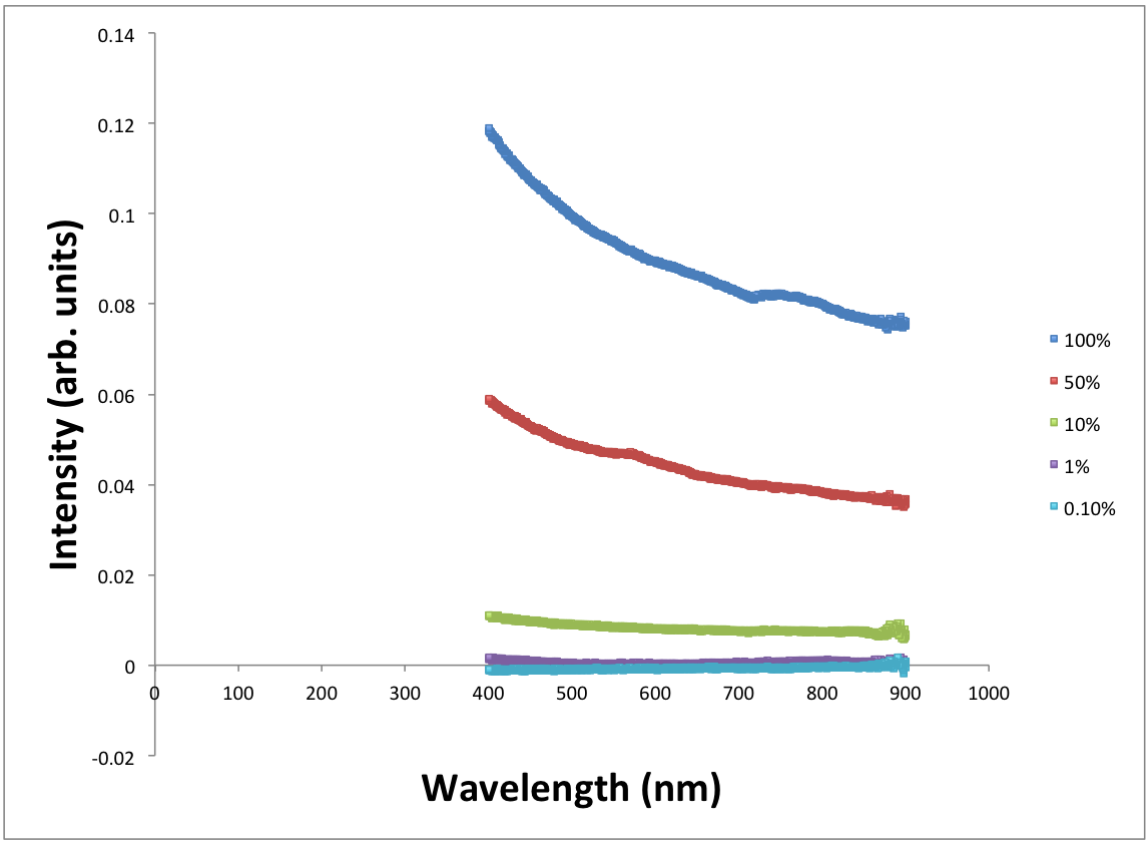

FIGURE C.9: UV-Vis spectra of suspensions of CNTs functionalized with amine groups to 7.0 wt% in the non-solvent bath. These suspensions were diluted four times from stock to 50%, 10%, 1%, and 0.1%, the spectra of each dilution is presented in the figure. From these UV-Vis spectra extrapolations of $CNT - NH_2$ functionalized to 7.0 wt% concentration are determined in unknown aqueous suspensions.

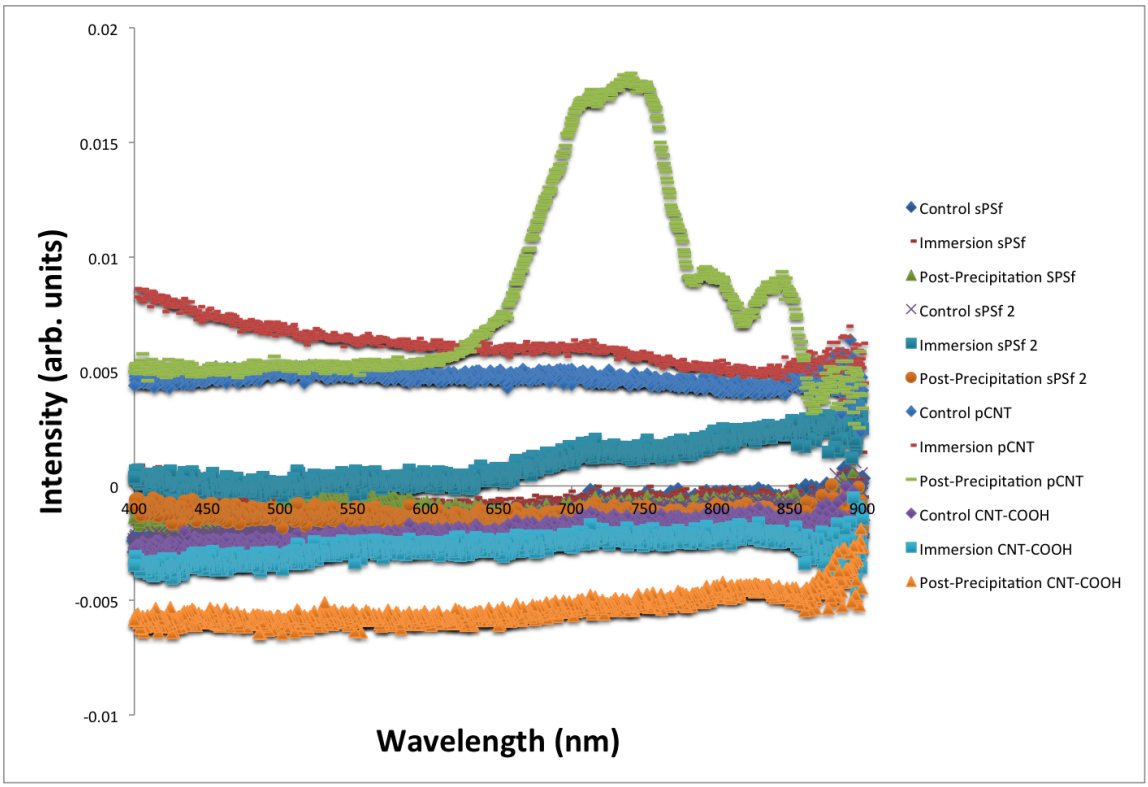

FIGURE C.10: The UV-Vis spectra of the non-solvent baths for membranes formed from pure sPSf, membranes formed from sPSf with prstine CNTs, and membranes formed from sPSf and carboxylated CNTs. Spectra were taken of the solutions in which the membranes were gelled and stored. These solutions were taken of the non-solvent bath before membrane gelation occurred (labeled 'Control'), of the non-solvent bath immediately after immersion precipitation occurred once the membranes were gelled ('Immersion'), and of the water bath the membranes rested in after two days. Duplicates were performed for the pure sPSf membranes to ensure that resutls were reproducible.

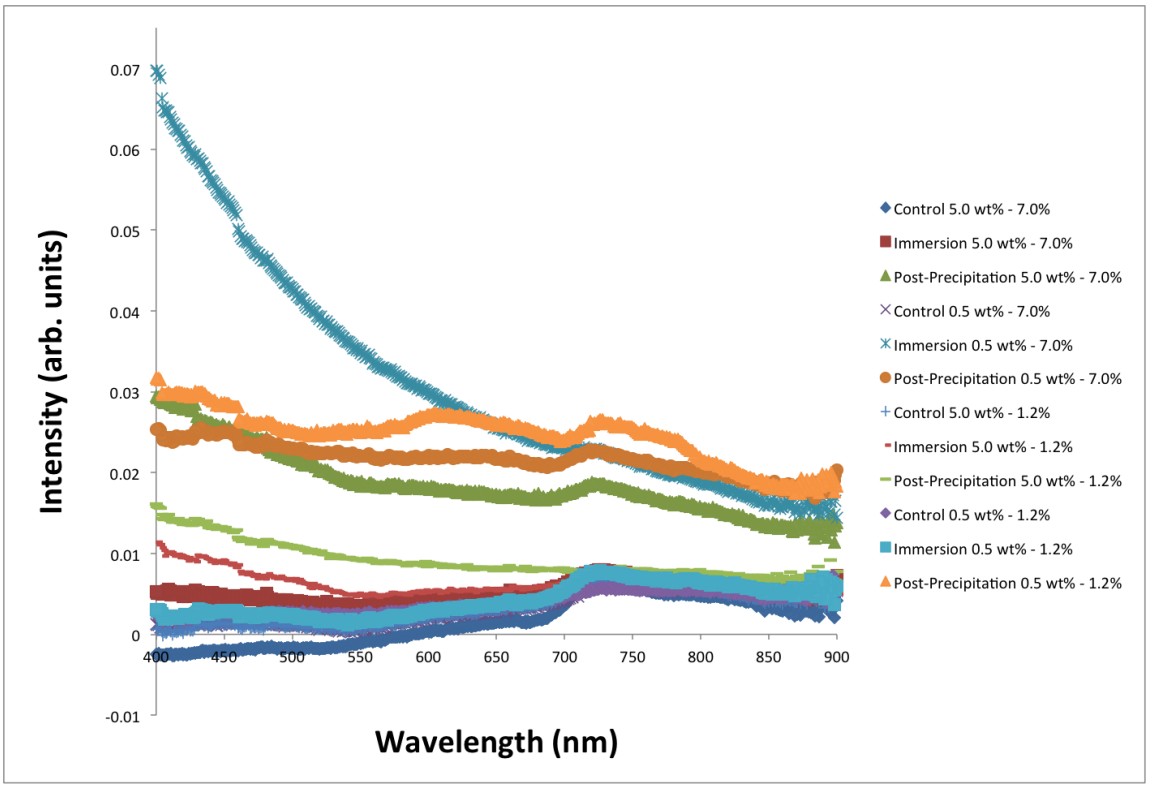

FIGURE C.11: The UV-Vis spectra of the non-solvent baths for membranes formed from sPSf with 5.0 wt% content of $CNT - NH_2$s functionalized to 7.0 wt%, sPSf with 0.5 wt% content of $CNT - NH_2$s functionalized to 7.0 wt%, sPSf with 5.0 wt% content of $CNT - NH_2$s functionalized to 1.2 wt%, and membranes formed from sPSf with 0.5 wt% content of $CNT - NH_2$s functionalized to 1.2 wt%. Spectra were taken of the solutions in which the membranes were gelled and stored. These solutions were taken of the non-solvent bath before membrane gelation occurred (labeled 'Control'), of the non-solvent bath immediately after immersion precipitation occurred once the membranes were gelled ('Immersion'), and of the water bath the membranes rested in after two days.

Bibliography

Abu Tarboush, B. J., Rana, D., Matsuura, T., Arafat, H. A., and Narbaitz, R. M. (2008), "Preparation of thin-film-composite polyamide membranes for desalination using novel hydrophilic surface modifying macromolecules," *Journal of Membrane Science*, 325, 166–175, 401ND Times Cited:11 Cited References Count:62.

Adeloju, S. B. and Wallace, G. G. (1996), "Conducting polymers and the bioanalytical sciences: new tools for biomolecular communication. A review," *Analyst*, 121, 699–703.

Ahmad, A. L., Sarif, M., and Ismail, S. (2005), "Development of an integrally skinned ultrafiltration membrane for wastewater treatment: effect of different formulations of PSf/NMP/PVP on flux and rejection," *Desalination*, 179, 257–263.

Akcora, P., Liu, H., Kumar, S. K., Moll, J., Li, Y., Benicewicz, B. C., Schadler, L. S., Acehan, D., Panagiotopoulos, A. Z., Pryamitsyn, V., Ganesan, V., Ilavsky, J., Thiyagarajan, P., Colby, R. H., and Douglas, J. F. (2009), "Anisotropic self-assembly of spherical polymer-grafted nanoparticles," *Nature Materials*, 8, 354–U121.

Angelopoulos, M. (2001), "Conducting polymers in microelectronics," *Ibm Journal of Research and Development*, 45, 57–75.

Antony, A., Low, J. H., Gray, S., Childress, A. E., Le-Clech, P., and Leslie, G. (2011), "Scale formation and control in high pressure membrane water treatment systems: A review," *Journal of Membrane Science*, 383, 1–16.

Baradie, B., Poinsignon, C., Sanchez, J. Y., PIffard, Y., Vitter, G., Bestaoui, N., Foscallo, D., Denoyelle, A., Delabouglise, D., and Vaujany, M. (1998), "Thermostable ionomeric filled membrane for H-2/O-2 fuel cell," *Journal of Power Sources*, 74, 8–16.

Bennewtiz, R., David, J., de Lannoy, C. F., Drevniok, B., Hubbard-Davis, P., Miura, T., and Trichtchenko, O. (2008), "Dynamic strain measurements in a sliding microstrained contact," *Journal of Physics - Condensed Matter*, 20.

Berndt, E. and Ulbricht, M. (2009), "Synthesis of block copolymers for surface functionalization with stimuli-responsive macromolecules," *Polymer*, 50, 5181–5191.

Biesheuvel, P. M. and van der Wal, A. (2010), "Membrane capacitive deionization," *Journal of Membrane Science*, 346, 256–262.

Boom, R. M., Wienk, I. M., Vandenboomgaard, T., and Smolders, C. A. (1992), "Microstructures in Phase Inversion Membranes .2. The Role of a Polymeric Additive," *Journal of Membrane Science*, 73, 277–292.

Cadotte, J. E., King, R. S., Majerle, R. J., and Petersen, R. J. (1981), "Interfacial Synthesis in the Preparation of Reverse-Osmosis Membranes," *Journal of Macromolecular Science-Chemistry*, A15, 727–755, Lg922 Times Cited:80 Cited References Count:14.

Celik, E., Park, H., Choi, H., and Choi, H. (2011), "Carbon nanotube blended polyethersulfone membranes for fouling control in water treatment," *Water Research*, 45, 274–282.

Chen, K. L., Song, L. F., Ong, S. L., and Ng, W. J. (2004), "The development of membrane fouling in full-scale RO processes," *Journal of Membrane Science*, 232, 63–72.

Chen, V., Mansouri, J., and Harrisson, S. (2010), "Strategies for controlling biofouling in membrane filtration systems: challenges and opportunities," *Journal of Materials Chemistry*, 20, 4567–4586.

Chiang, C. K., Park, Y. W., Heeger, A. J., Shirakawa, H., and Louis, E. J. Macdiarmid, A. G. (1978), "Conducting Polymers - Halogen Doped Polyacetylene," *Journal of Chemical Physics*, 69, 5098–5104.

Childress, A. E., Le-Clech, P., Daugherty, J. L., Chen, C., and Leslie, G. L. (2005), "Mechanical analysis of hollow fiber membrane integrity in water reuse applications," *Desalination*, 180, 5–14.

Choi, J. H., Jegal, J., and Kim, W. N. (2006), "Fabrication and characterization of multi-walled carbon nanotubes/polymer blend membranes," *Journal of Membrane Science*, 284, 406–415.

Ciofani, G., Obata, Y., Sato, I., Okamura, Y., Raffa, V., Menciassi, A., Dario, P., Takeda, N., and Takeoka, S. (2009), "Realization, characterization and functionalization of lipidic wrapped carbon nanotubes," *Journal of Nanoparticle Research*, 11, 477–484.

Coleman, J. N., Khan, U., Blau, W. J., and Gun'ko, Y. K. (2006), "Small but strong: A review of the mechanical properties of carbon nanotube-polymer composites," *Carbon*, 44, 1624–1652.

Coluci, V. R., Galvao, D. S., and Jorio, A. (2006), "Geometric and electronic structure of carbon nanotube networks: 'super'-carbon nanotubes," *Nanotechnology*, 17, 617–621.

Correa-Duarte, M. A., Grzelczak, M., Salgueirino-Maceira, V., Giersig, M., Liz-Marzan, L. M., Farle, M., Sierazdki, K., and Diaz, R. (2005), "Alignment of carbon nanotubes under low magnetic fields through attachment of magnetic nanoparticles," *Journal of Physical Chemistry B*, 109, 19060–19063.

Crittenden, J. C. and Harza, M. W. (2005), *Water treatment principles and design*, J. Wiley, Hoboken, N.J., 2nd edn.

Da Silva, L. V. F., Levi, J. E., Bento, C. N. O., Ramos, S. R. T. D., and Rozov, T. (1999), "PCR identification of Pseudomonas aeruginosa and direct detection in clinical samples from cystic fibrosis patients," *Journal of Medical Microbiology*, 48, 357–361, 237DL Times Cited:16 Cited References Count:17.

Daraei, P., Madaeni, S. S., Ghaemi, N., Khadivi, M. A., Astinchap, B., and Moradian, R. (2013), "Enhancing antifouling capability of PES membrane via mixing with various types of polymer modified multi-walled carbon nanotube," *Journal of Membrane Science*, 444, 184–191.

Datsyuk, V., Kalyva, M., Papagelis, K., Parthenois, J., Tasis, D., Siokou, A., Kallitsis, I., and Galiotis, C. (2008), "Chemical oxidation of multiwalled carbon nanotubes," *Carbon*, 46, 833–840.

Davies, D., Parsek, M., Pearson, J., Iglewski, B., Costerton, J., and Greenberg, E. (1998), "The involvement of cell-to-cell signals in the development of a bacterial biofilm," *Science*, 280, 295.

De, S., Lyons, P. E., Sorel, S., Doherty, E. M., King, P. J., Blau, W. J., Nirmalraj, P. N., Boland, J. J., Scardaci, V., and Joimel, J. (2009), "Transparent, flexible, and highly conductive thin films based on polymer-nanotube composites," *ACS Nano*, 3, 714–720.

de Lannoy, C. F., Jassby, D., Davis, D. D., and Wiesner, M. R. (2012), "A Highly Electrically Conductive Polymer-Multiwalled Carbon Nanotube Nanocomposite Membrane," *Journal of Membrane Science*, 415-416, 718 – 724.

de Lannoy, C. F., Jassby, D., Gloe, K., Gordon, A., and Wiesner, M. R. (2013a), "Aquatic Biofouling Prevention by Electrically Charged Nanocomposite Polymer Thin Film Membranes," *Environmental Science & Technology*, 47, 2760–2768.

de Lannoy, C. F., Soyer, E., and Wiesner, M. R. (2013b), "Optimizing Carbon Nanotube-Reinforced Polysulfone Ultrafiltration Membranes Through Carboxylic Acid Functionalization," *Journal of Membrane Science*, 447, 395–402.

Ding, J., Price, W., Ralph, S., and Wallace, G. (2003), "Recovery of gold cyanide using inherently conducting polymers," *Polymer international*, 52, 51–55.

Ebbesen, T. W., Lezec, H. J., Hiura, H., Bennett, J. W., Ghaemi, H. F., and Thio, T. (1996), "Electrical conductivity of individual carbon nanotubes," *Nature*, 382, 54–56.

Edwards, B. C. (2000), "Design and deployment of a space elevator," *Acta Astronautica*, 47, 735–744.

Elimelech, M. and Phillip, W. A. (2011), "The Future of Seawater Desalination: Energy, Technology, and the Environment," *Science*, 333, 712–717.

Falvo, M. R., Clary, G. J., Taylor, R. M., Chi, V., Brooks, F. P., Washburn, S., and Superfine, R. (1997), "Bending and buckling of carbon nanotubes under large strain," *Nature*, 389, 582–584.

Flemming, H. (1997), "Reverse osmosis membrane biofouling," *Experimental thermal and fluid science*, 14, 382–391.

Flemming, H. C. (2002), "Biofouling in water systems–cases, causes and countermeasures," *Appl Microbiol Biotechnol*, 59, 629–40.

Fritzmann, C., Lowenberg, J., Wintgens, T., and Melin, T.", k. . D. k. . R. (2007), "State-of-the-art of reverse osmosis desalination," *Desalination*, 216, 1 – 76.

Gao, G. and Vecitis, C. (2011), "Electrochemical Carbon Nanotube Filter Oxidative Performance as a Function of Surface Chemistry," *Environmental science & technology*.

Geise, G. M., Lee, H. S., Miller, D. J., Freeman, B. D., Mcgrath, J. E., and Paul, D. R. (2010), "Water Purification by Membranes: The Role of Polymer Science," *Journal of Polymer Science Part B-Polymer Physics*, 48, 1685–1718.

Geng, H. Z., Kim, K. K., So, K. P., Lee, Y. S., Chang, Y., and Lee, Y. H. (2007), "Effect of acid treatment on carbon nanotube-based flexible transparent conducting films," *Journal of the American Chemical Society*, 129, 7758–+.

Ghosh, A. K., Jeong, B. H., Huang, X., and Hoek, E. (2008), "Impacts of reaction and curing conditions on polyamide composite reverse osmosis membrane properties," *Journal of Membrane Science*, 311, 34–45.

Gijsbertsen-Abrahamse, A. J., Cornelissen, E. R., and Hofman, J. A. M. H. (2006), "Fiber failure frequency and causes of hollow fiber integrity loss," *Desalination*, 194, 251–258.

Greenberg, E. P., Costerton, J. W., and Stewart, P. S. (1999), "Bacterial biofilms: A common cause of persistent infections," *Science*, 284, 1318–1322.

Grossiord, N., Loos, J., Regev, O., and Koning, C. E. (2006), "Toolbox for dispersing carbon nanotubes into polymers to get conductive nanocomposites," *Chemistry of Materials*, 18, 1089–1099.

Guo, H., Wyart, Y., Perot, J., Nauleau, F., and Moulin, P. (2010), "Low-Pressure membrane integrity tests for drinking water treatment: A review," *Water Research*, 44, 41–57.

Hadlock, T., Elisseeff, J., Langer, R., Vacanti, J., and Cheney, M. (1998), "A tissue-engineered conduit for peripheral nerve repair," *Arch Otolaryngol Head Neck Surg*, 124, 1081–6.

Hall, N. (2003), "Twenty-five years of conducting polymers," *Chem Commun (Camb)*, pp. 1–4.

Hamon, M., Hui, H., Bhowmik, P., Itkis, H., and Haddon, R. (2002), "Ester-functionalized soluble single-walled carbon nanotubes," *Applied Physics A: Materials science & processing*, 74, 333–338.

Han, M. J. and Nam, S. T. (2002), "Thermodynamic and rheological variation in polysulfone solution by PVP and its effect in the preparation of phase inversion membrane," *Journal of Membrane Science*, 202, 55–61.

Han, Z. D. and Fina, A. (2011), "Thermal conductivity of carbon nanotubes and their polymer nanocomposites: A review," *Progress in Polymer Science*, 36, 914–944.

Harround, T., Koslowsky, M., Nieh, M. P., de Lannoy, C. F., Raghunathan, V., and Katsaras, J. (2005), "Comprehensive Examination of Mesophases Formed by DMPC and DHPC Mixtures," *Langmuir*, 21.

Herzberg, M. and Elimelech, M. (2007), "Biofouling of reverse osmosis membranes: role of biofilm-enhanced osmotic pressure," *Journal of Membrane Science*, 295, 11–20.

Herzberg, M. and Elimelech, M. (2008), "Physiology and genetic traits of reverse osmosis membrane biofilms: a case study with Pseudomonas aeruginosa," *Isme Journal*, 2, 180–194, 267ES Times Cited:25 Cited References Count:65.

Hinds, B. J., Chopra, N., Rantell, T., Andrews, R., Gavalas, V., and Bachas, L. G. (2004), "Aligned multiwalled carbon nanotube membranes," *Science*, 303, 62–65.

Hong, S., Jeong, J., Shim, S., Kang, H., Kwon, S., Ahn, K., and Yoon, J. (2008), "Effect of electric currents on bacterial detachment and inactivation," *Biotechnology and bioengineering*, 100, 379–386.

Hou, Y., Tang, J., Zhang, H. B., Qian, C., Feng, Y. Y., and Liu, J. (2009a), "Functionalized Few-Walled Carbon Nanotubes for Mechanical Reinforcement of Polymeric Composites," *Acs Nano*, 3, 1057–1062.

Hou, Y., Tang, J., Zhang, H. B., Qian, C., Feng, Y. Y., and Liu, J. (2009b), "Functionalized Few-Walled Carbon Nanotubes for Mechanical Reinforcement of Polymeric Composites," *Acs Nano*, 3, 1057–1062.

Hu, N. T., Zhou, H. W., Dang, G. D., Rao, X. H., Chen, C. H., and Zhang, W. J. (2007), "Efficient dispersion of multi-walled carbon nanotubes by in situ polymerization," *Polymer International*, 56, 655–659.

Huang, J. C., Chen, J. I., Tripathy, S. K., and Loh, I. H. (1989), "Electrically Conductive Membranes - Synthesis and Applications," *Abstracts of Papers of the American Chemical Society*, 198, 195–PMSE.

Huang, W. J., Lin, Y., Taylor, S., Gaillard, J., Rao, A. M., and Sun, Y. P. (2002), "Sonication-assisted functionalization and solubilization of carbon nanotubes," *Nano Letters*, 2, 231–234.

Huisman, I. H. and Williams, K. (2004), "Autopsy and failure analysis of ultrafiltration membranes from a waste-water treatment system," *Desalination*, 165, 161–164.

Iijima, S. (1991), "Helical Microtubules of Graphitic Carbon," *Nature*, 354, 56–58.

Janata, J. and Josowicz, M. (2003), "Conducting polymers in electronic chemical sensors," *Nature Materials*, 2, 19–24.

Jancar, J., Douglas, J. F., Starr, F. W., Kumar, S. K., Cassagnau, P., Lesser, A. J., Sternstein, S. S., and Buehler, M. J. (2010), "Current issues in research on structure-property relationships in polymer nanocomposites," *Polymer*, 51, 3321–3343.

Jeong, B. H., Hoek, E. M. V., Yan, Y. S., Subramani, A., Huang, X. F., Hurwitz, G., Ghosh, A. K., and Jawor, A. (2007), "Interfacial polymerization of thin film nanocomposites: A new concept for reverse osmosis membranes," *Journal of Membrane Science*, 294, 1 –7.

Jucker, C. and Clark, M. M. (1994), "Adsorption of Aquatic Humic Substances on Hydrophobic Ultrafiltration Membranes," *Journal of Membrane Science*, 97, 37–52.

Juuti, P., Katko, T., and Vuorinen, H. (2007), *Environmental History of Water*, 1 edn.

Kang, S., Herzberg, M., Rodrigues, D. F., and Elimelech, M. (2008), "Antibacterial effects of carbon nanotubes: Size does matter," *Langmuir*, 24, 6409–6413.

Kim, J. H., Kang, M. S., and Kim, C. K. (2005), "Fabrication of membranes for the liquid separation Part 1. Ultrafiltration membranes prepared from novel miscible blends of polysulfone and poly(1-vinylpyrrolidone-co-acrylonitrile) copolymers," *Journal of Membrane Science*, 265, 167–175.

Kim, S. S. and Lloyd, D. R. (1992), "Thermodynamics of Polymer Diluent Systems for Thermally Induced Phase Separation. 1. Determination of Equation of State Parameters," *Polymer*, 33, 1026–1035.

Kim, Y. A., Hayashi, T., Endo, M., Gotoh, Y., Wada, N., and Seiyama, J. (2006), "Fabrication of aligned carbon nanotube-filled rubber composite," *Scripta Materialia*, 54, 31–35.

Knoell, T., Safarik, J., Cormack, T., Riley, R., Lin, S. W., and Ridgway, H. (1999), "Biofouling potentials of microporous polysulfone membranes containing a sulfonated polyether-ethersulfone/polyethersulfone block copolymer: correlation of membrane surface properties with bacterial attachment," *Journal of Membrane Science*, 157, 117–138.

Koning, C. E., Grossiord, N., Loos, J., and Regev, O. (2006), "Toolbox for dispersing carbon nanotubes into polymers to get conductive nanocomposites," *Chemistry of Materials*, 18, 1089–1099.

Krishnan, A., Dujardin, E., Ebbesen, T. W., Yianilos, P. N., and Treacy, M. M. J. (1998), "Young's modulus of single-walled nanotubes," *Physical Review B*, 58, 14013–14019.

Kristensen, J. B., Meyer, R. L., Laursen, B. S., Shipovskov, S., Besenbacher, F., and Poulsen, C. H. (2008), "Antifouling enzymes and the biochemistry of marine settlement," *Biotechnology Advances*, 26, 471–481.

Lattemann, S. and Hopner, T. (2008), "Environmental impact and impact assessment of seawater desalination," *Desalination*, 220, 1–15.

Lee, K. P., Arnot, T. C., and Mattia, D. (2011), "A review of reverse osmosis membrane materials for desalination-Development to date and future potential," *Journal of Membrane Science*, 370, 1–22.

Lin, Y., Zhou, B., Fernando, K. A. S., Liu, P., Allard, L. F., and Sun, Y. P. (2003), "Polymeric carbon nanocomposites from carbon nanotubes functionalized with matrix polymer," *Macromolecules*, 36, 7199–7204.

Lin, Y., Meziani, M. J., and Sun, Y. P. (2007), "Functionalized carbon nanotubes for polymeric nanocomposites," *Journal of Materials Chemistry*, 17, 1143–1148.

Liu, J., Rinzler, A. G., Dai, H. J., Hafner, J. H., Bradley, R. K., Boul, P. J., Lu, A., Iverson, T., Shelimov, K., Huffman, C. B., Rodriguez-Macias, F., Shon, Y. S., Lee, T. R., Colbert, D. T., and Smalley, R. E. (1998), "Fullerene pipes," *Science*, 280, 1253–1256.

Liu, L. F., Liu, J. D., Gao, B., Yang, F. L., and Chellam, S. (2012), "Fouling reductions in a membrane bioreactor using an intermittent electric field and cathodic membrane modified by vapor phase polymerized pyrrole," *Journal of Membrane Science*, 394, 202–208.

Liu, M., Chen, Z., Yu, S., Wu, D., and Gao, C. (2011), "Thin-film composite polyamide reverse osmosis membranes with improved acid stability and chlorine resistance by coating N-isopropylacrylamide-co-acrylamide copolymers," *Desalination*, 270, 248–257.

Loh, I. H., Moody, R. A., and Huang, J. C. (1990), "Electrically Conductive Membranes - Synthesis and Applications," *Journal of Membrane Science*, 50, 31–49.

Lufrano, F., Squadrito, G., Patti, A., and Passalacqua, E. (2000), "Sulfonated polysulfone as promising membranes for polymer electrolyte fuel cells," *Journal Applied Polymer Science*, 70, 1250–1256.

Maartens, A., Swart, P., and Jacobs, E. P. (1998), "Humic membrane foulants in natural brown water: characterization and removal," *Desalination*, 115, 215–227.

Majumder, M., Chopra, N., Andrews, R., and Hinds, B. J. (2005), "Nanoscale hydrodynamics: Enhanced flow in carbon nanotubes (vol 438, pg 44, 2005)," *Nature*, 438, 930–930.

Mansouri, J. and Burford, R. P. (1994), "Novel Membranes from Conducting Polymers," *Journal of Membrane Science*, 87, 23–34.

Mansouri, J., Harrisson, S., and Chen, V. (2010), "Strategies for controlling biofouling in membrane filtration systems: challenges and opportunities," *Journal of Materials Chemistry*, 20, 4567–4586.

Matsunaga, T., Nakayama, T., Wake, H., Ozawa, K., and Nakamura, N. (1998), "Electrochemical prevention of marine biofouling on a novel titanium-nitride-coated plate formed by radio-frequency arc spraying," *Applied Microbiology and Biotechnology*, 50, 502–508.

McCullough, R. D. (1998), "The chemistry of conducting polythiophenes," *Advanced Materials*, 10, 93–+.

Mcneill, R., Weiss, D. E., Wardlaw, J. H., and Siudak, R. (1963), "Electronic Conduction in Polymers. 1. Chemical Structure of Polypyrrole," *Australian Journal of Chemistry*, 16, 1056 – end.

Moniruzzaman, M. and Winey, K. I. (2006), "Polymer nanocomposites containing carbon nanotubes," *Macromolecules*, 39, 5194–5205.

Mulder, M. (1996), *Basic principles of membrane technology*, Kluwer Academic, Dordrecht ; Boston, 2nd edn.

Nakashima, N. and Fujigaya, T. (2007), "Fundamentals and applications of soluble carbon nanotubes," *Chemistry Letters*, 36, 692–697.

Nakayama, T., Wake, H., Ozawa, K., Nakamura, N., and Matsunaga, T. (1998), "Electrochemical prevention of marine biofouling on a novel titanium-nitride-coated plate formed by radio-frequency arc spraying," *Applied Microbiology and Biotechnology*, 50, 502–508.

Nalwa, H. S. (2001), *Handbook of advanced electronic and photonic materials and devices*, Academic Press, San Diego, CA.

Ni, W. J., Wang, B., Wang, H. P., and Zhang, Y. M. (2006), "Fabrication and properties of carbon nanotube and poly(vinyl alcohol) composites," *Journal of Macromolecular Science Part B-Physics*, 45, 659–664.

Noshay, A. and Robeson, L. M. (1976), "Sulfonated Polysulfone," *Journal of Applied Polymer Science*, 20, 1885–1903.

Nystrom, M. and Jarvinen, P. (1991), "Modification of Polysulfone Ultrafiltration Membranes with Uv Irradiation and Hydrophilicity Increasing Agents," *Journal of Membrane Science*, 60, 275–296.

Osada, Y. and De Rossi, D. E. (2000), *Polymer sensors and actuators*, Macromolecular systems, materials approach, Springer, Berlin ; New York.

Ostuni, E., Chapman, R. G., Holmlin, R. E., Takayama, S., and Whitesides, G. M. (2001), "A survey of structure-property relationships of surfaces that resist the adsorption of protein," *Langmuir*, 17, 5605–5620.

Park, J. Y., Acar, M. H., Akthakul, A., Kuhlman, W., and Mayes, A. M. (2006), "Polysulfone-graft-poly(ethylene glycol) graft copolymers for surface modification of polysulfone membranes," *Biomaterials*, 27, 856–865.

Paul, D., Kim, Y. S., Ponnusamy, K., and Kweon, J. H. (2009), "Application of Quorum Quenching to Inhibit Biofilm Formation," *Environmental Engineering Science*, 26, 1319–1324.

Pei, Q. B., Yang, Y., Yu, G., Zhang, C., and Heeger, A. J. (1996), "Polymer light-emitting electrochemical cells: In situ formation of a light-emitting p-n junction," *Journal of the American Chemical Society*, 118, 3922–3929.

Peng, F. B., Huang, X. F., Jawor, A., and Hoek, E. M. V. (2010), "Transport, structural, and interfacial properties of poly(vinyl alcohol)-polysulfone composite nanofiltration membranes," *Journal of Membrane Science*, 353, 169–176.

Perez-Roa, R. E., Tompkins, D. T., Paulose, M., Grimes, C. A., Anderson, M. A., and Noguera, D. R. (2006), "Effects of localised, low-voltage pulsed electric fields on the development and inhibition of Pseudomonas aeruginosa biofilms," *Biofouling*, 22, 383–390.

Pieracci, J., Crivello, J. V., and Belfort, G. (2002), "Increasing membrane permeability of UV-modified poly(ether sulfone) ultrafiltration membranes," *Journal of Membrane Science*, 202, 1–16.

Pinnau, I. and Freeman, B. D. (2000), "Formation and modification of polymeric membranes: overview," *Membrane Formation and Modification*, 744, 1–22.

Plakas, K. V. and Karabelas, A. J. (2008), "Membrane retention of herbicides from single and multi-solute media: The effect of ionic enviornment," *Journal of Membrane Science*, 320, 325–334.

Porcelli, N. and Judd, S. (2010), "Chemical cleaning of potable water membranes: A review," *Septic Purification Technology*, 71, 137–143.

Price, W. E., Too, C. O., Wallace, G. G., and Zhou, D. (1999), "Development of membrane systems based on conducting polymers," *Synthetic Metals*, 102, 1338–1341.

Qin, Y., Shi, J., Wu, W., Li, X., Guo, Z. X., and Zhu, D. (2003), "Concise route to functionalized carbon nanotubes," *The Journal of Physical Chemistry B*, 107, 12899–12901.

Qu, L. W., Veca, L. M., Lin, Y., Kitaygorodskiy, A., Chen, B. L., McCall, A. M., Connell, J. W., and Sun, Y. P. (2005), "Soluble nylon-functionalized carbon nanotubes from anionic ring-opening polymerization from nanotube surface," *Macromolecules*, 38, 10328–10331.

Reddy, A. V. R., Mohan, D. J., Bhattacharya, A., Shah, V. J., and Ghosh, P. K. (2003), "Surface modification of ultrafiltration membranes by preadsorption of a negatively charged polymer I. Permeation of water soluble polymers and inorganic salt solutions and fouling resistance properties," *Journal of Membrane Science*, 214, 211–221.

Ruoff, R. S. and Lorents, D. C. (1995), "Mechanical and Thermal-Properties of Carbon Nanotubes," *Carbon*, 33, 925–930.

Saad, M. A. (1992), "Biofouling Prevention in Ro Polymeric Membrane Systems," *Desalination*, 88, 85–105.

Sahoo, N. G., Rana, S., Cho, J. W., Li, L., and Chan, S. H. (2010), "Polymer nanocomposites based on functionalized carbon nanotubes," *Progress in Polymer Science*, 35, 837–867.

Schoenbach, K. H., Peterkin, F. E., Alden, R. W., and Beebe, S. J. (1997), "The effect of pulsed electric fields on biological cells: Experiments and applications," *Ieee Transactions on Plasma Science*, 25, 284–292.

Shaffer, M. S. P. and Windle, A. H. (1999), "Fabrication and characterization of carbon nanotube/poly(vinyl alcohol) composites," *Advanced Materials*, 11, 937–+.

Shannon, M. A., Bohn, P. W., Elimelech, M., Georgiadis, J. G., Marias, B. J., and Mayes, A. M. (2008), "Science and technology for water purification in the coming decades," *Nature*, 452, 301–310.

Shawky, H. A., Chae, S. R., Lin, S. H., and Wiesner, M. R. (2011a), "Synthesis and characterization of a carbon nanotube/polymer nanocomposite membrane for water treatment," *Desalination*, 272, 46–50.

Shawky, H. A., Chae, S. R., Lin, S. H., and Wiesner, M. R. (2011b), "Synthesis and characterization of a carbon nanotube/polymer nanocomposite membrane for water treatment," *Desalination*, 272, 46–50.

Shim, S., Hong, S. H., Tak, Y., and Yoon, J. (2011), "Prevention of Pseudomonas aeruginosa adhesion by electric currents," *Biofouling*, 27, 217–224.

Shirakawa, H., Louis, E. J., Macdiarmid, A. G., Chiang, C. K., and Heeger, A. J. (1977), "Synthesis of Electrically Conducting Organic Polymers - Halogen Derviatives of Polyacetylene," *Journal of Chemical Society Chemical Communication*, pp. 578 – 580.

Strathmann, H. (2004).

Sun, Y. P., Huang, W. J., Lin, Y., Fu, K. F., Kitaygorodskiy, A., Riddle, L. A., Yu, Y. J., and Carroll, D. L. (2001), "Soluble dendron-functionalized carbon nanotubes: Preparation, characterization, and properties," *Chemistry of Materials*, 13, 2864–2869.

Sun, Y. P., Fu, K. F., Lin, Y., and Huang, W. J. (2002), "Functionalized carbon nanotubes: Properties and applications," *Accounts of Chemical Research*, 35, 1096–1104.

Tikhonov, V. E., Stepnova, E. A., Babak, V. G., Yamskov, I. A., Palma-Guerrero, J., Jansson, H. B., Lopez-Llorca, L. V., Salinas, J., Gerasimenko, D. V., Avdienko, I. D., and Varlamov, V. P. (2006), "Bactericidal and antifungal activities of a low

molecular weight chitosan and its N-/2(3)-(dodec-2-enyl)succinoyl/-derivatives," *Carbohydrate Polymers*, 64, 66–72.

Tsai, H. A., Huang, D. H., Ruaan, R. C., and Lai, J. Y. (2001), "Mechanical properties of asymmetric polysulfone membranes containing surfactant as additives," *Industrial & Engineering Chemistry Research*, 40, 5917–5922.

Tweddle, T. A., Kutowy, O., Thayer, W. L., and Sourirajan, S. (1983), "Polysulfone Ultrafiltration Membranes," *Industrial & Engineering Chemistry Product Research and Development*, 22, 320–326.

Ulbricht, M. (2006), "Advanced functional polymer membranes," *Polymer*, 47, 2217–2262.

Ulbricht, M. and Belfort, G. (1995), "Surface Modification of Ultrafiltration Membranes by Low-Temperature Plasma .1. Treatment of Polyacrylonitrile," *Journal of Applied Polymer Science*, 56, 325–343.

Ulbricht, M. and Belfort, G. (1996), "Surface modification of ultrafiltration membranes by low temperature plasma .2. Graft polymerization onto polyacrylonitrile and polysulfone," *Journal of Membrane Science*, 111, 193–215.

van der Borden, A. J., van der Werf, H., van der Mei, H. C., and Busscher, H. J. (2004), "Electric current-induced detachment of Staphylococcus epidermidis biofilms from surgical stainless steel," *Applied and Environmental Microbiology*, 70, 6871–6874.

Van der Bruggen, B. (2009a), "Chemical Modification of Polyethersulfone Nanofiltration Membranes: A Review," *Journal of Applied Polymer Science*, 114, 630–642.

Van der Bruggen, B. (2009b), "Chemical Modification of Polyethersulfone Nanofiltration Membranes: A Review," *Journal of Applied Polymer Science*, 114, 630–642.

Van der Bruggen, B., Vandecasteele, C., Van Gestel, T., Doyen, W., and Leysen, R. (2003), "A review of pressure-driven membrane processes in wastewater treatment and drinking water production," *Environmental Progress*, 22, 46–56.

Vecitis, C. D., Gao, G. D., and Liu, H. (2011a), "Electrochemical Carbon Nanotube Filter for Adsorption, Desorption, and Oxidation of Aqueous Dyes and Anions," *Journal of Physical Chemistry C*, 115, 3621–3629.

Vecitis, CD Vecitis, C. D., Schnoor, M. H., Rahaman, M. S., Schiffman, J. D., and Elimelech, M. (2011b), "Electrochemical Multiwalled Carbon Nanotube Filter for Viral and Bacterial Removal and Inactivation," *Environmental Science & Technology*, 45, 3672–3679.

Vrouwenvelder, J. S., von der Schulenburg, D. A. G., Kruithof, J. C., Johns, M. L., and van Loosdrecht, M. C. M. (2009), "Biofouling of spiral-wound nanofiltration and reverse osmosis membranes: A feed spacer problem," *Water Research*, 43, 583–594.

Wada, Y., Tsukada, M., Fujihira, M., Matsushige, K., Ogawa, T., Haga, M., and Tanaka, S. (2000), "Prospects and problems of single molecule information devices," *Japanese Journal of Applied Physics Part 1-Regular Papers Short Notes & Review Papers*, 39, 3835–3849.

Wallace, G. G., Ding, J., Price, W. E., and Ralph, S. F. (2003), "Recovery of gold cyanide using inherently conducting polymers," *Polymer International*, 52, 51–55.

Wang, Y. B., Iqbal, Z., and Malhotra, S. V. (2005), "Functionalization of carbon nanotubes with amines and enzymes," *Chemical Physics Letters*, 402, 96–101.

Wepasnick, K. A., Smith, B. A., Schrote, K. E., Wilson, H. K., Diegelmann, S. R., and Fairbrother, D. H. (2011), "Surface and structural characterization of multi-walled carbon nanotubes following different oxidative treatments," *Carbon*, 49, 24–36.

Wiesner, M. R., Bottero, J.-Y., and ebrary Inc. (2007), "Environmental nanotechnology applications and impacts of nanomaterials," .

Wilf, M. and Klinko, K. (2001), "Optimization of seawater RO systems design," *Desalination*, 138, 299–306.

Winey, K. I. and Moniruzzaman, M. (2006), "Polymer nanocomposites containing carbon nanotubes," *Macromolecules*, 39, 5194–5205.

Xia, T., Kovochich, M., Brant, J., Hotze, M., Sempf, J., Oberley, T., Sioutas, C., Yeh, J. I., Wiesner, M. R., and Nel, A. E. (2006), "Comparison of the abilities of ambient and manufactured nanoparticles to induce cellular toxicity according to an oxidative stress paradigm," *Nano Letters*, 6, 1794 – 1807.

Xie, X., Mai, Y., and Zhou, X. (2005a), "Dispersion and alignment of carbon nanotubes in polymer matrix: A review," *Materials Science and Engineering: R: Reports*, 49, 89–112.

Xie, X. L., Mai, Y. W., and Zhou, X. P. (2005b), "Dispersion and alignment of carbon nanotubes in polymer matrix: A review," *Materials Science & Engineering R-Reports*, 49, 89–112.

Yoon, J., Shim, S., Hong, S. H., and Tak, Y. (2011), "Prevention of Pseudomonas aeruginosa adhesion by electric currents," *Biofouling*, 27, 217–224.

Young, R. J. and Lovell, P. A. (1991), *Introduction to polymers*, Chapman & Hall, London ; New York, 2nd edn.

Young, R. J. and Lovell, P. A. (2011), *Introduction to polymers*, CRC Press, Boca Raton, 3rd edn.

Yu, M. F., Files, B. S., Arepalli, S., and Ruoff, R. S. (2000), "Tensile loading of ropes of single wall carbon nanotubes and their mechanical properties," *Physical Review Letters*, 84, 5552–5555.

Yue, G. Z., Qiu, Q., Gao, B., Cheng, Y., Zhang, J., Shimoda, H., Chang, S., Lu, J. P., and Zhou, O. (2002), "Generation of continuous and pulsed diagnostic imaging x-ray radiation using a carbon-nanotube-based field-emission cathode," *Applied Physics Letters*, 81, 355–357.

Zhang, X. W., Du, A. J., Lee, P. F., Sun, D. D., and Leckie, J. O. (2008), "TiO2 nanowire membrane for concurrent filtration and photocatalytic oxidation of humic acid in water," *Journal of Membrane Science*, 313, 44–51.

Zhao, Y. H., Qian, Y. L., Zhu, B. K., and Xu, Y. Y. (2008), "Modification of porous poly(vinylidene fluoride) membrane using amphiphilic polymers with different structures in phase inversion process," *Journal of Membrane Science*, 310, 567–576.

Zularisam, A. W., Ismail, A. F., and Salim, R. (2006), "Behaviours of natural organic matter in membrane filtration for surface water treatment - a review," *Desalination*, 194, 211–231.

Biography

Personal Information
Name: Charles-François Pedro Claude Karolek Ghislain de Lannoy
Date of Birth: 8th November 1984, North York, ON, Canada
Honours Bachelor of Science, H BSc., Honours Physics, McGill University
Philosophiae Doctor, Ph. D., Civil and Environmental Engieering, Duke University

Publications

1. Sengur, R.; Turken, T.; **de Lannoy, C. F.**; Wiesner, M.; Koyuncu, I., Hydroxylated and Carboxylated Multiwalled Carbon Nanotube / Polyethersulfone (PES) Hollow Fiber Membrane Fabrication and Characterization, *Journal of Membrane Science*, (under review)

2. **de Lannoy, C. F.**; Soyer, E.; Wiesner, M., Optimizing Carbon Nanotube–Reinforced Polysulfone Ultrafiltration Membranes Through Carboxylic Acid Functionalization. *Journal of Membrane Science*, 2013, 447, 395-402. (de Lannoy et al., 2013b)

3. **de Lannoy, C. F.**; Jassby, D.; Gloe, K.; Gordon, A.; Wiesner, M., Aquatic Biofouling Prevention by Electrically Charged Nanocomposite Polymer Thin Film Membranes, *Environmental Science and Technology*, 2013, 2760-2768, 47 (6) (de Lannoy et al., 2013a)

4. **de Lannoy, C. F.**; Jassby, D.; Davis, D.; Wiesner, M., A Highly Electrically Conductive Polymer–Multiwalled Carbon Nanotube Nanocomposite Membrane. *Journal of Membrane Science*, 2012, 415, 718-724. (de Lannoy et al., 2012)

5. Bennewitz, R.; David, J.; **de Lannoy, C. F.**; Drevniok, B.; Hubbard-Davis, P.; Miura, T.; Trichtchenko, O., Dynamic strain measurements in a sliding microstructured contact. *J Phys-Condens Mat*, 2008, 20 (1). Bennewtiz et al. (2008)

6. Harroun, T.; Koslowsky, M.; Nieh, M. P.; **de Lannoy, C. F.**; Raghunathan, V.; Katsaras, J., Comprehensive Examination of Mesophases Formed by DMPC and DHPC Mixtures. *Langmuir*, 2005, 21 (12).Harround et al. (2005)